

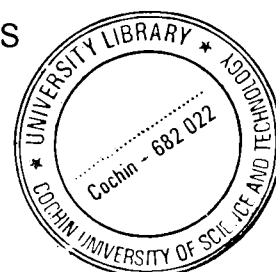
**METAMORPHISM AND FLUID INCLUSION STUDIES OF  
CHARNOCKITES AND ASSOCIATED ROCKS FROM THE  
MADURAI GRANULITE BLOCK, SOUTHERN INDIA WITH  
SPECIAL REFERENCE TO GRAPHITE MINERALIZATION**

09147

Thesis submitted to the  
**COCHIN UNIVERSITY OF SCIENCE AND TECHNOLOGY**  
*in partial fulfilment of the requirements*  
*for the degree of*

**DOCTOR OF PHILOSOPHY**

UNDER THE FACULTY OF MARINE SCIENCES



by  
**BAIJU K.R.**

Department of Marine Geology and Geophysics  
School of Marine Sciences  
Cochin University of Science and Technology  
Kochi – 682 016

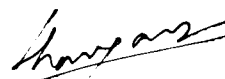
**SEPTEMBER 2006**

## CERTIFICATE

I certify that the thesis entitled “**Metamorphism and Fluid Inclusion Studies of Charnockites and Associated Rocks from the Madurai Granulite Block, Southern India with Special Reference to Graphite Mineralization**” has been prepared by Mr. Baiju K. R. under my supervision and guidance in partial fulfilment of the requirements for the degree of Doctor of Philosophy and no part thereof has been submitted for any other degree.

Kochi – 682 016

25<sup>th</sup> September 2006



**C.G. Nambiar**

(Research Supervisor)

Professor & Head

Department of Marine Geology and Geophysics

School of Marine Sciences

Cochin University of Science and Technology

Kochi – 682 016

# CONTENTS

	PAGE NO
PREFACE	
LIST OF TABLES	
LIST OF FIGURES AND PLATES	
MINERAL ABBREVIATIONS	
CHAPTER I	
<b>INTRODUCTION</b>	
1.1 GENERAL INTRODUCTION	1
1.2 INDIAN CRATONS - AN OUTLINE	4
1.3 CHARNOCKITES OF SOUTH INDIA	6
1.4 PRESENT STUDY	7
1.5 METHODOLOGY	9
CHAPTER II	
<b>MADURAI GRANULITE BLOCK-AN OUTLINE</b>	
2.1 INTRODUCTION	15
2.2 THE SOUTHERN GRANULITE TERRAIN (SGT)	15
2.3 GEOLOGICAL FRAMEWORK OF THE MADURAI GRANULITE BLOCK	17
CHAPTER III	
<b>FIELD RELATIONSHIPS AND PETROGRAPHY</b>	
3.1 INTRODUCTION	29
3.2 FIELD RELATIONSHIPS	29
3.3 PETROGRAPHY	37
CHAPTER IV	
<b>REACTION TEXTURES, MINERAL CHEMISTRY AND ESTIMATION OF PRESSURE – TEMPERATURE CONDITIONS</b>	
4.1 INTRODUCTION	41
4.2 TYPES OF P-T PATHS	42
4.3 P-T ESTIMATES FROM THE MGB	42
4.4 ROCK TYPES AND THE FIELD RELATIONSHIPS OF THE SAMPLES	44
4.5 REACTION TEXTURES	46
4.6 MINERAL CHEMISTRY	51
4.7 COMPARISON OF THE MINERAL CHEMISTRY OF PRESENT STUDIED ROCKS WITH SIMILAR ROCKS FROM ADJACENT TERRAINS	55

4.8	P-T ESTIMATION	57
4.9	CONCLUDING REMARKS	62

#### CHAPTER V

### **OCCURENCE, GENESIS AND MINERALOGICAL CHARACTERIZATION OF GRAPHITE**

5.1	INTRODUCTION	64
5.2	GRAPHITE FORMATION	65
5.3	GRAPHITE STRUCTURE	66
5.4	PREVIOUS STUDIES ON GRAPHITE MINERALIZATION IN THE MGB AND ADJACENT BLOCKS	68
5.5	FIELD RELATION AND OCCURRENCE OF GRAPHITE IN THE PRESENT STUDY	69
5.6	ANALYTICAL PROCEDURES	72
5.7	RESULTS	76
5.8	DISCUSSION	80
5.9	CONCLUDING REMARKS	81

#### CHAPTER VI

### **FLUID INCLUSION STUDIES**

6.1	INTRODUCTION	82
6.2	CRITERIA FOR RECOGNITION OF THE ORIGIN OF FLUID INCLUSIONS	85
6.3	CHANGES IN FLUID INCLUSION SINCE TRAPPING	88
6.4	COMPOSITION OF FLUID INCLUSIONS	89
6.5	FLUIDS IN METAMORPHIC ROCKS	90
6.6	ANALYTICAL PROCEDURES	90
6.7	FLUID INCLUSION STUDIES IN THE MGB	93
6.8	PRESENT STUDY	95
6.9	INTERPRETATIONS FROM THE FLUID INCLUSION DATA	108
6.10	CONCLUDING REMARKS	115

#### CHAPTER VII

### **MONAZITE DATING**

7.1	INTRODUCTION	117
7.2	ELECTRON MICROPROBE DATING OF MONAZITE	118
7.3	ANALYTICAL TECHNIQUES	120
7.4	FIELD RELATIONSHIP OF THE SAMPLES SELECTED FOR MONAZITE DATING	123
7.5	RESULTS AND DISCUSSION	125
7.6	GEOLOGICAL IMPLICATIONS	126

#### CHAPTER VIII

### **SUMMARY AND CONCLUSIONS**

127

**REFERENCES**

134

**APPENDIX I**

DETAILS OF THE MAJOR LOCATIONS AND THE ROCK  
TYPES FROM THE STUDY AREA

**APPENDIX II-**

MICROPROBE DATA OF MINERALS

**APPENDIX III**

DATA OF FLUID INCLUSION MICROTHERMOMETRY

## LIST OF TABLES

- Table 1.1 Summary of events in the Precambrian crust of the Indian craton
- Table 4.1 Representative microprobe data of garnets from garnet-biotite gneiss in MGB
- Table 4.2 Representative microprobe data of garnets from charnockite in MGB
- Table 4.3 Representative microprobe data of garnets from garnet-biotite-cordierite gneiss in ACS
- Table 4.4 Representative microprobe data of garnets from garnet-biotite gneiss in ACS
- Table 4.5 Representative microprobe data of garnets from charnockite in ACS
- Table 4.6 Representative microprobe data of biotites
- Table 4.7 Representative microprobe data of feldspars
- Table 4.8 Representative microprobe data of Orthopyroxenes
- Table 4.9 Representative microprobe data of clinopyroxenes
- Table 4.10 Representative microprobe data for hornblende
- Table 4.11 Microprobe data of cordierites
- Table 4.13 The summary of available P-T estimates in various parts of MGB and ACS
- Table 4.14 Temperature estimates from two pyroxene granulites of MGB at 8kb
- Table 4.15 Temperature estimates from garnet-biotite gneiss of MGB at 8kb
- Table 4.16 Temperature estimates from Charnockite of MGB at 8kb pressure
- Table 4.17 Temperature estimates from garnet-biotite-cordierite gneiss of ACS
- Table 4.18 Temperature estimates from garnet- biotite gneiss of ACS at 8 kb pressure
- Table 4.19 Temperature estimates from charnockite of ACS at 8kb pressure
- Table 4.20 Pressure estimates from charnockites of MGB at 800°C
- Table 4.21 Pressure estimates from charnockites of ACS at 800°C

- Table 4.22 Pressure estimates from garnet-biotite cordierite gneiss
- Table 5. 1 X-ray diffraction and calculated structural data of graphite samples
- Table. 6.1 Classification of Fluid-Inclusions
- Table 6.2 Details of the location and the major rock types present fro which the samples for fluid inclusion studies are taken
- Table 6.3 Halite solubility in weight percent as a function of temperature calculated.
- Table 7.1 Details of the samples selected for monazite dating
- Table 7.2 Electron probe analytical results for monazites of different samples from MGB

## LIST OF FIGURES AND PLATES

### FIGURES

- Fig. 1.1 Precambrian terrains in Indian subcontinent
- Fig. 1.2 Southern India showing different granulite blocks and major Proterozoic shear zones
- Fig. 2.1 Geological map of MGB
- Fig. 3.1 Traverses made during the field
- Fig. 4.1 Sampling locations for EPMA
- Fig. 4.2 Garnet composition from garnet-biotite gneiss of MGB
- Fig. 4.3 Variation in garnet composition from rim to core (Sample: CK16)
- Fig. 4.4 Garnet composition from charnockite of MGB
- Fig. 4.5 Variation in garnet composition from rim to core (Sample: CK58)
- Fig. 4.6 Garnet composition from garnet-biotite-cordierite gneiss of ACS
- Fig. 4.7 Variation in garnet composition from rim to core (Sample: CK37)
- Fig. 4.8 Garnet composition from garnet-biotite gneiss of ACS
- Fig. 4.9 Variation in garnet composition from rim to core (Sample: CK39)
- Fig. 4.10 Garnet composition from charnockite of the ACS
- Fig. 4.11 Variation in garnet composition from rim to core (Sample: CK40)
- Fig. 4.12 Biotite compositions plotted in the "ideal biotite plane" diagram
- Fig. 4.13 Si vs Ti plot for biotites showing primary and secondary biotites in the samples from MGB and ACS
- Fig. 4.14 Feldspar composition from different rocks of MGB & ACS
- Fig. 4.15 Clinopyroxene composition from the granulites of MGB
- Fig. 4.16 Plot for geothermometry of different rocks under study with respect to  $Al_2SiO_4$  triple junction using all possible garnet-biotite thermometers and garnet- plagioclase- orthopyroxene-quartz barometer.
- Fig. 4.17 Pressure-temperature fields of the rocks from MGB and ACS
- Fig. 5.1 Hexagonal and Rhombohedral lattice of graphite



- Fig. 5.2 Graphite sample locations
- Fig. 5.3. X-ray powder diffraction (002) peaks of selected graphite samples
- Fig 5.4 Interplanar spacing  $d(002)$  vs crystallite size,  $L_c(002)$  for the present studied graphite
- Fig. 5.5 Degree of graphitization of the graphite from the present study compared with the linear relationship for Ryoke pelites of Wada et al. (1994).
- Fig. 5.6 Comparison of metamorphic temperature of the MGB graphite derived from the curve of Ryoke pelites with the calculated temperatures
- Fig 5.7 Raman spectra of graphite samples from MGB
- Fig. 5.8 Histogram plot of the existing carbon isotope data from SGT, in comparison with the isotope data of the MGB graphite
- Fig. 6.1 Sample locations of fluid inclusion studies
- Fig. 6.2 Temperature of melting ( $T_M$ ) of monophase  $CO_2$  inclusions
- Fig. 6.3 Temperature of homogenisation ( $T_H$ ) of  $CO_2$  in monophase and biphasic inclusions
- Fig. 6.4 State of total homogenisation of the inclusions from different samples
- Fig. 6.5 Relationship between temperature of homogenisation and density of  $CO_2$  bearing inclusions
- Fig. 6.6 P-T diagram showing  $CO_2$  isochores and proposed fields of inclusions in the present study
- Fig. 7.1 Location of samples selected for monazite dating
- Fig. 7.2 Weighted-histogram representation of the investigated samples
- Fig. 7.3 Isochrones plotted from Th-Pb data
- Fig 7.4 U-Th-age diagram for the investigated samples displaying the relationship between individual ages and U-Th content.
- Fig. 7.5 Th equivalent age for the investigated samples

## PLATES

- Plates 3.1-3.6 Field occurrence of various rock types from the study area
- Plates 3.7-3.36 Photomicrographs of different mineral assemblages in the rocks under study

Plates 4.1-4.9	Photomicrographs explaining different reaction textures in the samples selected for EPMA
Plates 5.1-5.4	Field photos of graphite occurrence in MGB
Plates 6.1-6.6	Photomicrographs showing different types of fluid inclusions in the rocks under study
Plate 6.7	Fluid inclusion laboratory at IIT Bombay
Plates 6.8-6.9	Behaviour of fluid inclusions during microthermometry
Plate 6.10	Morphology of fluid inclusions showing effects of re-equilibration
Plates 7.1-7.3	Photo showing field occurrences of the rocks selected for monazite dating

## MINERAL ABBREVIATIONS

Qtz	Quartz
Pl	Plagioclase
Bt	Biotite
Grt	Garnet
Opx	Orthopyroxene
Cpx	Clinopyroxen
Hnb	Hornblende
Crd	Cordierite
Mag	Magnetite
Spl	Spinel
Ilm	: Ilminite

# CHAPTER 1

INTRODUCTION

---

## 1.1 GENERAL INTRODUCTION

Petrology is a term, which connotes the philosophical side of the study of rocks, and includes both petrography and petrogenesis (Tyrrel, 1926). From among various branches of petrology, metamorphic petrology is different and more challenging as it deals with the rocks that are formed secondarily at new sets of conditions resulting in extensive textural and mineralogical changes to the precursor rocks. Mostly metamorphism is regional, takes place in the deeper parts of orogenic belts and is termed metamorphic belts (Miyashiro, 1961). Depending on the intensity of temperature and pressure, the metamorphic rocks formed vary in the grade. As the grade of metamorphism increases, the appearance of new specific minerals is possible and in a terrain the zones between the appearances of two specific minerals (isograds) are termed mineral zones. Eskola (1915) introduced the concept of metamorphic facies based on these metamorphic zones.

In Eskola's classification, the granulite facies rocks are the highest grade that can be attained in crustal metamorphism. This facies was defined by the first appearance of orthopyroxenes in the rocks having considerable magnesium. However, origin of granulite facies rocks at high temperatures is widely accepted. Many geothermometric studies indicate that the temperature of formation of these rocks are above 750°C, while geobarometric studies conforming with depth conditions give a vivid picture ranging from low to high pressures. Therefore the occurrence of the rocks of granulite facies must be evaluated with respect to the mineral

assemblage of tectonic settings (Katz, 1978). So they provide important information on the nature of deep continental crust and its evolution with time. The tectonic and chemical processes responsible for the stabilization of the continents are enlightened through the study of granulites. The lower crustal origin of these rocks is confirmed as they apparently satisfy the overall density, seismic velocity and geothermal and geochemical characteristics of the lower crust (Katz, 1978; Harley, 1989). An argument in support of this view is the widespread exposure of Late Archaean and Proterozoic Precambrian terrains, which may be the result of extensive tectonic uplift and erosion (Heier, 1973). Reymer and Schubert (1984) corroborate the idea with an explanation that the 70% or more of the present crustal material had already separated from the mantle by about 2.5 Ga ago.

The granulite facies supracrustal rocks, of Precambrian terrains, those containing specific mineral assemblages suitable for experimental and empirical geothermobarometric computations are more important for P-T-t studies. Para metamorphic argillaceous (pelitic) rocks are particularly well suited for these empirical computations, as they contain low-variance mineral assemblages with conspicuous isograd minerals like biotite, garnet, the alumino-silicate polymorphs, cordierite, sillimanite, spinel and K-feldspar. The identification of isograd minerals allows for immediate, semi-quantitative estimates of peak metamorphic grade and its low-variance helps to estimate the thermobarometry (Berman, 1991) or it support in to the basis of differential thermodynamic modelling (Spear, 1993). The aspect of time of formation of the granulites is also an

important constraint in the description of the P-T-t paths. Earlier it was believed that the granulites were only formed during the Archaean-Proterozoic time, but later it has been proved that granulite metamorphism is not restricted to any particular part of the Earth's history but is associated with major continental crust formation and reworking episodes even continuing the present day and the recent granulite belts are yet to be exhumed through later tectonic episodes (Harley 1989). The Pan-African granulites of India and Sri Lanka (700-500 Ma), the Hercynian granulites of Europe (300 Ma) are some of the examples for Phanerozoic granulites.

The study of high-grade terrains helped geologists to pinpoint many of the aspects related to the petrogenetic evolution of the crust during the geological time. The internal structures and relationships between the rock types are generally complex due to the long evolutionary history, which these rocks have undergone. Most granulite terrains are comprised of a varied suit of rocks such as mafic and felsic orthogneisses and paragneisses derived from pelitic, quartzitic and calcareous precursors. A complex structural pattern is also noticed in most of the granulite terrains due to some partial melting processes, which took place at high grades, or due to some ductile deformation events. These complex frameworks come from a sequence of processes and geological events (deformation, intrusions, metamorphic phases, partial melting, recrystallisation, and assimilation) that tend to obliterate older structures by printing new features in the rocks. Thus the tectonic and chemical processes of granulite terrains are of greater interest since they form the windows for the better understanding of deep crustal materials.

Granulite studies are usually concentrated in four general areas; (i) thermometry and barometry, (ii) the nature and role of fluids, (iii) geochemical studies of lower crustal rocks with emphasis on their large-ion lithophile element content and (iv) tectonic modelling based on the field relationships, petrology and P-T-t data (Bohlen, 1987 and the references there in). The present study pertains to the Madurai Granulite Block (MGB), which is one of the important tectonic blocks of the Southern Granulite Terrain (SGT), South India. Some of the above said techniques were made use in the study to bring out the nature and evolution of deep continental crustal configuration of the terrain. The work is aimed at understanding the P-T conditions and the role of fluids in the metamorphism and processes of charnockitization. The presence of graphite in some specific regions of the terrain is kept in to consideration and an attempt is made in the present study to look into some of the important aspects like the occurrence, genesis, nature and grade of graphite. Finally, preliminary geochronological studies were carried out on some of the gneisses from the terrain using a novel technique of dating the monazites from the rock with the help of Electron Probe Micro Analyser (EPMA).

## **1.2 INDIAN CRATONS - AN OUTLINE**

Most of the granulite mobile belts are characterized with different rock types such as charnockites, layered mafic complexes, quartzo-feldspathic-migmatitic gneisses, granites and abundant conformable metasedimentary rocks including quartzites, marbles, garnet-sillimanite gneisses etc. In Indian arena the Precambrians are composed of Northern and Southern shields divided by a Central Indian tectonic zone. The



Northern shield is mainly dominated by the Aravalli craton including the Bundelkhand complex. The Southern shield consists of the Dharwar, Bastar, and Singhbhum cratons, which are bounded by granulite belts of Archaean and Proterozoic ages (Mahabaleswar *et al.*, 1995; Radhakrishna and Naqvi, 1986; Yoshida *et al.*, 1996). Fig. 1.1 gives a general outline of the Precambrian terrains in the Indian sub-continent.

The Indian shield has experienced two-stage course of cratonization (Mahadevan, 1994). An early period ending at 2500 Ma saw the cratonization of the Archaean greenstone-granite domain and the period of 2500 to 1600 Ma saw the progressive cratonization of the high-grade granulite domain. The boundary between the two domains is drawn in the south and east by the Fermor line, which is traced from the Orissa coast (north of Cuttack) through the Talchir coalfield the Nellore-Madras Coast and then across the shield to the west coast north of Mangalore (Pascoe, 1950). The western boundary of the greenstone-granite domain is determined by the eastern limits of the Mesozoic rift that ushered in the Deccan volcanism, placed along a line extending from east of Cambay through Nasik-Pune-Kolhapur and southwards (Mahadevan, 1994). On the north, the boundary of the greenstone-granite domain is rather diffused. The high-grade granulite domain covers a large part of the Chhotanagpur Gneissic Plateau (Majumdar, 1988; Mahadevan, 1992) and the western part of the Shillong plateau. Outcrops of high-grade granulites occur on the eastern and western flanks of the Delhi Super-group belt of the Aravalli range and to its south (Raja Rao, *et al.*, 1971; Fareeduddin *et al.*, 1991; Desai *et al.*, 1978). Charnockitic rocks occur over a 100 km long belt

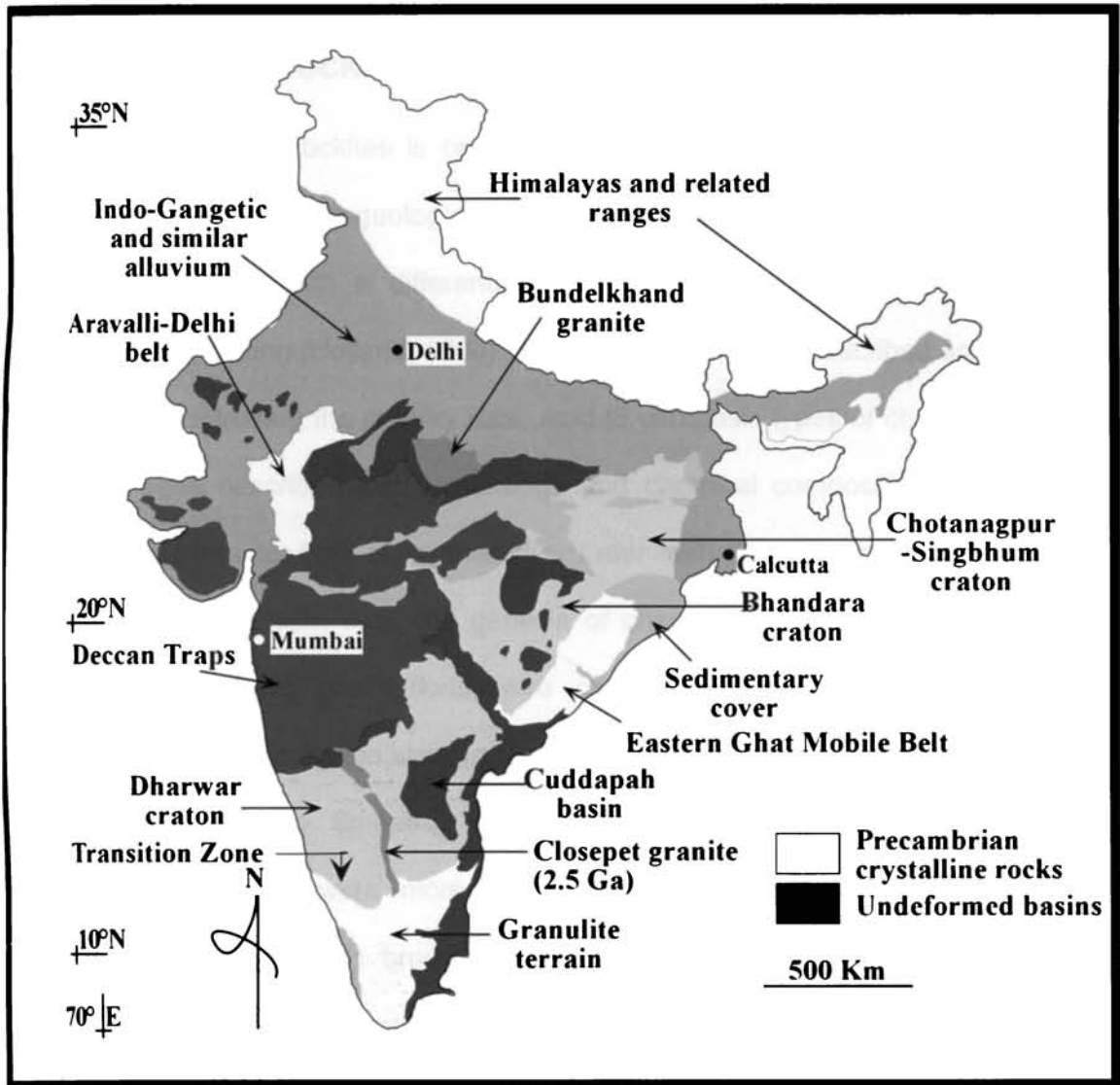


Fig 1.1 Precambrian terrains in Indian sub-continent

between the Sausars and Sakolis in central India (Pascoe, 1950; Yedekar *et al.*, 1990)

The chrono-stratigraphy incorporating the major events in the Precambrians of India is summarised as in Table 1.

### **1.3 CHARNOCKITES OF SOUTH INDIA**

Charnockites is one among the principal rocks of granulite facies terrain. In earlier geological literatures charnockites were given an igneous parentage with a differentiation series ranging from acid to ultrabasic composition (Holland, 1900). Their stratigraphy was described as a plutonic suit intruding the country rock. Acid to ultrabasic types of charnockites has been described with mineralogy and chemical composition from that of granites to that of pyroxenites. Later with the infusion of the idea of metamorphism in it, the genesis of charnockites got revised and earlier stratigraphic descriptions were changed. Therefore, many schools of elucidations on the stratigraphy of the SGT of India appeared in geological literature (eg. Smeeth, 1916; Rama Rao, 1945; Pichamuthu, 1953,1961 etc.), which were more or less inconclusive. However Fountain and Sallisbury (1981) brought out a conclusive and evident statement that charnockites are not stratigraphic units but are the deeper level equivalents of gneisses.

Crustal processes related to the formation and exhumation of charnockites has been a matter of discussion during the last two decades. About three major episodes of charnockitization were recognised so far. It includes (1) Late Archaean (~3.0 Ga) charnockites formed at dry lower crustal levels, (2) Early Proterozoic (~2.5 Ga) charnockites and (3) Late

**Table 1.1 Summary of events in the Precambrian crust of the Indian craton**  
(Compiled from various literatures)

EON	TIME (Ga)	MAJOR EVENTS
<b>RIPHEAN</b>	1.65- 0.57	<ul style="list-style-type: none"> <li>▪ Events related to Pan-African orogeny; Development of major shear zones in SGT, Incipient charnockitization episodes etc. (0.5 Ga)</li> <li>▪ Narmada–SonThrust Fault (1.0-0.5 Ga)</li> <li>▪ Additional metamorphism of Eastern Ghats belt (1.1 Ga).</li> <li>▪ Alkaline plutonism in Eastern Ghats Belts (1.3 Ga).</li> <li>▪ Thrust of Singhbhum copper belt, Advance of Eastern Ghats (1.65Ga)</li> </ul>
<b>PROTEROZOIC</b>	2.5-1.65	<ul style="list-style-type: none"> <li>▪ Eastern Ghats Orogeny (1.6 Ga)</li> <li>▪ Granite of Singhbhum and Bhandara cratons (2.2-2.1 Ga)</li> <li>▪ Aravalli sediments, Cuddapah sediments, Delhi sediments (2.5-1.8 Ga)</li> </ul>
<b>ARCHAIC</b>	ABOVE 2.0	<ul style="list-style-type: none"> <li>▪ Cratonization of Dravidian shield, Exhumation of Clospet, Chitradurga, Bundelkhand granites. Charnockites of South India and Eastern Ghats. (2.6 Ga).</li> <li>▪ Dharwar schist belts (3.0-2.6 Ga)</li> <li>▪ Major crust forming event; Peninsular gneisses and charnockites (3.3-3.0 Ga)</li> <li>▪ Khondalite metamorphism in Eastern Ghats (3.1 Ga)</li> <li>▪ Sargur enclaves (3.1-3.0 Ga)</li> <li>▪ Tonolites; Crust forming event (3.3 Ga). Banded Gneissic Complex of Aravalli craton (~3.4 Ga)</li> </ul>

Proterozoic (~550 Ma) Pan-African charnockites. The Proterozoic episodes are believed to be generated in the mid-to lower crustal levels by the lowering of partial pressures of H<sub>2</sub>O by CO<sub>2</sub>. Jayananda and Peucat (1996) and Mohan and Jayananda (1999) provide a perspective view into the metamorphic events in South Indian shield. A palaeo-pressure estimate of 4-9kb has been identified from the Karnataka Craton to Nilgiri hills. Further south, in Kerala Khondalite Belt the P-T were accorded at 4.5kb pressure and 700-750°C temperature. There are strong evidences of CO<sub>2</sub> influx promoting dehydration mechanism leading to extensive charnockitization (Santosh, 1989).

#### **1.4 PRESENT STUDY**

The three major subdivisions of the Precambrians of South India are the Dharwar craton (covering most of the Karnataka), the Southern Granulite Terrain (covering Tamil Nadu, Kerala and southern part of Karnataka) and the Eastern Ghats. The Southern Granulite Terrain (SGT) forms a tectonic collage of several crustal blocks separated by extensive Proterozoic shear zones. The MGB forms the largest and centrally located tectonic block in the SGT. The present study is concentrated in this block; the area falls approximately in between latitudes 8°40" N and 11°15" N and longitudes 76° 00" E - 79° 00" E. Structurally, it is bounded by the Palghat-Cauvery Shear zone (PCSZ) in the north and the Achankovil shear zone (ACS) in the south (Fig 1.2). Though Cenki and Kriegsman (2005) question the authenticity of the southern boundary concept, it is the popularly accepted by most workers and hence followed here.

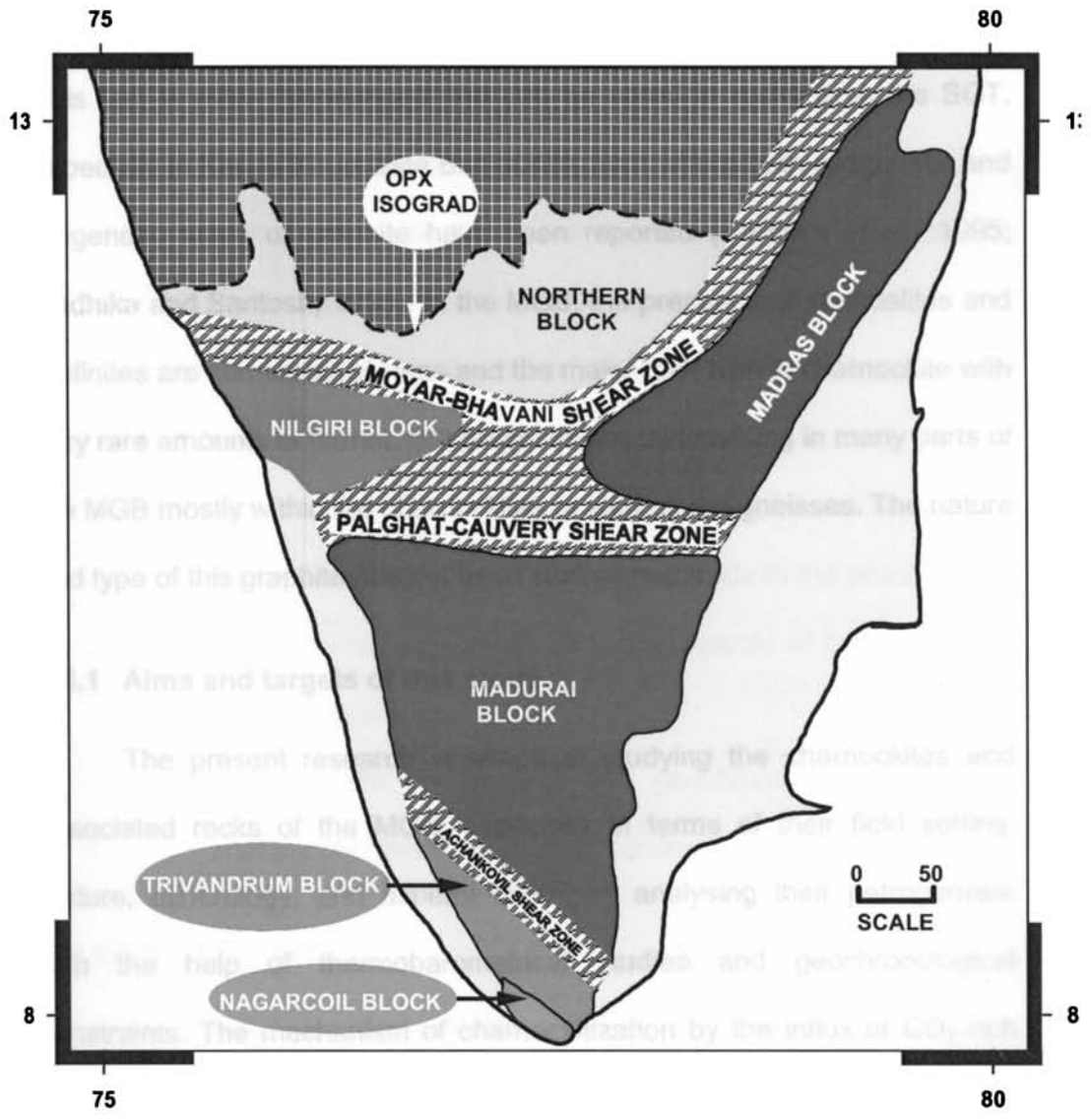


**Fig 1.2 Southern India showing different granulite blocks and major Proterozoic shear zones (After Santosh, 1996)**

Graphite is a common accessory mineral in high-grade metamorphic rocks, but it is more prominent in khondalites (garnet-biotite-silliminite gneiss) and leptinites (garnet-biotite gneiss) and very rarely in garnet bearing and orthopyroxene bearing anhydrous granulites (charnockite). This fact is more pronounced and can be noted in rocks from the SGT, especially in Kerala Khondalite Belt (KKB), from where both syngenetic and epigenetic types of graphite have been reported (Radhika *et al.*, 1995; Radhika and Santosh, 1996). In the MGB, the presence of khondalites and leptinites are comparatively less and the major rock type is charnockite with very rare amounts of garnet. But graphites are mineralising in many parts of the MGB mostly within the charnockites or associated gneisses. The nature and type of this graphite has not been studied much.

#### **1.4.1 Aims and targets of this study**

The present research is aimed at studying the charnockites and associated rocks of the MGB, especially in terms of their field setting, texture, mineralogy, and mineral chemistry analysing their petrogenesis with the help of thermobarometrical studies and geochronological constraints. The mechanism of charnockitization by the influx of CO<sub>2</sub> rich fluids and its relation to the graphite mineralization is actually a matter of discussion and study. But this aspect is not yet treated with all its possibilities in any of the previous studies. So in this study an attempt has been made in this line also, considering the widespread occurrence of graphite in the MGB.

The objectives of the present study are listed below:

- ❖ To delineate petrological and structural relationship of charnockites and associated gneissic rocks in the study area.
- ❖ To study the field and petrogenetic aspects of graphite mineralization in the MGB.
- ❖ To establish and re-evaluate the P-T conditions of formation of the rocks with the aid of thermobarometric computations and to compare with the earlier studies.
- ❖ Characterization of graphite with XRD, Raman spectroscopy and isotope studies together with a search in to its genesis and its relation to the high-grade metamorphism of the terrain.
- ❖ To evaluate the role of CO<sub>2</sub> bearing fluids in the processes of charnockitization as well as in the genesis of graphite within this high-grade terrain.
- ❖ To delineate the metamorphic geochronology of selected rocks using 'monazite dating' technique with EPMA.

## **1.5 METHODOLOGY**

The specific problem identified in the MGB is dissected and is scrutinised by a six-fold approach with an integration of different methods to summarize the results. Detailed field survey in the MGB was carried out in order to identify and characterize the different rock types and to delineate their field relationships. Special attention was given for finding the graphite occurrences in the terrain. This was followed by detailed hand specimen to thin-section scale petrographic observation and characterization of assemblages and reactions and textures. Petrogenetic modelling with real



mineral compositions gave good approximations of Pressure-Temperature conditions of peak and retrograde metamorphism. Fluid inclusion studies on selected specimens from the selected rocks in the area are carried out to comprehend different aspects of fluid activity during metamorphism and graphite mineralization. This was followed by the mineralogical characterization of graphites. Monazites from selected gneisses from the terrain are dated as the last stage to understand the period of its formation. All these data were compiled to formulate and model the evolution of the high-grade terrain of the MGB and to synthesise this with the processes of graphite mineralization.

#### **1.5.1 Field survey**

Extensive field studies were done in the major metamorphic terrains of the MGB for understanding the field relationship of different rocks. In the MGB the major rocks encountered in the field were charnockites, mafic granulites, hornblende-biotite gneiss, biotite gneiss, garnet-biotite gneiss, migmatitic gneisses, granites and other quartzo-feldspathic gneisses. Fresh samples from more than 150 locations were collected for the detailed laboratory investigations. About 20 locations of graphite mineralization were also found during that fieldwork. The field relationships of these graphites with respect to their host rocks were also studied. Details of the important locations from where samples and other data were collected are given in Appendix-I.

### **1.5.2 Petrography**

Detailed petrographic analysis of major rock types are carried out. More than 100 thin sections covering all the rock types were prepared by conventional methods. The petrography of each thin section was studied under a petrological microscope. The textural relationships of various minerals present in the rocks were studied in order to unearth the metamorphic reaction processes involved in the evolution of different rocks. Micrographs and photomicrographs were prepared using Leitz microscope with photographic attachment.

### **1.5.3 Electron Probe Micro Analysis (EPMA)**

Representative rock samples were used for the Electron Probe Micro Analysis (EPMA). For this doubly polished thin sections were prepared. The EPM analysis was carried out by Dr. M. Satish-Kumar at the Department of Biology and Geosciences, Shizuoka University, Japan. Details about the EPM and the conditions are given in section 4.6.

### **1.5.4 X-ray diffraction spectrometry**

X-ray powder diffraction data of representative graphite from ten locations in the western part of the MGB, mainly concentrating in the (002) reflection were collected using a SEIFERT diffractometer with Cu-K $\alpha$  radiation, installed at Cochin University of Science and Technology. Some of the analyses were repeated at the RIGAKU XRD at Shizuoka University, Japan with operating conditions same as those described in Wada *et al.* (1994). The details about the operation conditions are given in section 5.5.

The  $2\theta$ ,  $d$  values and full width of the peak at half-maximum are estimated from the diffractogram, from which an attempt has been done to calculate the metamorphic temperature of its formation.

#### **1.5.5 Raman Spectroscopy**

Raman spectra of graphite were obtained using Raman microprobe equipment comprising of a 30 cm single polychromater (Chromex, 250is) equipped with a CCD detector (Andor, DU-401-BR-DD SH) and an Ar<sup>+</sup> ion laser (514.5 nm; Ion Laser Technology, 5500A) set up in an optical microscope at the Laboratory for Earthquake Chemistry, University of Tokyo, Japan by Dr. M. Satish-Kumar. The details about the analysis are given in section 5.5.

#### **1.5.6 Carbon Isotope Studies**

Carbon isotope compositions of graphite were measured using a MAT 250 mass spectrometer housed at Shizuoka University, Japan. Analytical procedure follows those described in Wada and Ito (1990). Results are reported in standard delta notation in ‰ relative to PDB. Details about the analysis are given in section 5.5.

#### **1.5.7 Fluid Inclusion Studies**

Graphite hosted rocks from the study were selected for fluid inclusion studies. Doubly polished wafers of charnockite as well as some gneiss samples were made by conventional methods. The samples were selected after a detailed petrographic analysis. The study was concentrated on the inclusions in quartz. The microthermometric investigations on the

inclusions were done using a Linkam TH600 stage situated at Department of Earthsciences, IIT Bombay. Photomicrographs were taken using Leitz microscope with photographic attachment.

#### **1.5.8 Geochronological studies using monazite dating**

Electron microprobe dating of monazite is a novel method in geochronology, which has been employed in the present study to bring out the ages of some of the rocks from the MGB. For this monazite grains are identified from the samples thin sections using a petrological microscope. Some times the help of back-scattered electron images are made use to identify very small monazite grains found in matrix or as tiny inclusions in garnet. U, Th and Pb from monazites are analysed on an electron microprobe at the Mineralogisch-Petrologisches Institut, Universität Bonn, Poppelsdorfer Schloß, Germany. The analyses were done by Dr. Ingo Braun from the institute. The detailed procedure of the analysis is given in section 7.2.

#### **1.5.9 Data processing**

The work involved the calculation of petrochemical parameters, structural formulae of minerals, extrapolation of P-T value corresponding to phase equilibria etc. and preparation of various graphs and illustrations. These works were done using modern computing techniques with the help of relevant software. For the P-T calculations, computer programs like PTOXY (Nasir, 1994), PTMafic (Soto and Soto, 1995) and HbPI 1.2 (Holland and Blundy, 1994) were used.

The mineralogical characterisation of graphite from XRD data has been done using different techniques followed by many of the earlier workers like Tagiri (1981), Tagiri and Oba (1986), Pasteris and Chou (1998), Wopenka and Pasteris (1993) etc.

The fluid inclusion data obtained from microthermometry, were compiled and is used to extrapolate the density and volume fraction estimates of the fluid inclusions. The computer program package FLUIDS (Bakker, 2003) were made use of some of the computation purposes.

The raw data (EPMA) on the weight percentage of Th, U and Pb of the analysed rock specimens were compiled in Microsoft Excel programs to bring out the geochronology. It is further represented using different graphical and statistical methods. Isochrones were extrapolated from the Th-Pb data.

# CHAPTER 2

MADURAI GRANULITE BLOCK-AN OUTLINE

---

## 2.1 INTRODUCTION

Precambrian crust of the Earth constitutes nine cratons, namely regions in Asia and Indian subcontinent, Europe, Greenland, North America, South America, Africa, Australia and Antarctica. The Indian craton including Sri Lanka forms about 3% of the total area of Precambrian crust. The Indian Precambrian terrain include the Dravidian shield (the Western Dharwar craton, the Eastern Dharwar craton and the Southern Granulite Terrain) in the south, the Eastern Ghats in the east, the Chotanagpur-Singhbhum in the northeast and the Aravallis in the northwest (Goodwin, 1996) (Fig 1.1). The oldest rocks of Indian craton lie in the Aravallis, the Singhbhum and the Dharwar regions (~3.4 Ga). Major events of orogeny occurred during 3.0 Ga and 2.5 Ga, in which the later marks a boundary for Archaean-Proterozoic ages. It is further characterized by high-grade metamorphism, which in turn has resulted in consolidation of South Indian Shield (Goodwin, 1996, Jayananda and Peucat, 1996).

## 2.2 THE SOUTHERN GRANULITE TERRAIN (SGT)

The SGT is one of the best-exposed granulite terrains suited to address some fundamental problems concerning the origin and development of granulites. The contact between Dharwar craton and the SGT is marked by a series of crustal zone shear zones like the Moyar-Bhavani-Attur shear zone to the south of the regional orthopyroxene isograd. Geochronological studies reveal that the PCSZ forms a major divide between older Archaean granulite crust in the north and the younger supracrustal dominated crust in the south (Harris *et al.*, 1994, 1996;

Brandon and Meen, 1995; Loyd *et al.*, 2004). But the Noyil-Cauvery shear zone marks the tectonic boundary as well as the Archaean-Neoproterozoic boundary resulting from collision with a craton in Africa or Antarctica (Ramakrishnan, 2003), later through which some Pan-African granitic emplacement has taken place. Thus the major Proterozoic domains in India fall in the SGT and comprise of the Nilgiri Block (NB), the Madras Block (MB), the Madurai Granulite Block (MGB) and the Trivandrum Block (TB) (Hariss *et al.*, 1994; Jayananda and Peucat, 1996; Braun and Kriegsman, 2003). The major shear zones demarcating these blocks are, the Moyar shear zone (between the transition zone and the Nilgiri block), the Moyar-Bhavani and the Palghat-Cauvery shear zone (between Madras/Nilgiri Blocks and the Madurai Granulite Block) and the Achankovil shear zone (between the Madurai Block and the Trivandrum Block) (see Fig 1.2).

The NB and the MB are characterised by the occurrence of enderbites and charnockites where as the MGB and the TB are dominated by metasedimentary rocks with abundant tectonothermal activity in the Pan-African time (Choudhari *et al.*, 1992; Santosh *et al.*, 1992; Bartlett *et al.*, 1995; Jayananda *et al.*, 1995a). The main granulite facies metamorphism of most of the tectonic blocks of the SGT is found to be occurring around  $750 \pm 50^\circ\text{C}$  temperatures and 5-9kb pressure at 2.5Ga ago (Harris *et al.*, 1982; Peucat *et al.*, 1989; Choudhari *et al.*, 1992; Santosh *et al.*, 1992; Srikantappa *et al.*, 1992; Bartlett *et al.*, 1995; Jayananda *et al.*, 1995a; Jayananda and Peucat, 1996). But some models proposed in the recent studies display that granulite-facies metamorphism in the SGT has occurred as part of the east Gondwana (Eastern Africa,



Arabian–Nubian shield, Seychelles, India, Madagascar, Sri Lanka, East Antarctica and Australia) assemblage during 750-530 Ma (Meert, 2003) or by the collision between East and West Gondwana at a time span of 590-520 Ma (Meert *et al.*, 1995). Appropriate geochronological results infer protracted heating of the deep continental crust during this time, which is also referred as the poly phase Proterozoic evolution of the SGT. Abundant evidences put forth this Pan-African activity, which include amphibolite-facies gneiss formation at 550 Ma (Hansen *et al.*, 1985), the peak metamorphic age of the Kodaikanal granulites, just south of the Palghat-Cauvery lineament at ~550 Ma (from garnet-whole-rock Sm-Nd ages) (Jayananda *et al.*, 1995a). The Nd isotopic patterns also indicate considerable formation of juvenile crust and/or reworking of Archaean crust throughout the Proterozoic (Harris *et al.*, 1994; Brandon and Meen, 1995).

### **2.3 GEOLOGICAL FRAMEWORK OF THE MADURAI GRANULITE BLOCK**

The MGB occupies the largest portion of the SGT and it represents a composite mid to lower crustal domain. It has played a fundamental role in characterising the Proterozoic geodynamic evolution of the SGT and its position within East Gondwana. The location of the MGB defined by many early workers is as directly south of the PCSZ and north of the ACS. On contrary to the earlier studies, Cenki and Kriegsman (2005) highlights a poor structural control for different granulite blocks in the SGT as well as the rocks within it. The PCSZ and the ACS, which are defined as the northern and southern boundaries of the MGB, has been reconstructed in their new study. A recently defined lineament of Karur–Kambam–Painavu–

Trissur (KKPT) proposed by Ghosh et al (1998) runs within the MGB. An Achankovil Nd unit (AU) is defined by the workers as a relatively young unit (of Nd modal ages 1.3-1.6 Ga) approximately overlaps the ACS in the western half where as it is diverged in the east.

The MGB is a high-grade granulite facies terrain and the major rock types in the block include charnockites, mafic granulites and different gneisses (Fig 2.1). The MGB can be lithologically divided into a western region and an eastern region; MBK in Kerala and MBTN in Tamil Nadu (Cenki and Kriegsman, 2005). The MBK is characterised by two different groups of hornblende–biotite and orthopyroxene–biotite (charnockite) gneisses, one being quartz rich and the other feldspar rich. While the eastern part, MBTN is composed of massive charnockites and enderbites with heterogeneously distributed quartzites and calc silicate series of rocks (Cenki and Kriegsman, 2005). Garnetiferous rocks are relatively less in the MGB when compared with the adjacent blocks, but hornblende, biotite and orthopyroxenes are present all over the area. A sharp boundary between hornblende and garnet occur in the southern boundary of the MGB, which is elucidated as the difference in composition of protolith rather than a difference in the metamorphic grade. Cenki and Kriegsman (2005) propose a volcano-sedimentary sequence in the MGB.

### **2.3.1 Lithology**

The important rock types found in the MGB, their physico-chemical properties and the characteristic mineral assemblages are given below.

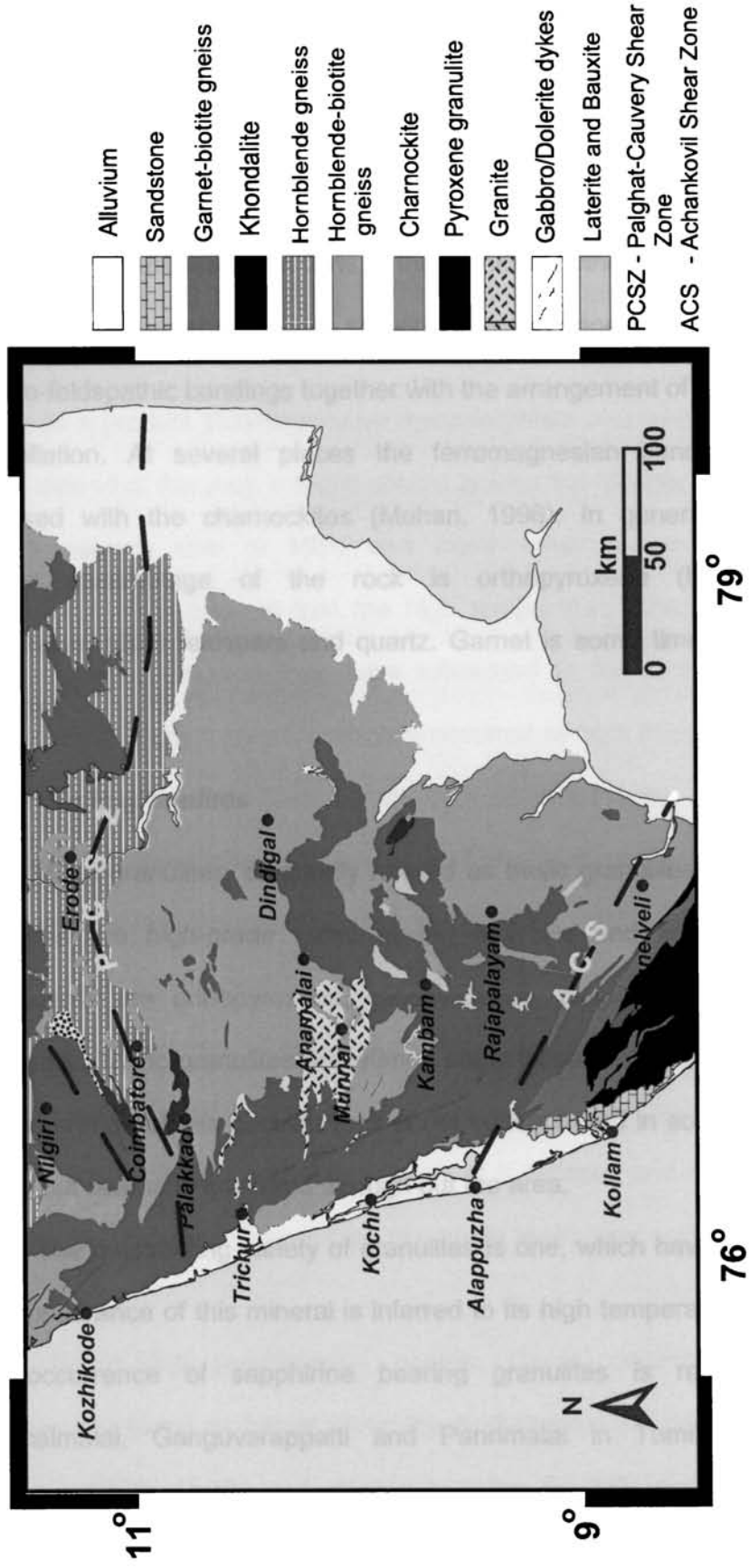


Fig 2.1. Geological map of MGB (compiled after GSI, 1995)

### **2.3.1a Charnockites**

Charnockites present in the block are typically coarse to medium grained with overall grey colour. Presence of smoky/blue quartz as well as plagioclase feldspars is the causative factor for this appearance. The mafic minerals constitute less than 25% in these rocks. Other than the massive varieties, there are charnockites showing gneissic appearances due to the quartzo-feldspathic bandings together with the arrangement of pyroxenes in the foliation. At several places the ferromagnesian bands are seen mobilised with the charnockites (Mohan, 1996). In general the major mineral assemblage of the rock is orthopyroxene (hypersthene), plagioclase, alkali feldspars and quartz. Garnet is some times present in the rock.

### **2.3.1b Mafic granulites**

Mafic granulites, differently referred as basic granulites or pyroxene granulites are high-grade rocks having high Fe and Mg. The major constituents are orthopyroxene, clinopyroxene, plagioclase, hornblende and quartz. Mafic granulites sometimes show foliated nature. In the MGB the occurrence of this peculiar rock is not concentrated in some particular zones, but seems to scattered through out the area.

The outstanding variety of granulites is one, which have sapphirine. The appearance of this mineral is inferred to its high temperature genesis. The occurrence of sapphirine bearing granulites is reported from Perumalmalai, Ganguvarappatti and Panrimalai in Tamil Nadu, the northeastern part of the MGB (Mohan *et al.*, 1996b; Brown *et al.*, 1992;

Sivasubramanian *et al.*, 1991; Grew, 1982). The major mineral assemblage in this rock is sapphirine, orthopyroxene, sillimanite, spinel, and phlogopite. Garnet is rarely present.

### **2.3.1c Gneisses**

Hornblende-biotite gneiss: Hornblende-biotite gneiss forms a major rock type in the MGB. Usually this rock is found associated with charnockite bodies as a product of retrogressive metamorphism occurred in the block. A vast extend of this rock is found almost around the Munnar granitic body on the eastern side of MBK and many other places adjacent to charnockites. It is inferred that the high temperature effects during the Munnar granitic intrusion may have influenced in the formation of this gneissic body. Dehydration mechanism occurred by high thermal influx has led to the development of hornblende from orthopyroxenes. As the name indicates the major minerals present in this gneiss are hornblende and biotite with intermittent quartzo-feldspathic bands.

Garnet-biotite gneiss: The occurrence of garnet-biotite gneiss (Leptinite) is mostly traced in the southern margin of the MGB, and in some parts of central Kerala and Tamil Nadu. These rocks are characterised by a massive fabric due to the predominance of K-feldspar and quartz. These rocks associated with charnockites are some times host rock for graphite mineralization.

Garnet-cordierite-sillimanite gneiss: Garnet-cordierite sillimanite gneisses are found as bands along the Kodaikannal and Madurai region (Prakash, 1999). Biotite and sillimanite define the foliations in the rock. Garnet is usually found as porphyroblasts. Patches of cordierite sillimanite

gneisses are seen in the southern part of the MGB in close association with ACS (Sinha-Roy *et al.*, 1984; Santosh, 1987) and another occurrence is reported from Kottayam district, central Kerala. The cordierite bearing gneisses are generally coarse grained with quartz, plagioclase, perthite, cordierite, garnet and biotite as the major minerals. Varghese (1990) has reported the presence of hypersthene or sillimanite also in this gneiss.

Migmatitic gneisses: Migmatite, a megascopically composite rock consists of two or more petrographically different components, one of them may be the country rock generally in a more or less metamorphic stage termed as "mesosome", the other is of pegmatitic, aplitic, granitic or generally plutonic appearing phase termed as "leucosome". The presence of relict orthopyroxenes in quartzo-feldspathic gneisses gives evidences of the magmatic activity that had affected in the MGB. These quartzo-feldspathic gneisses that are showing a mixed texture are termed as migmatitic gneisses. Such rocks in the MGB are sometimes referred to as migmatitic charnockites (Mohan1996). These rocks are noted in the contact zones of sapphirine bearing granulites in the MBTN, in the eastern side of the MBK, in and around the Munnar granites etc. Gneissic layerings of dark and white bands are seen in the rock. The dark bands are mostly biotite rich. The quartzo-feldspathic bands are rich in K-feldspar, perthite with minor quartz and garnet.

### **2.3.1d Intrusives**

Alkali granites and syenites occur widely in the East Gondwana continents such as India, Sri Lanka, Madagascar, East Antarctica and Australia. Most of these alkaline magmatic activities are associated with the

Proterozoic lineaments and contemporaneous with the Pan-African activities widely reported in different parts of the Gondwana fragments (Rajesh and Santosh, 1996 and Rajesh *et al.*, 1996). The major alkaline plutons in the MGB are the granite bodies of Chengannoor, Pathanamthitta, Athiringal, Munnar, Pariyaram, Kizhakkanchery, Vadakkanchery and syenite bodies of Sholayar, Mannappra and a carbonatite body at Kambammettu. These intrusives are metaluminous to peralkaline in nature with high SiO<sub>2</sub> and low CaO and Sr resembling the characteristics of A-type granites (Santosh and Nair, 1983a; Santosh *et al.*, 1983; Santosh and Thara, 1985; Santosh 1989; Thampi *et al.*, 1993; Rajesh and Santosh, 1996; Rajesh, 2004 etc).

Mafic dykes, which have intruded in almost all parts of the Peninsular India, plays a significant role in the geologic history of the Precambrian terrain, but no much studies are available on this. The MGB is also characterised with abundant mafic dyke swarms. They show a general trend of NNW-NW. Minor sets of dykes are also noticed with ENE-WSW trend (along the Bhavani valley). NW-SE trending dyke swarm in the MGB, which in turn extends up to ACS, is truncating a major dyke swarm in the northern Kerala region. This basic magmatism is also considered as representing Proterozoic as well as Cretaceous magmatic events (Radhakrishna *et al.*, 1986, 1990; Murthy, 1995).

### **2.3.2 Structure**

The Precambrian crystalline rocks of the SGT are multiply deformed at different periods in the geologic past. The major shear zones can be considered as one of the products of those complex deformational

histories. These are but comparatively of younger age. Deformations in the MGB, reflects the partial reorientation and transposition of earlier foliation into later trends, with altering low strain and high strain domains. The Western Ghats is a major geomorphic feature, which divides the MGB in to the Kerala part and the Tamil Nadu part. It forms the western limb of a NNW plunging synclinorium. The axis of the synclinorium extends from Belgaum in the north to Tuticorin in the south (Soman, 2002). The overall geometry reflects the superposition of at least two regional fold generations reworking the main gneissic layering. Structural evolution around three groups of structures are noticed in the MGB; D1, D2, and D3 (Cenki and Kriegsman, 2005). D1 is the main foliation-forming event, which is synchronous to the main ultra high temperature metamorphic event. It has affected in a regional scale and produced a well-developed gneissic layering. The regional strikes of the D1 is NW-SE TO WNW-ESE, with a steep dip towards SW. D2 are less pervasive deformation and are less affected to the internal fabric of the rocks. This actually represent the regional scale refolding of the earlier structure during 700-800 Ma (Ghosh *et al.*, 2004) with a NNE-SSW trend in the highlands and a NE-SW trend at the northern most part of the lowlands of the MGB. D3 is characterised by strain partitioning in to localized high strain zones with WNW-ESE and W-E trend (the ACS and the Palghat lineament respectively). This is believed to be of early Paleozoic age (530-550 Ma), which is normally found coexisting with the Pan-African orogeny, major charnockitization, granitic intrusions etc in the MGB (Ghosh *et al.*, 2004).



Based on these conclusions a biphasic structural model has been put forward by Cenki and Kriegsman (2005). It says that in the first phase the region has undergone the D1 deformation which is dominated by regional top-to-the-N displacement, but locally close to the PCSZ, top-to-the S displacement. The second phase comprises of a more complicated refolding episodes, but giving a general movement, which ended in sub horizontal shortening.

### **2.3.3 Metamorphism**

#### **2.3.3a Previous P-T estimates**

P-T estimates of Indian Peninsular Shield from mineral equilibria and fluid inclusion studies fall in the range of 5-10kb and 650°C to 950°C, where as the peak metamorphic grade is in a higher range as revised by Mahadevan (1996). In general, the P-T estimates for the different tectonic blocks of the SGT is as follows: an intermediate pressure of 6kb and 750° ± 50°C has been reported from Madurai Granulite block and a high P-T range of 8kb and 800°± 50°C is reported from Nilgiri block. The KKB and the rocks in Kodaikanal gave an intermediate pressure of 6kb and a temperature near to the Madurai Granulite block assemblage (Mahabaleshwar, 1993). A combination of mineral equilibria studies and studies on fluid phases in the rocks of KKB by Santosh (1986b, 1987) define a similar P-T range.

In the northern Madurai block peak metamorphic conditions of 800°C and 8kb have been observed from the sapphirine-bearing granulites of Ganguvarpatti (Mohan and Windley, 1993; Mohan *et al.*, 1996). Similarly

Ravindrakumar and Chacko (1994) report a high-grade metamorphism (9-10kb pressure and 900°C) in and around the Palghat gap region. Near peak metamorphic conditions of 10.2kb and 900°C are reported from the Nilgiri block (Raith *et al.*, 1990; Srikantappa *et al.*, 1992). However the peak metamorphic temperatures recorded by the charnockites, calc silicate rocks, and sapphirine bearing granulites from the SGT are more than 900°C, but the pressure falls in a wide range (Chacko, *et al.*, 1996, Brown and Raith, 1996; Raith *et al.*, 1997; Satish-Kumar *et al.*, 2001).

### 2.3.4 Geochronology

Isotopic dating during the last two decades has played a relevant role in understanding the geochronological framework of the SGT. Based on these techniques different age provinces with distinct pre-crustal histories have been recognized in the SGT. Earlier workers believed that the whole south Indian shield was evolved in a common granulite facies event at the end of Archaean. But the recent studies put forth different age history ranging from 3000 Ma to 550 Ma for the terrain (Yoshida *et al.*, 1996). New results on U/Pb/Th single zircon and monazite dates from six structural transects across regional shears signifies seven tectono-thermal events in the SGT during 2.5 Ga, 2.0 Ga, 1.6 Ga, 1.0 Ga, 0.8 Ga, 0.6 Ga, 0.55 Ga and two episodes of charnockitization at 2.5 Ga and .55 Ga (Ghosh *et al.* 2004). The oldest rock reported from the terrain is of  $3358 \pm 66$  Ma age (Beckinsale *et al.*, 1980). In the Dharwar Craton U-Pb SHRIMP of detrital zircon is reported by Nutman *et al.*, 1992, is of about 3580 – 3130 Ma. Comparatively younger ages (2.6 – 2.5 Ma) are reported from the southern margin of Dharwar Craton—around Kolar–Bangalore, Krishnagiri,

Southern Closepet batholith and Gundepet areas (Krogstad *et al.*, 1991; Peucat *et al.*, 1989, 1993; Jayananda *et al.*, 1995b), which are resulted from the juvenile accretion associated with reworking of older continental crust.

The MGB, which is the largest tectonic part in the SGT, is characterised by some of the highland granulite massifs in South India like, the Palani, the Anamalai and the Cardamom hills. Ages of these granulite massifs range from Mid- to late Proterozoic (i.e. from 2.5 Ga. to 0.5 Ga) (Jayananda *et al.*, 1995a; Miller *et al.*, 1996; Mohan and Jayananda, 1999). The MGB is an ancient crust with preserved protolith ages, which has been reworked in the Pan-African tectonothermal event, with considerable additions from the mantle. U-Pb data on zircon has gained 1.85 Ga where as a whole rock isochron age from a charnockite body from Kodaikanal show  $553 \pm 15$  Ma (Jayananda *et al.*, 1995a). The major Protolith in this block has been reported to be of ages around 2.5 Ga. (Bartlett *et al.*, 1998) and Pan-African tectonothermal events evidenced as incipient charnockite are of 550-560 Ma age. (Jayananda *et al.*, 1995a; Bartlett *et al.*, 1995). These ages corresponds with the Rb-Sr whole rock isochron ages by Hansen *et al.* (1985). The Nd model ages (3.0-2.0 Ga) and zircon ages (2.43-2.1 Ga) from the MGB, which is a marked discrepancy reflect that the Proterozoic crust as a remobilised basement. Due to the lack of sufficient age data for different components and due to the difficulties in delineating such components of the terrain it is not clear how much of the crust represents the original basement and how much is added later.

### 2.3.5 Economic mineral deposits

The Proterozoic era is considered to be the greatest and varied period of mineralization all over the world. The world's leading deposits of gold, gemstones, graphite, molybdenite, iron, chromium, copper and manganese, other rare metals, mica, cordierite etc were formed during this period.

One of the major economic minerals reported from the MGB is graphite. The geological and structural features of the graphite occurrences of Kerala indicate their similarity to some world famous graphite deposits in Sri Lanka and Madagascar (Rajesh-Chandran *et al.* 1996). In the MGB, graphite is concentrated in Kottayam, Ernakulam, and Idukki districts of Kerala state (Radhika *et al.*, 1995; Soman, 2002) and some isolated pockets in Tamil Nadu. Based on the mode of occurrence the graphite deposits of the MGB can be classified into four major categories.

- 1) Disseminated flakes and segregations in high grade rocks
- 2) Graphites in pegmatites
- 3) Shear /fracture zone hosted graphites
- 4) Graphites concentrated in weathered rocks and laterites

Molybdenite is another economic mineral reported from the MGB. It is usually associated with the Pan-African alkaline magmatism. So the mineral is found in the granite and syenite plutons in the terrain. Chengannur granite is a major molybdenite bearing pluton in the southern boundary of the MGB. Spatial relationship of individual molybdenite occurrences and their parent rocks with seismically active deep folds and shear margins suggest a metallogenic episode related to taphrogenesis of

the continental margin (Santosh and Nair, 1983b). Molybdenite is also seen as disseminations in quartz, K-feldspar and hornblende in the pegmatites.

Many other salient mineralizations were also reported from the MGB. Odara pegmatite near Thiruvalla, Kerala is having columbite and tantalite together with aquamarine variety of beryl (Santosh, 1984). Books of mica are reported from Alleppey and Punalur. Sillimanite has been reported from Alleppey, Ernakulam, Kottayam, and Palghat districts in Kerala and from many places in Tamil Nadu. Minor deposits of magnetite are found in Kottayam, Plaghat and Trichur in Kerala and magnetite-quartzite bands from places like Selam in Tamil Nadu (Rajesh-Chandran *et al.*, 1996). Rich placer concentrations of monazite, ilmenite, rutile, zircon, cheralite, sillimanite and garnet are common in the coasts of Kerala and Tamil Nadu, and the MGB is among the presence for these deposits.

".....They were first found in full variety at St. Thomas' Mount and Pallavaram, 10 miles south of Madras city; from quarries in these localities large quantities of rocks have been obtained for building and ornamental purposes in Madras. Subsequently the same rocks were found to make up the mountain masses of the Shevaroyes, Nilgiris, the Palnis and the great ridge of high ground forming part of the Western Ghats, stretching southwards as far as Cape Comorin and reappearing above the sea level in Cylone".

- Thomas Holland

## CHAPTER 3

### FIELD RELATIONSHIPS AND PETROGRAPHY

---

### 3.1 INTRODUCTION

The Madurai Granulite Block falls in the Survey of India degree sheets 58B, 58C, 58F and 58G and forms an area of about 50,000 km<sup>2</sup>. Since it covers such a large area a detailed field mapping are not feasible in the present work, even then the area has been studied by several field surveys covering most of the quarries along the western and south eastern parts of the MGB giving more emphasis to the occurrence and mutual field relations of the metamorphic rocks as well as the major intrusives.

### 3.2 FIELD RELATIONSHIPS

The concept of different tectonic blocks in the SGT separated by extensive Proterozoic shear zones came in to discussion at the early eighties (Drury and Holt, 1980; Drury *et al.*, 1984). The MGB, which is located between the Palghat-Cauvery Shear Zone and the Achankovil Shear Zone, generally comprises of charnockites in prominence associated with retrogressed or synmetamorphic gneisses. Charnockites are concentrated more in the western side of the block while the eastern side is dominated by gneisses - hornblende-biotite gneiss - as described in Fig 2.1. But in the local scenario it can be noticed that the gneisses show wide variations. They are some times migmatitic gneisses, garnet-biotite gneisses or simply biotite gneisses. Major felsic/alkaline intrusive bodies of Munnar granite, Pariyaram granite (central MGB), Wadakkancherry syenite (northern MGB), Chengannur granite, Pathanamthitta granite and Athiringal granite (southern MGB, along ACS) have a major role in the formation of

gneisses in the area. The intrusives are generally elongated or elliptical bodies having sharp contacts with the country rocks and are always associated with major lineaments in the block.

On detailed mapping of the terrain different types of field relationships between the rock types were traced out. For convenience of description the entire block is subdivided according to six regional traverses (and several sub-traverses within it) made during the fieldwork as given below (Fig 3.1).

### **3.2.1 Trichur-Palghat traverse (Traverse 1)**

The traverses were along the Northwestern part of the MGB. In this traverse fine to medium grained charnockites some times showing faint foliations but mostly massive in appearance are noted. Most of this charnockites were felsic in appearance some times rich in feldspars. Medium to coarse-grained K-feldspars were noticed in enormous in some pockets. The massive charnockites with closely spaced vertical joints were seen in some quarries near Malayatoor. Highly deformed biotite gneisses were found in contact with the charnockites, which gives the signs of some retrogressive reaction. Pegmatite veins of different widths were also noticed cutting across the charnockites in certain areas (Plate 3.1).

Towards the eastern side of this traverse along Chalakkudi-Athirappilli, the predominance of charnockites is lost and are replaced by large exposures of hornblende-biotite gneiss. Here also the K-feldspar is dominant in some parts of the exposures. Charnockites are found as patches within the gneisses inferred to be incipient. Some felsic charnockite



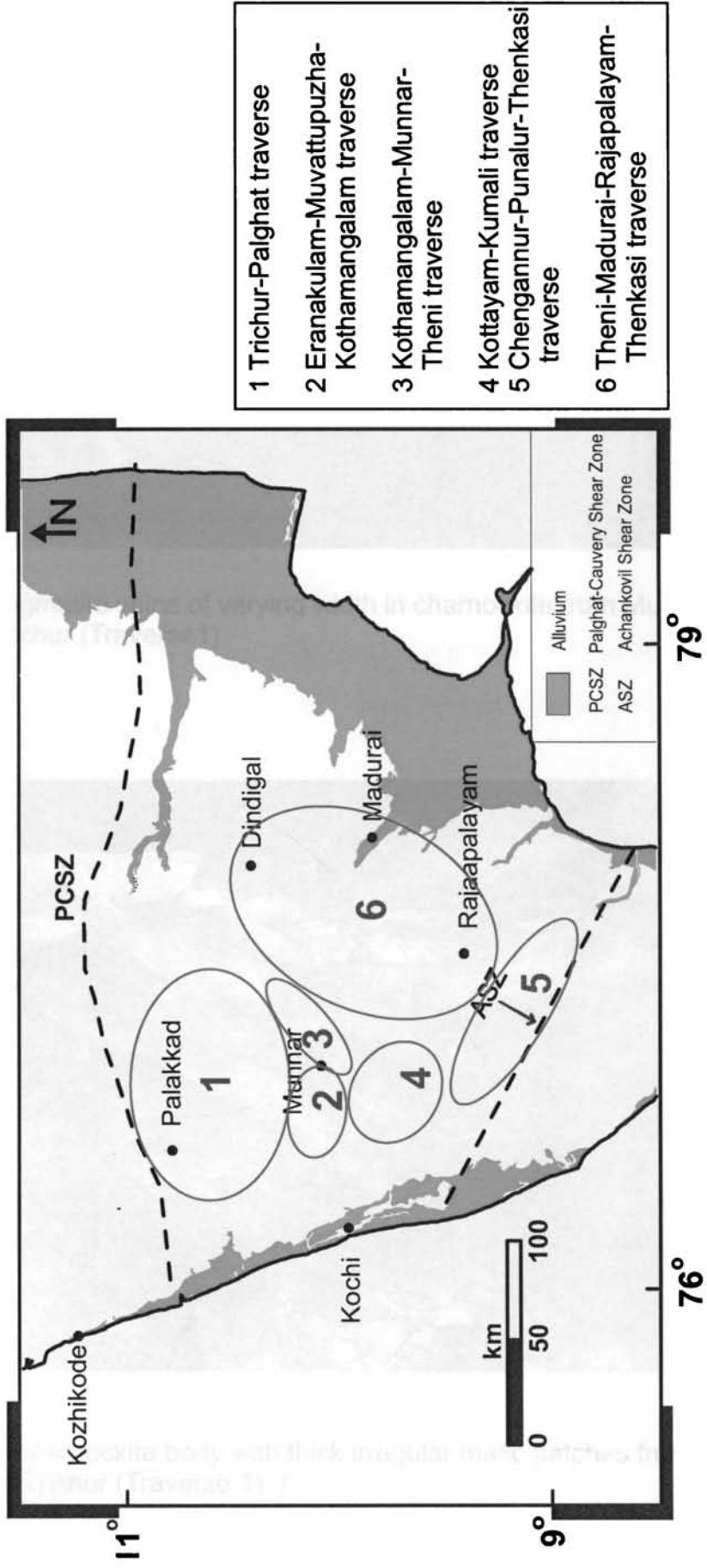


**Fig. 3.1 Traverses made during the fieldwork**

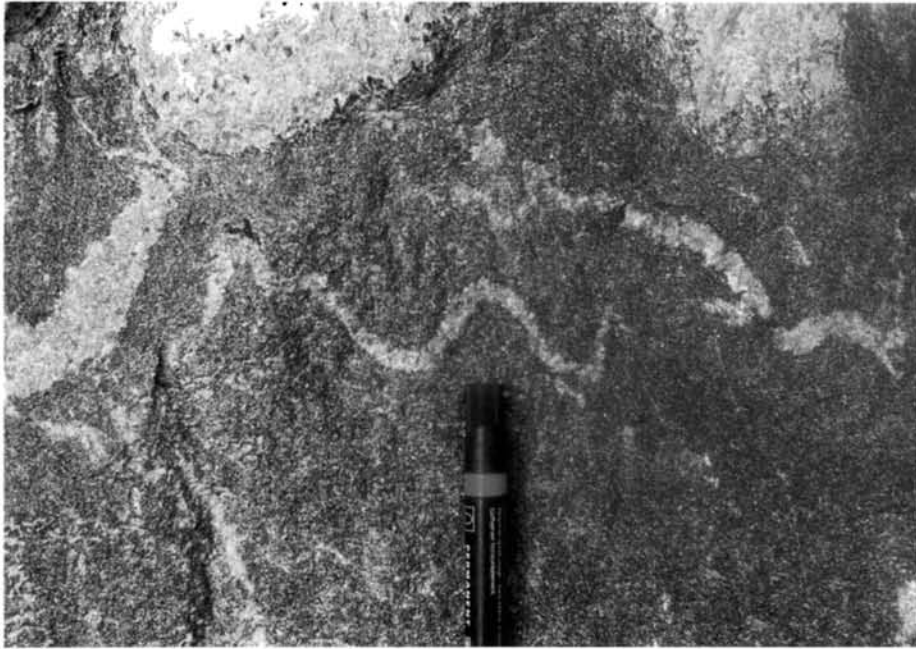


**Plate 3.1** Pegmatite veins of varying width in charnockite from Mudikode, Trichur (Traverse1)



**Plate 3.2** Felsic charnockite body with thick irregular mafic patches from Orappana quarry, Trichur (Traverse 1)

bodies with thick irregular mafic patches were also noticed in some quarries (Plate. 3.2).

### **3.2.2 Ernakulam-Muvattupuzha-Kothamangalam traverse (Traverse 2)**

In this traverse, towards the western side (Ernakulam) the major rock type found is charnockite, with very less retrogressive changes. Massive charnockite in some areas (especially at Mamala quarry near Thrippunithura) show very much faulted appearance with vertical to sub-vertical fault planes. Good amount of mylonitization are also noticed. The charnockites all along the area differ in their appearance (grain size and colour), but are always rich in plagioclase. Towards NE of Ernakulam, near Kakkanad, the massive charnockite is found intruded by a NE-SW trending granite body of 10-15m wide exposures. Further north to the location large bands of graphite has been found within thick laterites. This graphitic band appears to be occurring in NW-SE trend up to Ambalamugal.

In Muvattupuzha area, the two varieties of charnockites, the incipient variety as well as the massive type with or without foliations form the prominent rock type. Retrogressive product of charnockite, the biotite gneisses with or without hornblendes is noticed in some parts. The massive variety of charnockite differs in their grain size, felsic composition etc from place to place all along the traverse. Pegmatite veins of considerable width (~15-30cm) are also found cutting across the foliation planes. The incipient variety of charnockites appears as highly mafic patches, some times surrounded by gneisses or the felsic charnockites itself (Plate 3.3). However a general observation that can be made in the rocks of this



**Plate 3.3** Incipient charnockite occurrence in hornblende-biotite gneiss in a quarry near Kothamangalam (Traverse 2)

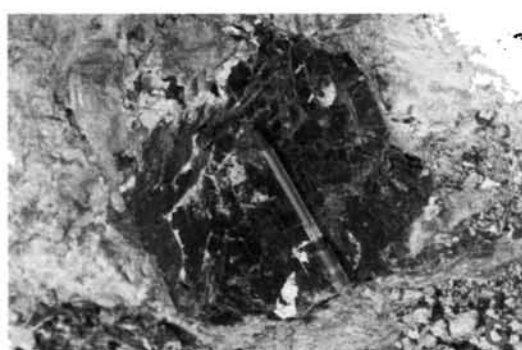


**Plate 3.4** (A) Migmatite gneiss quarry at Munnar (Traverse 3)  
 (B) Contact between biotite gneiss and the Munnar granite  
 relicts of precursor biotite and pyroxenes seen within the granite  
 (C) Large flake of relict biotite preserved in the granite body

traverse is the total deficiency of garnets and the overall felsic nature of the charnockites present. Near Muvattupuzha town a large pluton of diorite has been intruded the country rock and it stands out as a hill. Spheroidally weathered boulders of diorite are seen along the slopes of the hill. Some portions of the diorite body are characterized by molybdenite mineralization.

### **3.2.3 Kothamangalam-Munnar-Theni traverse (Traverse 3)**

Towards the east of Kothamangalam, the effect of Munnar granite intrusion can be noticed in the country rock. It can be understood that the precursor rock was charnockite due to the presence of the relict patches of pyroxenes as well as biotite flakes available within the migmatites and the intruded granitic body in and around Munnar (Plate 3.4). The precursor charnockites present in some places are felsic in appearance and shows highly deformed foliated nature (Plate3.5). Hypersthene is found recrystallized to hornblende in many places and is visible even in hand specimens. Sometimes the host charnockites are characterized with aplitic veins. In some areas around Munnar small veins of charnockite (2-4cm wide) are found within the migmatitic gneiss having relict pyroxenes and appearances of newly formed hornblende. The veins are always cutting across the gneissosity. The geological history that can be traced out from these petrological relations is that the precursor charnockite has got migmatized and retrogressed by the granitic intrusion and a later generation incipient charnockites were formed as veins due to the CO<sub>2</sub> dehydration processes through some weaker planes. Towards the eastern



**Plate 3.5** Highly deformed charnockite gneiss from Munnar area (Traverse 3)



**Plate 3.6** Graphite bearing garnet-biotite sillimanite gneiss from Muthukudi, Tamil Nadu (Traverse 6)

flank of the Munnar granite (at Bodinaykkannur and Theni), the reappearance of non-migmatized charnockites confirms that the original country rock of the area was massive charnockite.

#### **3.2.4 Kottayam-Kumali traverse (Traverse 4)**

As noticed in the above traverses here also, charnockite forms the major rock type. The retrogressive reactions have taken place in most of the charnockites and are evidenced in the form of associated gneisses in many outcrops. Massive charnockites of mafic to felsic appearance are noticed all along the traverse. Felsic varieties are rich in plagioclase feldspars. In some charnockites gneissosity is seen. In Kuthattukulam area gneissic charnockites are found with augen structures and pyroxene crystals. Presence of pegmatite veins of varying width is noticed in the majority of exposures. Garnet assemblages are rarely noticed. But garnet is observed in some of the felsic charnockites at Karukachal and Manimala. In some areas charnockites are tending to enderbitic in nature where as in some parts the charnockites characterized with more K-feldspars. A large stretch of cordierite gneiss has been traced out about 3km east of Kottayam (Vadavathoor), which is further found near Ettumanoor (north of Kottayam) and Moolavattom (South of Kottayam). From this it can be generalized that the exposure is having a N-S trend. Some other workers like Sinha-Roy, *et al.* (1984) have reported another exposure of the rock near Changanasserry, further south of Moolavattom. All these form the western end of the large cordierite belt, running sub parallel to the Achankovil shear.

Minor faults were identified in many exposures most of them are vertical to sub-vertical generally trending NW-SE to N-S.

### **3.2.5 Chengannur-Punalur-Thenkasi traverse (Traverse 5)**

The traverse was almost along the ACS, and the exposures noticed are on either sides of the Achankovil River. The shear zone can be considered as a sequence of two NW-SE trending strike-slip shears, the Achankovil shear and the Thenmala shear. Kinematic and textural analyses of the rocks in the shear zone indicate primarily a dextral shear sense (Sacks *et al.*, 1997), with localized sinistral nature (Rajesh *et al.*, 1998). The northern end of the shear zone is characterized by the Chengannur granitic pluton. It has been intruded puncturing the major country rock of the area – the charnockites. The charnockites of the area are sometimes cordierite bearing and gneissic. Minor specks of molybdenite were seen in some exposures of the pink variety of granite.

Towards south of Chengannur, in and around Panthalam along the shear the occurrence of garnet-biotite gneiss (leptinite) and garnet-biotite-sillimanite gneiss (khondalite) have been noticed in considerable amount. The rocks always show high amount of shearing, some times showing good augen structures with the development of coarse, “eye like” oriented feldspar crystals. Garnets occur as porphyroblasts of irregular, rounded or semi rounded nature. The khondalite shows a general mineralogy of K-feldspars, quartz, garnet, biotite, sillimanite, cordierite, spinel, and plagioclase, with graphite, apatite and zircon as major accessories. Garnet, biotite, cordierite and spinel define the compositional bands. At places



garnets show recrystallisation into large porphyroblasts, sometimes exhibiting 'snow ball' texture. A peculiar feature observed in some of the garnet grains is its flattened nature, caused by the shearing. Pegmatitic veins are found common in most of the exposures sometimes containing coarser crystals of graphite and often cordierite. The veins are always discordant to the gneissosity and highly distorted or folded.

In some locations near Punalur, charnockites are also found in association with the gneisses, which are some times recognized as the incipient variety. At Nedumpara quarry, north of Punalur large area is covered by cordierite gneiss characterized by the presence of gemmy violet cordierites. Pink granite veins are found intruding the gneiss. Relicts of pyroxenes are noticed at some places in the gneiss giving an inference of precursor charnockite. The granitic veins are also observed in some other nearby locations in and around Punalur and Pathanapuram. The foliations in the area are also highly distorted; sub vertical and dipping NNW to NNE.

The above said rock assemblages are noted all along the shear up to Thenkasi.

### **3.2.6 Theni-Madurai-Rajapalayam-Thenkasi traverse (Traverse 6)**

The traverse covered almost major portion of the Tamil Nadu part of the MGB. Massive charnockites of comparatively high mafic appearance are the noticeable feature observed in this terrain. Felsic charnockites are also found, but not as much in the Kerala part. A granitic emplacement near Madurai is the major plutonic outcrop encountered during the traverse. Graphite bearing garnet-biotite gneiss ± sillimanite is noticed in some parts

near Supplapuram and Muthukidi (Plate 3.6). It appears to be a retrogressed product, while some incipient charnockites are found in some of the outcrops. Garnet is also found in some charnockites.

### **3.2.7 Rock types and their field relationship from the rest of the MGB**

The above traverses do not cover the entire area of the MGB. So the details on the remaining areas of the block are compiled from available literature and are reviewed below, in order to have a complete picture.

The Palghat region is dominant with hornblende-biotite and biotite gneisses that are closely associated with charnoenderbites. Conspicuous spotty appearance of mafic minerals was also found in the gneisses. This indicates that the area has undergone extensive amphibolite facies retrogression. Arrested charnockite were also reported from the region exclusively in migmatitic hornblende-biotite gneiss (Ravindrakumar and Chacko, 1994; Ravindrakumar, 2004).

The Kodaikanal massif, one of the largest highland blocks of granulites in South India (Drury *et al.* 1984) encompasses the Anamalai, the Palani and Cardamom hills. The Palani hill ranges form a part of the Kodaikanal massif and is composed of common granulites. The major portion of the massif is made up of highly deformed enderbitic granulites. The eastern margin of the massif is in contact with thick sequence of metasedimentary rocks like interbanded quartzites, calc-silicates, marbles, garnet-biotite-sillimanite gneisses, garnetiferous gneisses and graphitic schists. Diatexitic garnet-cordierite sillimanite gneisses occur as layers and rafts within and at the immediate contacts with the enderbitic charnockites

(Raith *et al.*, 1997 and references cited therein). Occurrences of sapphirine granulites were also reported from Ganguvarppati area in this massif by many workers (Grew, 1982; Mohan *et al.*, 1985; Mohan and Windley, 1993). Migmatitic gneisses are noted at the contact of sapphirine granulites (Raith *et al.*, 1997; Prakash, 1999).

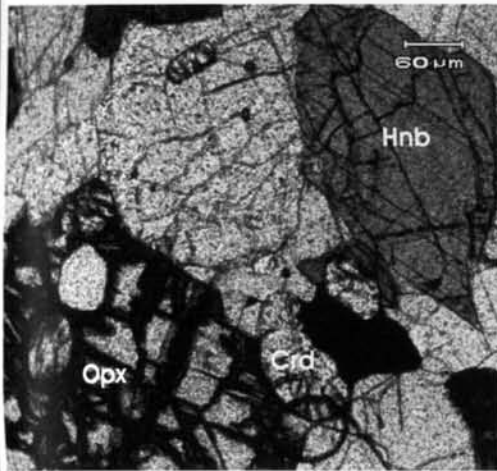
The Achankovil metasedimentary sequence consists of cordierite bearing metapelite, calc silicate rock and marble. Cordierite-bearing rocks occur as elongate patches and appear to have partially replaced garnet bearing assemblages. Towards the eastern side of the ACS the sequences are diopside rich/calcite rich marble and metapelitic gneisses are also common (Satish-Kumar *et al.*, 2001 and references cited there in).

### 3.3 PETROGRAPHY

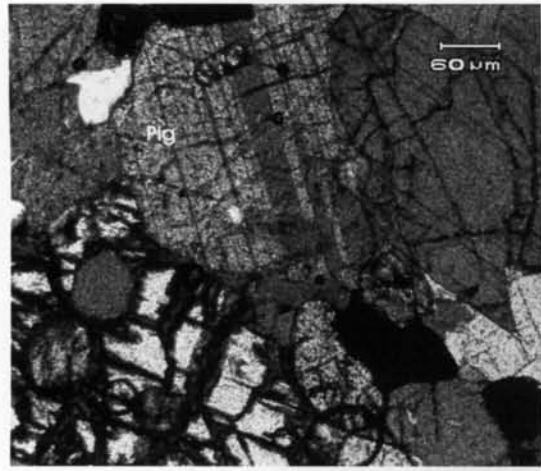
Generalized petrographic descriptions of South Indian granulites have been published in many classical works by many prominent geologists (Rama Rao, 1945; Pichamuthu, 1953, 1979; Howie, 1955; Subramaniam, 1967), more detailed petrography, and mineral chemistry in recent works. (Raith *et al.*, 1983; Chacko *et al.*, 1987; Brown, *et al.*, 1992; Ravindra Kumar and Chacko, 1994; Srikantappa, 1993, 1996; Santosh, 1996; Mohan, 1996; Satish-Kumar, 2000, Ravindra Kumar, 2005). But very less studies are there concentrating on the rocks of the MGB (Mohan *et al.*, 1985; Mohan, 1996; Mohan *et al.*, 1996b; Satish-Kumar 2000) and none of it give a complete picture as the block is too vast and complex. So the present study aims to bring out some of the important petrographic features encountered in the charnockites and associated gneisses of the MGB.

In traverse 1 at many outcrops the appearance of the charnockite in contact with the hornblende ± biotite gneiss is noticed. The petrography also confirms these retrogressive assemblages with the co-existence of orthopyroxene and hornblende. Plate 3.7 shows one of these assemblages from a location near Malayattoor. Presence of cordierite also gives evidences of retrogressive reaction. The biotite and orthopyroxene eaten up by large plagioclase indicate some reaction caused by the secondary intrusion of pegmatite veins in the charnockite (Plate 3.8). The presence of cordierite can also be explained by associated fluid influx. Development of quartz-cordierite symplectites at the magnetite rims in the presence of hornblendes is also an evidence of retrogressive metamorphism (Plate 3.9). The formation of incipient charnockite is evidenced by the development of newly formed orthopyroxenes within the hornblende ± biotite gneiss of Chalakkudi area (Plates 3.10 and 11). Quartz-plagioclase myrmekites are noticed in the hornblende ± biotite gneiss from Vadakkanchery (Plate 3.12).

Garnets are very rarely occurring in the rocks of the second traverse. Some are seen in the Muvattupuzha area among the charnockites. Plate 3.13 shows such an occurrence of garnet in a felsic charnockite body, which can be inferred as a prograde metamorphic reaction. The typical granuloblastic texture with significant amount of orthopyroxene is characterized in certain charnockites in the area (Plate 3.14). Much amount of biotites mostly concentrated in the felsic matrix is also noticed in the thin sections from many locations (Plate 3.15). Plate 3.16 shows a typical assemblage of Orthopyroxene, biotite and plagioclase in a charnockite.

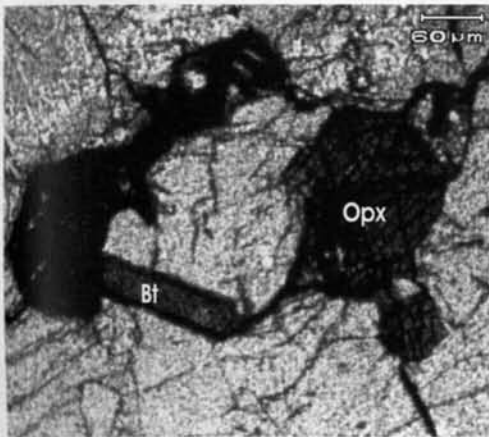


Open polars

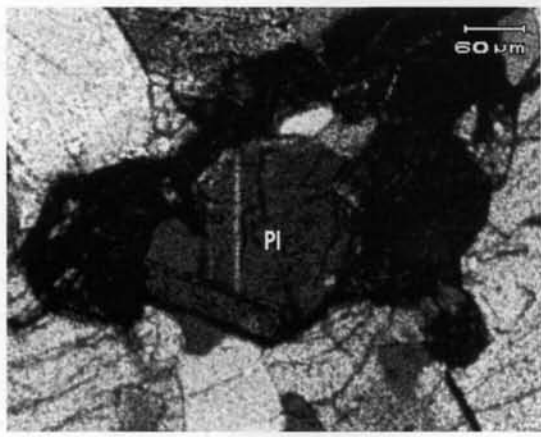


Closed polars

**Plate 3.7** Coexistence of hornblende and orthopyroxene in the presence of cordierite indicating retrogressive reaction. Sample from a quarry near Malayattoor (Traverse 1)

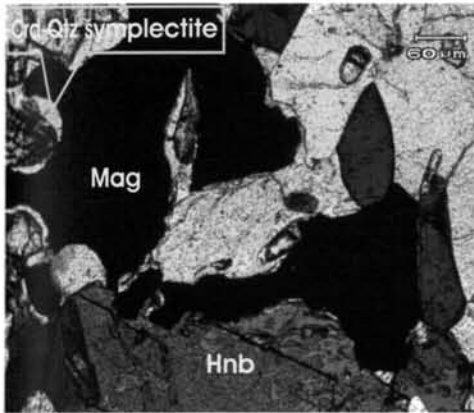


Open polars



Closed polars

**Plate 3.8** Biotite and orthopyroxene eaten up by plagioclase. Sample from traverse 1. Location: Illithodu, Malayattoor; Sample No. CK 78A

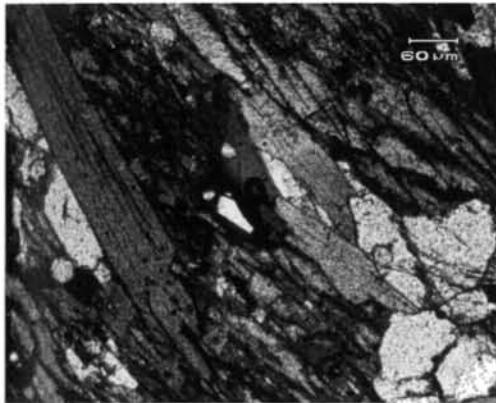


Open polars

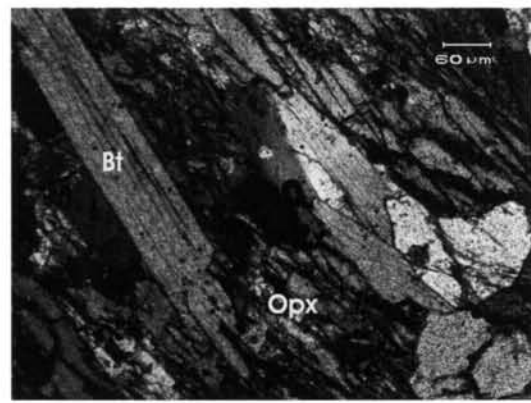


Crossed polars

**Plate 3.9** Development of quartz-cordierite symplectites at Interstitial magnetite and hornblende, evidence for retrogressive metamorphism in traverse 1. Location illithodu, Malayattoor; Sample No. CK 78 B.

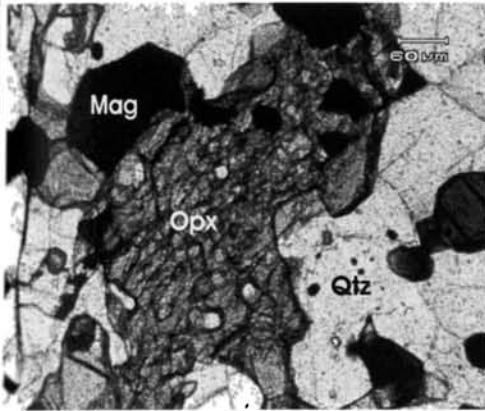


Open polars

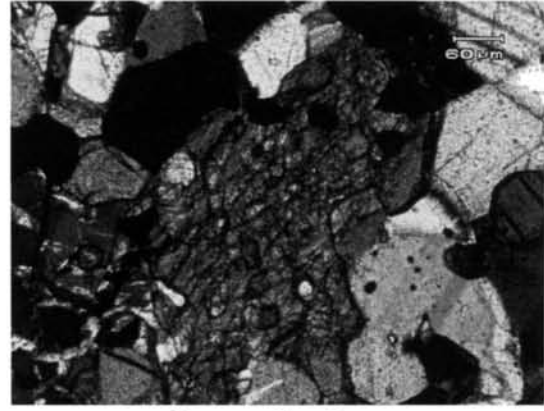


Crossed polars

**Plate 3.10** Development of orthopyroxenes in biotite gneiss from traverse 1  
Location: Amballur, Thrissur; Sample No. CK 101A

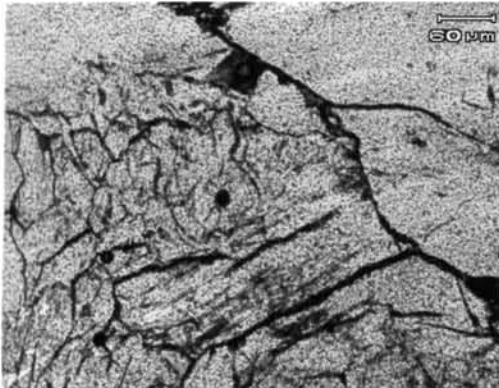


Open polars

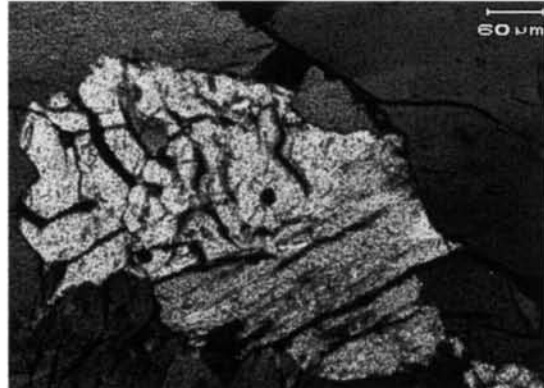


Crossed polars

**Plate 3.11** Large orthopyroxene crystals in felsic matrix in gneiss in incipient charnockite. Location: Amballur, Thrissur; Sample No. CK 101B.

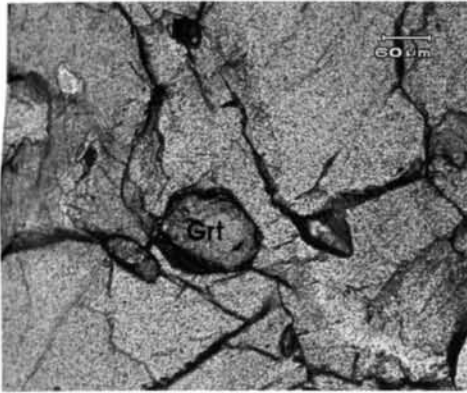


Open polars

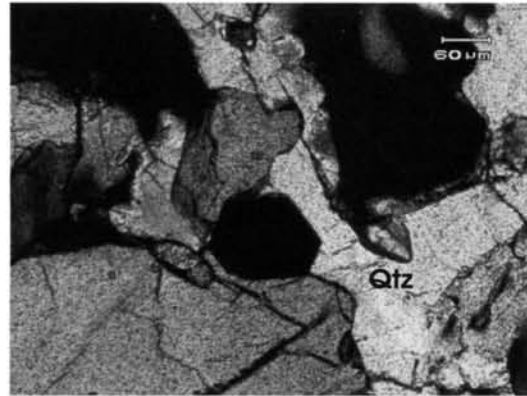


Crossed polars

**Plate 3.12** Quartz-plagioclase myrmekite noticed in traverse 1  
Location: Vadakkancherri, Thrissur; Sample No. CK 94B

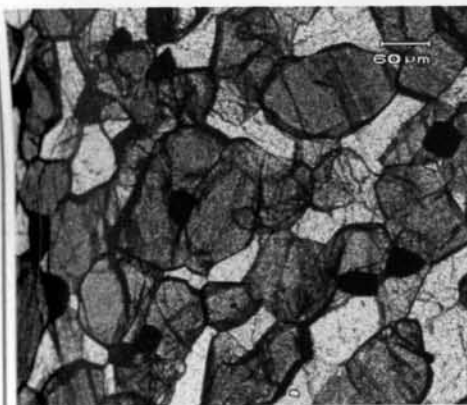


Open polars

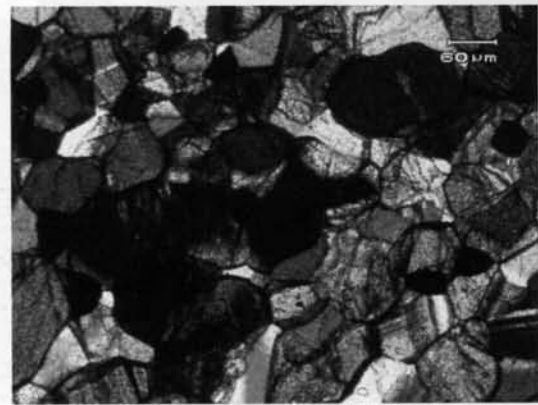


Crossed polars

**Plate 3.13** Small garnet crystal in a felsic charnockite from Muvattupuzha (Traverse 2). Sample No. CK 6



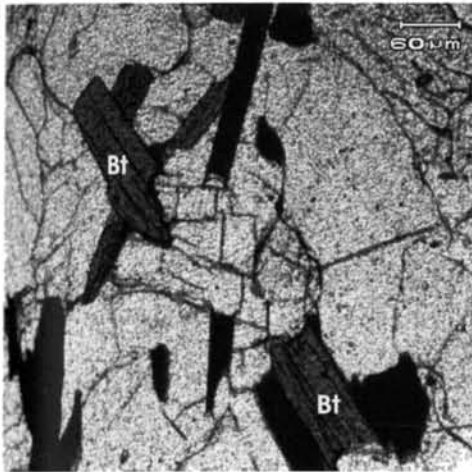
Open polars



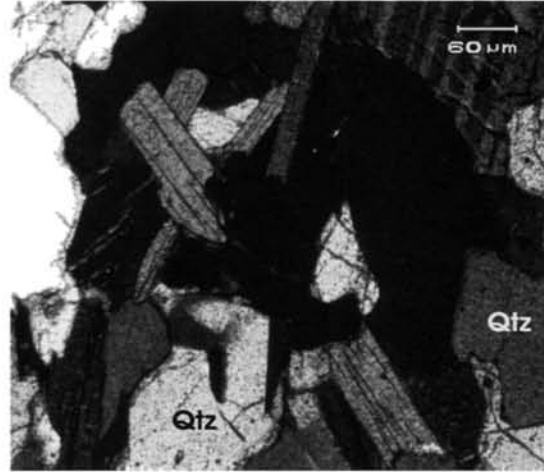
Crossed polars

**Plate 3.14** Typical granuloblastic texture in charnockite (Traverse 2).  
Location: Muvattupuzha, Sample No. CK 8B



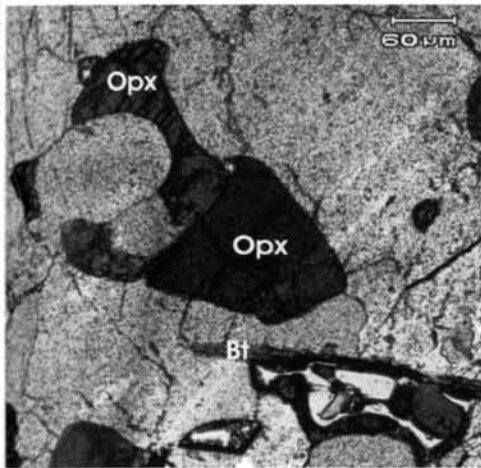


Open polars

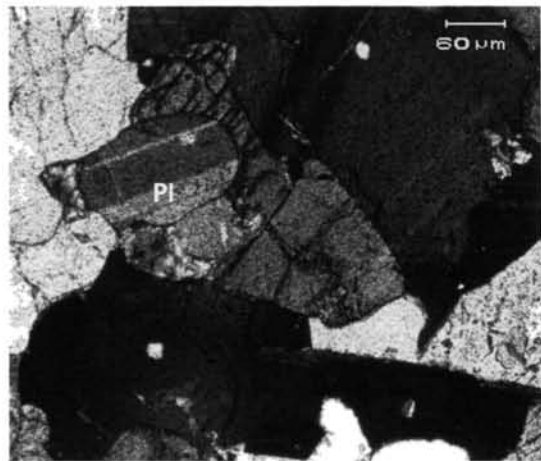


Crossed polars

**Plate 3.15** Biotites concentrated in felsic matrix (Traverse 2).  
Location: Pettamala, Perumbavoor; Sample No. CK 28A



Open polars



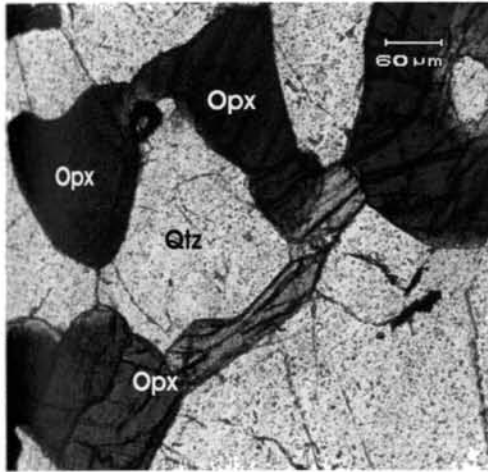
Crossed polars

**Plate 3.16** Opx-Pl-Bt assemblage in charnockite (Traverse 2).  
Location: Kanalpalam, Perumbavoor; Sample No. CK 29

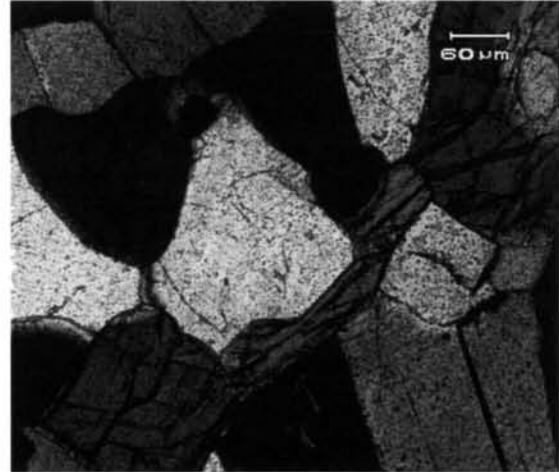
Development of secondary quartz replacing orthopyroxene can be explained as result of quartz vein intrusions in the charnockites (Plate 3.17). Formation of hornblendes in contact with orthopyroxenes is also noted in some samples denoting retrogression (Plate 3.18). Garnet porphyroblasts are seen in the charnockite from Mamala quarry recording a high temperature metamorphism (plate 3.19) (for details see chapter IV).

Highly deformed orthopyroxenes are characteristic of the charnockites from the third traverse. The effect of migmatization has been evident in the rock from its typical texture (Plate 3.20). Secondary quartz inclusions in the orthopyroxenes are also evidence for the migmatization (Plate 3.21). Relict pyroxenes within the biotite trails confirm the retrogressive changes occurred to the precursor charnockites during the intrusion of Munnar granitic pluton (Plates 3.22 and 3.23).

The MGB is usually referred as a garnet deficient terrain (Mohan, 1996), so the petrologists search for garnet bearing rocks. The 4<sup>th</sup> traverse in the present study, which follows a path along the central part of the MGB, also agrees this with some exceptions. In this traverse garnet bearing assemblages are identified in some isolated locations. The assemblages found are garnet-biotite (Plate 3.24) and garnet porphyroblasts in felsic charnockite (Plate 3.25). Another peculiar assemblage noticed in the thin section is the magnetite-biotite-quartz and orthopyroxene (Plate 3.26) in which magnetite is some times surrounded by orthopyroxenes (Plate 3.27). Myrmekites are common in felsic charnockites (Plate 3.28). The usual retrograde reaction textures are also found in some

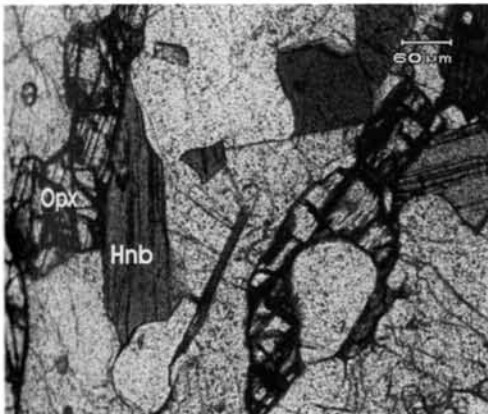


Open polars



Crossed polars

**Plate 3.17** Development of quartz replacing orthopyroxenes (Traverse 2).  
Location: Kanalpalam, Perumbavoor; Sample No. CK 29

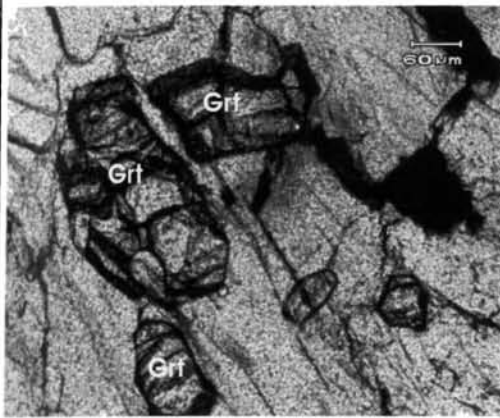


Open polars

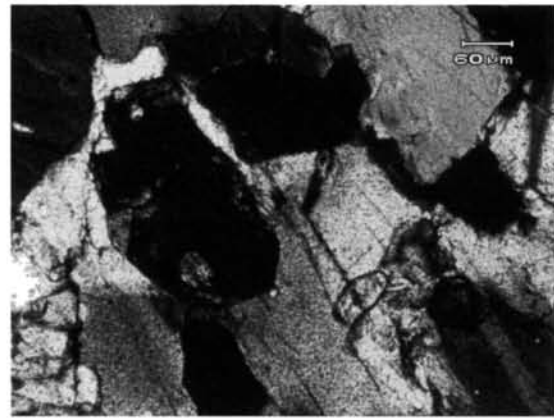


Crossed polars

**Plate 3.18** Hornblende-orthopyroxene assemblage indicating retrogression  
Location: Vekuvalli, Perumbavoor; Sample No. CK 30

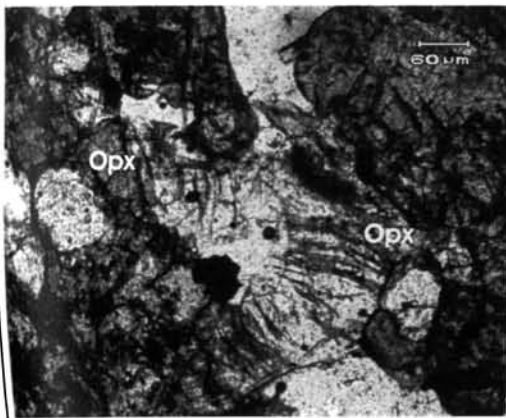


Open polars

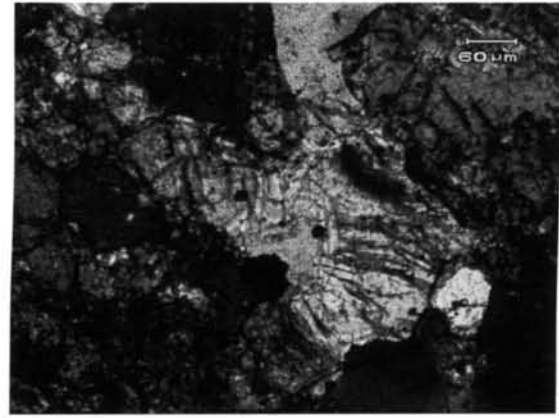


Crossed polars

**Plate 3.19** Garnet porphyroblasts in charnockite from Mamala quarry (Traverse 2)  
Location: Mamala, Ernakulam; Sample No. CK 57

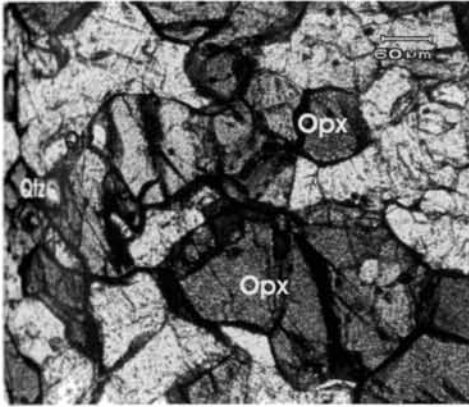


Open polars

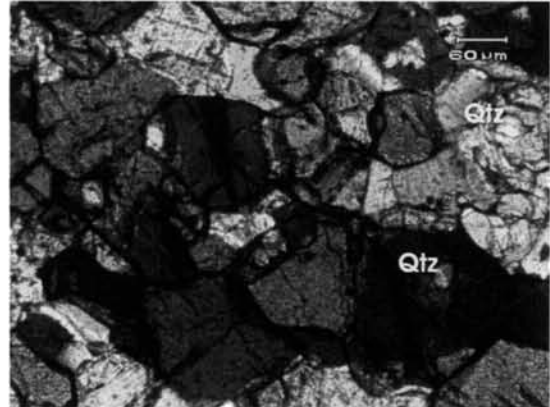


Crossed polars

**Plate 3.20** Highly deformed and schillerised orthopyroxene due to the effect of migmatization (Traverse 3).  
Location: Adimali; Sample No. CK 46B

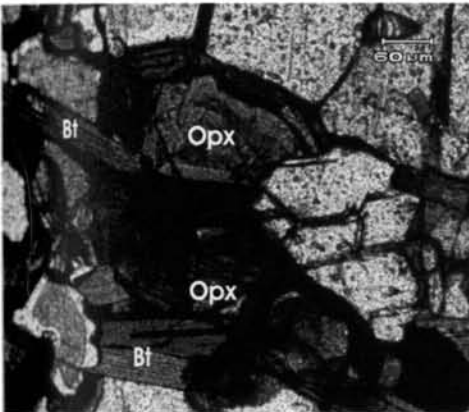


Open polars

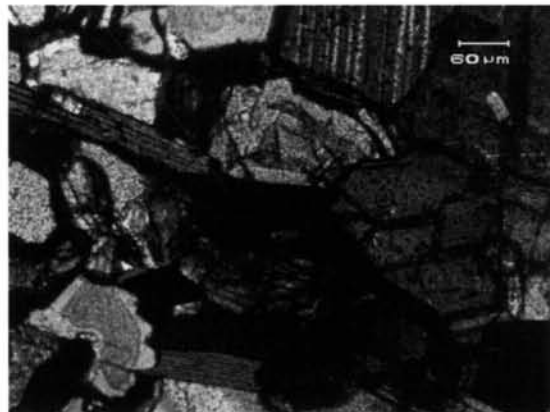


Crossed polars

**Plate 3.21** Secondary quartz inclusions in charnockite replacing orthopyroxene (Traverse 3). Location: Adimali; Sample No. CK 46B

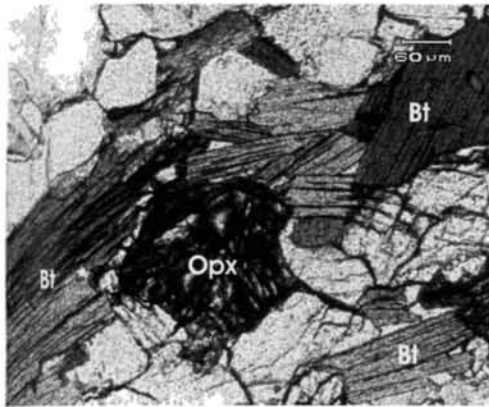


Open polars

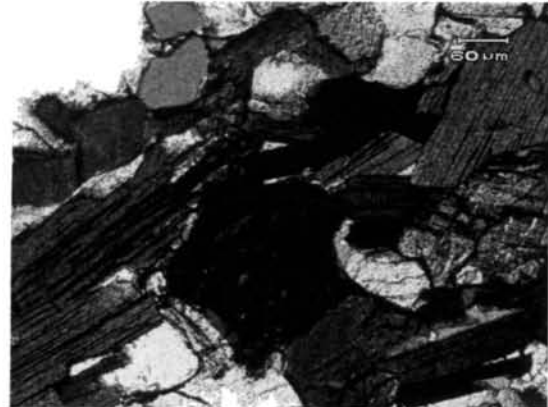


Crossed polars

**Plate 3.22** Relict pyroxenes in biotite from migmatite (Traverse 3). Location: Munnar; Sample No. CK 50

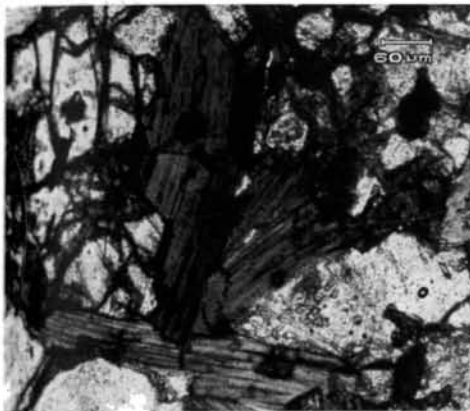


Open polars

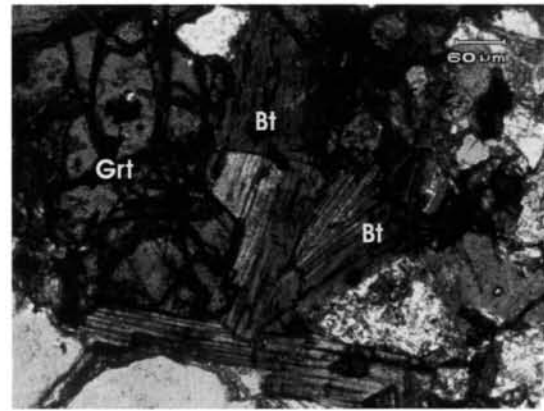


Crossed polars

**Plate 3.23** Relict pyroxene in a mesh of biotite in migmatitic gneiss (Traverse 3) Location: Munnar; Sample No. CK 50

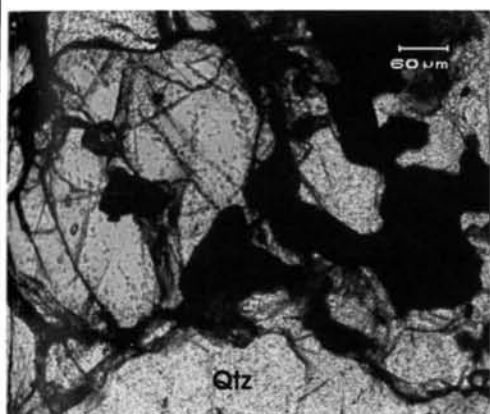


Open polars

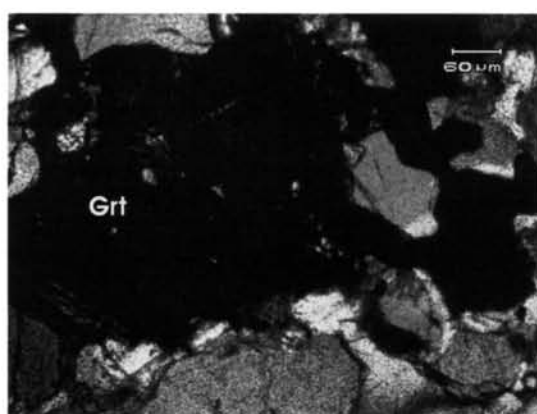


Crossed polars

**Plate 3.24** Garnet porphyroblasts in garnet-biotite gneiss from traverse 4. Location: Karukachal, Kottayam; Sample No. CK 16

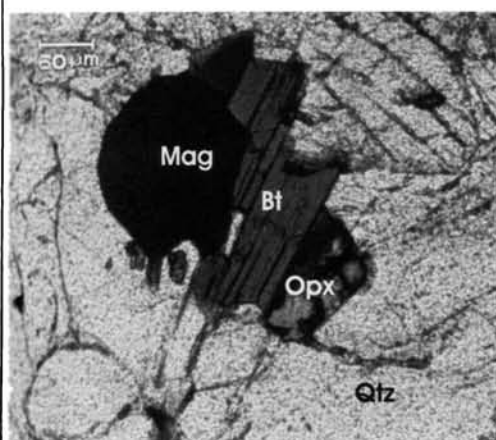


Open polars

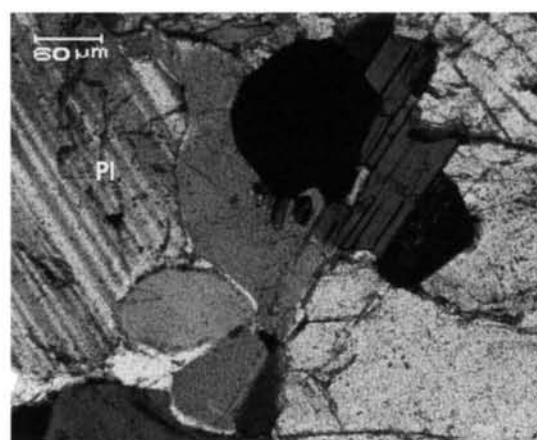


Crossed polars

**Plate 3.25** Garnet porphyroblast in felsic charnockite(Traverse 4)  
 Location: Kappilikkunnu, Kottayam; Sample No. CK 75B



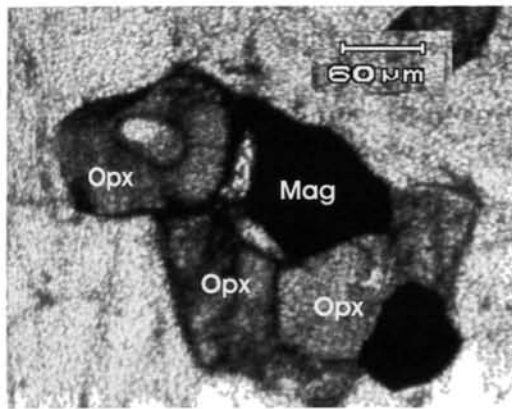
Open polars



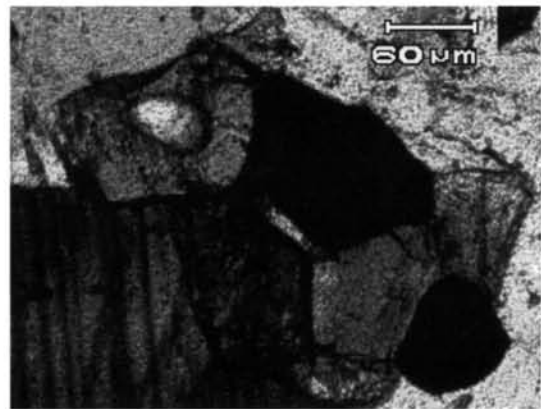
Crossed polars

**Plate 3.26** Magnetite-biotite-quartz-orthopyroxene in charnockite from traverse 4  
 Location: Neelampara, Karukachal; Sample No. CK 19





Open polars



Crossed polars

**Plate 3.27** Magnetite surrounded by orthopyroxenes in charnockite from traverse 4. Location: Neelampara, Karukachal; Sample No. CK 19

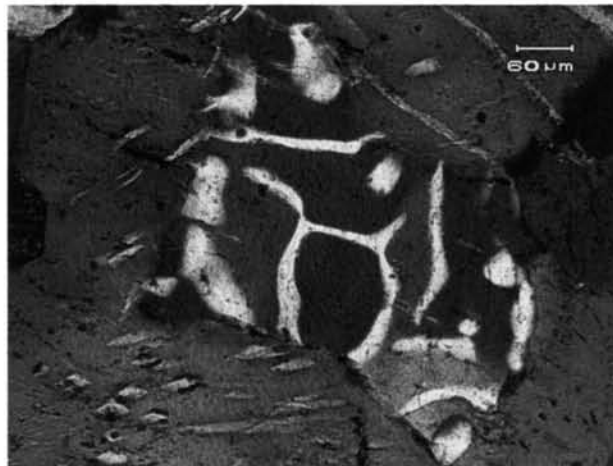


**Plate 3.28** Myrmekitic texture in felsic charnockite from traverse 4. Location: Ayarkkunnam, Kottayam; Sample No. CK 14

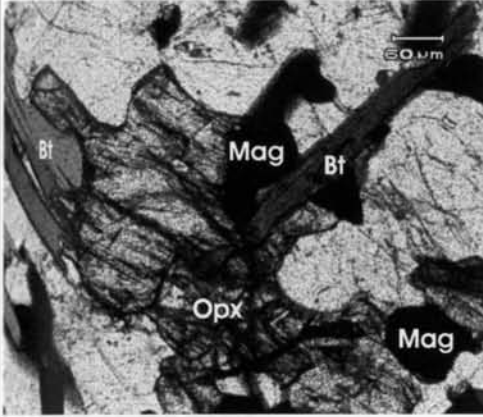


samples as the formation of secondary biotites at orthopyroxene rims together with magnetite and quartz (Plate 3.29).

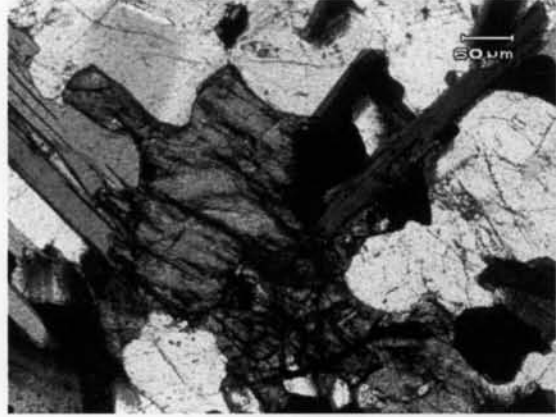
Traverse 5 covered the transition area between the meta-sedimentaries of the KKB and the charnockites of the MGB (the ACS). So the rock types encountered are characterized with many mineral assemblages and textures that show these transitional changes. The coexisting hornblende and garnet is one among them (Plate 3.30). Another assemblage is garnet + hornblende + spinel + magnetite + quartz (Plate 3.31). This assemblage denotes a fluid involved reaction (more discussed in Chapter IV). Garnet-biotite assemblages are also common in the terrain (Plate 3.32), but a peculiar reaction noted is the development of magnetite around biotite (Plate 3.33). The garnet-biotite occurrence also points to some more retrogressive changes since biotites are radiating into garnets (Plate 3.34 and 3.35).

The region covered by traverse 6 is mostly characterized by less retrogressed massive charnockites giving typical granuloblastic texture (Plate 3.36)

The metamorphic conditions of the rocks studied are discussed further with mineral chemistry data in Chapter 4.



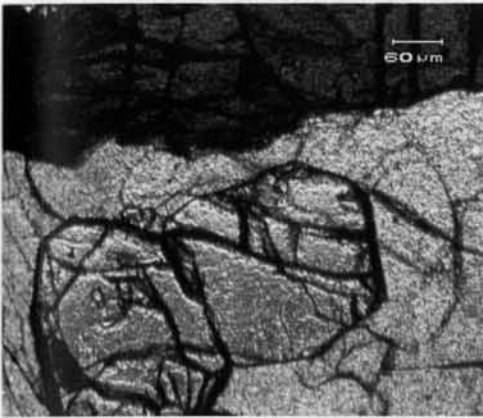
Open polars



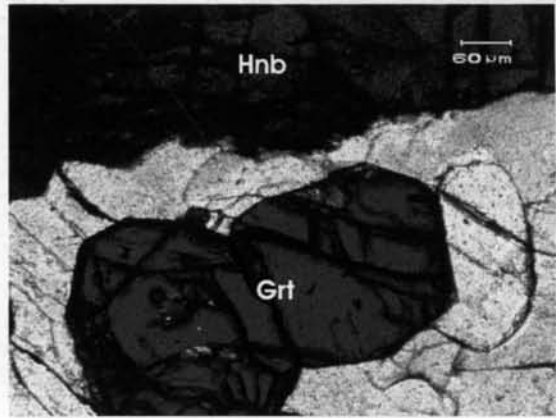
Crossed polars

**Plate 3.29** Secondary biotite at orthopyroxene rims together with magnetite (Traverse 4). Location: Uzhavoor, Kottayam; Sample No. CK 67

Sample No. CK 67



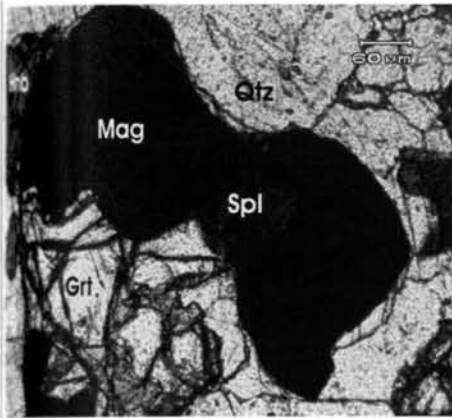
Open polars



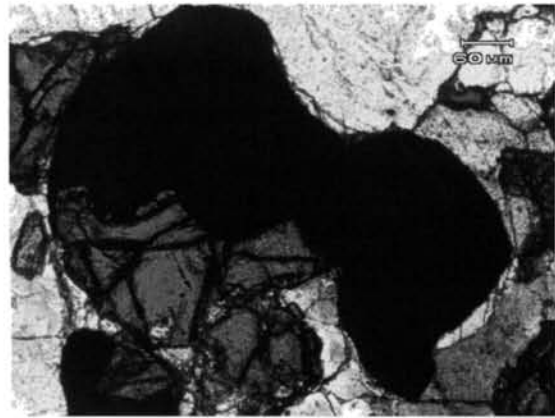
Crossed polars

**Plate 3.30** Coexisting garnet and hornblende in charnockite (Traverse 5) Location: Punalur-Thenmala road; Sample No. CK 34

Sample No. CK 34

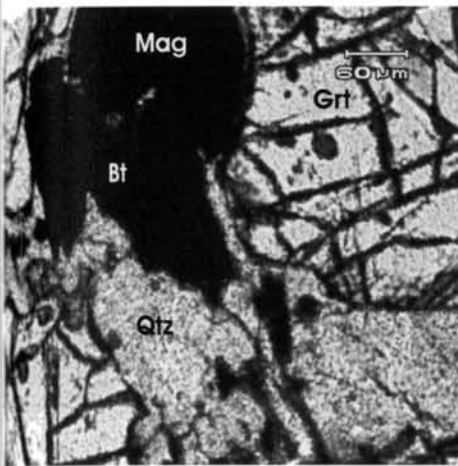


Open polars

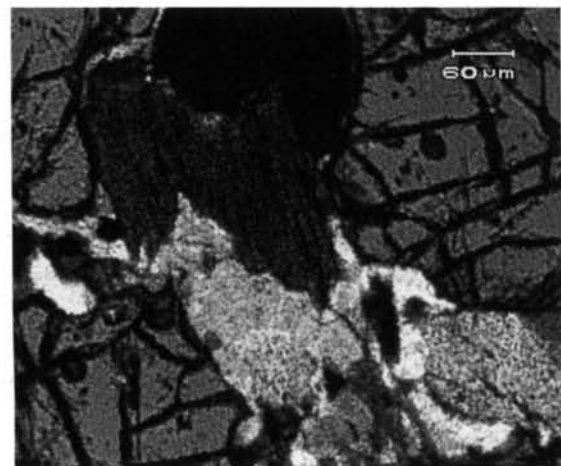


Crossed polars

**Plate 3.31** Garnet-hornblende-magnetite-spinel-quartz assemblage in gneiss from traverse 5. Location: Punalur-Thenmala road; Sample No. CK 34

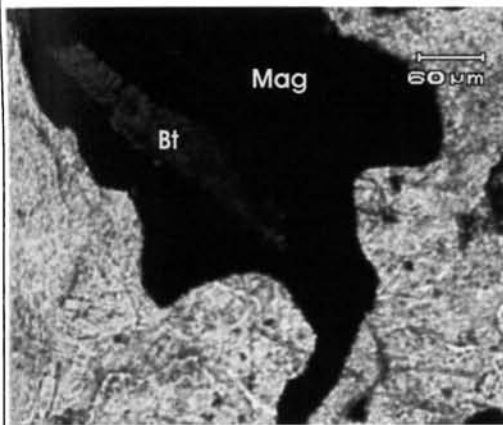


Open polars

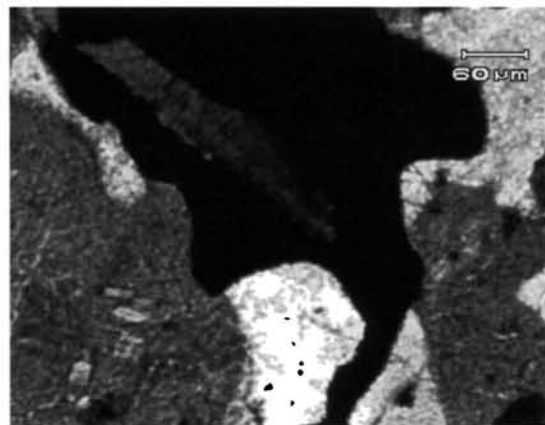


Crossed polars

**Plate 3.32** Garnet biotite gneiss a specific textural assemblage from traverse 5. Location: Punalur-Thenmala road; Sample No. CK 34

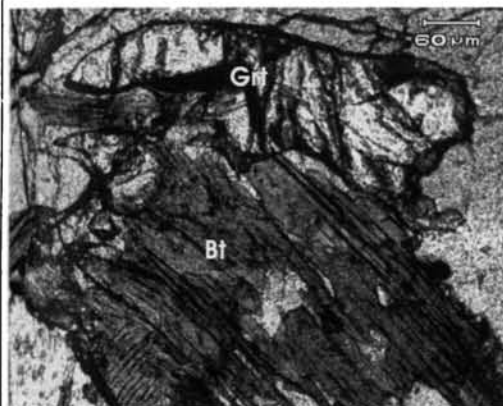


Open polars

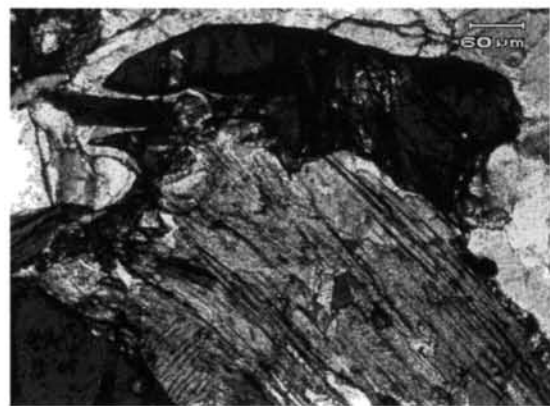


Crossed polars

**Plate 3.33** Accretion or development of magnetite around biotite flake (Traverse 5) Location: Punalur-Thenmala road; Sample No. CK 34B

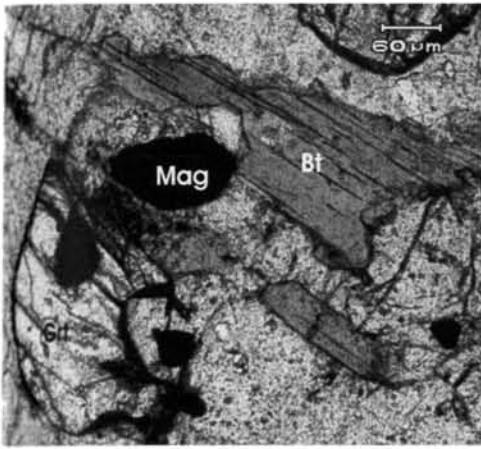


Open polars

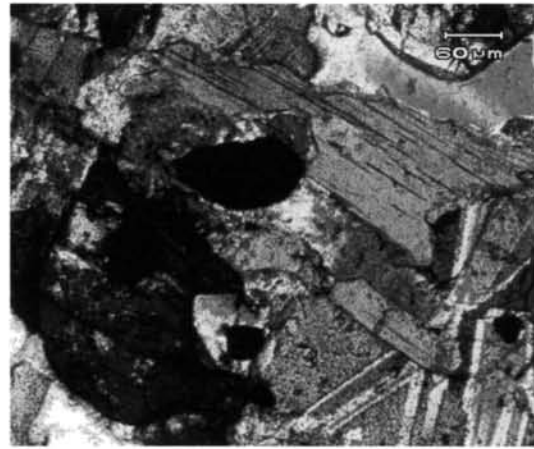


Crossed polars

**Plate 3.34** Biotites radiating into garnet; effect of retrogression (Traverse 5) Location: Nedumpara, Pathanapuram; Sample No. CK 38

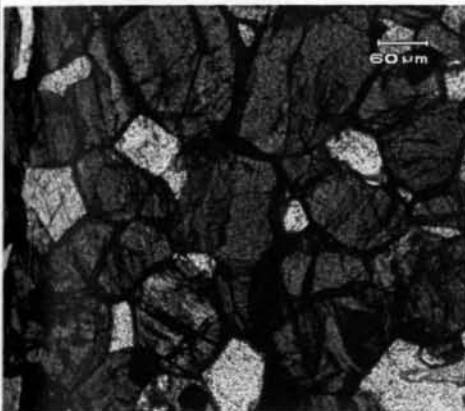


Open polars

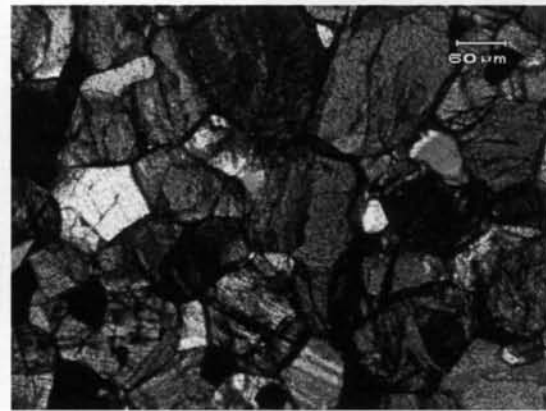


Crossed polars

**Plate 3.35** Garnet break down to biotite and newly formed quartz and feldspar embaying into it. (Traverse 5). Location: Nedumpara, Pathanapuram; Sample No. CK 38



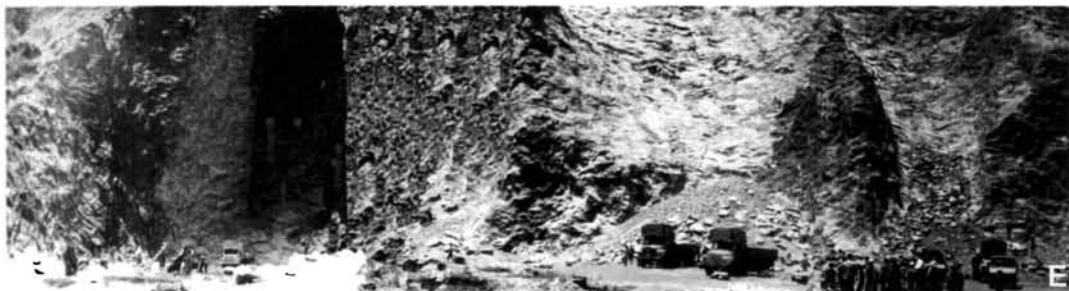
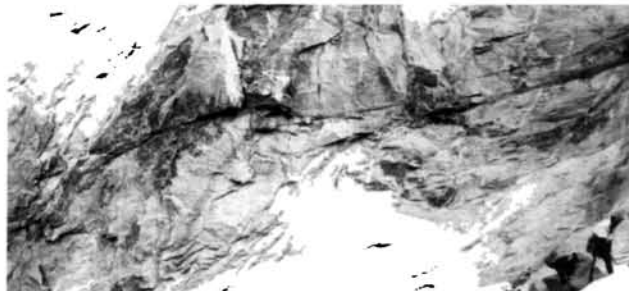
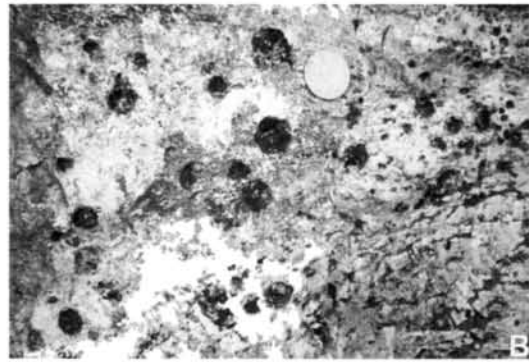
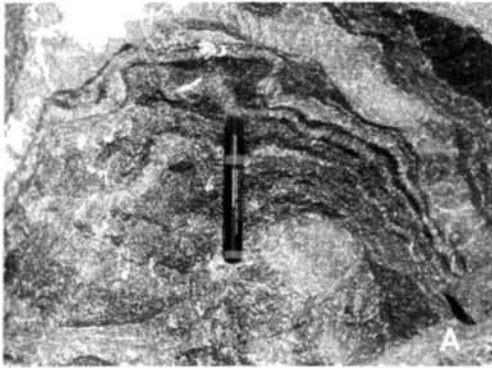
Open polars



Crossed polars

**Plate 3.36** Typical granuloblastic texture from charnockite encountered in traverse 6. Location: Iswaramalli, Thirumangalam, Tamil Nadu; Sample No. CTN 121

**SOME MORE GLIMPSES FROM THE FIELD WORK**



- A. Highly folded charnockite from Illithodu, Trichur
- B. Weathered garnet-biotite gneiss with garnet porphyroblasts from Kakkanad
- C. Distant view of Madurai granitic intrusive
- D. Charnockite relicts in the Madurai granite
- E. A huge cordierite-biotite gneiss quarry in the ACS
- F. Incipient charnockitization in hornblende-biotite gneiss. Location near Palghat.
- G. Charnockite hillock near Theni
- H. Migmatitic gneiss which forms the part of Western Ghats. Location near Bodimett

**THE PLATES ARE NOT MENTIONED IN THE TEXT**

# CHAPTER 4

REACTION TEXTURES, MINERAL CHEMISTRY  
AND ESTIMATION OF PRESSURE – TEMPERATURE  
CONDITIONS

---

## 4.1 INTRODUCTION

Granulite facies rocks are really the exposed examples of ancient deep crustal materials. So for those who are involved in studying the evolutionary history of the Earth, it is of great interest to understand the tectonic and chemical processes that form granulite terrains. To unravel their petrogenetic history, the studies on granulite rocks have been concentrated in four general areas like, thermobarometry, the nature and role of fluids in their genesis, geochemical studies, and tectonic modeling. Since metamorphism is a non-static process, characterized by changing conditions of pressure and temperature the understanding of these changes with respect to time is more important. In a regime of tectonic activity there will be perturbation in the thermal structure of the crust. This thermal disturbance will slowly settle down to a steady state value after the stoppage of tectonism. Pressure-Temperature-time (P-T-t) history of a rock is the function of this tectonic perturbations and the subsequent thermal decay. Every volume of rock follows an individual unique P-T path in space and time during the tectonics. So the retrieval of quantitative P-T-t information from the mineral assemblages in the rocks under study is considered as the primary goal in understanding the history of the rock. This knowledge in turn gives a better picture of the tectonic processes that formed the deep continental crust.



## 4.2 TYPES OF P-T PATHS

Harley (1989) in his review on the types of P-T paths of granulites and their implications for the origin of granulite terrains has recognized a path of nearly isothermal decompression (ITD) and a path of nearly isobaric cooling (IBC). Both the cases are equally occurring in many of the granulite terrains. Nevertheless, there are workers who argue that most of the granulite terrains follow the IBC path (eg. Bohlen, 1987). Bohlen (1991) has formulated a three-fold classification for the P-T-t paths of granulite terrains.

They are:

- (i) Clock wise (CW) paths where  $P_{\max}$  attained before  $T_{\max}$ , isothermal decompression (ITD).
- (ii) Anticlockwise (ACW) where  $T_{\max}$  attained before  $P_{\max}$  isobaric cooling (IBC),
- (iii) IBC paths with no recognizable precursor path (from Sandiford and Powel, 1986).

These P-T-t paths are believed to be of prime evidence, which can describe the tectonic settings for the granulite formation. The type (i) path is characteristic of continent-continent collision environments, the type (i) and (ii) some times of continental magmatic arc regions and (ii) and (iii) representing rift environments and hot spots (Bohlen, 1991).

## 4.3 P-T ESTIMATES FROM THE MGB

Though a few thriving works on the P-T conditions of the metamorphic rocks of the MGB are available, a comprehensive picture of the tectonic block and the P-T evolution of the block in relation to adjoining crustal units is yet to be worked out. P-T conditions in the MGB has been

calculated by many early workers and which gave a range of temperatures from 500° C to 1000° C and pressures up to 8 kb. The P-T conditions of the granulite facies metamorphism have produced a unique range but in reality they preserve a spectrum of diverse petrogenetic features, which may be due to the difference in their mode of formation (Harley, 1989). These PT range represent both prograde as well as retrograde metamorphic conditions (eg. Harris *et al.*, 1982; Raith *et al.*, 1983; Ravindrakumar and Chacko, 1994; Prakash, 1999; Satish-Kumar *et al.*, 2002; John *et al.*, 2005 and the references there in). So P-T conditions, which we estimate from an available mineral assemblage, cannot form a generalized picture of the terrain, especially in the case of a large tectonic block like the MGB. Another difficulty, which comes forth in the P-T estimates of the terrain, is the widely retrogressed assemblages in the rocks and the lack of garnet (a common high grade mineral) bearing assemblages.

Keeping all the above constraints, an attempt is made in the present study to correlate the P-T conditions of representative rock samples from the MGB. The study is more concentrated in the southern part of the block, since the P-T estimates from the area is scarce, as much of the available data is from the northern and northeastern parts. An idea is also there to correlate the P-T estimates of the adjoining ACS with the nearby locations of the MGB. The rocks selected show some peculiar mineral assemblages and the study is more concentrated to determine retrogressive effects of the terrain with the help of possible thermobarometers. The garnet-biotite thermometers are found suitable for most of the rocks and are mostly relied

in the present study. The P-T estimates are further used to merge with the fluid inclusion data available from the charnockites of the MGB to bring out the source of CO<sub>2</sub> fluids and its relation with the graphites in this high-grade terrain (see Chapter VI).

Samples from the MGB include CK 8, CK16 and CK58 and the samples from the ACS are CK37, CK39, and CK40. The locations from which the samples are taken are shown in Fig 4.1.

#### **4.4 ROCK TYPES AND THE FIELD RELATIONSHIPS OF THE SAMPLES**

Brief description on the field setup of the samples selected for EPMA and thermobarometric studies from the MGB and the adjoining areas are given below:

- 1) Sample No. CK8: Mafic charnockite (two pyroxene granulite) having major mineral assemblage of clinopyroxene, orthopyroxene, hornblende, and plagioclase. In the field the rock is very dark in appearance due to the presence of high amount of mafic minerals. Quartz and biotite is also found in the rock. Texturally the rock is medium grained and equigranular, except for the larger crystals of hornblende (porphyroblasts).
- 2) Sample No. CK16 (Garnet-biotite gneiss): The major rock type of the area is felsic charnockite. Garnet is found occurring in some parts of the rock. At places, gneissosity is preserved with good amount of biotite and garnet resembling tonalitic gneiss. The EPMA was carried out on the gneissic

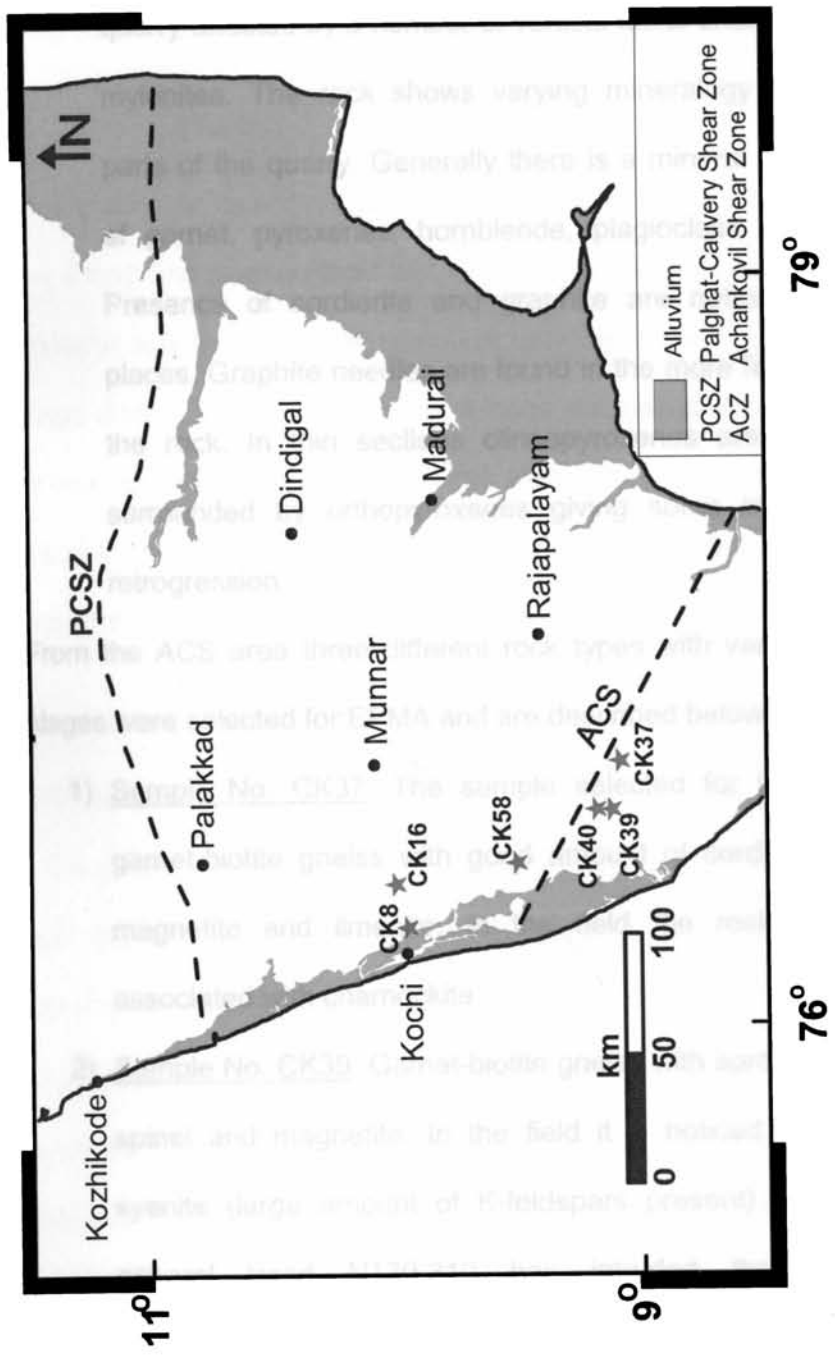


**Fig 4.1 Sampling locations for EPMA**

sample having prominent assemblage of garnet, biotite and spinel.

- 3) Sample No. CK58: This sample is from a massive charnockite quarry affected by a number of vertical faults characterised by mylonites. The rock shows varying mineralogy in different parts of the quarry. Generally there is a mineral assemblage of garnet, pyroxenes, hornblende, plagioclase and quartz. Presence of cordierite and graphite are noticed in some places. Graphite needles are found in the more felsic parts of the rock. In thin sections clinopyroxenes are sometimes surrounded by orthopyroxenes giving some inferences of retrogression.

From the ACS area three different rock types with variant mineral assemblages were selected for EPMA and are described below:

- 1) Sample No. CK37: The sample selected for the study is garnet-biotite gneiss with good amount of cordierite, spinel magnetite and ilmenite. In the field the rock is closely associated with charnockite.
- 2) Sample No. CK39: Garnet-biotite gneiss with some amount of spinel and magnetite. In the field it is noticed that a pink syenite (large amount of K-feldspars present) vein with a general trend N130-310 has intruded through felsic charnockite and this may have some effects in the genesis of this gneiss. The attitude of the foliations measured are 75/N 150, 80/N210, 82/N250.

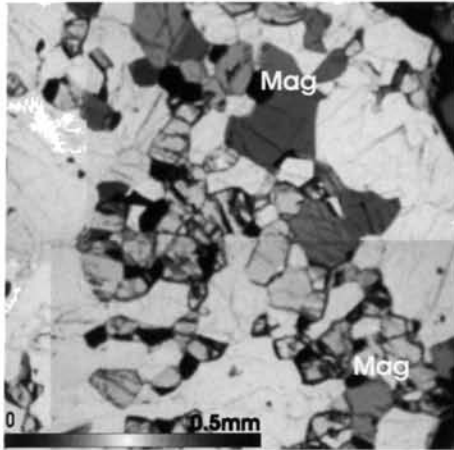
- 3) Sample No. CK40: Massive charnockite intruded by large granitic veins. Gneissosity is preserved in the charnockite. The major mineral assemblage includes garnet, orthopyroxene, biotite and plagioclase.

#### **4.5 REACTION TEXTURES**

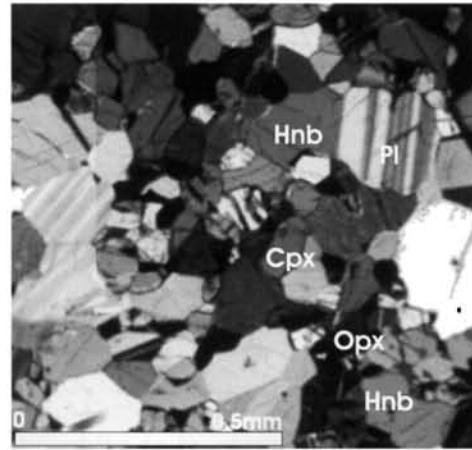
Recognition of distinctive patterns in the occurrence of minerals in rocks has a long and distinguished history in the development of petrology. A metamorphic reaction is an expression of how the minerals got to a new assemblage during metamorphism, but it does not necessarily tell us the path that was actually taken to arrive at this state. We can deduce the path by means of a reaction mechanism. It suggests additional opportunities for investigating chemical and physical processes during metamorphism.

##### **4.5.1 Samples from the MGB**

CK8 is characterized with mineral grains of typical granoblastic texture. The grains are comparatively fine in size and the maximum size is less than 0.5mm. The major minerals present are clinopyroxene, orthopyroxene, hornblende, magnetite and plagioclase. The coexisting  $Pl+Opx+Cpx+Hbl$  ( $\pm Qtz, Bt$ ) assemblage denotes a mafic origin, which in turn is similar to gabbroic assemblage (Raith *et al.*, 1983). Texturally the rock shows much difference than charnockites and shows slightly hydrated assemblage with the presence of primary hornblende (Plate 4.1). Comparatively coarse-grained nature of the hornblende, which is almost similar to the size of plagioclase grains, indicates that it is a primary assemblage and the pyroxenes are formed later. Opaques in the rock are

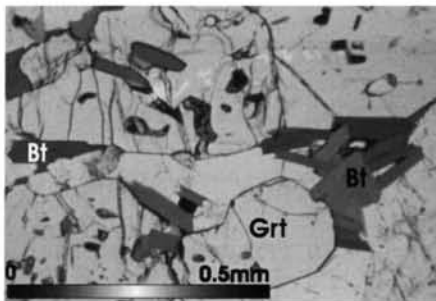


Open polars

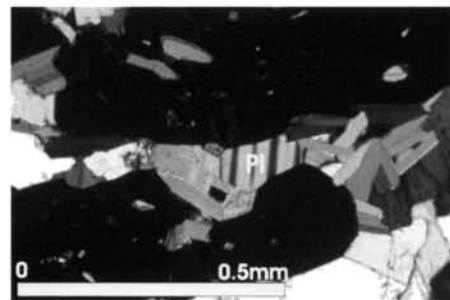


Crossed polars

**PLATE 4.1** Pl-Hnb-Opx-Cpx assemblage from sample CK.8. Mag noticed at Hnb rim



Open polars



Crossed polars

**PLATE 4.2** Garnet porphyroblasts surrounded by biotite flakes in sample CK.16

always found associated with hornblende and usually found in their rims, from which it can be inferred that the release of Fe during the recrystallisation of hornblende to pyroxenes may have caused the formation of opaques (Plate 4.1).

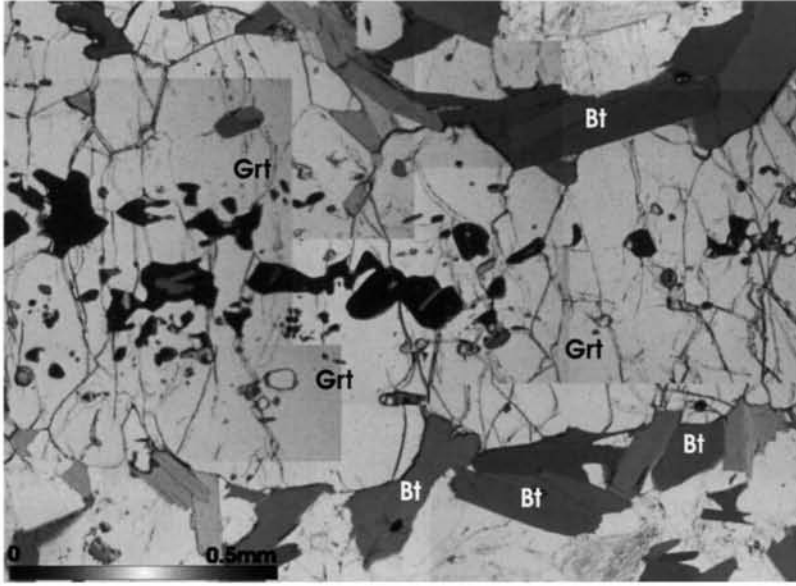
$$\text{Hbl} + \text{Qtz} = \text{Opx} + \text{Cpx} + \text{Pl} + \text{H}_2\text{O} \quad (\text{eq: 4.1}) \text{ (de Waard, 1967; Sen, 1970)}$$

This breakdown reaction of hornblende in granulite facies has been further suggested for the mafic granulites by Sen and Ray (1971). The presence of opaques (especially ilmenite) adjacent to hornblende is explained as a result of Ti release from the hornblende. This kind of oxide release prior to hornblende-orthopyroxene prograde reaction is documented for the northern Kerala mafic granulites (Nambiar *et al.*, 1992).

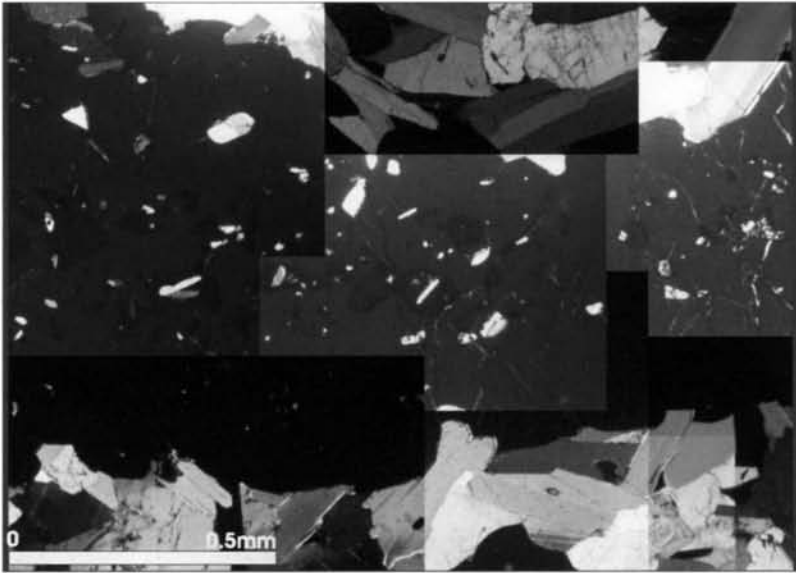
CK16 petrographically is typical tonalitic gneiss, rich in feldspars. The feldspars are mostly plagioclase and among them some are showing perthitic texture, which is relict from the original precursor rock. The other major minerals present are garnet, biotite, and spinel. Garnet porphyroblasts of 1-2mm diameter are found within the layer of biotites. Garnet porphyroblasts are highly fractured and fragmented. Biotite seems to be surrounding the garnet grains or sometimes within the garnet giving an inference that they both had crystallized simultaneously replacing the precursor feldspars (Plate 4.2). Opaques and spinel are arranged in arrays and sometimes found as relicts within the garnet grains (Plate 4.3).

In CK58 the mineral assemblage is garnet-clinopyroxene-hornblende-plagioclase-quartz. Garnet is found as porphyroblastic grains surrounded by plagioclase, hornblende and quartz (Plate 4.4). Another



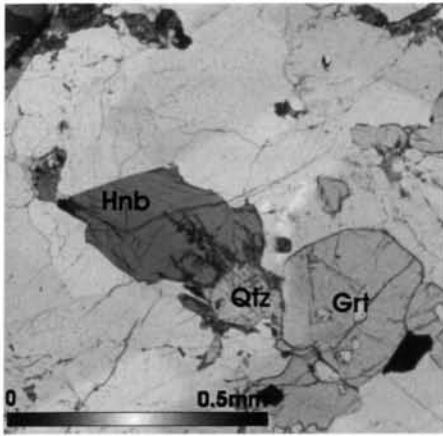


Open polars

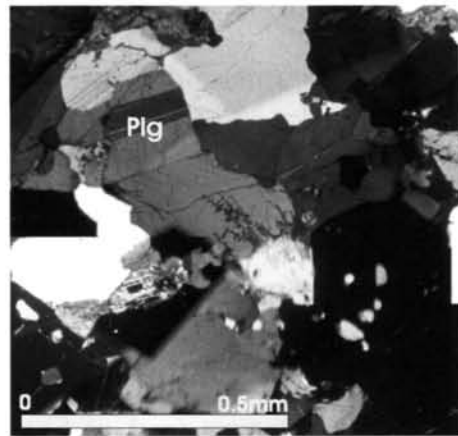


Crossed polars

**PLATE 4.3** Arrays of opaques and spinel within garnet porphyroblasts from sample CK16

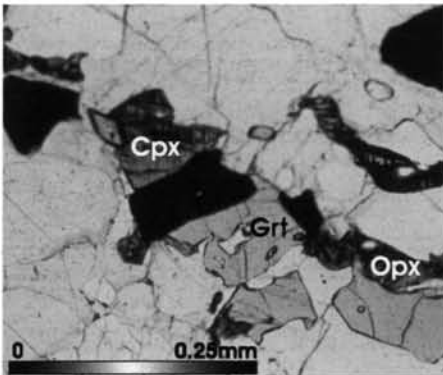


Open polars

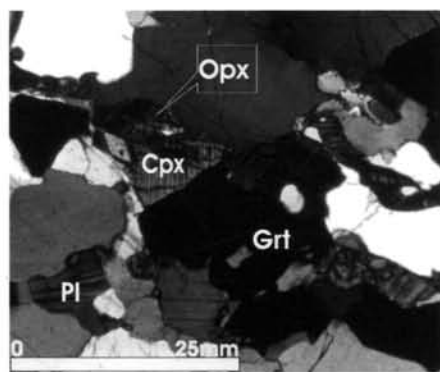


Crossed polars

**PLATE 4.4** Grt-Hnb-Pl-Qtz assemblage from sample CK.58



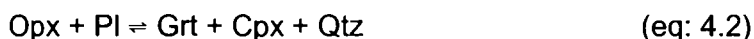
Open polars



Crossed polars

**PLATE 4.5** Charnockite showing newly formed Grt and Cpx replacing Opx from sample CK.58.

noticeable feature is that, even though the rock shows the charnockitic appearance, orthopyroxenes are found rare in thin sections and those occurring are with clinopyroxene overgrowths at the rim (Plate 4.5), which is a typical reaction representative of isobaric cooling history described by Harley (1989)



In high-pressure conditions where plagioclase is comparatively more, the orthopyroxene gets consumed to form garnet, clinopyroxene, plagioclase, quartz assemblage. In intermediate pressure conditions the assemblage will be having orthopyroxenes in close proximity (Pattison, 2003 and the references there in). The sample CK58 points to be of intermediate pressure genesis since there are traces of orthopyroxenes, within the assemblage.

The orthopyroxene free  $\text{Grt} + \text{Cpx} + \text{Pl} \pm \text{Qtz}$  assemblages are considered either in the granulite or the eclogite facies. But there was a self-rejected view by Turner (1948), that this assemblage can be grouped into almandine-diopside-hornblende subfacies of the granulite facies. The presence of hornblende in the present sample substantiates this. There were many more discussions on this specific assemblage. de Waard (1965, 1967) asserted this into a clinopyroxene-almandine ( $\pm$  hornblende) subfacies, which was supported by Green and Ringwood (1967). Still there are controversies as to whether  $\text{Grt} + \text{Cpx} + \text{Pl} \pm \text{Qtz}$  without orthopyroxenes should be regarded as definitive of high-pressure granulites (Pattison, 2003).

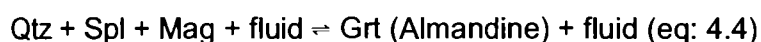
Similarly the presence of garnet embedded in clinopyroxene (Plate 4.6) suggests the formation of garnet by the reaction:



This reaction is again indicative of isobaric cooling.

#### 4.5.2 Samples from the ACS

The samples analysed from the ACS show some reaction textures, which are, evidences for prograde metamorphism as well as some others showing retrogressive reaction. The garnets are seen as porphyroblasts of size 1-1.5mm surrounded by magnetite, spinel (hercynite), biotite and quartz (Plate 4.7). This assemblage represents a fluid involved reaction,

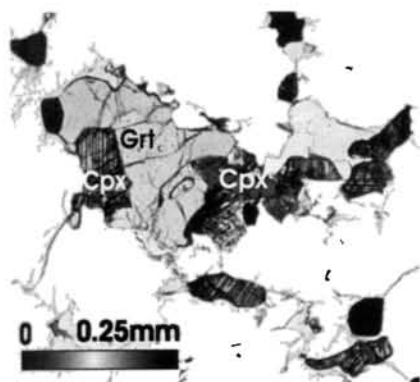


Cordierites form some symplectitic intergrowth with quartz, biotite and spinel and are mostly concentrated at the rim of the garnet. Cordierites are found anhedral and fine grained. Some times biotites are present as inclusions in cordierite and at cordierite margins. Intergrowth of cordierite and greenish spinel are well noticed along with composite grains of ilmenite and magnetite (Plate 4.7). This texture gives a picture of garnet breakdown during some retrograde processes to form corona of cordierite–quartz symplectite along grain boundary. This represents a melt-involved reaction,

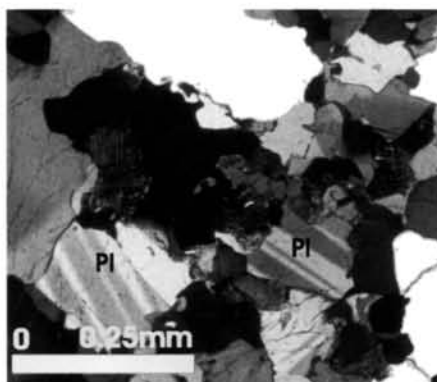


Similarly the presence of cordierite–biotite association in the presence of garnet and spinel can be explained by the reaction,



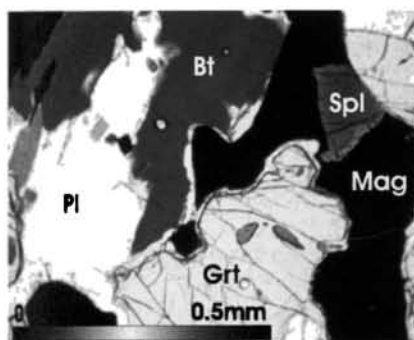


Open polars

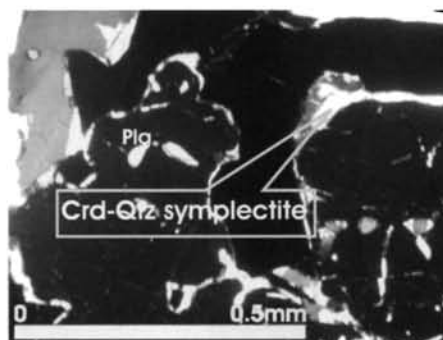


Crossed polars

**PLATE 4.6** Garnet embedded in clinopyroxene plagioclase matrix from sample CK 58.



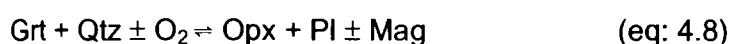
Open polars



Crossed polars

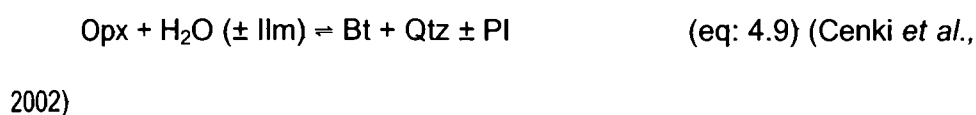
**PLATE 4.7** Grt-Mag-Spl-Bt-Qtz assemblage from sample CK.37 Crd-Qtz symplectitic intergrowth noticed along the garnet rim

CK40 is having major mineral assemblage of garnet, orthopyroxene, biotite, plagioclase, magnetite and spinel in which Opx + Bt + Plg + Mag forms one specific assemblage and Grt + Opx + Pl + Qtz forms another. The reaction textures give evidence for the breaking of garnets. So the assemblage points to garnet breaking down to plagioclase and orthopyroxene (Plate 4.8).

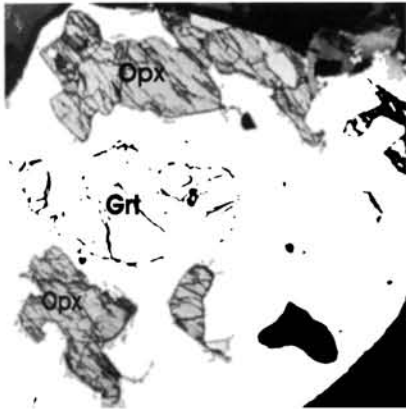


This garnet breaking down is indicative of isothermal decompression rather than isobaric cooling (Harley, 1989; Ravindrakumar and Chacko, 1994; John *et al.*, 2005)

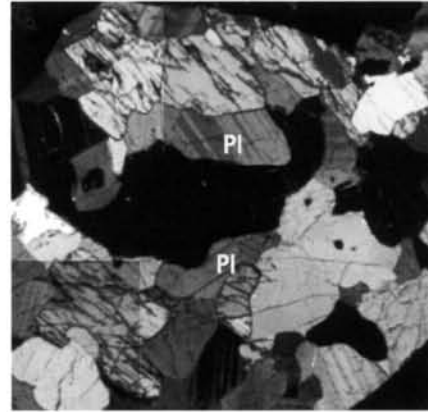
Some biotites are found radiating into the orthopyroxene boundary indicating that the biotites are after the orthopyroxenes (Plate 4.9). These secondary biotites also show symplectitic assemblage with quartz points towards some hydration mechanism (retrogression). The presence of secondary biotite is further confirmed from the mineral chemistry (see section 4.6). In orthopyroxene-bearing quartzo-feldspathic gneisses, biotites or biotites + quartz or hornblende + quartz intergrowth replaces orthopyroxenes and clinopyroxenes during hydration (Kundu *et al.*, 1998).



Cordierite–quartz symplectites are also found at the rim of the garnet grains, indicating retrogressive metamorphism.

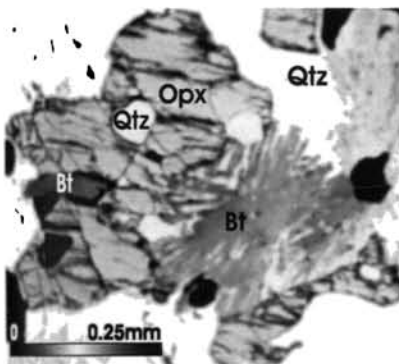


Open polars

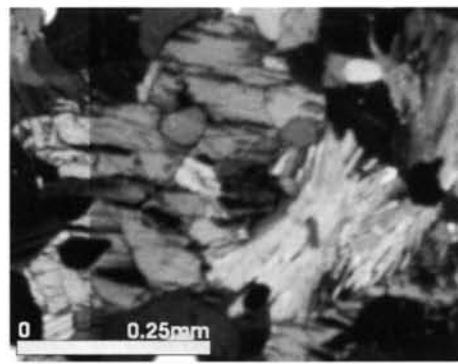


Crossed polars

**PLATE 4.8** Garnet breaking down into plagioclase and orthopyroxene in charnockite( sample CK.40) from ACS.



Open polars



Crossed polars

**PLATE 4.9** Biotites radiating into Opx boundary giving inferences of retrogressive reaction in charnockite (sample CK.40) from ACS.

#### 4.6 MINERAL CHEMISTRY

Chemistry of the constituent minerals were determined using a wave dispersive EPM housed at Shizuoka University (JEOL 733), Japan. Measurement conditions were 12 nA, 15 kV accelerating voltage at with a minimum beam diameter (2-3 $\mu$ m). Natural and synthetic mineral standards were used. Bence and Albee (1968) corrections were performed throughout. Representative mineral analyses are presented in tables 4.1 to 4.12.

The chemistry of different minerals at different locations are summarised below.

In the MGB locations the garnet compositions have characteristic almandine-pyrope solid solution with minor amounts of grossular and spessartine. In garnet-biotite gneiss the almandine content varies from 65-70% (Fig 4.2) with a slight decrease from rim to core. Pyrope, spessartine and grossular are very negligible (Fig 4.3). The  $X_{Mg}$  values show a range of 0.26-0.31; the recalculation of  $X_{Mg}$  after deducting  $Fe^{3+}$  from Fe total also almost similar values of  $X_{Mg}$  indicating no pronounced oxidation effects (calculated  $Fe^{3+}$  was negligible) (Table 4.1). The FM ( $Fe/Fe+Mg$ ) falls in a range 0.68-0.75 in which the higher value points are observed where the garnets are in contact with biotites i.e., usually along the rim. But flat FM values are also observed in some grains. In charnockite from the MGB the grossular-andradite content is comparatively more than the pyrope fraction and the almandine has a range of 66-69% (Table 4.2) (Fig. 4.4). All the gamets show an Mg enriched core and Fe enriched rim. Towards the core pyrope content is increasing with simultaneous decrease of spessartine



**Table 4.1 Representative microprobe data of garnets from garnet-biotite gneiss in MGB**

	core	rim	core	rim	core	rim	core	rim
SiO <sub>2</sub>	39.250	39.319	38.475	39.075	39.275	39.485	38.759	39.846
TiO <sub>2</sub>	0.110	0.075	0.084	0.065	0.074	0.073	0.065	0.079
Al <sub>2</sub> O <sub>3</sub>	20.784	21.498	21.541	21.403	21.534	21.776	20.718	22.128
Cr <sub>2</sub> O <sub>3</sub>	0.001	0.016	0.025	0.040	0.047	0.286	0.077	0.063
FeO	32.396	30.045	32.536	31.634	30.513	29.871	30.239	30.113
MnO	0.523	0.424	0.461	0.422	0.467	0.349	0.519	0.412
MgO	5.758	7.525	6.650	6.981	7.549	7.649	7.820	7.394
CaO	1.246	1.236	1.057	1.221	1.257	1.277	1.257	1.228
Na <sub>2</sub> O	0.000	0.000	0.000	0.000	0.000	0.020	0.002	0.010
K <sub>2</sub> O	0.031	0.021	0.038	0.025	0.024	0.022	0.024	0.012
ZnO	0.000	0.000	0.000	0.000	0.000	0.000	0.000	0.000
<b>Total</b>	<b>100.099</b>	<b>100.159</b>	<b>100.867</b>	<b>100.866</b>	<b>100.740</b>	<b>100.808</b>	<b>0.000</b>	<b>0.000</b>
O	12.000	12.000	12.000	12.000	12.000	12.000	12.000	12.000
Si	3.081	3.048	3.001	3.031	3.034	3.037	3.038	3.048
Ti	0.006	0.004	0.005	0.004	0.004	0.004	0.004	0.005
Al	1.923	1.964	1.980	1.957	1.961	1.974	1.914	1.995
Cr	0.000	0.001	0.002	0.002	0.003	0.017	0.005	0.004
Fe	2.127	1.948	2.122	2.052	1.972	1.922	1.982	1.926
Mn	0.035	0.028	0.030	0.028	0.031	0.023	0.034	0.027
Mg	0.674	0.869	0.773	0.807	0.869	0.877	0.914	0.843
Ca	0.105	0.103	0.088	0.101	0.104	0.105	0.106	0.101
Na	0.000	0.000	0.000	0.000	0.000	0.003	0.000	0.001
K	0.003	0.002	0.004	0.002	0.002	0.002	0.002	0.001
Zn	0.000	0.000	0.000	0.000	0.000	0.000	0.000	0.000
<b>Total Cation</b>	<b>7.953</b>	<b>7.967</b>	<b>8.005</b>	<b>7.986</b>	<b>7.980</b>	<b>7.965</b>	<b>8.000</b>	<b>7.950</b>
Fe <sup>3+</sup>	-0.142	-0.101	0.016	-0.042	-0.059	-0.105	-0.001	-0.151
Fe <sup>2+</sup>	2.269	2.049	2.106	2.094	2.030	2.027	1.983	2.078
Fe <sup>3+</sup> /Fe <sup>2+</sup>	-0.063	-0.049	0.008	-0.020	-0.029	-0.052	0.000	-0.073
Alm	0.736	0.672	0.703	0.691	0.669	0.669	0.653	0.682
Spe	0.011	0.009	0.010	0.009	0.010	0.008	0.011	0.009
Pyr	0.219	0.285	0.258	0.266	0.286	0.289	0.301	0.277
Grs	-0.032	-0.073	0.022	0.079	0.179	-0.074	0.033	-0.027
Adr	0.066	0.107	0.008	-0.045	-0.145	0.108	0.002	0.060
XMg <sup>+</sup>	0.229	0.298	0.268	0.278	0.300	0.302	0.315	0.289
XMg	0.241	0.309	0.267	0.282	0.306	0.313	0.315	0.304

\* The entire data is given in Appendix IIIa

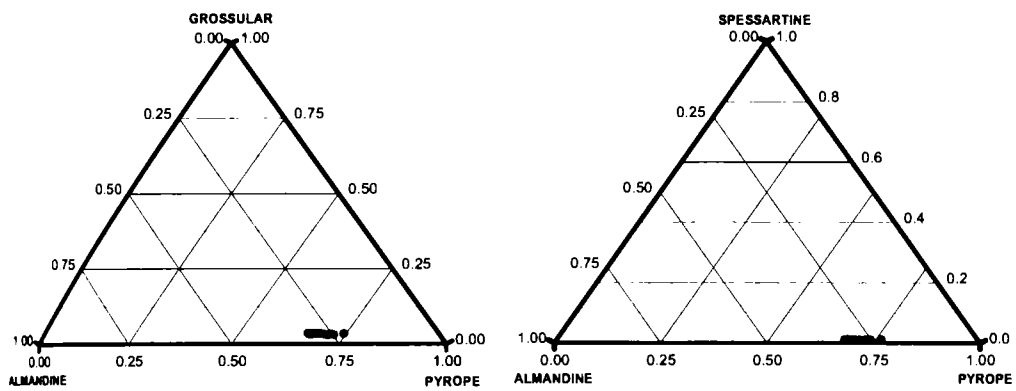


**Fig. 4.2 Garnet composition from garnet-biotite gneiss of MGB**

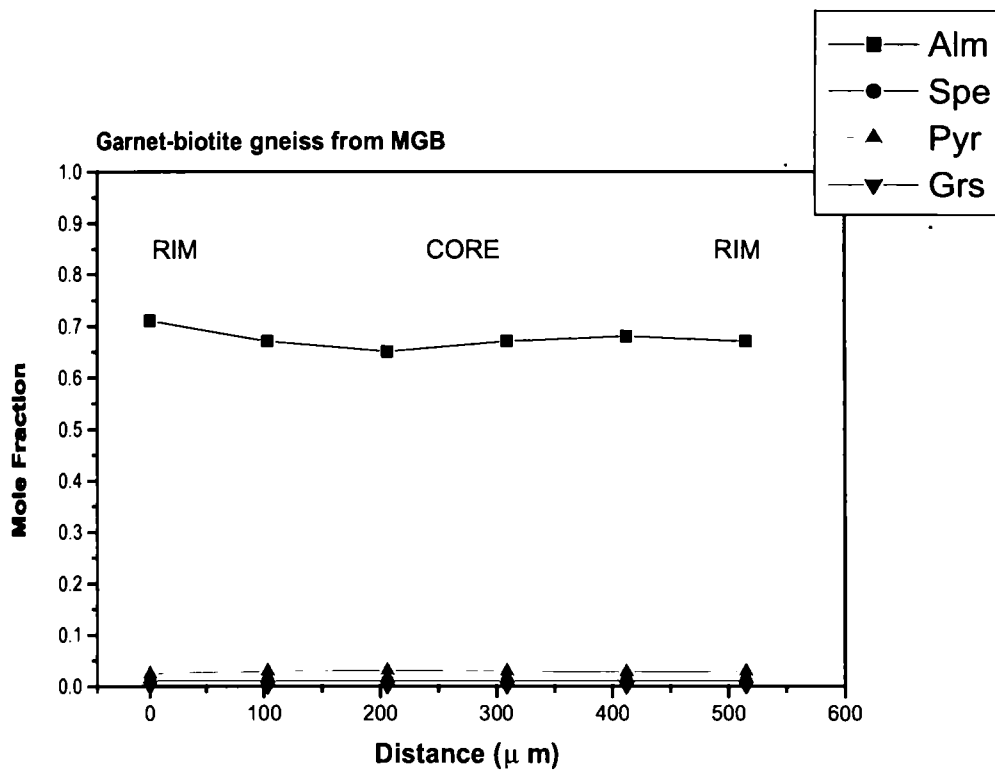


**Fig. 4.3 Variation in garnet composition from rim to core (Sample CK16)**

**Table 4.2 Representative microprobe data of garnets from charnockite in MGB**

	core	rim	core	rim	core	rim	core	rim
SiO <sub>2</sub>	37.908	37.691	37.251	36.905	37.779	37.993	36.847	36.969
TiO <sub>2</sub>	0.371	0.380	0.379	0.376	0.363	0.354	0.583	0.384
Al <sub>2</sub> O <sub>3</sub>	20.048	20.177	19.526	19.897	19.955	20.417	19.606	19.917
Cr <sub>2</sub> O <sub>3</sub>	0.149	0.144	0.141	0.153	0.125	0.116	0.103	0.170
FeO	31.434	31.044	30.634	30.612	30.943	31.166	30.937	31.111
MnO	2.637	2.556	2.684	2.528	2.746	2.555	2.537	2.282
MgO	1.094	1.107	1.109	0.941	1.029	1.063	0.880	1.183
CaO	7.560	7.612	7.666	7.755	7.782	7.705	7.622	7.593
Na <sub>2</sub> O	0.094	0.098	0.089	0.089	0.081	0.100	0.089	0.083
K <sub>2</sub> O	0.097	0.096	0.104	0.096	0.104	0.101	0.094	0.089
ZnO	0.000	0.000	0.000	0.000	0.000	0.000	0.000	0.000
<b>Total</b>	<b>101.392</b>	<b>100.905</b>	<b>99.583</b>	<b>99.352</b>	<b>100.907</b>	<b>101.570</b>	<b>99.298</b>	<b>99.781</b>
O	12.000	12.000	12.000	12.000	12.000	12.000	12.000	12.000
Si	3.025	3.018	3.027	3.006	3.027	3.020	3.008	2.999
Ti	0.022	0.023	0.023	0.023	0.022	0.021	0.036	0.023
Al	1.885	1.904	1.870	1.910	1.885	1.913	1.886	1.905
Cr	0.009	0.009	0.009	0.010	0.008	0.007	0.007	0.011
Fe	2.097	2.079	2.082	2.085	2.074	2.072	2.112	2.111
Mn	0.178	0.173	0.185	0.174	0.186	0.172	0.175	0.157
Mg	0.130	0.132	0.134	0.114	0.123	0.126	0.107	0.143
Ca	0.646	0.653	0.667	0.677	0.668	0.656	0.667	0.660
Na	0.015	0.015	0.014	0.014	0.013	0.015	0.014	0.013
K	0.010	0.010	0.011	0.010	0.011	0.010	0.010	0.009
Zn	0.000	0.000	0.000	0.000	0.000	0.000	0.000	0.000
<b>Total Cation</b>	<b>8.018</b>	<b>8.016</b>	<b>8.023</b>	<b>8.023</b>	<b>8.016</b>	<b>8.012</b>	<b>8.022</b>	<b>8.031</b>
Fe <sup>3+</sup>	0.054	0.047	0.068	0.070	0.048	0.036	0.065	0.092
Fe <sup>2+</sup>	2.043	2.032	2.014	2.016	2.025	2.035	2.047	2.018
Fe <sup>3+</sup> /Fe <sup>2+</sup>	0.026	0.023	0.034	0.035	0.024	0.018	0.032	0.046
Alm	0.682	0.680	0.671	0.676	0.674	0.681	0.683	0.678
Spe	0.059	0.058	0.062	0.059	0.062	0.058	0.059	0.053
Pyr	0.043	0.044	0.045	0.038	0.041	0.042	0.036	0.048
Grs	0.182	0.187	0.183	0.187	0.191	0.193	0.179	0.174
Adr	0.034	0.031	0.040	0.040	0.032	0.026	0.043	0.048
XMg <sup>*</sup>	0.060	0.061	0.063	0.054	0.057	0.058	0.050	0.066
XMg	0.058	0.060	0.061	0.052	0.056	0.057	0.048	0.063

\* The entire data is given in Appendix IIIb

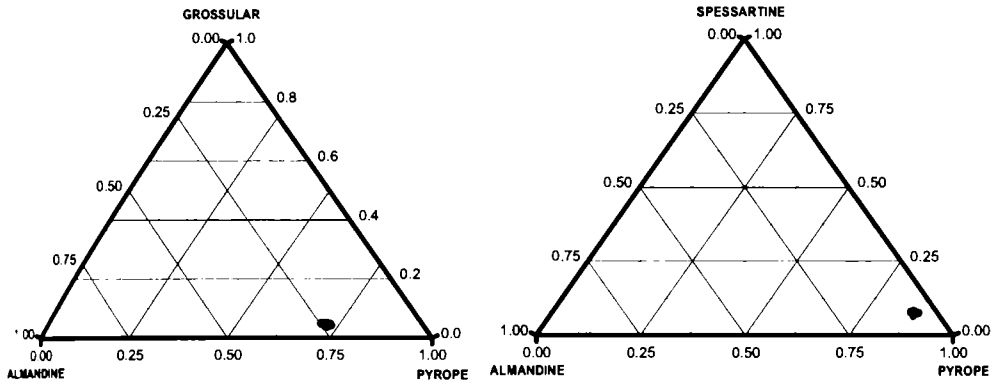


Fig. 4.4 Garnet composition from charnockite of MGB

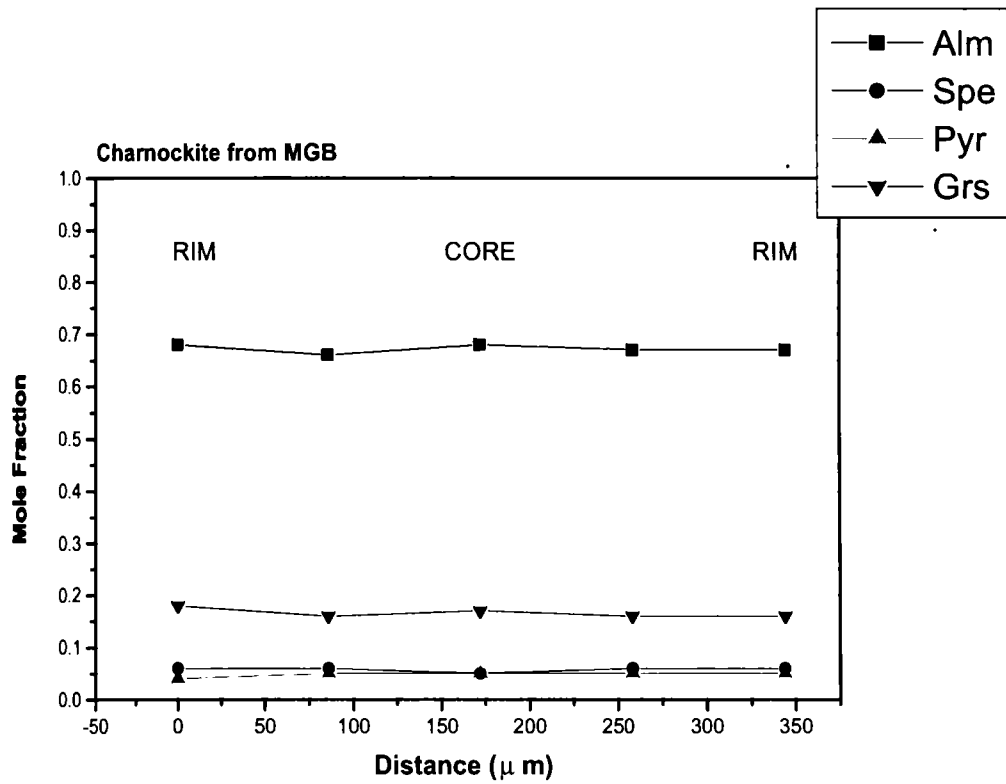


Fig. 4.5 Variation in garnet composition from rim to core (Sample: CK58)

(Fig 4.5). This represents the typical retrograde diffusion zoning of garnet (Toriumi and Nomizo, 2000). The FM value from this sample almost remains constant and high (0.94-0.95) due to the absence of biotites in the sample. Comparatively overall Mn content is higher in garnets from charnockite and are concentrated towards the core indicating that some retrogression has affected the garnet (Cherneva and Gerdjikov, 2004)

The ACS samples chemically show almost same type of garnets with almandine predominance. In garnet-biotite-cordierite gneiss from this area almandine content is between 0.54 and 0.65 (Table 4.3) (Fig 4.6). Here also there is a fall of almandine fraction towards the core, whereas the pyrope content has a gradual increase from rim to core (Fig 4.7). In garnet-biotite gneiss the almandine content follows almost a steady value of 0.56 (Table 4.4) (Fig 4.8) and the rest also showing no remarkable variations (Fig 4.9). The FM values of garnets from both the samples, falls in a range 0.58-0.64 locally showing high values at the rims as in the gneiss from MGB. Similarly, the garnets in the charnockites of the ACS give almandine measure around 0.6 (Table 4.5) (Fig 4.10) without any notable change from rim to core. The other components also show constant values though out the crystals (Fig 4.11). On contrary to the charnockite from MGB, here the FM value is approximately 0.65, due to the presence of biotites. Comparatively the garnets from the ACS are having less almandine content than the garnets from the MGB.

From the over all mineral chemistry of garnets slight amount of grossular zoning with increasing and decreasing trends is noted especially in the gneisses of ACS. This denotes a prograde growth of garnet (Storm

**Table 4.3 Representative microprobe data of garnets from garnet-biotite-cordierite gneiss in ACS**

	core	rim	core	rim	core	rim	core	rim
SiO <sub>2</sub>	39.943	40.816	40.162	39.702	40.240	40.304	39.333	39.600
TiO <sub>2</sub>	0.333	0.369	0.311	0.327	0.340	0.334	0.112	0.056
Al <sub>2</sub> O <sub>3</sub>	21.561	22.883	22.754	21.244	21.941	22.229	22.229	21.386
Cr <sub>2</sub> O <sub>3</sub>	0.115	0.135	0.170	0.109	0.123	0.121	0.000	0.000
FeO	26.067	24.883	25.010	25.927	25.318	25.120	29.199	26.156
MnO	2.673	2.396	2.408	2.581	2.648	2.387	3.039	2.412
MgO	9.032	9.785	9.480	9.802	9.830	9.570	6.861	9.276
CaO	1.199	1.241	1.222	1.144	1.159	1.005	0.961	0.890
Na <sub>2</sub> O	0.078	0.070	0.083	0.084	0.084	0.105	0.000	0.000
K <sub>2</sub> O	0.087	0.090	0.088	0.091	0.096	0.097	0.037	0.030
ZnO	0.000	0.000	0.000	0.000	0.000	0.000	0.000	0.000
<b>Total</b>	<b>101.088</b>	<b>102.668</b>	<b>101.688</b>	<b>101.011</b>	<b>101.779</b>	<b>101.272</b>	<b>101.771</b>	<b>99.806</b>
O	12.000	12.000	12.000	12.000	12.000	12.000	12.000	12.000
Si	3.042	3.029	3.017	3.026	3.030	3.040	3.018	3.050
Ti	0.019	0.021	0.018	0.019	0.019	0.019	0.006	0.003
Al	1.935	2.002	2.015	1.909	1.947	1.976	2.010	1.941
Cr	0.007	0.008	0.010	0.007	0.007	0.007	0.000	0.000
Fe	1.660	1.545	1.571	1.653	1.594	1.585	1.874	1.685
Mn	0.172	0.151	0.153	0.167	0.169	0.153	0.197	0.157
Mg	1.025	1.082	1.061	1.114	1.103	1.076	0.784	1.065
Ca	0.098	0.099	0.098	0.093	0.094	0.081	0.079	0.073
Na	0.012	0.010	0.012	0.012	0.012	0.015	0.000	0.000
K	0.008	0.009	0.008	0.009	0.009	0.009	0.004	0.003
Zn	0.000	0.000	0.000	0.000	0.000	0.000	0.000	0.000
<b>Total Cation</b>	<b>7.978</b>	<b>7.954</b>	<b>7.964</b>	<b>8.008</b>	<b>7.985</b>	<b>7.962</b>	<b>7.973</b>	<b>7.978</b>
Fe <sup>3+</sup>	-0.066	-0.137	-0.110	0.024	-0.046	-0.116	-0.083	-0.067
Fe <sup>2+</sup>	1.726	1.682	1.681	1.629	1.641	1.701	1.956	1.752
Fe <sup>3+</sup> /Fe <sup>2+</sup>	-0.038	-0.082	-0.065	0.015	-0.028	-0.068	-0.042	-0.038
Alm	0.571	0.558	0.561	0.543	0.546	0.565	0.648	0.575
Spe	0.057	0.050	0.051	0.056	0.056	0.051	0.065	0.052
Pyr	0.339	0.359	0.354	0.371	0.367	0.357	0.260	0.349
Grs	0.126	-0.042	-0.083	0.018	0.057	-0.033	-0.058	-0.066
Adr	-0.093	0.075	0.116	0.013	-0.025	0.060	0.085	0.090
XMg*	0.373	0.392	0.387	0.406	0.402	0.387	0.286	0.378
XMg	0.382	0.412	0.403	0.403	0.409	0.404	0.295	0.387

\* The entire data is given in Appendix IIIc

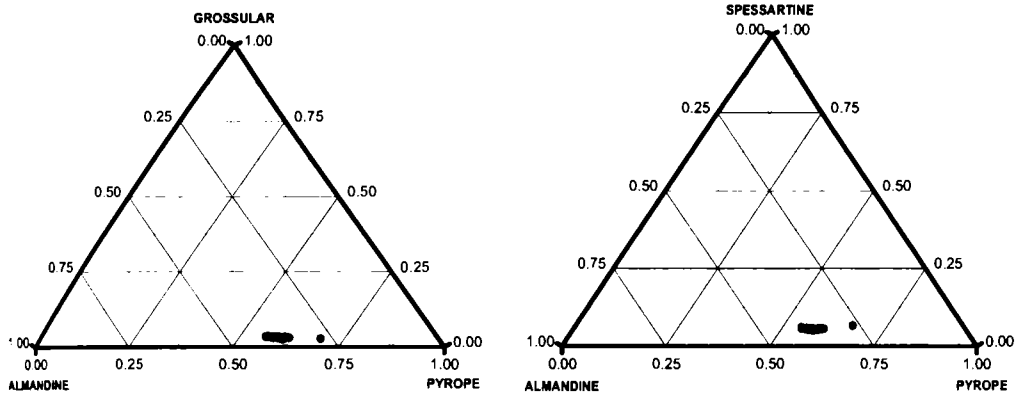


**Fig. 4.6. Garnet composition from garnet-biotite-cordierite gneiss of ACS**

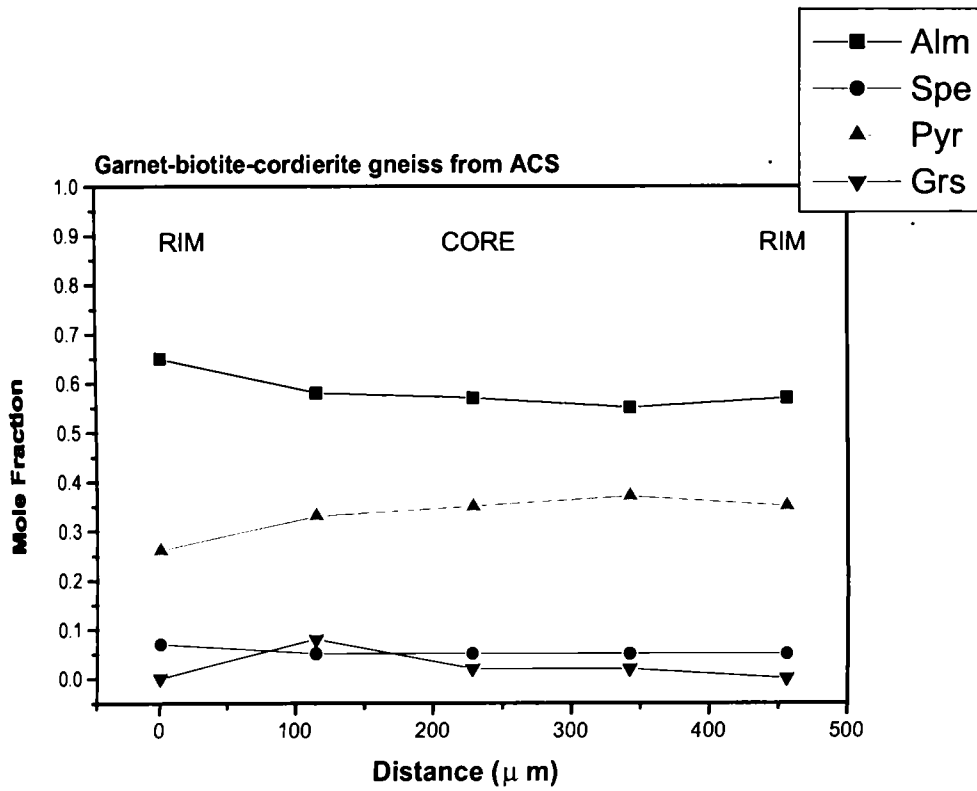


**Fig. 4.7 Variation in garnet composition from rim to core (Sample: CK37)**

**Table 4.4 Representative microprobe data of garnets from garnet-biotite gneiss in ACS**

	core	rim	core	rim	core	rim	core	rim
SiO <sub>2</sub>	39.043	39.091	39.098	38.037	38.352	38.315	38.675	38.405
TiO <sub>2</sub>	0.356	0.356	0.336	0.328	0.311	0.311	0.335	0.330
Al <sub>2</sub> O <sub>3</sub>	21.084	20.757	21.139	21.411	21.103	20.821	21.299	21.273
Cr <sub>2</sub> O <sub>3</sub>	0.130	0.142	0.140	0.140	0.146	0.149	0.138	0.143
FeO	26.404	26.847	26.877	27.058	27.382	26.789	27.561	27.405
MnO	2.183	1.815	1.867	2.068	2.132	1.862	2.146	1.953
MgO	9.110	9.004	8.993	8.778	9.262	9.163	8.986	9.306
CaO	1.231	1.221	1.194	1.182	1.120	1.155	1.265	1.360
Na <sub>2</sub> O	0.071	0.075	0.071	0.072	0.074	0.080	0.086	0.068
K <sub>2</sub> O	0.095	0.088	0.094	0.101	0.106	0.112	0.089	0.096
ZnO	0.000	0.000	0.000	0.000	0.000	0.000	0.000	0.000
<b>Total</b>	<b>99.707</b>	<b>99.396</b>	<b>99.809</b>	<b>99.175</b>	<b>99.988</b>	<b>98.757</b>	<b>100.580</b>	<b>100.339</b>
O	12.000	12.000	12.000	12.000	12.000	12.000	12.000	12.000
Si	3.022	3.038	3.025	2.974	2.979	3.003	2.986	2.971
Ti	0.021	0.021	0.020	0.019	0.018	0.018	0.019	0.019
Al	1.924	1.901	1.928	1.974	1.932	1.923	1.938	1.940
Cr	0.008	0.009	0.009	0.009	0.009	0.009	0.008	0.009
Fe	1.709	1.745	1.739	1.770	1.779	1.756	1.780	1.773
Mn	0.143	0.119	0.122	0.137	0.140	0.124	0.140	0.128
Mg	1.051	1.043	1.037	1.023	1.072	1.070	1.034	1.073
Ca	0.102	0.102	0.099	0.099	0.093	0.097	0.105	0.113
Na	0.011	0.011	0.011	0.011	0.011	0.012	0.013	0.010
K	0.009	0.009	0.009	0.010	0.011	0.011	0.009	0.009
Zn	0.000	0.000	0.000	0.000	0.000	0.000	0.000	0.000
<b>Total Cation</b>	<b>8.001</b>	<b>7.997</b>	<b>7.998</b>	<b>8.026</b>	<b>8.044</b>	<b>8.024</b>	<b>8.032</b>	<b>8.045</b>
Fe <sup>3+</sup>	0.003	-0.010	-0.007	0.077	0.130	0.072	0.096	0.135
Fe <sup>2+</sup>	1.707	1.754	1.746	1.693	1.649	1.684	1.684	1.638
Fe <sup>3+</sup> /Fe <sup>2+</sup>	0.002	-0.006	-0.004	0.045	0.079	0.043	0.057	0.082
Alm	0.568	0.581	0.581	0.574	0.558	0.566	0.568	0.555
Spe	0.048	0.040	0.041	0.046	0.047	0.042	0.047	0.043
Pyr	0.350	0.345	0.345	0.347	0.363	0.360	0.349	0.363
Grs	0.025	0.029	0.028	0.014	0.009	0.013	0.013	0.012
Adr	0.009	0.005	0.005	0.020	0.022	0.019	0.022	0.026
XMg*	0.381	0.373	0.373	0.377	0.394	0.389	0.380	0.396
XMg	0.381	0.374	0.374	0.366	0.376	0.379	0.367	0.377

\* The entire data is given in Appendix III d



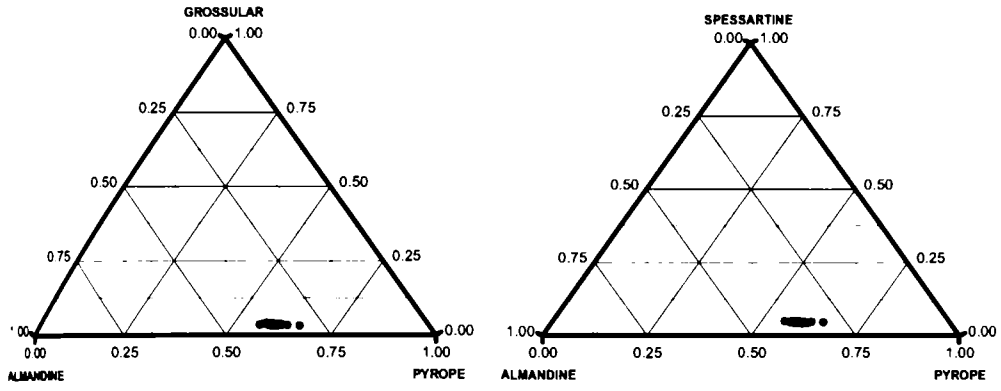


Fig. 4.8 Garnet composition from garnet-biotite gneiss of the ACS

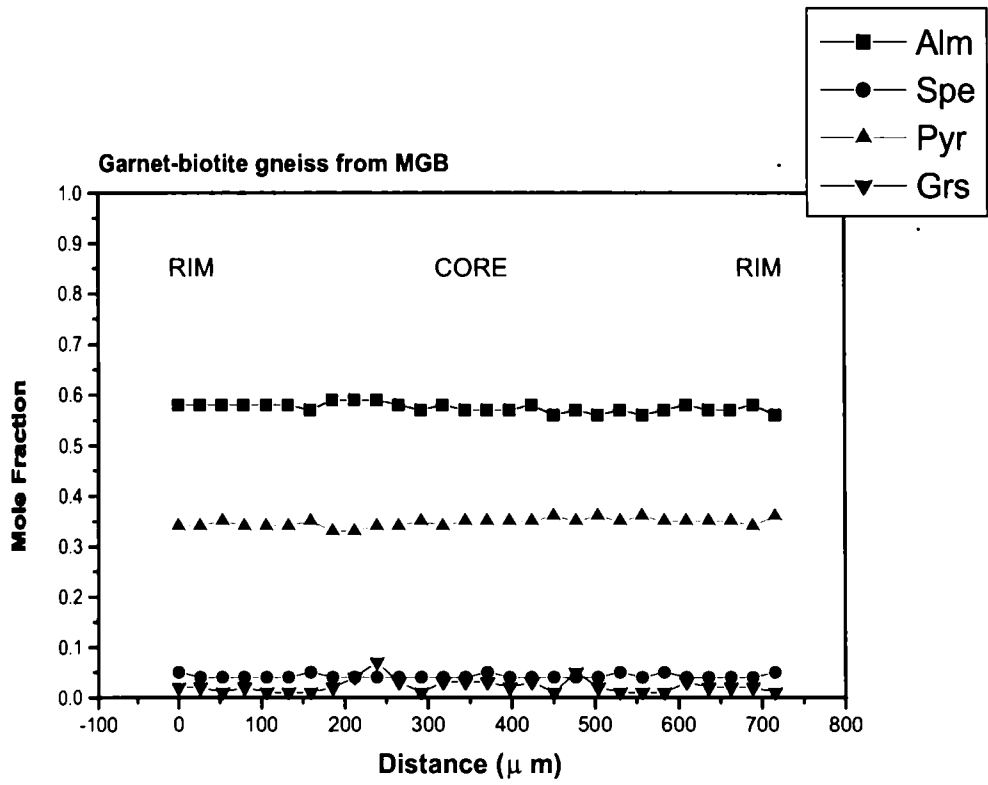


Fig. 4.9 Variation in garnet composition from rim to core (Sample: CK37)

**Table 4.5 Representative microprobe data of garnets from Charnockite in ACS**

	core	rim	core	rim	core	rim	core	rim
SiO <sub>2</sub>	39.886	39.470	39.673	40.040	39.045	39.870	39.893	40.309
TiO <sub>2</sub>	0.089	0.065	0.048	0.065	0.048	0.077	0.071	0.058
Al <sub>2</sub> O <sub>3</sub>	20.511	21.818	20.982	21.970	21.115	22.313	22.404	22.374
Cr <sub>2</sub> O <sub>3</sub>	0.018	0.000	0.006	0.038	0.000	0.000	0.033	0.003
FeO	26.792	26.750	26.786	27.333	27.511	26.959	26.847	27.767
MnO	2.564	2.313	2.535	2.358	2.495	2.299	2.584	2.443
MgO	8.219	7.886	8.100	8.030	8.176	8.272	8.171	7.941
CaO	0.926	0.977	0.975	0.967	0.949	0.929	1.006	1.022
Na <sub>2</sub> O	0.002	0.022	0.000	0.003	0.000	0.012	0.019	0.010
K <sub>2</sub> O	0.015	0.026	0.029	0.023	0.024	0.022	0.021	0.024
ZnO	0.000	0.000	0.000	0.000	0.000	0.000	0.000	0.000
<b>Total</b>	<b>99.022</b>	<b>99.327</b>	<b>99.134</b>	<b>100.827</b>	<b>99.363</b>	<b>100.753</b>	<b>101.049</b>	<b>101.951</b>
O	12.000	12.000	12.000	12.000	12.000	12.000	12.000	12.000
Si	3.108	3.060	3.087	3.061	3.046	3.044	3.040	3.052
Ti	0.005	0.004	0.003	0.004	0.003	0.004	0.004	0.003
Al	1.884	1.994	1.925	1.980	1.941	2.008	2.012	1.996
Cr	0.001	0.000	0.000	0.002	0.000	0.000	0.002	0.000
Fe	1.746	1.734	1.743	1.748	1.795	1.722	1.711	1.758
Mn	0.169	0.152	0.167	0.153	0.165	0.149	0.167	0.157
Mg	0.954	0.911	0.939	0.915	0.951	0.941	0.928	0.896
Ca	0.077	0.081	0.081	0.079	0.079	0.076	0.082	0.083
Na	0.000	0.003	0.000	0.000	0.000	0.002	0.003	0.001
K	0.001	0.003	0.003	0.002	0.002	0.002	0.002	0.002
Zn	0.000	0.000	0.000	0.000	0.000	0.000	0.000	0.000
<b>Total Cation</b>	<b>7.946</b>	<b>7.942</b>	<b>7.949</b>	<b>7.945</b>	<b>7.982</b>	<b>7.949</b>	<b>7.951</b>	<b>7.949</b>
Fe <sup>3+</sup>	0.003	0.000	0.000	0.000	0.010	0.000	0.000	0.000
Fe <sup>2+</sup>	1.743	1.734	1.743	1.748	1.785	1.722	1.711	1.758
Fe <sup>3+</sup> /Fe <sup>2+</sup>	0.001	0.000	0.000	0.000	0.006	0.000	0.000	0.000
Alm	0.592	0.603	0.595	0.604	0.599	0.596	0.592	0.608
Spe	0.057	0.053	0.057	0.053	0.055	0.051	0.058	0.054
Pyr	0.324	0.317	0.320	0.316	0.319	0.326	0.321	0.310
Grs	0.023	0.026	0.026	0.026	0.021	0.024	0.027	0.027
Adr	0.004	0.002	0.001	0.002	0.005	0.002	0.002	0.002
XMg*	0.354	0.344	0.350	0.344	0.347	0.353	0.352	0.338
XMg	0.353	0.344	0.350	0.344	0.346	0.353	0.352	0.338

\*The entire data is given in Appendix IIIe

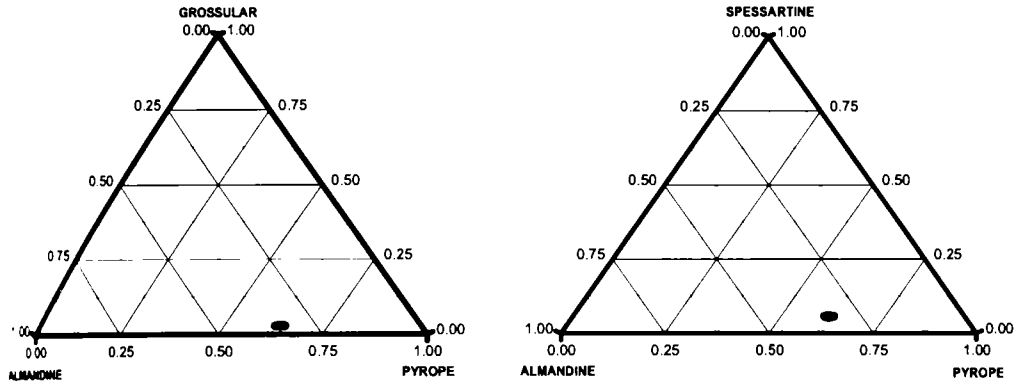


Fig. 4.10 Garnet composition from charnockite of the ACS

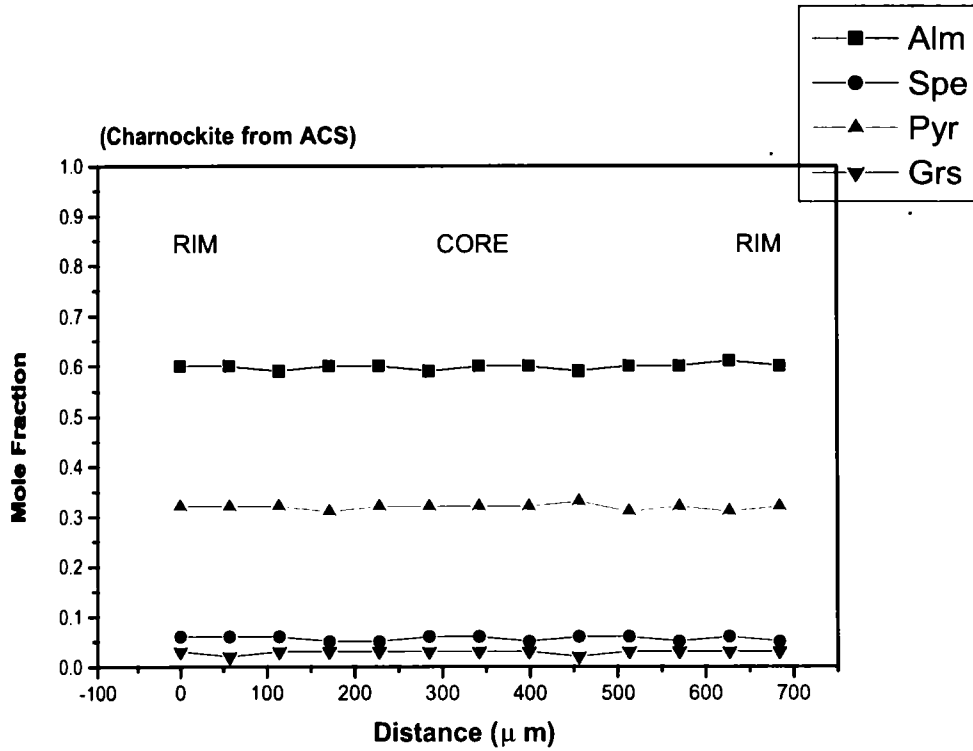
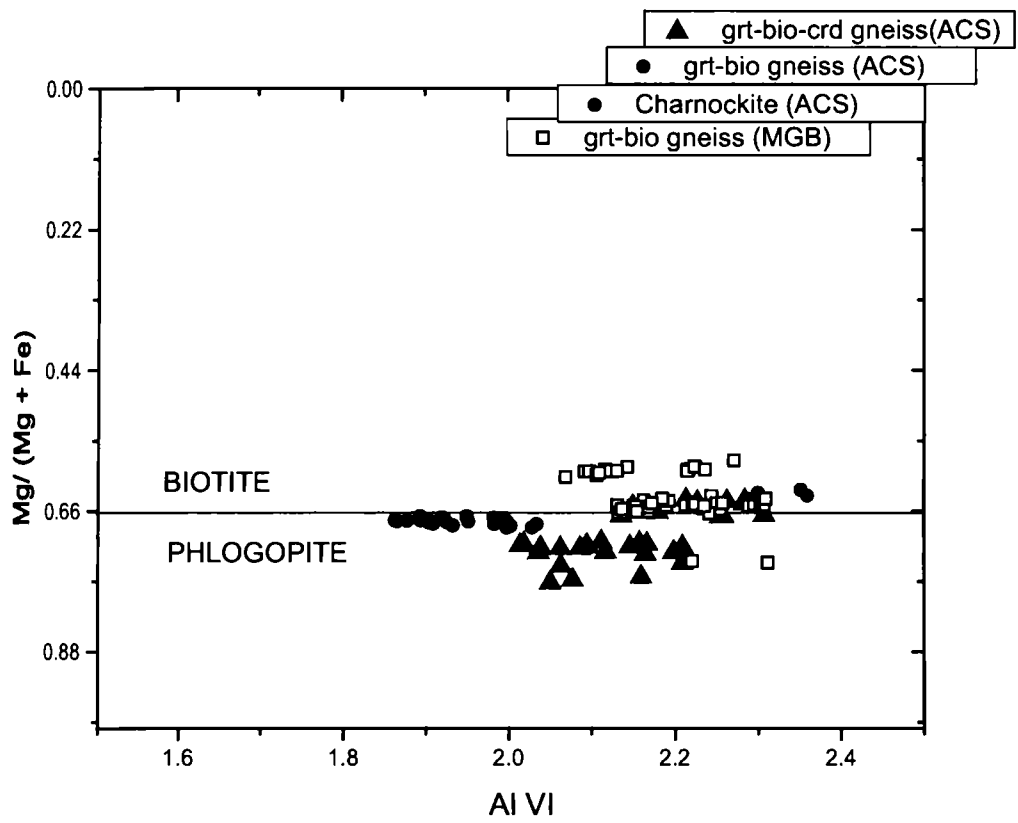


Fig. 4.11 Variation in garnet composition from rim to core (Sample: CK40)

and Spear, 2005) in these samples. The total calcium composition ( $X_{Ca}$ ) from these samples is also comparatively higher (mostly above 0.03) than the other samples. This type of conditions is identified as evidence for differential timing of garnet nucleation and growth (Storm and Spear, 2005).

Biotite is a major constituent mineral in most of the rocks selected for EPMA. For a comparative study, the entire biotite compositions are plotted in the "ideal biotite plane" diagram of Guidotti (1984) (Fig 4.12). Arbitrary division between phlogopites and biotites ( $Mg:Fe = 2:1$ ) are taken from Deer et al. (1966). From the figure it is noticed that most of the mica under study are in the biotite-phlogopite boundary with comparatively high  $Al^{IV}$  content. The  $X_{Mg}$  of biotite shows a range of 0.58-0.77 and the higher ranges of  $X_{Mg}$  are shown by the biotites, which are occurring as inclusions in garnet and as remnants in reaction zones. Moderate water activities are suggested by the estimated  $H_2O$  content in all the analysed biotites ( $H_2O^* = 3.9-4.2$  wt%) (Table 4.6). The Ti content in some of the biotites especially from sample CK 16 (0.548-0.6) and CK 40 (0.594-0.603) show comparatively depleted values indicating that they are secondary in origin where as in other biotites the Ti ranges between 0.604- 0.696 (Fig. 4.13). Very meager amount of chromium is present in the biotites of all locations but even then they show variations with respect to the presence of spinel in the country rock. Generally  $Cr_2O_3$  ranges from 0-0.3wt%.

Plagioclase occurs as a subordinate phase in most of the rock types under this study except in the tonalitic gneiss. In comparison most of them are albite rich, and are labradorites (An percentage 50-70). The alkali feldspars found in some of the samples especially in metapelites from the



**Fig 4.12 Biotite compositions plotted in the "ideal biotite plane" diagram of Guidotti (1984). Arbitrary division between phlogopites and biotites (Mg:Fe = 2:1) are taken from Deer et al. (1966).**

**Table 4.6 Representative microprobe data of biotites**

	grt-bio gneiss (MGB)		grt-bio gneiss (ACS)		grt-bio-crd gneiss (ACS)		charnockite (ACS)	
SiO <sub>2</sub>	37.493	37.783	37.336	37.583	36.926	36.311	37.777	37.094
TiO <sub>2</sub>	5.836	5.855	5.678	5.714	5.787	5.742	5.246	5.474
Al <sub>2</sub> O <sub>3</sub>	14.534	14.161	15.721	15.153	14.384	14.614	16.575	16.589
Cr <sub>2</sub> O <sub>3</sub>	0.229	0.225	0.129	0.155	0.163	0.105	0.000	0.024
FeO	15.457	15.512	11.279	11.409	13.190	13.539	14.286	14.160
MnO	0.026	0.041	0.174	0.148	0.167	0.179	0.067	0.080
MgO	12.892	12.945	15.817	16.241	15.484	15.294	13.470	13.594
CaO	0.029	0.045	0.133	0.121	0.143	0.139	0.043	0.042
Na <sub>2</sub> O	0.127	0.149	0.134	0.128	0.231	0.226	0.023	0.019
K <sub>2</sub> O	9.189	9.280	9.492	9.323	9.799	9.850	9.532	9.606
F	0.000	0.000	0.000	0.000	0.000	0.000	0.000	0.000
Cl	0.000	0.000	0.000	0.000	0.000	0.000	0.000	0.000
F=O	0.000	0.000	0.000	0.000	0.000	0.000	0.000	0.000
Cl=O	0.000	0.000	0.000	0.000	0.000	0.000	0.000	0.000
Total	95.812	95.996	95.893	95.975	96.274	95.999	97.019	96.682
H <sub>2</sub> O*	4.032	4.037	4.106	4.111	4.063	4.038	4.116	4.093
Total*	99.844	100.033	99.999	100.086	100.337	100.037	101.135	100.775
Si	5.577	5.613	5.453	5.483	5.450	5.392	5.505	5.435
Ti	0.653	0.654	0.624	0.627	0.642	0.641	0.575	0.603
Al	2.548	2.479	2.706	2.605	2.502	2.558	2.846	2.865
Cr	0.027	0.026	0.015	0.018	0.019	0.012	0.000	0.003
Fe	1.922	1.927	1.377	1.392	1.628	1.681	1.741	1.735
Mn	0.003	0.005	0.022	0.018	0.021	0.023	0.008	0.010
Mg	2.859	2.867	3.444	3.532	3.407	3.386	2.926	2.970
Ca	0.005	0.007	0.021	0.019	0.023	0.022	0.007	0.007
Na	0.037	0.043	0.038	0.036	0.066	0.065	0.006	0.005
K	1.743	1.759	1.768	1.735	1.845	1.866	1.772	1.795
O	22.000	22.000	22.000	22.000	22.000	22.000	22.000	22.000
F	0.000	0.000	0.000	0.000	0.000	0.000	0.000	0.000
Cl	0.000	0.000	0.000	0.000	0.000	0.000	0.000	0.000
OH	4.000	4.000	4.000	4.000	4.000	4.000	4.000	4.000
XMg*	0.778	0.778	0.853	0.854	0.830	0.826	0.795	0.799
XMg	0.598	0.598	0.714	0.717	0.677	0.668	0.627	0.631
XFe	0.402	0.402	0.286	0.283	0.323	0.332	0.373	0.369

\* The entire data is given in Appendix IIIf

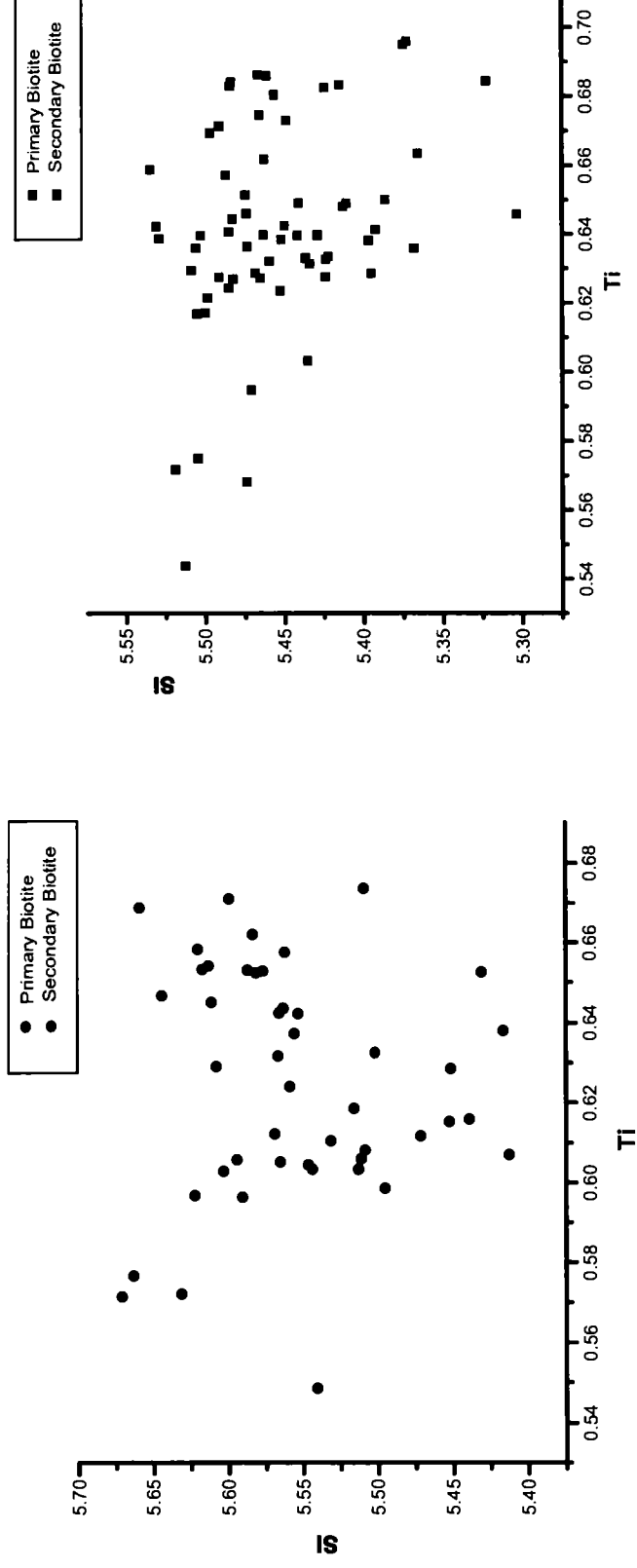


**Fig. 4.13 Si vs Ti plot for biotites showing primary and secondary biotites in the samples from MGB and ACS**

ACS, is orthoclase (~90%) with minor amount of albite (Table 4.7) (Fig 4.14).

Orthopyroxenes from both the group of samples show hypersthene chemistry with  $X_{Mg}$  ranging from 0.55-0.61 and low contents of Ti, Mn and Ca. The total Al ( $X_{Al}$ ) in cations show considerable anomaly between the metapelitic rock of the ACS and the two-pyroxene granulite rock from the MGB. Obviously the later show very low aluminum content (0.018-0.032). Even in the ACS sample the  $X_{Al}$  ranges from 0.13-0.15 (Table 4.8). Clinopyroxenes are found only in the MGB locations. Compositionally the Cpx from the two-pyroxene granulite are salite or augite, whereas in some other locations it is showing compositions of ferrosalite or ferroaugite (Table 4.9) (Fig 4.15).

The amphiboles are found in the MGB samples only. They belong to the calcium amphibole sub group (hornblende), where the  $Ca > Na$ . The CaO ranges from 10.7 –11.9 wt% and  $Na_2O$  ranges between 1.5 and 1.9 wt% (Table 4.10).

As the reaction texture says cordierites can be treated as of secondary origin and is only found in the metapelitic rock (garnet-biotite-cordierite gneiss) from the ACS. The  $X_{Mg}$  values do not show much variation but the total oxide weight percentage varies considerably reflecting the role of volatiles. Cordierites forming simplectite with quartz and biotites exhibit a very low oxide total (97.427 wt%) suggesting high volatile content within the crystal structure (Table 4.11).

Spinel is present in garnet-biotite gneisses (metapelites) from both the MGB and the ACS. Only green spinel (hercynite) is noticed from



**Table 4.7 Representative microprobe data of feldspars**

	Mafic granulite (MGB)		Grt-bio gneiss (MGB)		Charnockite (MGB)		Grt-bio-crld gneiss (ACS)		Charnockite (ACS)	
SiO <sub>2</sub>	57.186	57.693	61.848	61.728	60.514	60.622	60.784	64.266	61.745	61.935
TiO <sub>2</sub>	0.000	0.000	0.000	0.000	0.252	0.258	0.021	0.045	0.000	0.017
Al <sub>2</sub> O <sub>3</sub>	28.313	27.232	23.202	23.551	24.269	22.924	24.875	20.344	23.608	24.322
Cr <sub>2</sub> O <sub>3</sub>	0.000	0.000	0.000	0.000	0.108	0.120	0.042	0.000	0.000	0.000
FeO	0.097	0.145	0.028	0.068	0.209	0.399	0.045	0.047	0.033	0.067
MnO	0.000	0.000	0.002	0.000	0.131	0.109	0.014	0.027	0.011	0.000
MgO	0.010	0.013	0.017	0.011	0.062	0.070	0.009	0.001	0.000	0.010
CaO	9.322	9.476	5.889	6.068	7.757	7.416	6.223	0.126	5.549	5.570
Na <sub>2</sub> O	5.968	6.023	7.923	7.825	7.118	7.166	7.728	0.901	7.700	7.745
K <sub>2</sub> O	0.345	0.358	0.217	0.149	0.318	0.259	0.510	14.607	0.701	0.786
<b>Total</b>	<b>101.241</b>	<b>100.940</b>	<b>99.126</b>	<b>99.400</b>	<b>100.738</b>	<b>99.343</b>	<b>100.251</b>	<b>100.36</b>	<b>99.347</b>	<b>100.452</b>
O	8.000	8.000	8.000	8.000	8.000	8.000	8.000	8.000	8.000	8.000
Si	2.534	2.566	2.766	2.753	2.686	2.726	2.699	2.939	2.758	2.738
Ti	0.000	0.000	0.000	0.000	0.008	0.009	0.001	0.002	0.000	0.001
Al	1.479	1.427	1.223	1.238	1.270	1.215	1.302	1.096	1.243	1.267
Cr	0.000	0.000	0.000	0.000	0.004	0.004	0.001	0.000	0.000	0.000
Fe	0.004	0.005	0.001	0.003	0.008	0.015	0.002	0.002	0.001	0.002
Mn	0.000	0.000	0.000	0.000	0.005	0.004	0.001	0.001	0.000	0.000
Mg	0.001	0.001	0.001	0.001	0.004	0.005	0.001	0.000	0.000	0.001
Ca	0.443	0.452	0.282	0.290	0.369	0.357	0.296	0.006	0.266	0.264
Na	0.513	0.519	0.687	0.677	0.613	0.625	0.665	0.080	0.667	0.664
K	0.020	0.020	0.012	0.008	0.018	0.015	0.029	0.852	0.040	0.044
<b>Total cation</b>	<b>4.992</b>	<b>4.990</b>	<b>4.972</b>	<b>4.970</b>	<b>4.984</b>	<b>4.975</b>	<b>4.996</b>	<b>4.978</b>	<b>4.974</b>	<b>4.982</b>
An	0.454	0.456	0.287	0.297	0.369	0.358	0.299	0.007	0.273	0.271
Ab	0.526	0.524	0.700	0.694	0.613	0.627	0.672	0.085	0.686	0.683
Or	0.020	0.020	0.013	0.009	0.018	0.015	0.029	0.908	0.041	0.046

\* The entire data is given in Appendix IIIg

**Table 4.8 Representative microprobe data of Orthopyroxenes**

	<b>Mafic granulite (MGB)</b>				<b>Charnockite (ACS)</b>			
	core	rim	core	rim	core	rim	core	rim
SiO <sub>2</sub>	52.856	52.235	54.380	53.738	49.208	49.658	48.931	48.883
TiO <sub>2</sub>	0.092	0.088	0.111	0.111	0.182	0.161	0.172	0.170
Al <sub>2</sub> O <sub>3</sub>	1.193	1.145	1.141	0.811	6.811	6.244	6.823	6.761
Cr <sub>2</sub> O <sub>3</sub>	0.000	0.000	0.000	0.000	0.000	0.031	0.006	0.001
FeO	24.633	24.143	24.227	23.973	25.112	24.863	25.389	24.953
MnO	0.754	0.720	0.835	0.713	0.634	0.689	0.731	0.767
MgO	20.191	20.415	19.888	20.728	17.680	17.986	17.465	17.481
CaO	0.693	0.619	0.649	0.561	0.113	0.097	0.087	0.122
Na <sub>2</sub> O	0.014	0.029	0.027	0.011	0.000	0.017	0.000	0.003
K <sub>2</sub> O	0.032	0.021	0.019	0.015	0.024	0.024	0.020	0.014
<b>Total</b>	<b>100.458</b>	<b>99.415</b>	<b>101.277</b>	<b>100.661</b>	<b>99.764</b>	<b>99.770</b>	<b>99.624</b>	<b>99.155</b>
O	6.000	6.000	6.000	6.000	6.000	6.000	6.000	6.000
Si	1.981	1.977	2.011	2.000	1.860	1.874	1.856	1.860
Ti	0.003	0.003	0.003	0.003	0.005	0.005	0.005	0.005
Al	0.053	0.051	0.050	0.036	0.303	0.278	0.305	0.303
Cr	0.000	0.000	0.000	0.000	0.000	0.001	0.000	0.000
Fe	0.772	0.764	0.749	0.746	0.794	0.785	0.805	0.794
Mn	0.024	0.023	0.026	0.022	0.020	0.022	0.023	0.025
Mg	1.128	1.151	1.096	1.150	0.996	1.012	0.987	0.991
Ca	0.028	0.025	0.026	0.022	0.005	0.004	0.004	0.005
Na	0.001	0.002	0.002	0.001	0.000	0.001	0.000	0.000
K	0.002	0.001	0.001	0.001	0.001	0.001	0.001	0.001
<b>Total cation</b>	<b>3.991</b>	<b>3.997</b>	<b>3.963</b>	<b>3.980</b>	<b>3.984</b>	<b>3.983</b>	<b>3.987</b>	<b>3.984</b>
Al <sup>IV</sup>	0.014	0.022	-0.029	-0.010	0.133	0.117	0.138	0.133
Al <sup>VI</sup>	0.039	0.029	0.080	0.045	0.172	0.162	0.168	0.172
Al <sup>6</sup> /Al <sup>4</sup>	2.696	1.340	-2.712	-4.732	1.295	1.375	1.220	1.297
Al <sup>6</sup> /Al <sup>T</sup>	0.731	0.573	1.599	1.274	0.567	0.581	0.551	0.567
X <sub>Al</sub>	0.026	0.026	0.025	0.018	0.152	0.139	0.153	0.152
Fe <sup>3+</sup>	-0.027	-0.009	-0.112	-0.060	-0.048	-0.052	-0.039	-0.048
Fe <sup>2+</sup>	0.799	0.773	0.861	0.806	0.842	0.837	0.845	0.842
Fe <sup>3+</sup> /Fe <sup>2+</sup>	-0.034	-0.012	-0.130	-0.074	-0.057	-0.062	-0.047	-0.057
Fe <sup>3+</sup> /Fe <sup>T</sup>	-0.035	-0.012	-0.150	-0.080	-0.061	-0.066	-0.049	-0.061
X <sub>Mg</sub> <sup>+</sup>	0.585	0.598	0.560	0.588	0.542	0.547	0.539	0.541
X <sub>Mg</sub>	0.594	0.601	0.594	0.606	0.556	0.563	0.551	0.555
Fs	0.400	0.393	0.400	0.389	0.442	0.436	0.448	0.443
En	0.585	0.593	0.585	0.599	0.555	0.562	0.550	0.554
Wo	0.014	0.013	0.014	0.012	0.003	0.002	0.002	0.003
Ac	0.001	0.001	0.001	0.000	0.000	0.001	0.000	0.000

\*The entire data is given in Appendix IIIh

**Table 4.9 Representative microprobe data of clinopyroxenes**

	<b>Mafic granulite (MGB)</b>				<b>Charnockite (MGB)</b>			
SiO <sub>2</sub>	52.961	53.231	53.089	52.587	48.866	48.982	49.209	49.441
TiO <sub>2</sub>	0.323	0.271	0.210	0.326	0.509	0.526	0.488	0.481
Al <sub>2</sub> O <sub>3</sub>	2.287	2.004	1.610	2.247	1.183	1.035	1.143	1.004
Cr <sub>2</sub> O <sub>3</sub>	0.006	0.000	0.019	0.001	0.149	0.143	0.147	0.122
FeO	10.585	9.414	8.911	10.040	23.299	22.460	23.798	23.764
MnO	0.292	0.317	0.324	0.290	0.741	0.700	0.688	0.653
MgO	13.277	13.352	13.323	12.821	4.470	4.503	4.287	4.434
CaO	21.108	22.550	22.441	21.725	19.525	20.309	19.687	20.306
Na <sub>2</sub> O	0.481	0.446	0.444	0.522	0.373	0.337	0.368	0.339
K <sub>2</sub> O	0.016	0.022	0.025	0.023	0.111	0.101	0.113	0.095
<b>Total</b>	<b>101.336</b>	<b>101.607</b>	<b>100.396</b>	<b>100.582</b>	<b>99.226</b>	<b>99.096</b>	<b>99.928</b>	<b>100.639</b>
O	6.000	6.000	6.000	6.000	6.000	6.000	6.000	6.000
Si	1.956	1.959	1.973	1.957	1.969	1.972	1.972	1.968
Ti	0.009	0.007	0.006	0.009	0.015	0.016	0.015	0.014
Al	0.100	0.087	0.071	0.099	0.056	0.049	0.054	0.047
Cr	0.000	0.000	0.001	0.000	0.005	0.005	0.005	0.004
Fe	0.327	0.290	0.277	0.313	0.785	0.756	0.797	0.791
Mn	0.009	0.010	0.010	0.009	0.025	0.024	0.023	0.022
Mg	0.731	0.732	0.738	0.711	0.268	0.270	0.256	0.263
Ca	0.835	0.889	0.894	0.867	0.843	0.876	0.845	0.866
Na	0.034	0.032	0.032	0.038	0.029	0.026	0.029	0.026
K	0.001	0.001	0.001	0.001	0.006	0.005	0.006	0.005
<b>Total cation</b>	<b>4.003</b>	<b>4.007</b>	<b>4.002</b>	<b>4.003</b>	<b>4.002</b>	<b>4.000</b>	<b>4.001</b>	<b>4.007</b>
Al <sup>IV</sup>	0.045	0.045	0.028	0.044	0.032	0.028	0.029	0.035
Al <sup>VI</sup>	0.054	0.042	0.043	0.054	0.024	0.021	0.025	0.012
Al <sup>6</sup> /Al <sup>4</sup>	1.210	0.944	1.526	1.228	0.754	0.771	0.860	0.335
Al <sup>6</sup> /Al <sup>T</sup>	0.547	0.485	0.604	0.551	0.430	0.435	0.462	0.251
X <sup>Al</sup>	0.050	0.043	0.035	0.049	0.028	0.025	0.027	0.024
Fe <sup>3+</sup>	0.008	0.020	0.006	0.010	0.007	0.001	0.004	0.022
Fe <sup>2+</sup>	0.319	0.269	0.271	0.302	0.778	0.755	0.793	0.769
Fe <sup>3+</sup> /Fe <sup>2+</sup>	0.024	0.076	0.023	0.034	0.009	0.002	0.005	0.028
Fe <sup>3+</sup> /Fe <sup>T</sup>	0.023	0.070	0.022	0.033	0.009	0.002	0.005	0.028
X <sup>Mg*</sup>	0.696	0.731	0.732	0.702	0.257	0.264	0.244	0.255
X <sup>Mg</sup>	0.691	0.717	0.727	0.695	0.255	0.263	0.243	0.250
Fs	0.170	0.149	0.143	0.162	0.408	0.392	0.414	0.406
En	0.379	0.377	0.380	0.369	0.139	0.140	0.133	0.135
Wo	0.433	0.458	0.461	0.449	0.438	0.454	0.439	0.445
Ac	0.018	0.016	0.016	0.020	0.015	0.014	0.015	0.013

\* The complete data is given in Appendix IIIi

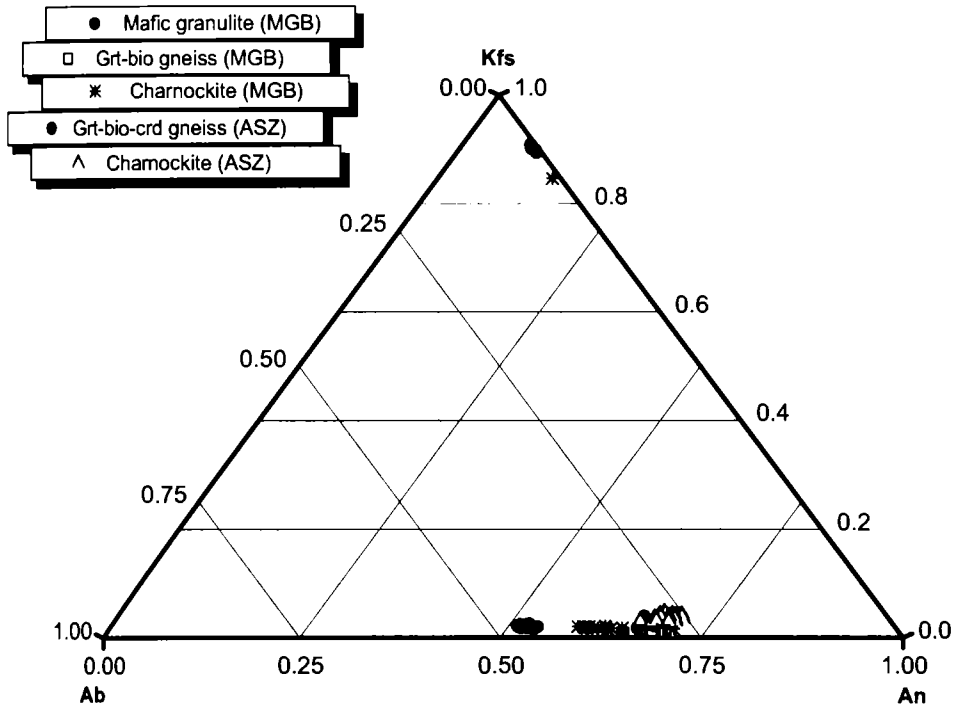


Fig. 4.14 Feldspar composition from different rocks of MGB & ACS

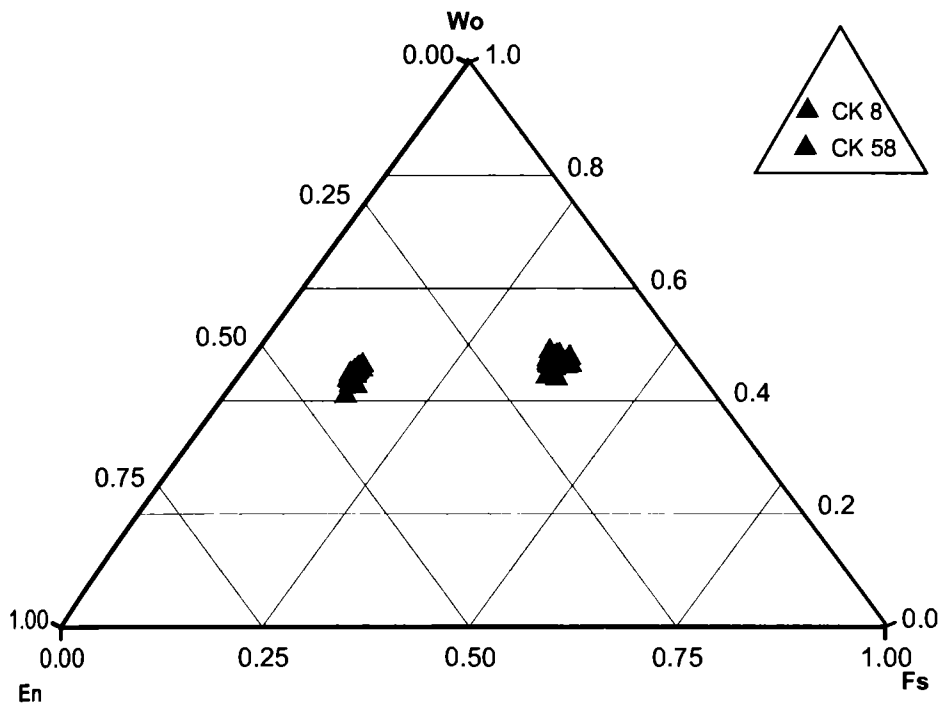


Fig. 4.15 Clinopyroxene composition from the granulites of MGB

**Table 4.10 Representative microprobe data for hornblende**

	<b>Mafic granulite (MGB)</b>				<b>Charnockite (MGB)</b>			
SiO <sub>2</sub>	45.618	45.938	45.197	45.800	41.971	41.214	41.280	41.358
TiO <sub>2</sub>	2.187	2.396	2.423	2.493	2.857	2.854	2.908	2.953
Al <sub>2</sub> O <sub>3</sub>	10.264	10.827	11.230	11.276	10.113	10.028	10.091	9.841
Cr <sub>2</sub> O <sub>3</sub>	0.003	0.020	0.020	0.010	0.091	0.120	0.169	0.109
FeO	13.963	14.416	14.672	14.774	26.300	27.288	27.417	27.564
MnO	0.150	0.150	0.178	0.178	0.437	0.416	0.378	0.478
MgO	11.964	11.554	11.421	11.233	2.834	2.888	2.761	2.841
CaO	11.862	11.713	11.413	11.541	10.814	10.801	10.672	10.791
Na <sub>2</sub> O	1.549	1.708	1.816	1.844	1.627	1.645	1.668	1.742
K <sub>2</sub> O	1.320	1.206	1.198	1.237	2.065	2.138	2.042	2.154
<b>Total</b>	<b>98.880</b>	<b>99.928</b>	<b>99.568</b>	<b>100.386</b>	<b>99.109</b>	<b>99.392</b>	<b>99.386</b>	<b>99.831</b>
O	23.000	23.000	23.000	23.000	23.000	23.000	23.000	23.000
Si	6.663	6.641	6.549	6.599	6.554	6.466	6.473	6.471
Ti	0.240	0.261	0.264	0.270	0.336	0.337	0.343	0.348
Al	1.767	1.845	1.918	1.915	1.861	1.854	1.865	1.815
Cr	0.000	0.002	0.002	0.001	0.011	0.015	0.021	0.013
Fe <sup>3+</sup>	0.029	0.020	0.179	0.040	0.000	0.000	0.000	0.000
Fe <sup>2+</sup>	1.677	1.723	1.599	1.740	3.434	3.580	3.595	3.606
Mn	0.019	0.018	0.022	0.022	0.058	0.055	0.050	0.063
Mg	2.605	2.490	2.467	2.413	0.660	0.676	0.645	0.663
Ca	1.856	1.814	1.772	1.782	1.809	1.815	1.793	1.809
Na	0.439	0.479	0.510	0.515	0.493	0.500	0.507	0.528
K	0.246	0.222	0.221	0.227	0.411	0.428	0.408	0.430
Zr	0.000	0.000	0.000	0.000	0.000	0.000	0.000	0.000
<b>TOTAL</b>	<b>15.541</b>	<b>15.515</b>	<b>15.503</b>	<b>15.524</b>	<b>15.626</b>	<b>15.727</b>	<b>15.699</b>	<b>15.746</b>

\* The complete data is given in Appendix IIIj

**Table 4.11 Microprobe data of cordierites**

	<b>Cordierite</b>	<b>Cordierite</b>	<b>Cordierite Symplectite</b>
SiO2	50.185	50.680	48.636
TiO2	0.163	0.127	0.192
Al2O3	35.901	36.039	33.881
Cr2O3	0.000	0.000	0.000
FeO	3.155	3.116	3.053
MnO	0.186	0.090	0.083
MgO	11.553	11.404	11.392
CaO	0.055	0.056	0.066
Na2O	0.067	0.026	0.073
K2O	0.002	0.000	0.004
ZnO	0.000	0.000	0.000
<b>Total</b>	<b>101.267</b>	<b>101.538</b>	<b>97.380</b>
O	18.000	18.000	18.000
Si	4.903	4.930	4.940
Ti	0.012	0.009	0.015
Al	4.135	4.132	4.056
Cr	0.000	0.000	0.000
Fe	0.258	0.254	0.259
Mn	0.015	0.007	0.007
Mg	1.682	1.653	1.725
Ca	0.006	0.006	0.007
Na	0.013	0.005	0.014
K	0.000	0.000	0.001
Zn	0.000	0.000	0.000
<b>Total cation</b>	<b>11.024</b>	<b>10.997</b>	<b>11.024</b>
Fe3+	0.000	0.000	0.018
Fe2+	0.258	0.254	0.241
Fe3+/Fe2+	0.000	0.000	0.075
XMg <sup>+</sup>	0.867	0.867	0.877
XMg	0.867	0.867	0.869

all the locations. These are found in association with cordierites, sometimes forming intergrowth textures mainly concentrated in the proximity of garnets. Garnets with inclusions of spinel also found common. The cordierite bearing gneisses show comparatively higher  $X_{Mg}$  values (0.47-0.49) for spinel, whereas the Fe amount is found less (Table 4.12). The  $Fe^{3+}$  content is higher in spinels enclosed in garnets, which gives an inference that there exists a higher oxidation state for spinel inclusions than the spinels in matrix.

The opaque phases are found in all the samples analysed by microprobe. They generally show the composition of ilmenite and locally ilmenite-magnetite solid solution.

#### **4.7 COMPARISON OF THE MINERAL CHEMISTRY OF PRESENT ROCKS WITH SIMILAR ROCKS FROM ADJACENT TERRAINS**

Comparison of the mineral chemistry of the present study and similar rocks from previous works in the area as well as in the adjacent blocks can give a better picture to elucidate the conditions of metamorphism. This type of attempt is made in the following session.

Garnet: Studies on progressive charnockitization in KKB by Srikantappa et al. (1985) bring out the similarity in chemistry of garnets present in both the charnockites as well as the precursor leptinites and that they are rich in almandine component. The gradual increase in the grossular component as the almandine content increases is explained to be due to the non-ideality of the Fe-Ca exchange (Ganguly and Kennedy, 1974). Garnets from the metapelites of Madagascar are also rich in

Table 4.12 Microprobe data of spinels

	Grt-Bio gneiss (MGB)		Grt-Crd-Bio gneiss (ACS)				Grt-Bio gneiss (ACS)	
	Spl in Grt	Spl in Grt	Spl	Spl	Spl	Spl	Spl	Spl
SiO2	0.000	0.000	0.162	0.163	0.170	0.164	0.165	0.165
TiO2	0.081	0.051	0.334	0.693	0.300	0.285	0.346	0.308
Al2O3	57.195	57.597	61.677	61.862	60.359	60.279	58.131	58.687
Cr2O3	0.443	0.448	0.545	0.470	0.460	0.398	0.452	0.397
FeO	32.814	32.600	24.124	24.365	25.320	25.124	32.739	32.166
MnO	0.043	0.055	0.286	0.291	0.388	0.344	0.378	0.341
MgO	7.843	8.120	12.814	11.896	12.736	12.831	6.845	6.759
CaO	0.040	0.053	0.139	0.145	0.132	0.150	0.144	0.158
Na2O	0.061	0.091	0.183	0.192	0.222	0.201	0.204	0.198
K2O	0.015	0.021	0.090	0.093	0.094	0.096	0.090	0.090
ZnO	0.000	0.000	0.000	0.000	0.000	0.200	0.000	0.000
Total	98.535	99.036	100.354	100.170	100.181	100.072	99.494	99.269
O	4.000	4.000	4.000	4.000	4.000	4.000	4.000	4.000
Si	0.000	0.000	0.004	0.004	0.005	0.004	0.005	0.005
Ti	0.002	0.001	0.007	0.014	0.006	0.006	0.007	0.006
Al	1.912	1.912	1.933	1.944	1.910	1.910	1.924	1.939
Cr	0.010	0.010	0.011	0.010	0.010	0.008	0.010	0.009
Fe	0.778	0.768	0.537	0.543	0.569	0.565	0.769	0.754
Mn	0.001	0.001	0.006	0.007	0.009	0.008	0.009	0.008
Mg	0.331	0.341	0.508	0.473	0.510	0.514	0.286	0.282
Ca	0.001	0.002	0.004	0.004	0.004	0.004	0.004	0.005
Na	0.003	0.005	0.009	0.010	0.012	0.010	0.011	0.011
K	0.001	0.001	0.003	0.003	0.003	0.003	0.003	0.003
Zn	0.000	0.000	0.000	0.000	0.000	0.004	0.000	0.000
Total cation	3.039	3.041	3.023	3.011	3.037	3.033	3.028	3.022
Fe3+	0.104	0.107	0.061	0.030	0.097	0.092	0.075	0.058
Fe2+	0.675	0.661	0.476	0.513	0.472	0.473	0.694	0.696
Fe3+/Fe2+	0.154	0.162	0.127	0.059	0.204	0.195	0.108	0.084
XMg	0.299	0.307	0.486	0.465	0.473	0.476	0.271	0.272
XMg*	0.329	0.340	0.516	0.480	0.519	0.521	0.292	0.289
YCr	0.005	0.005	0.006	0.005	0.005	0.004	0.005	0.004
YAl	0.944	0.942	0.964	0.980	0.947	0.950	0.958	0.967
YFe3	0.051	0.053	0.030	0.015	0.048	0.046	0.037	0.029
Cr#	0.005	0.005	0.006	0.005	0.005	0.004	0.005	0.005



almandine content and is having Mg enriched core and Fe rich rim (Markl *et al.*, 2000). Similar are the chemistry of garnets analysed in the present.

Biotite: The high  $X_{Fe}$  ratios noticed in the biotites in the leptinites and charnockites of KKB are due to the strong reducing conditions of metamorphism, which resulted in the formation of opaque mineral assemblage of graphite, ilmenite and pyrrhotite (Srikantappa *et al.*, 1985). Comparatively the biotites in the leptinites have lesser Fe than the biotites in charnockites. The biotites from South Madagascar metapelites are Al and Ti rich. Ti is positively correlated with  $X_{Fe}$  (Markl *et al.*, 2000). In the present samples also high Ti is noted in the primary biotites from MGB as well as ACS, but Ti depletion is noted in secondary biotites. These types of occurrences are also reported earlier elsewhere in KKB (Shabeer, 2004).

Orthopyroxenes: The orthopyroxenes from KKB charnockites are mostly ferrohypersthene with significant higher Fe ratios when compared with the orthopyroxenes of similar metamorphic grade (Srikantappa *et al.*, 1985). The Al content but shows a good positive correlation with  $X_{Mg}$  and the Ca, Mn, Ti, Cr contents are very low. In the present studied samples orthopyroxenes are mostly ferrohypersthene but with comparatively high Al content (0.27-0.3)

Feldspars: The rocks from KKB show unzoned plagioclase with less effects of alteration. The alkali-feldspars show a variety of exsolution micro textures (Srikantappa *et al.*, 1985). This shows almost similar characteristics with the feldspars in the present study.

Cordierites: The Madagascar cordierites, are unzoned and Mg rich with  $X_{Fe}$  ranging between 0.21-0.35. It does not show the presence of any

fluid species since most of the total reach values are >99% (Markl *et al.*, 2000). The cordierites in and around ACS studied by Santosh (1987) gives  $X_{Mg}$  values ranging from 0.78-0.83. It is having analytical totals less than 100% indicating the presence of channel filling molecular species such as H<sub>2</sub>O or CO<sub>2</sub>. The cordierites in the present study also resemble the samples of Santosh (1987), but the influence of fluid species is noted.

#### 4.8 P-T ESTIMATION

The peak thermobarometric conditions for granulites are found in a range of 700-1000°C and 4-12kb (Newton and Perkins, 1982; Bohlen *et al.*, 1983; Bohlen, 1987; Harley, 1989; Bohlen, 1991; Indares and Martignole, 2003). Despite this general range there exist a diversity as noticed in the in the P-T conditions those deduced from mineral textures and thermobarometry. Determination of peak metamorphic P-T regime in high-temperature granulites is often hampered by retrograde reactions and diffusional cation exchange resulted in compositional changes of mineral phases (Harley, 1989, 1998; Fitzsimons and Harley, 1994). In the present study an attempt is made to find out the peak metamorphic conditions by selecting suitable samples that are affected by less retrogressive reactions. The available P-T data from different parts of the MGB are summarised in Table 4.13.

In this study, pressures and temperatures have been calculated using different models and these give a wide range of temperature and pressure estimates for any given sample. Due to the heterogeneity in the mineral assemblages it is found difficult to infer the P-T conditions of formation in a regional scale. P-T estimation software PTOXY (Nasir, 1994)

**Table 4.13** The summary of available P-T estimates in various parts of MGB and ACS (Ravindrakumar and Chacko, 1994; Prakash, 1999; Satish-Kumar et al., 2002; John et al., 2005; Cenki et al 2002)

Author	Region/ Area	Thermometer	Barometer	Temperature (°C)	Pressure (kb)
Ravindrakumar and Chacko (1994)	Pighat gap (Northern MGB)	Grt-Cpx	Grt-Cpx-Pl-Qtz	682-916	6.9-9.5
Prakash (1999)	Kodaikanal (NE part of MGB)	Grt-Opx	Grt-Opx-Pl-Qtz	676-1040	6.6-10.9
		Grt-Bt	-----	752	-----
		Grt-Opx	Grt-Opx-Pl-Qtz	685-763	4.7-5.7
Satish-Kumar et al. (2002)	Eastern part of MGB	Grt-Crd	Grt-Crd-Sil-Qtz	591-681	5.0-5.9
		Grt-Bt	-----	646-797	-----
		Crd-Sp	-----	662-740	-----
		-----	Grt-Sil-Pl-Qtz	-----	5.6-7.7
John et al. (2005)	Northern part of MGB	Grt-Cpx	Grt-Cpx-Pl-Qtz	535-916	4.4-11
Cenki et al. (2002)	ACS	Grt-Opx	-----	945	7.0

is mainly made use for the P-T calculations. The obtained result is further crosschecked by conventional geothermobarometric methods as well as with the help of some other software like PTMAFIC (Soto and Soto, 1995) and HbPI 1.2 (Holland and Blundy, 1994). But with the available thermometers and barometers an attempt has been made to correlate the different metamorphic conditions of each rock type. For all samples the metamorphic temperatures have been estimated at assumed pressure of 8kb, and pressures has been calculated at an assumed temperature of 800°C, to facilitate inter-comparison.

#### **4.8.1 Temperature estimates**

For the mafic granulite (two pyroxene granulite) from the MGB, Cpx-Opx thermometers by Wood and Banno (1973), Brey and Köhler (1990) are used. Since the rock is also constituted with hornblende-plagioclase assemblage, the thermometer by Blundy and Holland (1990) and Nasir (1991) is made use for confirmation. The results obtained are almost same and the temperature ranges in between 669-837 °C. But a different value at higher temperature of 1050 °C is obtained from another thermometer by Nehru and Wyllie (1974) (Table 4.14). Using the garnet-biotite thermometer, temperature of 471-740°C is obtained for garnet-biotite gneiss from the MGB (Table 4.15). Difference is noted between temperatures at the rim and core of the garnets. Here, the rim temperature ranges from 590-629°C and the core temperature falls in arrange of 619-740°C. For charnockite, grt-cpx thermometer proposed by Raheim and Green (1974), Ellis and Green (1979), Krogh (1988), Newton (1989) gives temperature in between 500-800 °C, whereas temperatures more than

**Table 4.14 Temperature estimates from two pyroxene granulites of MGB at 8kb pressure.**

<b>Clinopyroxene-Orthopyroxene</b>	<b>°C</b>
Wood & Banno 1973(W&B ' 73)	837
Brey & Köhler 1990 (B&K ' 90)	
Ca partitioning	740 ± 15
Na partitioning	919 ± 56
Nehru & Wyllie 1974(N&W ' 74)	1050
<b>Hornblende-Plagioclase</b>	
Blundy & Holland, 1990 (B&H ' 90)	759
Nasir, 1991(N ' 91)	669

**Table 4.15 Temperature estimates from garnet-biotite gneiss of MGB at 8kb pressure.**

<b>Garnet –Biotite</b>	<b>°C</b>	
	<b>Core</b>	<b>Rim</b>
Ferry & Spear, 1978 (F&S ' 98)	697	597
Goldman & Albee, 1977 (G&A ' 77)	628	559
Thompson, 1977 (T ' 77)	639	565
Perchuk & Larvent'eva, 1983 (P&L ' 83)	635	582
Hoinkes, 1986 (H ' 86)	740	629
Ganguly & Saxena ,1984 (G&S ' 84)	619	523
Hodges & Spear, 1982 (H&S ' 82)	697	595
Williams & Grambling, 1990 (W&G ' 90)	620	536
Dasgupta et al., 1991(D' 91)	667	590

1000 °C are obtained from the same thermometer developed by some other workers like Sengupta *et al.* (1989) But some other thermometers like grt-hnb, grt-cpx-hnb, hnb-pl agrees with the earlier temperature range (Table 4.16). Within this range the rim and core temperature ranges are 692-1135°C and 717-1167°C respectively.

The different rock types from the ACS has been analysed with grt-bio thermometer and is noticed that the temperature at 8kb pressure is found falling in between 600 and 900 °C irrespective of the rock type (Table 4.17-4.19). But in these rocks also there is disparity between garnet rim-core temperatures. The garnet-biotite gneiss gives the minimum temperature for rim at 675°C and maximum at 872°C. For the core it ranges between 691 and 891. From the reaction textures and the mineral chemistry it is evident that the garnets of ACS are not affected by less retrogressive changes. So the temperature obtained from garnet-biotite thermometer can be considered to be of peak metamorphic time in which the garnet rim temperatures fall in 538-789°C and the core temperatures in 555-832°C range (Table 4.17). The grt-crd thermometer used for grt-bio-crd gneiss only gives lesser values (500-600°C). The temperature estimates for charnockite using grt-opx thermometer also gives comparatively higher values (750-900°C) and the rim-core temperatures are at 694-910°C and 697-909v respectively (Table 4.19).

#### **4.8.2 Pressure estimates**

The pressure estimates using the available and suitable barometers for the given rock types produce a vivid picture. The reference temperature for all the calculation is kept as 800 °C. The charnockite from the MGB is

**Table 4.16 Temperature estimates from Charnockite of MGB at 8kb pressure**

<b>Garnet-Clinopyroxene</b>	<b>°C</b>	
	Core	Rim
Rahiem & Green, 1974 (R&G ' 74)	717	692
Ganguly, 1979(G ' 79)	1167	1135
Krogh, 1988(K ' 88)	775	739
Ellis & Green, 1979 (E&G ' 79)	809	777
Dahl, 1980 (D ' 80)	1041	982
Powell, 1985 (P ' 85)	792	760
Sengupta et al., 1989 (S ' 89)	1165	1120
<b>Garnet-Hornblende</b>		
Graham & Powell, 1984(G&P ' 84)		
Fe <sup>2+</sup> /Fe <sup>3+</sup> estimated	782	746
Total iron as Fe	761	735
<b>Garnet-Clinopyroxene-Hornblende</b>		
Nasir & Abu-Aljarayesh ,1992 (N&AA ' 92)	789	767
<b>Hornblende-Plagioclase</b>		
Blundy & Holland, 1990 (B&H ' 90)	743	
Nasir, 1991(N ' 91)	642	

**Table 4.17 Temperature estimates from garnet-biotite-cordierite gneiss of ACS at 8kb pressure**

<b>Garnet -Biotite</b>	<b>°C</b>	
	<b>Core</b>	<b>Rim</b>
Ferry & Spear, 1978 (F&S ' 98)	784	745
Goldman & Albee, 1977 (G&A ' 77)	737	706
Thompson, 1977 (T ' 77)	697	669
Perchuk & Larvent'eva, 1983 (P&L ' 83)	675	655
Hoinkes, 1986 (H ' 86)	832	789
Ganguly & Saxena ,1984 (G&S ' 84)	710	671
Hodges & Spear, 1982 (H&S ' 82)	784	745
Williams & Grambling, 1990 (W&G ' 90)	693	662
Dasgupta et al., 1991(D' 91)	785	731
<b>Garnet-Cordierite</b>		
Thompson, 1979 (T ' 79)	580	562
Wells, 1979 (W ' 79)	555	538
Clifford et al., 1981 (C ' 81)	555	538
Perchuk et al., 1981 (P ' 81)	580	562



**Table 4.18 Temperature estimates from garnet-biotite gneiss of ACS at 8kb pressure**

Garnet–Biotite	°C	
	Core	Rim
Ferry & Spear, 1978 (F&S ' 98)	818	784
Goldman & Albee, 1977 (G&A ' 77)	715	684
Thompson, 1977 (T ' 77)	720	697
Perchuk & Larvent'eva, 1983 (P&L ' 83)	691	675
Hoinkes, 1986 (H ' 86)	873	834
Ganguly & Saxena ,1984 (G&S ' 84)	740	706
Hodges & Spear, 1982 (H&S ' 82)	818	784
Williams & Grambling, 1990 (W&G ' 90)	723	696
Dasgupta et al., 1991(D' 91)	891	872

**Table 4.19 Temperature estimates from charnockite of ACS at 8kb pressure**

<b>Garnet -Biotite</b>	<b>°C</b>	
	<b>Core</b>	<b>Rim</b>
Ferry & Spear, 1978 (F&S ' 98)	832	826
Goldman & Albee, 1977 (G&A ' 77)	773	764
Thompson, 1977 (T ' 77)	729	725
Perchuk & Larvent'eva, 1983 (P&L ' 83)	697	694
Hoinkes, 1986 (H ' 86)	878	871
Ganguly & Saxena, 1984 (G&S ' 84)	748	743
Hodges & Spear, 1982 (H&S ' 82)	832	826
Williams & Grambling, 1990 (W&G ' 90)	744	739
Dasgupta et al., 1991(D' 91)	732	732
<b>Garnet-Orthopyroxene</b>		
Harley, 1984 (H ' 84)	810	810
Lee & Ganguly, 1988 (L&G ' 88)	909	910
Lal 1993 (L ' 93)	755	757
Bhattacharya et al., 1991 (B ' 91)	850	851

estimated to be formed at 4.0-5.6kb pressure (Table 4.20) while the ACS charnockite gives pressure estimates between 5.0 and 7.8 kb (Table 4.21). The grt-bio-crd gneiss gives comparatively higher pressures (6.6-8.3 kb) when estimated with grt-crd barometer (Table 4.22). All the samples show minor variation of pressures from rim to core of garnets up to a maximum of 1kb.

### 4.8.3 Discussion

In most of the temperature estimates available for the region, the garnet-biotite thermometer is used irrespective of the rock type. Majority of the rocks in this study is having this assemblage. Distribution of Mg and Fe between the garnet and biotite phases is largely a function of temperature and pressure, as the partitioning of elements decreases with increasing temperature. The temperature estimates derived from the rocks using garnet-biotite thermometer ranges between 550-875°C at 8kb pressure. The observed mineral chemistry displays slight rim ward increase of FM in garnets of the gneisses and the charnockite from ACS. These can be interpreted as a manifestation of retrograde reaction (Storm and Spear, 2005). This is probably due to the Fe-Mg exchange reaction between garnet and biotite (Tracy *et al.*, 1976; Ferry and Spear, 1978). The exchange produces increasingly Fe rich garnet and Mg rich biotite through cooling until the rock passes through the garnet-biotite Fe-Mg closure temperature of 500-600°C (Storm and Spear, 2005). So the temperature estimates from the garnet biotite thermometer will be of peak metamorphism only if it is above 600°C and the lower temperature may

**Table 4.20 Pressure estimates from charnockites of MGB at 800°C**

<b>Garnet-Clinopyroxene-Plagioclase-Quartz</b>	<b>kb</b>	
	Core	Rim
Newton & Perkins, 1982 (N&P ' 82)	5.2	4.4
Powell, 1978 (P ' 78)	5.5	4.8
Eckert et al., 1991(E ' 91)	4.8	4.0
<b>Garnet-Hornblende-Plagioclase</b>		
Kohn & Spear, 1989, 1990 (K&H ' 89, ' 90)	5.6	5.6

**Table 4.21 Pressure estimates from charnockites of ACS at 800°C**

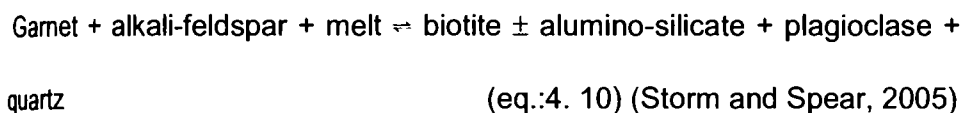
<b>Garnet-Orthopyroxene</b>	<b>kb</b>	
	Core	Rim
Wood, 1974 (W ' 74)	7.7	7.8
Nickel & Green, 1985 ( N&G ' 85)	5.1	5.2
Brey & Koehler, 1990 (B&K ' 90)	6.7	6.8
<b>Garnet-Orthopyroxene-Plagioclase-Quartz</b>		
Wells, 1979 (W ' 79)	5.7	5.6
Newton & Perkins, 1982 (N&P ' 82)	6.1	6.0
Eckert et al., 1991(E ' 91)	5.6	5.6

**Table 4.22 Pressure estimates from garnet-biotite cordierite gneiss of ACS at 800°C**

<b>Garnet- Cordierite</b>	<b>kb</b>	
	C	R
Wells, 1979 (W ' 79)	8.1	8.0
Clifford et al., 1981(C ' 81)	8.2	8.3
Perchuk et al., 1981(P ' 81)	6.7	6.6

denote the temperature of retrogression. From the reaction textures this can be distinguished by the presence of secondary biotites (eq: 4.9).

Another probable cause for this retrogression is the retrograde net-transfer reaction (ReNTR) defined as below:



However the retrogressive effects are very minimal in the samples since no abrupt and anomalous change of FM is noticed anywhere and there is a great amount of homogeneity noticed in most of the grains.

It is doubtful that any metamorphic terrain worldwide is devoid of at least some mineralogical effects of retrograde metamorphism, and, in the extreme, some samples from some terrains are composed almost entirely of retrograde minerals. The cordierites can be considered one among them and its appearance is usually secondary in nature. So the garnet-cordierite thermometer denotes a secondary temperature, which cannot be treated as the peak ( $\sim 550 \pm 50$ ). Thus the cordierite formation represents a lower-temperature, higher-pressure event localized along the southern boundary of the MGB. This is an indication of the shearing effects of the ACS, which is a major transcurrent shear (Sacks *et al.*, 1997).

The two-pyroxene granulites from the MGB signify the prograde nature of metamorphism from its reaction textures. Here the cpx-opx thermometer gives a temperature above 800 °C, which can be considered, as the peak temperatures since the hornblende–plagioclase thermometer renders only  $700 \pm 50$ °C. This further ratifies that the pyroxenes are formed at expense of hornblende (eq: 4.1).

Garnet and clinopyroxene that has been formed as a progressive reaction product, this thermometer will give a peak temperature of formation. The charnockite from the MGB gives general temperature of formation at around 800°C and  $5.0 \pm 0.5$  kb pressures while using garnet-clinopyroxene-plagioclase-quartz barometer. Similarly the charnockite from the ACS also gives a temperature of formation at  $800 \pm 50$  °C.

The barometry of these samples is hardly available and the available pressure is from the garnet-plagioclase-orthopyroxene-quartz barometers (Wells, 1979; Newton and Perkins, 1982; Eckert *et al.*, 1991). Since this barometer is reliable and is compatible with garnet-biotite thermometer (Spear, 1995) the P-T derived from these geothermobarometers are plotted with respect to  $Al_2SiO_5$  triple boundary (Fig. 4.16). From the figure it is clear that there is not much change in the pressure ( $\sim 4-6$  kb) as the temperature increases.

From the reaction textures it can be noted that the MGB samples shows evidences of isobaric cooling where as the ACS samples indicates isothermal decompression paths. The P-T estimates of the rocks bearing garnet and biotite (especially from ACS) (Fig 4.16) also express the conditions of ITD path. The pressure-temperature fields for the rocks from MGB and ACS demarcating the garnet rim-core differences are given in Fig 4.17, from which a better picture is available on the IBC, ITD nature of the two blocks.

#### 4.9 CONCLUDING REMARKS

- ❖ The samples selected the analysis are different in various aspects, especially in the occurrence, mineralogy and

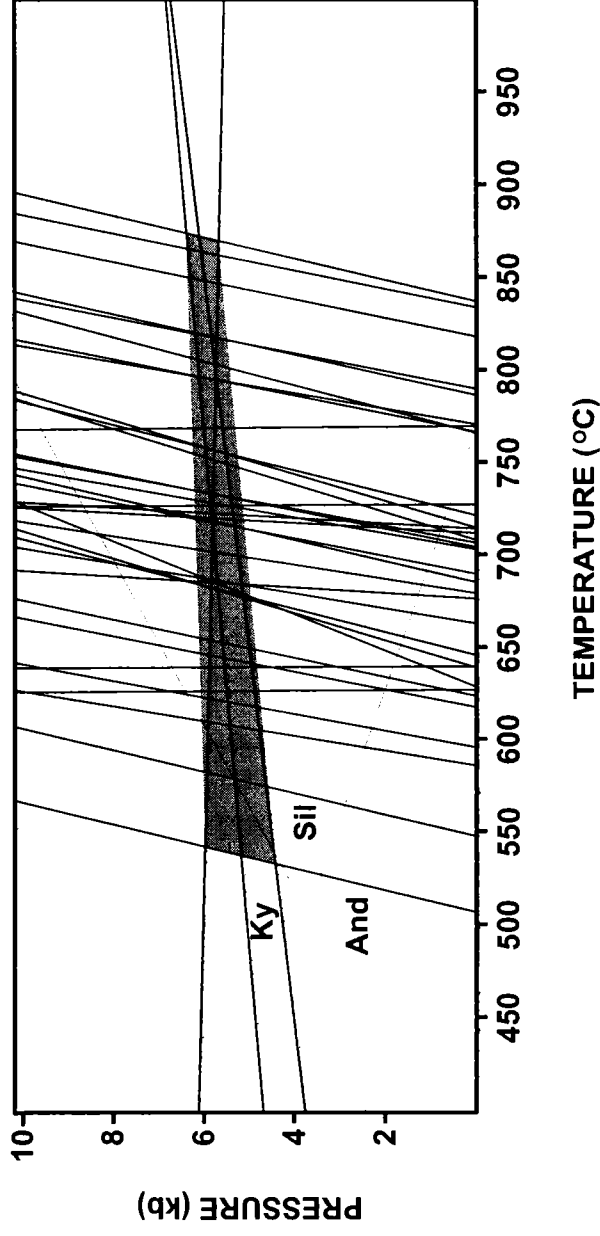
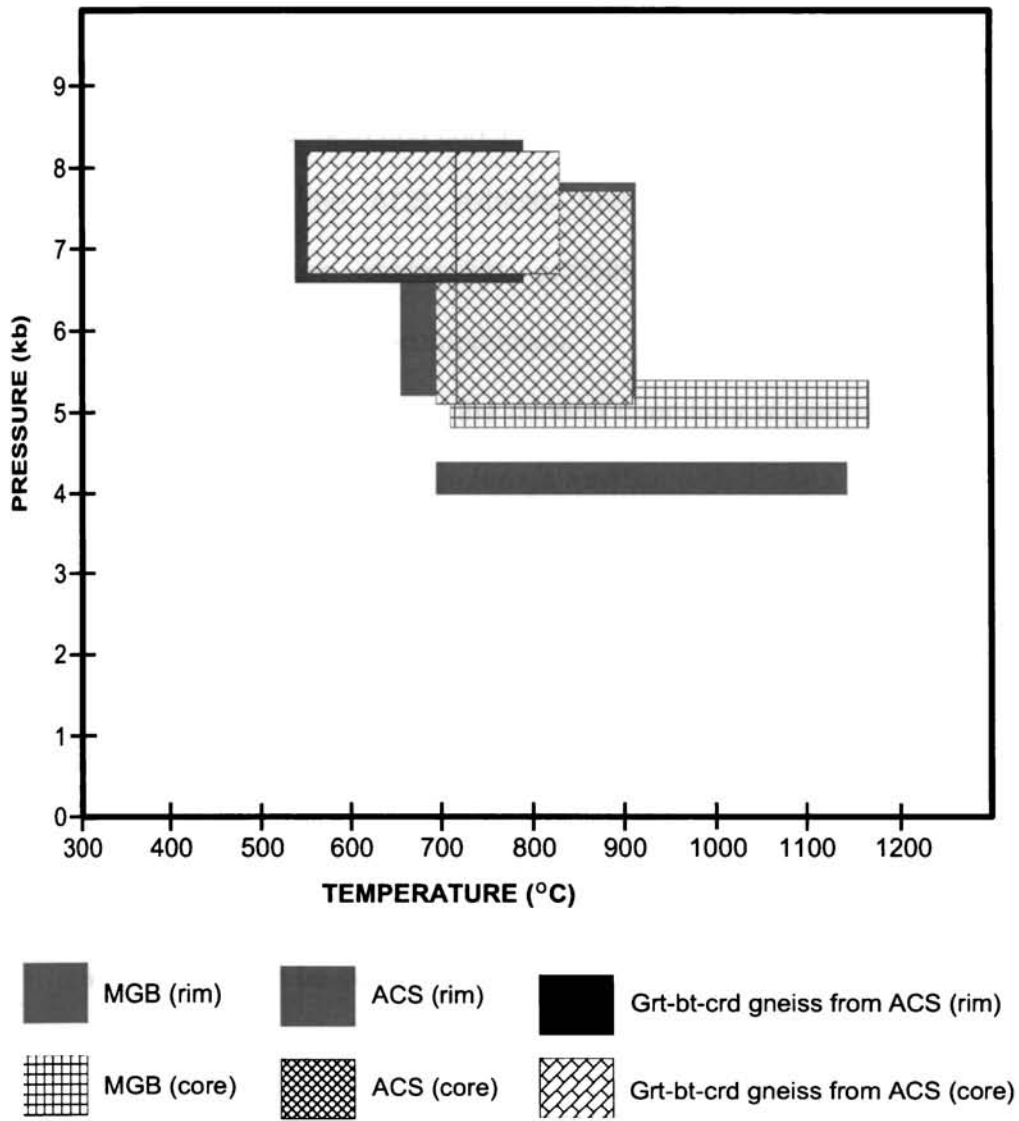


Fig. 4.16 Plot for geothermometry of different rocks under study with respect to  $\text{Al}_2\text{SiO}_5$  triple junction using all possible garnet-biotite thermometers and garnet-plagioclase-orthopyroxene-quartz barometer.



**Fig. 4.17 Pressure-temperature fields of the rocks from MGB and ACS**



chemistry. Therefore, a complete picture on metamorphic events cannot be brought out from the analysis. But it gives a broad idea on the P-T-t paths of the selected terrains.

- ❖ The reaction textures of mafic granulites and charnockites from the MGB express more progressive metamorphism with very less retrogression and conditions of isobaric cooling.
- ❖ Gneisses from the ACS exhibits melt involved mineral reactions and the charnockite exhibits specific reaction textures of isothermal decompression.
- ❖ In the rocks having biotites, the mineral chemistry of garnets exhibit pronounced Fe-Mg exchange reaction with biotites.
- ❖ The temperature and pressure obtained from the rocks of the MGB is  $800 \pm 50^{\circ}\text{C}$  and  $5.0 \pm 0.5\text{kb}$  respectively. Some extreme temperatures above  $1000^{\circ}\text{C}$  are also noted.
- ❖ Rocks from ACS give peak metamorphic temperatures at  $800 \pm 50^{\circ}\text{C}$  and pressure  $\sim 4\text{-}6\text{kb}$ .
- ❖ From the reaction textures as well as the available P-T estimates it can be concluded that rocks of the MGB followed IBC path where as the ACS rocks gives signatures of ITD.

# CHAPTER 5

OCCURRENCE, GENESIS AND MINERALOGICAL  
CHARACTERIZATION OF GRAPHITE

---

## 5.1 INTRODUCTION

Carbon is an element widely spread in igneous, metamorphic and sedimentary rocks. In sedimentary rocks it commonly occurs in the form of organic debris, but in igneous and metamorphic rocks pure carbon is usually seen in the form of graphite. Graphite is essentially formed from the organic materials by different geological processes that are associated with metamorphism. Another type of graphite formation is by the direct crystallisation from hydrothermal fluids (Landis, 1971; Wada *et al.*, 1994; Luque *et al.*, 1998; Pasteris, 1999). However graphite can be considered as an end product of elemental carbon metamorphism. Thus graphite is petrologically significant as an indicator of its host rocks, condition of formation and the role of carbon in its formation (Pasteris and Chou, 1998).

The conversion of biogenic materials to graphite is actually a complex process and not all carbons will be graphitised by metamorphism. There are carbons that never show graphitization even after heating to 3000°C and this is due to the difference in the structure and composition of their hydrocarbon precursors. The process of graphitization is initiated by the removal of hydrogen, nitrogen and oxygen by the process of polymerisation and is formed into more complex carbon units together with the development of ordered, planar layers of carbon that can be stacked in to parallel layers which characterize the graphite structure (Buseck and Bo-Jun, 1985). However, the final development to well crystallized graphite is by the effect of high P-T conditions. Landis (1971) determined a minimum temperature of 300°C for the initiation of graphitization with fully ordered

graphite appearing at 450°C and pressure of 2-6 kb. But according to Diessel and Offler (1975) graphitization begins at chlorite zone of green schist facies and will be complete before the beginning of amphibolite facies, i.e., temperature at ~ 400°C and pressure at ~3 kb.

Graphite is usually found as flaky, disseminated specks in metamorphosed siliceous or calcareous sediments such as gneisses, schists and marbles, and the fluid deposited graphite as veins along fractures and brittle shears (Dissanayake, 1981; Katz, 1987; Radhika *et al.*, 1995, Santosh and Wada, 1993a; Radhika and Santosh, 1996; Satish-Kumar *et al.*, 2002; Binu-Lal *et al.*, 2003). Graphite is reported from many of the Precambrian crustal fragments of East Gondwana, such as Peninsular India, Sri Lanka, Madagascar and East Antarctica (Desai, 1968; Krishnaswami, 1979; Dissanayake, 1981; Santosh and Wada, 1993a; Satish-Kumar and Wada, 2000; Parthasarathy *et al.*, 2003). In Peninsular India graphite has been reported from the Eastern Ghat province (Rao and Rao, 1965) and in different parts of Southern Granulite Terrain (SGT) and the Dharwar craton (Radhika *et al.*, 1995; Sharma *et al.*, 1998).

## 5.2 GRAPHITE FORMATION

There are basically three different processes leading to the formation of graphite deposits (Harben and Kuzvart, 1996), They are:

- 1) Contact metamorphism affected to coal deposits: These deposits are usually of low quality.
- 2) Epigenetic graphite deposits: These are formed from carbonic fluids and are usually found as massive polycrystalline vein deposits to well

ordered euhedral crystals or spherulites in metamorphic and igneous rocks (Rumble *et al.*, 1986; Luque *et al.*, 1998; Pasteris, 1999). Industrially this graphite is classified as vein or lump type. The formation of these deposits is assumed to involve the following reactions



- 3) Syngenetic graphite deposits: These graphites are usually flaky in nature and its formation is from the metamorphic alteration of organic matter. This metamorphic process is very much complex (Bonijoly *et al.*, 1982) and the formation is controlled by many factors like, nature of the hydrocarbon precursor, partial pressures of CO<sub>2</sub>, CO, CH<sub>4</sub>, H<sub>2</sub>O and H<sub>2</sub>, regional P-T conditions etc.

In nature graphite has some other modes of occurrences also which are considerably rare. Graphites were reported from many meteorites, in which they occur as nodules, spheres, and as a polycrystalline variety called 'cliftonite' (Brett and Higgins, 1967; Bernatowicz *et al.*, 1991; Mostefaoui *et al.*, 2005). Graphite pseudomorphs after diamonds were also reported (Pearson, *et al.*, 1989).

### 5.3 GRAPHITE STRUCTURE

Graphite is a crystalline polymorphic form of elementary carbon. It has a heterodesmic-layered structure. The structure of graphite consists of six-membered rings in which each carbon atom has three near neighbours

at the apices of an equilateral triangle. Within the large planar layers there are linkages intermediate between atomic and metallic bonds. Van der Waal's bonding forces of energy of 0.2 eV/atom hold the layers in the structure together. Perfect basal cleavage readily takes place between the layers along the (001) plane. Weak bonding perpendicular to the layers gives rise to easy gliding parallel to the sheets. Natural graphite is found in different morphologies like, flat, fibrous and spherical. Large crystals of graphite usually are hexagonal flakes with strong metallic lustre and perfect basal cleavage.

Two structural forms are possible for graphites due to the difference in the spatial arrangement of carbon layers.

- i. The hexagonal structure of graphite with the spatial sequence ABABAB.....(Fig. 5.1a). In this sequence every carbon atom lies over the centre of a hexagon consisting of carbon atoms of the preceding layer, i.e., every layer is transitionally identical with respect to the c-axis. The unit cell in the lattice of hexagonal graphite contains four atoms with coordinates (000), (00(1/2)), ((2/3)(1/3)0) and ((1/2)(2/3)(1/2)). It has a space group  $D_{6h}^4$ -P6<sub>3</sub>/mmc and unit cell dimension:  $a_0 = 2.46 \text{ \AA}$ ,  $c_0 = 6.70 \text{ \AA}$ , interlayer distance ( $c/2$ ) =  $3.3539 + 0.0001 \text{ \AA}$ . Hexagonal graphite is stable up to a temperature of 2000°C and pressure up to 130kb.
- ii. The rhombohedral modification with the sequence ABCABC..... (Fig. 5.1b). This is a metastable phase, which is not available at elevated temperatures. It has a space group  $D_{3d}^5$ -R3m with unit cell parameters:  $a_0 = 2.46 \text{ \AA}$ ,  $c_0 = 10.038 \text{ \AA}$ , and the atoms occupying the

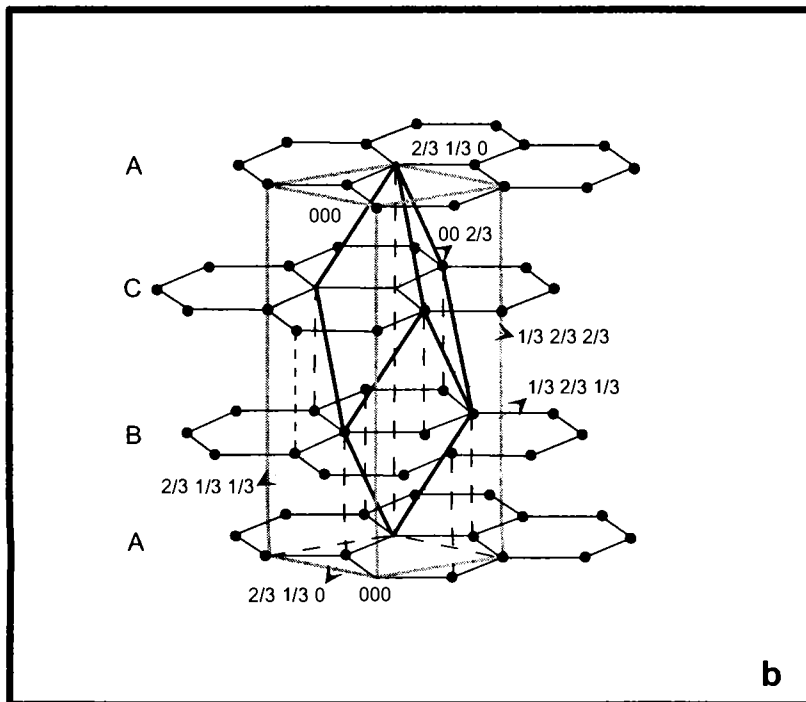
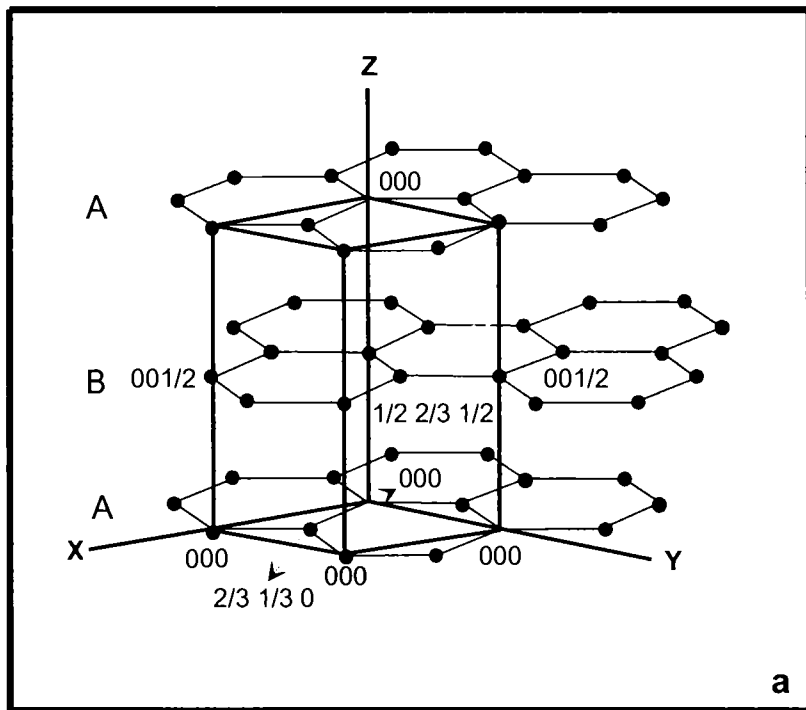


**Fig 5.1 Hexagonal and Rhombohedral lattice of graphite (Reynolds, 1968)**

positions:  $(000)$ ,  $((2/3)(1/3)0)$ ,  $(00(2/3))$ ,  $((2/3)(1/3)(1/3))$ ,  
 $((1/3)(2/3)(1/3))$ ,  $((1/3)(2/3)(2/3))$ .

(The above details extracted from Kwiecinska and Petersen, 2004).

### 5.2.1 Importance of the structural analysis of graphite

The structural analysis of graphite enables inferences about the physical conditions under which it is formed. Based on the genesis of graphite, whether they are from metamorphosed organic matter or precipitated from C-O-H fluids their occurrence will be different. Usually dispersed graphite flakes are described in a syngenetic deposit whereas vein type or pod type deposits are formed from fluid derived graphites. Even then it is difficult to distinguish the genetic type simply from the mode of occurrence. One important difference that can be noted is the degree of crystallinity exhibited by the two genetic types of graphite. The term crystallinity refers to the length-scale of continuity within the crystal lattice i.e. the crystallite size.

## 5.4 PREVIOUS STUDIES ON GRAPHITE MINERALIZATION IN THE MGB AND ADJACENT BLOCKS

In the SGT, graphite is mostly seen associated with metapelites, charnockites and other high-grade gneisses of the Kerala Khondalite Belt (KKB) and the MGB. In the MGB, graphite is an accessory mineral within different metamorphic rocks of medium- to high-grade and associated pegmatites. It is more commonly noticed in altered rocks like laterite. Towards the eastern side of the MGB graphite is seen in calc-silicate rocks and marbles (Satish-Kumar *et al.*, 2002). However, in the western region of



the peninsula, especially in the KKB, graphite is found in granulite facies rocks such as khondalites, charnockites and gneisses (Soman *et al.*, 1986; Radhika *et al.*, 1995). The occurrence of graphite in the MGB, dominated by massive charnockites, is genetically more significant because its origin may relate to the CO<sub>2</sub>-rich fluid conditions that prevailed during charnockitization. One interesting aspect about graphite in metamorphic rocks is their variable crystallinity, which is correlatable with the grade of metamorphism of the host rocks (Tagiri, 1981; Wada *et al.*, 1994; Yui *et al.*, 1996; Sharma *et al.*, 1998; Parthasarathy and Sharma, 2001; Parthasarathy *et al.*, 2003). Such studies were mostly carried out on samples from low- to medium- grade terrains, relating to the prograde metamorphism. It is believed that graphite is highly inert with respect to its structural and isotopic characteristics, a unique property useful in recording geological events (Thrower and Mayor, 1978.).

## **5.5 FIELD RELATION AND OCCURRENCE OF GRAPHITE IN THE PRESENT STUDY**

The sixteen graphite locations where the samples were collected are shown in the Fig. 5.2. In most of the locations graphite is an accessory mineral in the host rock (charnockite or associated gneiss). In some locations the actual relation between the host rock and the graphites cannot be traced out since the fresh rock is unavailable in the area and the graphite is occurring within the weathered equivalents of the host rock (laterites) (Plate 5.1). However the most prominent type of occurrence of graphite seen in fresh rocks of the area is as disseminations parallel or sub parallel to the gneissosity (Plate 5.2). The size of individual flakes range between 1

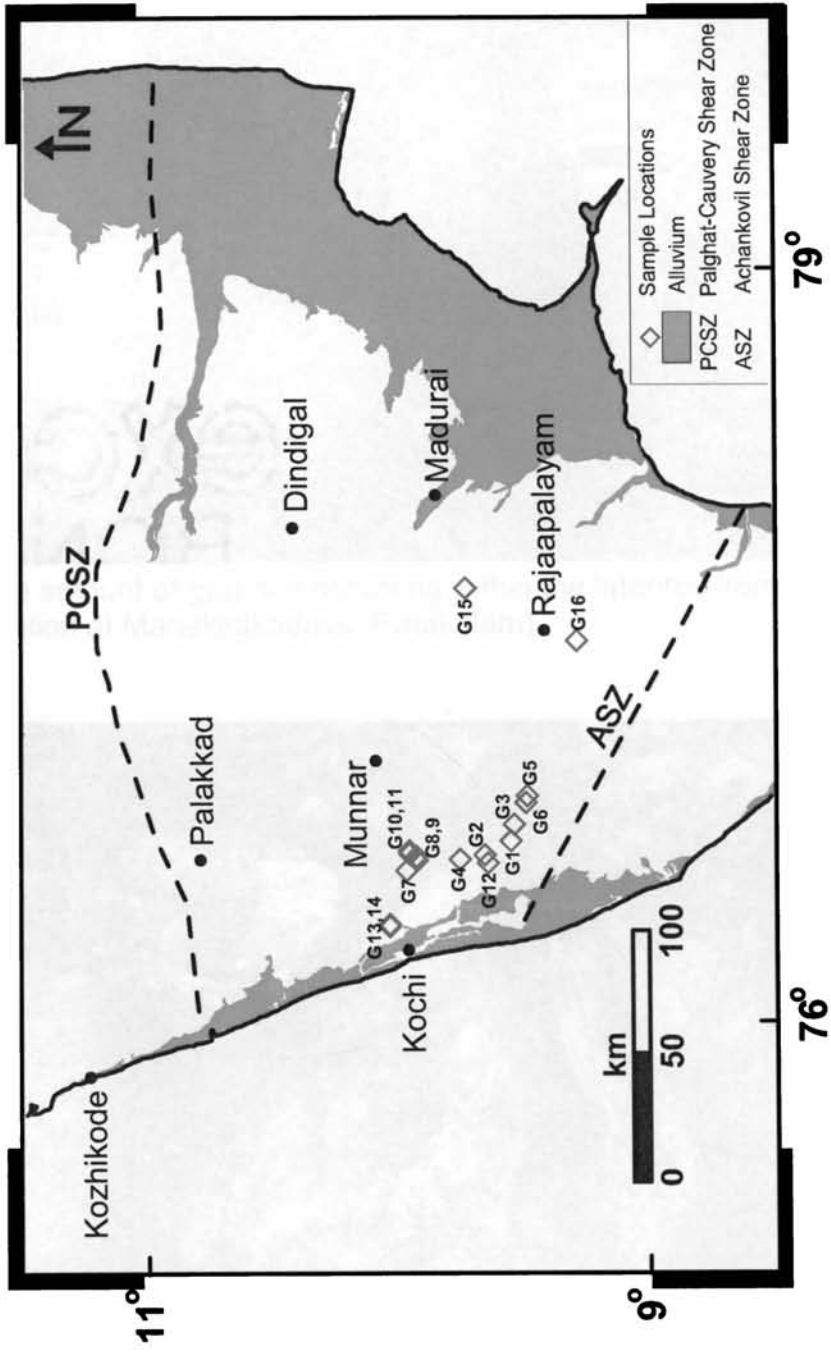
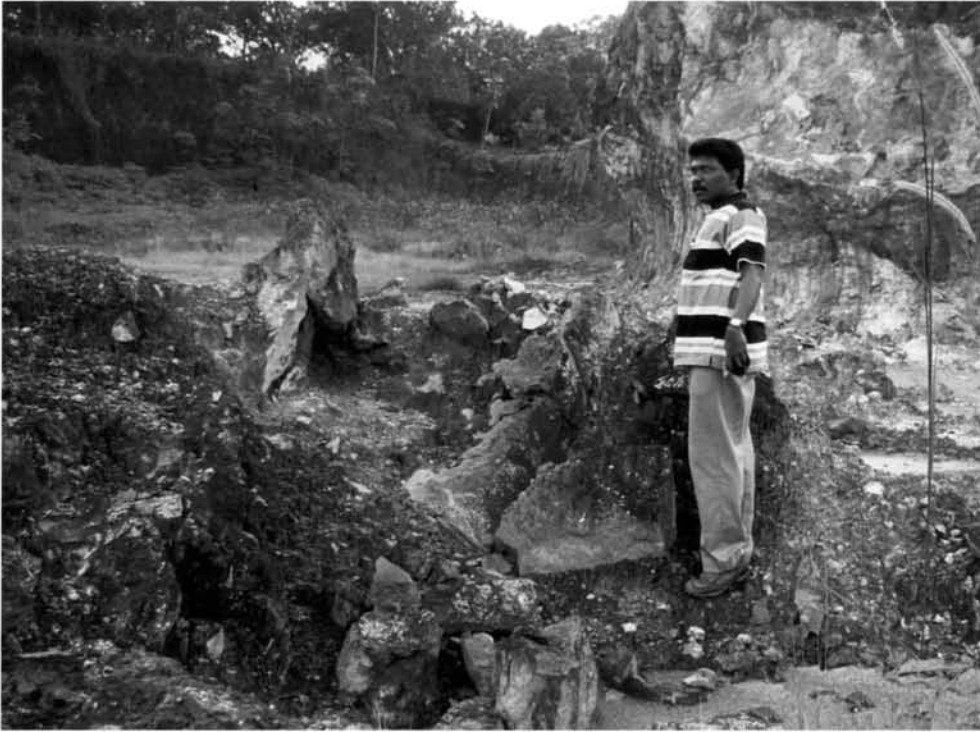


Fig 5.2 Graphite sample locations



Large amount of graphite occurring within the laterites from MGB  
(Location at Manakkakadavu, Ernakulam)



Lumps of graphite flakes occurring along with weathered feldspars  
(Location at Mannakkakkadavu, Ernakulam)

**Plate 5.1**



**Plate 5.3** Graphite flakes occurring in weathered pegmatite vein

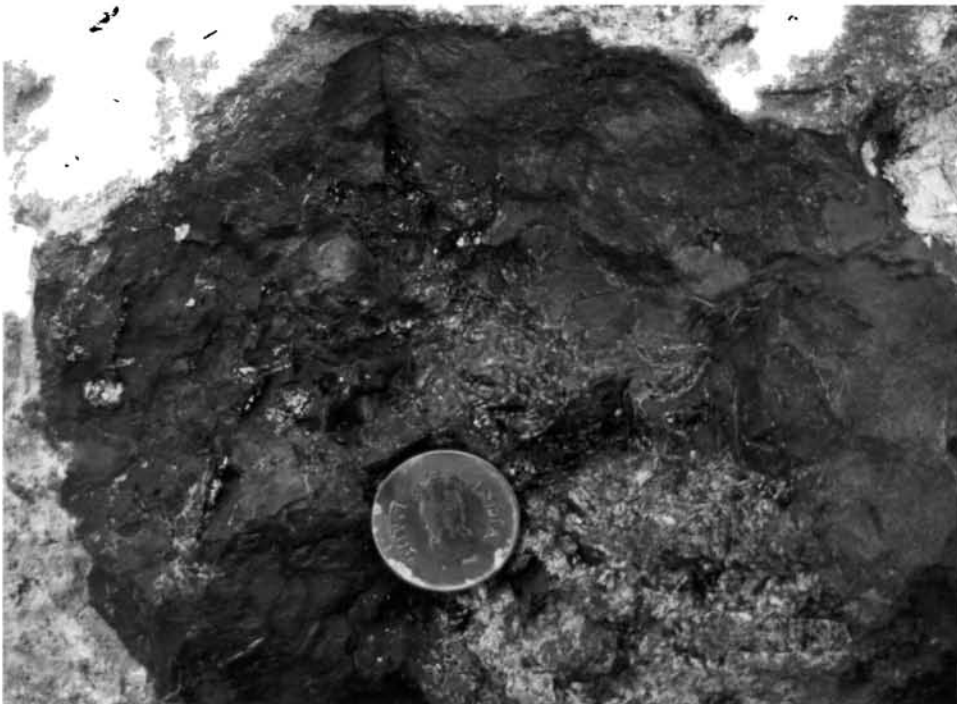


**Plate 5.4** Graphite pocket in duricrust

to 5mm. In many areas where graphite occurs in laterite is concentrated in particular zones or sometimes as isolated pockets. This type of occurrences was reported in many Precambrian terrains all over the world (Radhika *et al.*, 1995; Rajesh-Chandran *et al.*, 1996). Graphite is also been located along with pegmatite veins emplaced within the gneisses and charnockites. This graphite is found occurring together with the feldspar grains (Plate 5.3).

The specific field relations of graphite that can be traced out from the locations can be described as below.

Kodungoor, Idamula and Chirakkadavu: These are the respective locations where the samples G1, G2 and G3 were collected. In these locations the exposures of the hard rock are not seen. These are somewhat near by locations and the whole area is covered by thick laterite. Laterites are highly reddish in colour indicating the high percentage of Fe in the precursor rock. Graphite flakes are found disseminated in nature in some places where as in some other it is found along the relict foliation planes within the laterites. At Chirakkadavu small veins of pure graphite have been identified in lateritised charnockite. A working quarry noticed near Idamula is characterized with massive charnockite, but graphites are not found in the rock. In some parts of the quarry the rock is showing gneissic nature.

Valavoor: The graphites occurring in this location are along with pegmatites and gneisses (sample: G4). The major type of the rock exposed in the area is massive charnockites. But the charnockites are devoid of the graphites. The gneisses are formed in contact with the charnockites and are

leptynitic in nature (i.e. garnet- biotite gneiss). Veins of pegmatite and quartz are traversing all over the charnockites and gneisses.

Punchavayal and Kannimala: Both the locations are massive charnockite quarries and graphite (Sample: G5andG6) is occurring as accessory phase in both the exposures.

Peringazha: Graphite is found in association with garnet-biotite gneiss. Graphite flakes (sample: G7) of few centimetres in size are seen along the foliation planes of the rock. The lateritic equivalent of the rock is also found in the area, which is flourished with large amount of graphite. Weathered pegmatite veins having graphite were also detected in the area.

Piralimattom: Samples G8 and G9 were collected from two near by locations at Piralimattom. In both the locations the host rock could not be determined because the area is devoid of any rock exposures. But the rock type in the near by areas is massive charnockite. So it can be assumed to be the same. Graphite flakes are found in highly ferruginous laterites.

Kallurkkad and Nagapuzha: The locations are similar to Piralimattom, that the area is having thick lateritic cover. The samples G10 and G11 were collected from the locations respectively. In Kallurkkad, there is high amount of graphite where some activities of mining is progressing.

Mattakkara: The area is characterised by massive charnockite. But graphite is hardly identified in the hand specimens. The overlying laterite is having disseminated flakes of graphite but concentrated in certain parts only.

Manakkakkadavu: This is an area where more than 50m thick laterite cover is found. Graphite (sample: G13, G14) is found parallel to the

preserved gneissic banding within the laterites. The graphite bands are about 30-45cm thick. Relicts of weathered garnet and biotites can be identified in the laterites. So it can be assumed that the host rock is garnet bearing gneiss. Thick duricrust is found capping the laterite. Usually the graphites are found within the felsic clay under the duricrust (Plate 5.4).

Supplapuram and Muthukudi: These are two locations from Tamil Nadu. The samples G15 and G16 were collected from the locations respectively. In Supplapuram the graphites are found in the garnet-biotite gneiss, which is associated with charnockite. Graphite is mainly found along the foliation planes in the gneiss. Some flakes of graphite are also present within the charnockites. Pegmatitic veins traversing zig-zag path all along the gneisses and charnockite.

In Muthukudi graphite is found as disseminated flakes in garnet biotite gneiss. Charnockites identified in the area is of arrested type.

## **5.6 ANALYTICAL PROCEDURES**

The degree of carbon crystallisation depends on the extent and intensity of metamorphism. The structural studies of such carbonaceous material provide considerable information regarding metamorphism (eg. Landis, 1971; Wopenka and Pasteris, 1993). Whereas in the case of fluid deposited graphite the crystallinity is a complex function of temperature, pressure, fluid composition and time (Pasteris and Chou, 1998). The X-ray diffraction (XRD) and Raman spectroscopic studies provide valuable information on these physical (metamorphic) conditions of graphite formation whereas the carbon isotopes give information about the nature of



**Plate 5.3** Graphite flakes occurring in weathered pegmatite vein



**Plate 5.4** Graphite pocket in duricrust



graphite precursors (e.g. Pasteris and Wopenka, 1991; Santosh and Wada, 1993a; Luque *et al.*, 1998; Parthasarathy *et al.*, 2006).

Graphite samples meant for the XRD study were separated from the laterites, gneisses or charnockites by hand picking or by using a sharp knife. The separated samples were powdered in an agate mortar. These were then treated with HF and HCl to remove carbonate and silicate phases. The resultant residue was washed with distilled water until the acid relicts were completely removed. The graphite flakes left over were then dried in the hot air oven at about 80°C for about 4 hours. The graphite was then sieved through a 270 mesh (ASTM) in the acetone medium. X-ray powder diffraction data were collected using a SEIFERT diffractometer with Cu-K $\alpha$  radiation, installed at Cochin University of Science and Technology. The operating conditions were, accelerating voltage 20 KV; current 10 nA; scanning speed 1°/min; chart speed 60 mm/min and slit system having 0.5 mm width at the source side and 0.05 mm width at the detector side. Some of the analyses were repeated at the RIGAKU XRD at Shizuoka University, Japan with operating conditions same as those described in Wada *et al.* (1994).

Ten locations in the western part of the MGB were selected for the XRD analysis mainly concentrating in the (002) reflection and from which an attempt has been done to calculate the metamorphic temperature of its formation. The  $2\theta$ ,  $d$  values and full width of the peak at half-maximum are estimated from the diffractogram. The crystallite size ( $L_c$ ) along stacking direction is then calculated from Scherrer's equation:

$$L_{C(002)} = K\lambda / \beta_{(002)} \cos \theta,$$

where  $K$  is the shape constant, assumed to be 0.9 (Griffin, 1967; Tagiri and Tsuboi, 1979) and  $\beta_{(002)}$  is the full width of the peak at half-maximum in radian and  $\lambda$  is the X-ray wave length in angstroms and  $\theta$  is the angle of diffraction in radian. Further the graphitization degree (GD) has been calculated from the equation (Tagiri, 1981):

$$GD = \{[d_{(002)} - 3.7] / [\log Lc_{(002)} / 1000]\} \times 100$$

Raman spectroscopy is a vibrational spectroscopic technique, which monitors the inelastic scattering of monochromatic visible light as it interacts with covalent bonds in solids, liquids and gases. Thus it provides the information on the way that atoms are bonded to each other, reflecting both the symmetry of the bonds and the relative atomic masses of bonded atoms. Raman spectroscopy is sensitive to the molecular and crystalline structure as well as the composition of a material. So it is used as a means to identify the species or to quantitatively assess the degree of crystallinity of materials like graphite. Peak positions are monitored in frequency units ( $\text{cm}^{-1}$ ), and are recorded in terms of the peak displacement (Raman shift) with respect to the frequency of the exciting laser radiation ( $\Delta\text{cm}^{-1}$  or  $R\text{ cm}^{-1}$ )

Raman spectra of graphite samples of the present study were obtained using Raman microprobe equipment comprising of a 30 cm single polychromator (Chromex, 250is) equipped with a CCD detector (Andor, DU-401-BR-DD SH) and an  $\text{Ar}^+$  ion laser (514.5 nm; Ion Laser Technology, 5500A) set up in an optical microscope at the Laboratory for Earthquake Chemistry, University of Tokyo, Japan. A 50x objective lens (Olympus UMPlan FL, NA = 0.80) was used to obtain Raman spectra and the

diameter of laser beam was 2 microns. The laser power on the surface of samples was approximately 15 mW and low enough for the present samples to prevent artificial downshift of Raman spectra caused by laser-induced heating (Kagi *et al.*, 1994). Individual spectra were obtained with an exposure time of 10 seconds and the spectral resolution of the system was about  $1.5\text{cm}^{-1}$ . Peak positions were determined by fitting with Lorentzian functions and Raman shift was calibrated using naphthalene as a standard material.

Carbon isotope geochemistry provides an important tool to decipher the source of carbon in different geological environments. Studies have indicated that the kinetics of isotopic exchange within graphite are sluggish, so a graphite once fully crystallised is virtually inert and does not exchange with subsequent fluids even under high P-T conditions (Valley and O'Neil, 1981; Chacko *et al.*, 1991) So the isotopic composition of graphite serves as a potential tool to demarcate the source characteristics of carbon. The relative proportion of two isotopes of carbon namely  $^{12}\text{C}$  and  $^{13}\text{C}$  is expressed by the conventional ' $\delta$ ' notation. Carbon isotope compositions of graphite were measured using a MAT 250 mass spectrometer housed at Shizuoka University, Japan. Graphite samples were cleaned using HF and HCl and oxidised to  $\text{CO}_2$  using  $\text{V}_2\text{O}_5$  in preheated Vycor glass tubes at  $1000^\circ\text{C}$ . Analytical procedure follows those described in Wada and Ito (1990). Results are reported in standard delta notation in ‰ relative to PDB. Carbon isotope values have reproducibility better than  $0.1\text{‰}$ .

## 5.7 RESULTS

### 5.7.1 X-ray diffraction studies

High quality data on graphite using X-ray powder diffraction is difficult to obtain since carbon has a very low mass absorption coefficient for X-rays, which contribute to errors, associated with displacement and peak broadening. Also, it is difficult to prepare graphite samples, having strong preferred orientation and less textured (Howe *et al.*, 2003). Due to this problem the diffraction pattern reflects a non-random averaging of crystal orientation, with some enhanced peaks and some missing ones (Sharma *et al.*, 1998; Parthasarathy *et al.*, 2003). This plays a serious impediment in the structural studies of graphite. To avoid these complications, what is generally followed is to concentrate on the characteristics of the (002) peak, since it is the first appearing and the highest- intensity peak of well-crystallized graphite. The sharpness of this peak is also very much related to the regularity of the structure and size of crystallites (Radhika *et al.*, 1995; Sharma *et al.*, 1998).

The X-ray diffraction patterns of graphite samples are shown in Fig. 5.3, and the calculated structural data are presented in Table 5.1. From this it can be noted that the  $d_{(002)}$  values are not coinciding exactly with either the JCPDS CARD NO. 41-1487 (hexagonal graphite) or the CARD NO. 26-1079 (rhombohedral graphite) and is lesser than the card values. Such decrease in the basal spacing is attributable to the high temperature (more than 400°C) metamorphic recrystallization of graphite (Wada *et al.*, 1994). Wada *et al.*, 1994 have analysed several samples of carbonaceous matter

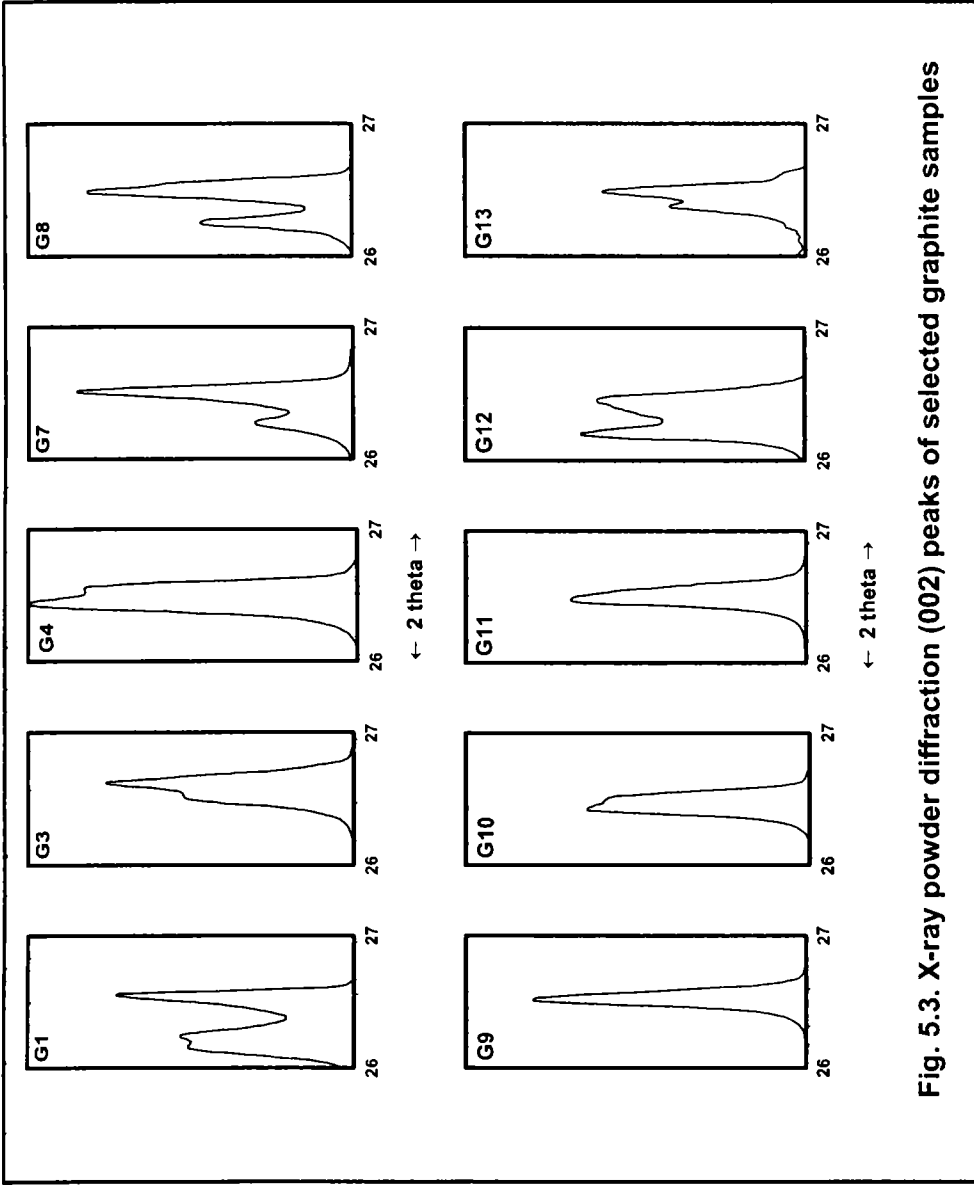


Fig. 5.3. X-ray powder diffraction (002) peaks of selected graphite samples

**Table 5. 1. X-ray diffraction and calculated structural data of graphite samples**

Sample No.	2 $\theta$ °	$\beta_{200}$ (°)	$d_{(002)}$ Å	$L_c$ (002) Å	GD Å	$\delta^{13}C_{PDB}$ (‰)	Metamorphic Temperature (T°C)
G1	26.52	0.122	3.358	669	196	-19.8	907
G3	26.56	0.174	3.353	469	105	-16.8	616
G4	26.4	0.149	3.373	544	124	-11.8	677
G7	26.47	0.109	3.365	749	267	-26.8	1134
G8	26.46	0.143	3.366	572	138	-15	722
G9	26.5	0.126	3.361	647	180	-14.8	856
G10	26.41	0.126	3.372	648	174	--	836
G11	26.47	0.149	3.365	544	127	--	686
G12	26.19	0.143	3.399	571	123	--	674
G13	26.57	0.126	3.352	648	185	--	872

from limestone and pelitic rocks of Ryoke metamorphic terrain and has derived a linear correlation between GD and peak metamorphic temperature. According to the relation;

$$T (^{\circ}\text{C}) = 3.2 \times \text{GD} (\text{\AA}) + 280$$

Substituting the values from the present study the corresponding metamorphic temperatures are calculated (Table 5.2). For further clarification a comparison has been made with the present data and the data of the carbonaceous samples of Kasuga contact aureole and the Ryoke metamorphic terrain studied by Wada *et al.*, (1994) The MGB samples have comparatively higher  $L_{c(002)}$  values but display comparable  $d_{(002)}$  values. A binary plot of  $L_{c(002)}$  vs  $d_{(002)}$  (after Tagiri and Oba, 1986) shows that the samples belong to the well crystallized graphite phase (Fig. 5.4). On extrapolation of the plot showing the linear relationship between the metamorphic temperature and GD values of Wada *et al.* (1994), the MGB samples cluster around 650°C and 800°C, with a few extreme values, especially sample G7 showing a temperature of more than 1000°C and G3 showing 550°C (Fig 5.5). The comparison of the calculated metamorphic temperatures of the graphite samples with temperatures obtained from Fig. 5.5 shows slight differences (about 50°C), but gives an almost similar curve (Fig. 5.6), which confirms the accuracy of the temperature obtained. However, two extreme values obtained in both the plots, which can be ruled out while considering the factors like local Lithology. Concisely the metamorphic temperature of graphite crystallization for the present samples of the order of  $700 \pm 100^{\circ}\text{C}$  can reasonably be estimated.

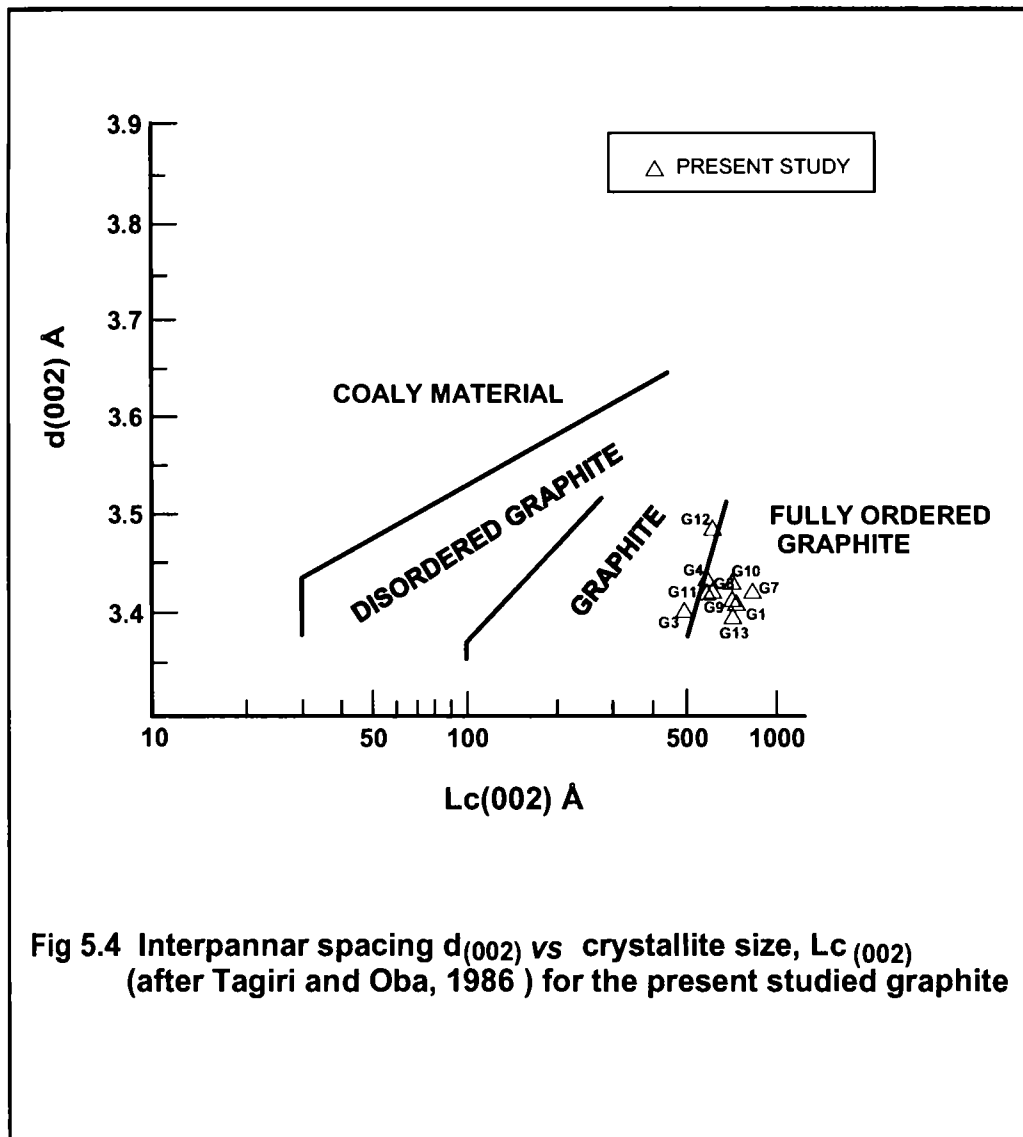


**Fig 5.4 Interplanar spacing  $d(002)$  vs crystallite size,  $L_c(002)$  (after Tagiri and Oba, 1986 ) for the present studied graphite**



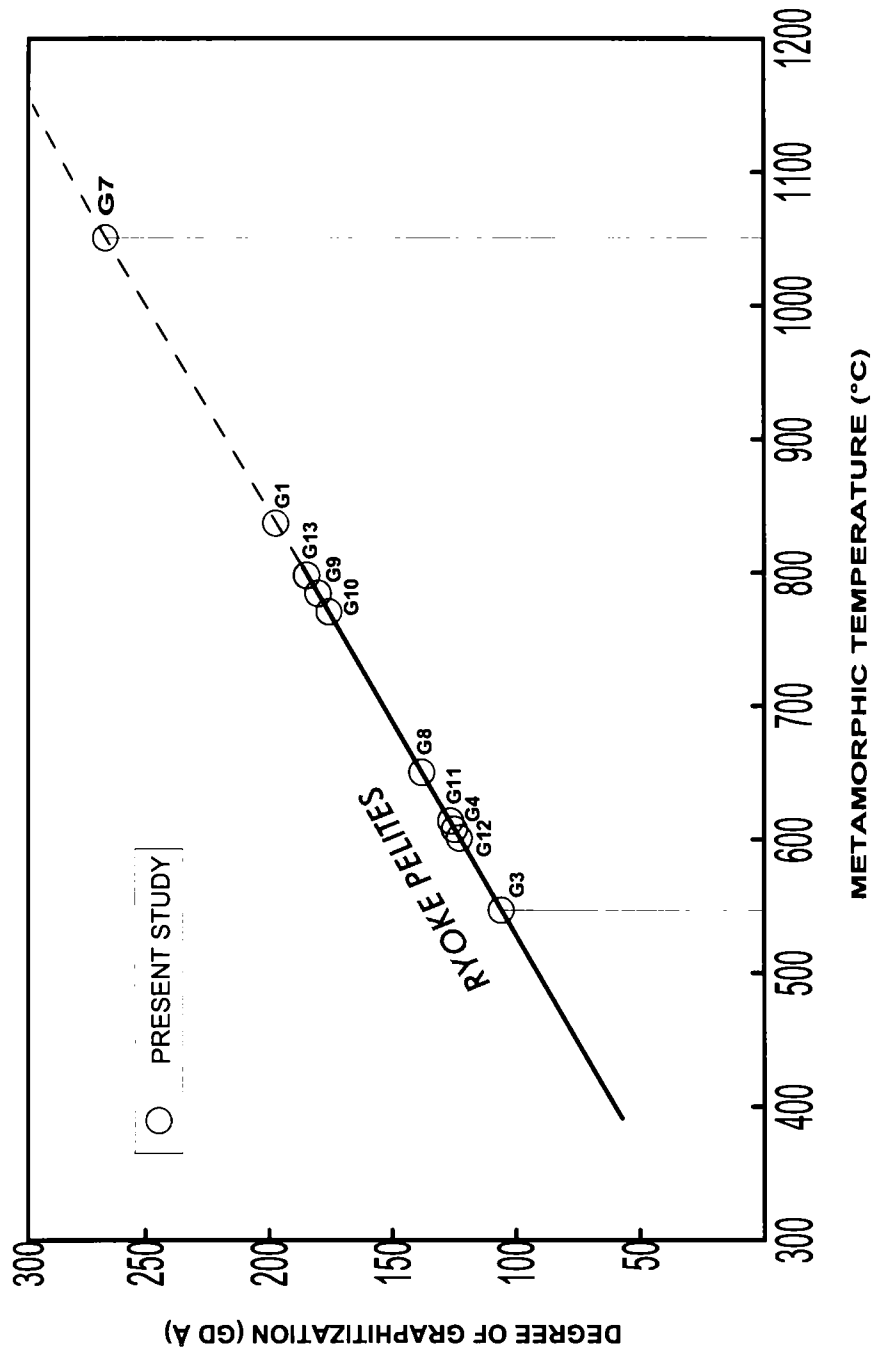


**Fig. 5.5. Degree of graphitization of the graphite from the present study compared with the linear relationship for Ryoke pelites of Wada et al. (1994). The broken line is extrapolation of Ryoke pelite relationship for higher temperatures. The derived metamorphic temperatures for the present samples falls between 665 °C and 875 °C.**

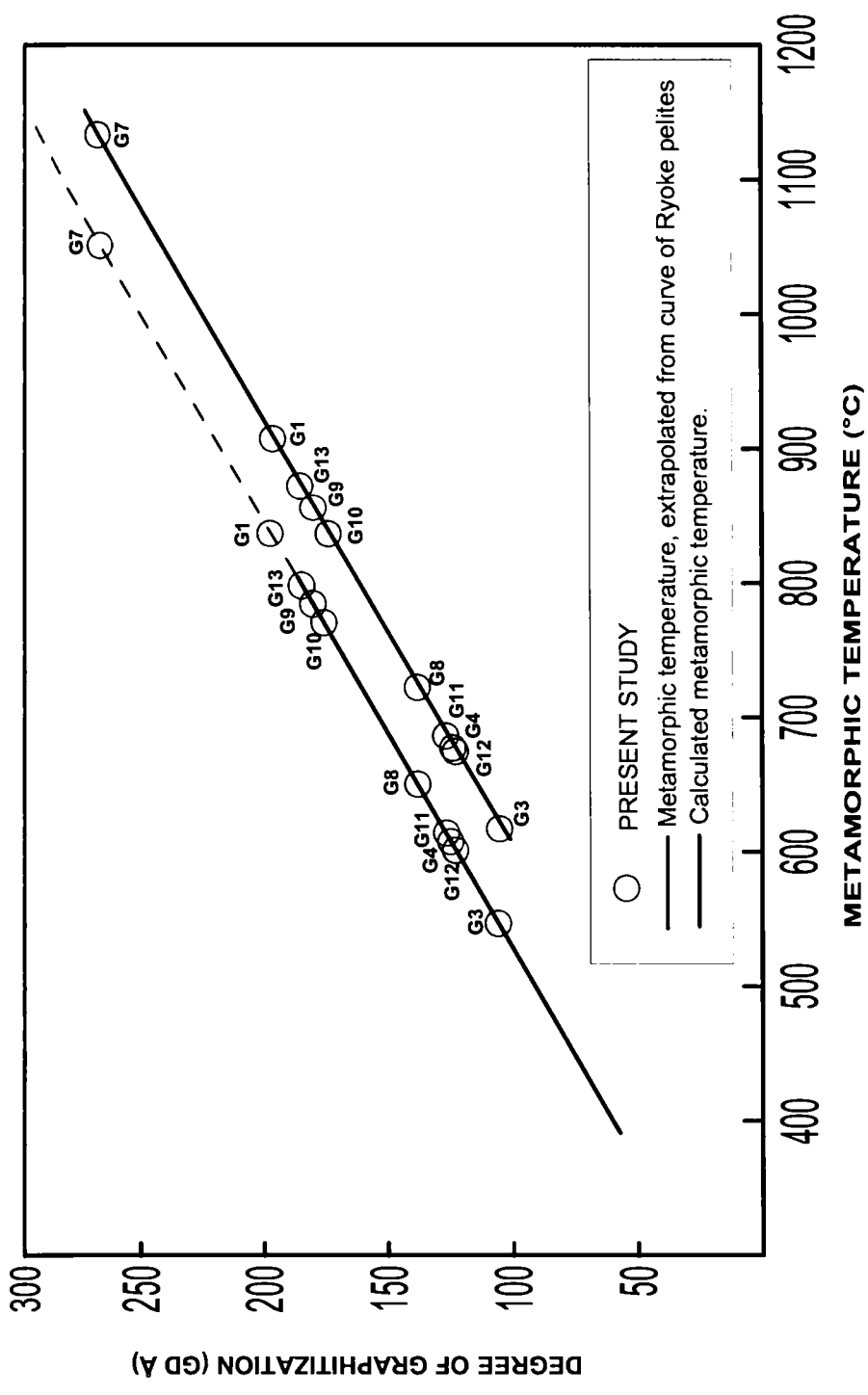


Fig. 5.6 Comparison of metamorphic temperature of the MGB graphite derived from the curve of Ryoike pelites with the calculated temperatures

## 5.7.2 Raman spectroscopy

The Raman spectrum of a graphitic material is a sensitive function of its degree of crystallinity, most specially the length scale of continuity within the (0001) basal plane of the graphite (eg. Wopenka and Pasteris, 1993; Sharma *et al.*, 2000 etc.). The degree of crystallinity of graphite is indicated in two portions of Raman Spectrum. The highly ordered, totally crystalline, pure carbon material that is properly called graphite has a single first order Raman peak or ordered peak (O) at approximately  $1580\text{ cm}^{-1}$  and an unresolved doublet/disordered peak or secondary peak (S) at about  $2725\text{ cm}^{-1}$ . If the S:O ratio is smaller the  $L_c$  will be small and more disordered the graphite will be (Pasteris and Chou, 1998). The Fig.5.7 shows typical Raman spectra of graphite samples from the MGB. It shows an ordered peak at  $1584\text{cm}^{-1}$  and disordered peak at  $2732\text{cm}^{-1}$ . From the values itself it is evident that the graphite is ordered. In comparison with the laboratory-produced fluid deposited graphite by Pasteris and Chou (1998) and graphite from vein materials of Water Hen, Duluth Complex, MN. (Luque *et al.*, 1998), the samples of present study lack the disordered peak suggestive of their highly ordered form. There is a striking similarity of Raman peaks of the graphites of the MGB and Duluth Complex. The graphite from hydrated altered troctolites of Duluth Complex, of fluid deposited origin, has ordered peak at  $1581\text{cm}^{-1}$  and secondary peak at  $2726\text{cm}^{-1}$ . This is estimated to be formed at temperatures above  $600^\circ\text{C}$  (Wopenka and Pasteris, 1993). From the similarity in the values (O

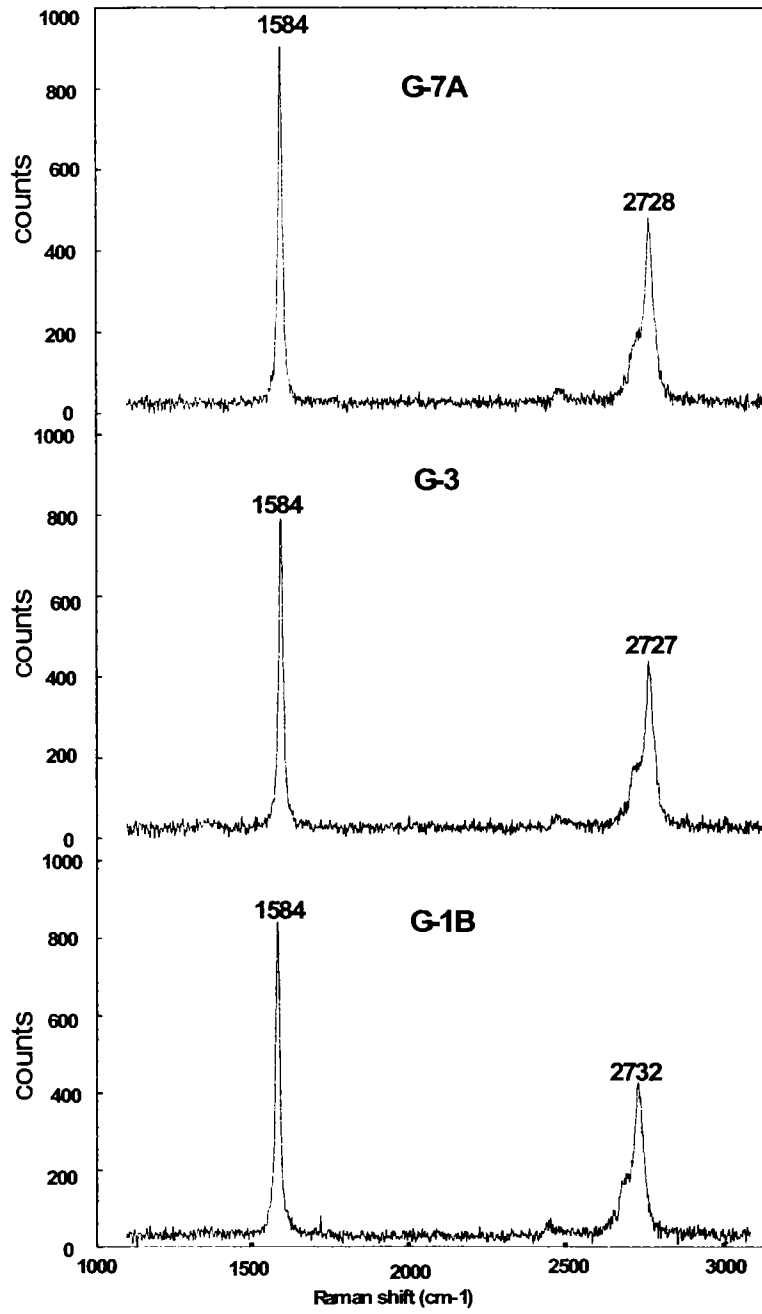
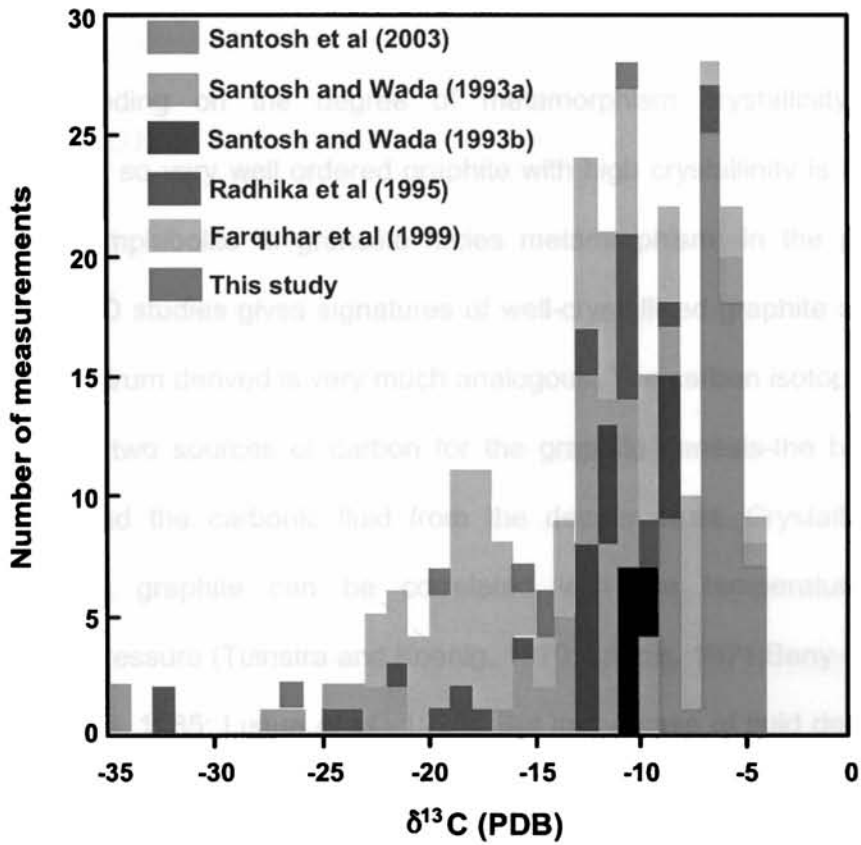


Fig 5.7. Raman spectra of graphite samples from MGB

=1584cm<sup>-1</sup>, S = 2732cm<sup>-1</sup>) it can be inferred that the MGB graphite also formed during high-temperature metamorphism.

### 5.7.3 Carbon isotope geochemistry

Preliminary results of carbon isotope composition of graphite from Thodupuzha-Kanjirappally Belt show a range of isotope signatures between -11.8 to -26 ‰ (Table. 5.1). Typical ancient and modern organic carbon has  $\delta^{13}\text{C}$  values lower than -25‰ due to the fractionation during photosynthesis (Eichman and Schidlowsky, 1975). Then the 'heavy' carbon may be precipitated from C-O-H fluids derived from magmatic sources or by dissociation of carbonate lithologies. Therefore in the present study the carbon isotope compositions suggest at least two sources, the heavier isotopes indicating a fluid precipitated origin and the lighter values showing a biogenic origin. Comparing with the existing carbon isotope data on graphite from the Kerala Khondalite Belt in southern India (Fig. 5.8), the carbon isotope compositions of graphite in the MGB show many similarities. (Farquhar and Chacko, 1991; Santosh and Wada, 1993a, b; Radika *et al.*, 1995; Farquhar *et al.*, 1999; Satish-Kumar *et al.*, 2002; Santosh *et al.*, 2003). In the KKB, graphite occurs in different settings, such as disseminations in metapelitic rocks, as epigenetic veins, flaky graphite in brittle shears and in pegmatites. Since the graphite samples of the present study were collected from lateritized horizons, a direct comparison is difficult. However, the carbon isotope results and field relation with the respective rock types indicate that depleted isotope values correlate with the biogenic graphite that occur as disseminations in metasedimentary



**Fig. 5. 8 Histogram plot of the existing carbon isotope data from SGT, in comparison with the isotope data of the MGB graphite (modified after Santosh et al., 2003).**

**The carbon isotope data of the MGB graphite show a spread in isotope values suggesting different carbon source such as biogenic or igneous.**

gneisses. However signatures correspond to the graphite formed from the precipitation of CO<sub>2</sub> rich fluids (Farquhar and Chacko, 1991; Santosh and Wada, 1993b).

## **5.8 DISCUSSION**

### **5.8.1 Structural characterization of graphite**

Depending on the degree of metamorphism crystallinity often changes and so very well ordered graphite with high crystallinity is seen in the upper amphibolite to granulite facies metamorphism. In the present samples XRD studies gives signatures of well-crystallised graphite and the Raman spectrum derived is very much analogous. The carbon isotope data, which gives two sources of carbon for the graphite genesis-the biogenic precursor and the carbonic fluid from the deeper crust. Crystallinity of metamorphic graphite can be correlated with the temperature and lithological pressure (Tuinstra and Koenig, 1970; Landis, 1971; Beny-Bassez and Rouzaud, 1985; Luque *et al.*, 1998). But in the case of fluid deposited graphite it always a matter of controversy that the crystallinity has no much relation with the temperature of formation. But the fluid deposited graphite through out the world often shows high crystallinity and the low-crystalline graphites of this type are comparatively less (Luque *et al.*, 1998).

### **5.8.2 Metamorphic Condition During Graphitization**

The present temperature estimate for the crystallization of graphite is in agreement with the earlier thermometric estimates for the high-grade metamorphic rocks of the terrain as well as the P-T range estimated in this

work (Chapter 4). Further, the narrow range of temperature observed in the samples indicates that processes like exhumation and retrogression have not affected the graphite crystallinity. This aspect of the irreversible nature of graphite formation that has earlier been reported for lower grade metamorphic terrains (Grew, 1974; Pasteris and Wopenka, 1991), thus hold good for the high-grade rocks as well.

## 5.9 CONCLUDING REMARKS

- The  $d_{(002)}$  values of the graphite crystals and their high crystallite size  $L_{C(002)}$  suggests that the graphite occurring in the MGB is well ordered.
- The calculated graphitization degree suggests a high temperature formation of the graphite of the order of  $700 \pm 100^{\circ}\text{C}$ , which is in agreement with the available geothermometry data for the terrain.
- The present study extends the idea that the graphite crystallization is always a progressive reconstruction process even to the highest grades of metamorphism and is an irreversible phenomenon, which has the potential to be used as a metamorphic thermometer to assess the peak metamorphic temperature.
- Raman spectral properties of graphite also attest the high degree of crystallinity and thereby its high temperature origin.
- Based on the preliminary carbon isotope results it can be considered that there exists more than one source for carbon in the graphite deposits in the MGB.



".....The story of granulite fluids is just beginning to be told....."

-Prof. Robert C. Newton

# CHAPTER 6

## FLUID INCLUSION STUDIES

---

## 6.1 INTRODUCTION

The thermodynamically isolated micro geochemical systems entrapped in various minerals during their growth are popularly known as "fluid inclusions". Fluid and melt inclusions provide a wealth of information on the genetic and evolutionary history of the mineral assemblages in a rock or ore formation as they furnish valid clues for the physico-chemical interpretations. They represent ideal samples of the fluid or melt, which were in equilibrium with host mineral either during its genesis or at later stages. These fluids can be trapped in a crystal along the growth zones or crystal edges or in any imperfection of the crystal growth. These are called primary inclusions. When a mineral is fractured during growth syngenetic micro-cracks will be healed in the presence of a fluid, which may be trapped as pseudosecondary inclusions. Any stress after crystal growth will lead to epigenetic fractures and secondary inclusions may be the result of their recrystallisation. Primary and pseudosecondary inclusions will thus contain the fluid from which the host crystal has grown. Therefore they can provide information on the fluid composition of the corresponding environment (magmatic hydrothermal fluids, basinal brines, heated meteoric waters, etc.) (Shepherd *et al.* 1985). But secondary inclusions provide information on the later geological history of a crystal. A fluid inclusion represents a closed (isochoric) system, which is defined by pressure (P), temperature (T), volume (V) and chemical composition (X). Two of these parameters (V, X) are fixed during formation of an inclusion while P and T remain variable after trapping.

At room temperature most fluid inclusions contain two phases, a vapour bubble and (aqueous) solution. But other phase combinations as two immiscible liquids (liquid CO<sub>2</sub> and water for example) with or without a vapour bubble are also common. Different occurrence of fluid inclusion and their classifications are illustrated in table 6.1.

**Table. 6.1 Classification of Fluid-Inclusions**

TYPE	BRIEF ACCOUNT
I	Vapor / Gas-rich / Monophase Fluid Inclusion
II	Biphase, Vapor / Gas-rich Fluid Inclusion (Gas> Liquid)
III	Biphase, Liquid-rich Fluid Inclusion (Liquid>Gas)
IV	Triphase, Immiscible Liquid-rich Fluid Inclusion (Aqueous Phase >CO <sub>2</sub> Liquid >CO <sub>2</sub> Gas)
V (a)	Polyphase, Gas-rich, High Saline (Gas >Liquid >Solid)
V(b)	Polyphase, Liquid-rich, High Saline (Liquid >Solid > Vapor)
V(c)	Polyphase, Solid-rich, High Saline (Solid>Liquid>Gas)

Additional solids may occur, which are termed daughter crystals if they are precipitated from the trapped solution. Halite is by far the most common solid phase observed. A distinction is made between these solids and 'captive' or captured mineral phases accidentally trapped together with a proportion of the fluid. In practice a distinction between captured and daughter minerals is difficult. The best way is to visually check the phase ratios. It will be more or less constant in inclusions of different size in a

given generation, since the probability of trapping captive minerals giving constant liquid/solid volume ratio is very low. Also the captive minerals will be often anomalously large compared to their host inclusion, Thirdly, if the solid phases also occur as solid inclusion within the crystal it is quite likely, that they represent accidental trapping of materials nucleating or settling on to the surface of the crystal. As a general rule, only one crystal of each daughter mineral is developed within a single inclusion in geological samples.

The aim of any fluid inclusion study is the reconstruction of the PTVX properties. The most applied method is microthermometry which, means the observation of individual fluid inclusions on a heating and freezing stage under the microscope at a temperature range of  $-180^{\circ}\text{C}$  (i.e. cooling with liquid nitrogen) to  $+600^{\circ}\text{C}$ . After complete freezing (solidification) the inclusions are carefully warmed or heated and any observable phase change up to total homogenization (one-phase state) is recorded. Initial melting of any solid phase permits the identification of the involved aqueous and also gaseous systems ( $\text{H}_2\text{O}-\text{NaCl}$ ,  $\text{H}_2\text{O}-\text{CO}_2$ ,  $\text{CO}_2-\text{CH}_4$ , etc.). Final melting temperatures (or temperatures of dissolution) point to the concentration of individual components in the corresponding system. The freezing-point depression of ice in aqueous inclusions, for example, is a measure of the total salt concentration (salinity), which is commonly expressed as weight percent NaCl equivalent. The temperature of total homogenization of an inclusion defines its density. Furthermore the homogenization temperature means the minimum trapping temperature (Roedder, 1984; Belkin, 1994 etc).

## **6.2 CRITERIA FOR RECOGNITION OF THE ORIGIN OF FLUID INCLUSIONS**

The distinction of various types of inclusions is quite significant in fluid inclusion studies. The main features of different categories of inclusions as given by Roedder (1984) are summarised below.

### **6.2.1 Primary origin**

Fluid inclusions of primary origin usually are found as single crystal with or without evidence of direction of growth or growth zonation. It will occur as a single inclusion (or isolated group) in an otherwise inclusion free crystal. The other notable characteristics include:

- Large size of inclusion(s) relative to enclosing crystal and of equant shape.
- Isolated occurrence of inclusions away from other inclusions.
- Random three -dimensional occurrences of inclusions in crystal.
- Occurrence of daughter minerals of the same type as occurs as solid inclusions in the host crystal or contemporaneous phases

#### **6.2.1.a *Single crystals showing evidence of directional growth***

- Occurrence of inclusions along boundary between two different stages of growth.
- Occurrence of inclusions in a growth zone beyond a visible healed crack in earlier growth stage.

- Occurrence of inclusions between boundaries between sub-parallel growth zones.
- Occurrence of inclusions at intersection of growth spirals.
- Occurrence of relatively large, flat inclusions in the core or parallel to external crystal faces.
- Occurrence of inclusion(s) at the intersection of two crystal faces.

#### **6.2.1.b *Single crystals showing evidence of growth zonation***

- Occurrence of different frequencies or morphologies of fluid inclusions adjacent growth zones.
- Occurrence of planar arrays outlining growth zones (unless parallel to cleavage directions).

#### **6.2.1.c *Crystals evidencing growth from heterogeneous or changing fluid***

- Occurrence of inclusions with differing contents in adjacent growth layers (e.g. gas inclusions in one layer, liquid and water in another layer etc).
- Occurrence of inclusions containing some growth medium at points where crystals have overgrown and surrounding adhering globules of an immiscible phase (e.g. oil droplets).
- Occurrence of primary appearing inclusions with “unlikely” growth medium (e.g. Mercury in Chlorite, oil in Fluorite and Calcite etc).

#### **6.2.1.d Host other than single crystal**

- Occurrence of inclusions at growth surfaces of non-parallel crystals (these have been often leaked and could be secondary).
- Occurrence of inclusions in polycrystalline hosts.
- Occurrence in non-crystalline hosts.

#### **6.2.2 Secondary origin**

The major criteria for the identification of secondary inclusions are:

- Occurrence of inclusions in planer groups along planes those cross cut crystals or that parallel cleavages.
- Occurrence of very thin, flat and obviously “necking-down” inclusions.
- Occurrence of primary inclusions with filling representative of secondary conditions.
- Occurrence of inclusions along a healed fracture.
- Occurrence of empty inclusions in portions of crystals where all other inclusions are filled.
- Occurrence of inclusions that exhibit much lower (or more rarely, much higher) filling temperature than adjacent inclusions.

#### **6.2.3 Pseudo-secondary origin**

- Occurrences of secondary like inclusions with a fracture visibly terminating within a crystal.

- Occurrence of equant and negative crystal shaped inclusions.
- Occurrence of inclusions in each pit crosscutting growth zones.

### **6.3 CHANGES IN FLUID INCLUSION SINCE TRAPPING**

Most fluid inclusions will be trapped as a homogeneous fluid at elevated temperatures and pressures. During the subsequent cooling, the fluid may have separated into liquid and vapour, because the fluid contracts much more than the solid host mineral. Immiscible fluids may separate on cooling, and daughter crystals, usually halite or sylvite, may precipitate as saturation of fluid occurs. Many inclusions do not now have the shape they originally had because of solution and deposition in different parts of the inclusion cavity. In general, inclusions will tend, by solution and re-deposition, to reduce surface area to become more equant. Through this process, elongated inclusions may separate into several more equant inclusions as a result of "necking down". If the necking down occurs after biphasic separation, the process may isolate the vapour bubble in one of the new inclusions while leaving another new inclusion completely fluid filled. As a result, neither inclusion would be representative of the originally trapped fluid, nor the information that could be derived accurate. Larger flat primary inclusions or secondary cracks may undergo considerable recrystallisation in which one large inclusion is reduced to many small ones occupying the same region within the crystal. Leakage, the movement of material in or out of the original inclusion, can occur but is not that common; one exception may be high grade metamorphism in which recrystallisation



can markedly alter inclusions. It is evident, however, when one observes planes containing large number of inclusions, all of which are empty. Generally, quartz, fluorite, calcite and sphalerite are free from leakage problems; barite and gypsum are more prone to such problems.

#### **6.4 COMPOSITION OF FLUID INCLUSIONS**

By far the most abundant type of fluid inclusion is that which contains a low viscosity liquid and a smaller volume of gas or vapour bubble. The liquid is generally aqueous has a pH within one unit of neutral, and contains a total salt concentration between 0 and 40 weight percent. The salts contain major amounts of  $\text{Na}^+$ ,  $\text{K}^+$ ,  $\text{Ca}^{2+}$ ,  $\text{Mg}^{2+}$ ,  $\text{Cl}^-$  and  $\text{SO}_4^{2-}$  ions, with minor amount of  $\text{Li}^+$ ,  $\text{Al}^{3+}$ ,  $\text{BO}_3^{3-}$ ,  $\text{H}_4\text{SiO}_4$ , and bicarbonate and carbonate ions. Na and Cl ions are usually dominant.  $\text{CO}_2$  in both liquid and gas form and liquid hydrocarbon are fairly common. Liquid hydrogen sulphide has also been observed, but is rare. Carbon dioxide occurs as a supercritical fluid above  $31^\circ\text{C}$ , its critical point. Daughter minerals, usually cubes of halite or sylvite form when nearly saturated fluids cool from the initial temperature of entrapment. Other crystals that are observed but are not simple precipitates of a supersaturated solution include sulphides, quartz, anhydrite, calcite, hematite and gypsum. Such crystals either form before the inclusion was finally sealed, as a result of secondarily introduced fluids or even through oxidation resulting from hydrogen diffusion (Roedder, 1979).

## 6.5 FLUIDS IN METAMORPHIC ROCKS

Studies on the genesis, composition and petrological relationship of the inclusive fluids in the metamorphic minerals have become one of the most active fields of research in metamorphic petrology. Fluid phase plays an essential role in metamorphic rock forming processes (Touret, 2001). Element transport, kinetics of crystal growth etc are some among them. But a good amount of complexity and difficulties are employed in the study of this fluid-mineral interaction. Therefore most of the workers are doubtful on the reliability of this study. This attitude is not justified since fluid inclusions are the part of the rock and they occupy as almost the same volume of the accessory minerals present in a rock. Studies on fluid inclusion in rocks of different metamorphic grade shows that there is a consistent relation of composition of fluids found in inclusion to the metamorphic conditions and the variation will be only according to the difference in grade (Crawford, 1981; Touret, 1981; Roedder, 1984; Crawford and Hollister, 1986). In a host mineral, the inclusions behave as closed volumes and during its path to exhumation in a definite P-T trajectory it maintains 'isochoric behaviour' (Touret, 1992). So in high-grade metamorphic rocks all most all the generation fluids are well preserved rather than in low-grade rocks which makes the studies much easier. (Touret, 2001; Frezzotti *et. al.*, 2004).

## 6.6 ANALYTICAL PROCEDURES

The conventional fluid inclusion analysis includes three major steps ie., the observation, measurements and interpretation. Observation usually focuses on the identification and the determination of relative chronology of

major inclusion types using a petrological microscope. The measurements are made usually by non-destructive microthermometric analysis to specify the composition and density of different fluid types. The interpretation part is based on the P-T conditions of metamorphism and the fluid inclusion isochores.

### **6.6.1 Optical examination of fluid inclusion**

Fluid inclusions are best seen and studied in cut mineral plates that are thick enough to contain the undamaged inclusion, but thin enough to readily transmit light and are doubly polished to minimize the interference of the sample imperfections and excessive diffuse light scattering. For most samples 1-1.5 mm thickness is quite satisfactory. The samples are then polished and reduced in thickness on the lapping machine using 80 mesh and 220 mesh carborundum powder in succession. After this, polishing is carried out on a glass plate using carborundum powder of 400, 600, 800, 1000 and 2000 mesh sizes respectively. Polishing using chromium oxide on the canvas cloth follows this. The final polishing is done on a satin cloth. The inclusions vary in size between 10 microns- 40 microns and a large variety of geometrical sizes were observed as perfectly rounded, tubular, rectangular, cubical, triangular and ellipsoidal. The inclusions vary largely in size and can mostly be seen with a 50X magnification.

A surprising amount of data can be obtained on the physical and chemical properties of fluid inclusions using simple optical examination. One of the most important parameters is the overall density of the inclusion at the time of trapping. The density estimate can then be utilized to define

an approximate P-T isochore and thereby calculate the minimum trapping temperature. The CO<sub>2</sub>:H<sub>2</sub>O ratios in inclusions containing immiscible CO<sub>2</sub> rich liquid aqueous solution can also be determined from phase ratios and the partial homogenization temperature of the CO<sub>2</sub> phase.

### 6.6.2 Degree of fill (F) and calculation of overall density

The degree of fill (F) is defined as the volumetric proportion of liquid (V<sub>L</sub>) relative to the total volume of the inclusion (V<sub>TOT</sub>).

$$F = (V_L) / (V_L + V_V), \text{ where } V_V + V_L = V_{TOT}$$

F is related to the total density of the inclusion (D<sub>TOT</sub>) by the following expression:

$$D_{TOT} = D_L F + D_V (1-F)$$

Where, D<sub>L</sub> = density of the liquid phase, D<sub>V</sub> = density of the vapour phase

In most cases it can be assumed that the density of the vapour phase is zero.

$$\text{Thus, } D_{TOT} = D_L F$$

The value of D<sub>L</sub> for a salt solution varies linearly as the salt concentration.

### 6.6.3 Estimation of phase proportions

Fluid inclusion volumes are relatively easy to estimate if the inclusions have a regular geometrical shape. Measurements of various dimensions in the plane of focus of the microscope are easily made with a calibrated, graduated ocular, and reasonable estimates also made of the depth dimensions of the inclusions. Bubble diameters fix the volume of the

vapour bubble (provided it is free to move and is not flattened) enabling the  $V_L$  and  $V_V$  to be calculated. Appropriate measurements for the solid phase allow  $V_s$  to be calculated. The procedure is even more straightforward if the inclusions are very flat since the assumption that “area=volume” is valid.

## 6.7 FLUID INCLUSION STUDIES IN THE MGB

Previous works on the fluid inclusions in the metamorphic rocks of the SGT include Santosh and Tsunogae (2003), Mohan *et al.* (1996a), Santosh (1991), Santosh *et al.* (1991), Santosh (1986a) etc from the MGB; some studies from the adjacent Kerala Khondalite Belt by Nandakumar and Harley (2000), Santosh (1986b); Raith *et al.* (1990), Srikantappa and others (1992) from Nilgiri granulites; and Satish-Kumar *et al.* (2001), about the fluid rock interactions in Ambasamudram area in the ACS.

Even though several studies are there on the fluids of the SGT in general, it is intricate to portray the complete picture about the types of fluids found in the different rocks of the terrain, the MGB in specific. But in garnet free terrains like the MGB, where the PT calculation, especially the palaeopressure calculations are difficult using the conventional methods of EPMA fluid inclusion studies is an effective tool. Santosh (1998) studied the fluid inclusion in the massive charnockites of the MGB and has found that pure CO<sub>2</sub> with uniform densities was the ambient fluid species during peak metamorphic time.

There are many other studies also concentrating on the carbonic inclusions and their role in the charnockitization processes. Mohan *et al.* (1996a) studied quartz from the charnockites of Kodaikanal massif and has

reported three fluid inclusions types: (1) monophasic high density CO<sub>2</sub>-rich (0.968–1.014g/cm<sup>3</sup>) as the dominant fluid phase; (2) aqueous biphasic CO<sub>2</sub>-H<sub>2</sub>O (0.888–0.915 g/cm<sup>3</sup>) and (3) late minor aqueous H<sub>2</sub>O inclusions with no visible CO<sub>2</sub>. CO<sub>2</sub>-isochores for the high density fluid inclusions yield a pressure limit of ca. 6.5kb, at granulite facies temperatures of ca. 800°C, which is in accordance with the estimation from mineralogical thermobarometry. The P-T path delineated from combined mineralogical and density data on carbonic inclusions is characteristically T-convex suggesting an isothermal decompression path and rapid uplift followed by cooling of a tectonically thickened crust. Recently, Sukumaran *et al.* (2005) in his study on the fluid inclusions from different rock types of Palghat brought out three generations of fluid inclusions viz., CO<sub>2</sub>, CO<sub>2</sub>-H<sub>2</sub>O, and CO<sub>2</sub>-H<sub>2</sub>O-NaCl. The CO<sub>2</sub> inclusions are of variable densities between 1.03 g/cm<sup>3</sup> and 0.71 g/cm<sup>3</sup> and it is stated that the inclusions were trapped at different stages of high-grade metamorphism. From the Trivandrum Block (TB), Fonarev *et al.* (2003) has also identified three generations of CO<sub>2</sub> bearing inclusions among which one is a high-density species (1.041-1.012 g/cm<sup>3</sup>). Relatively fewer amounts of aqueous inclusions and their low salinity are pointed out there to rule out any metasomatic processes involved in charnockite formation. However the three generations of CO<sub>2</sub> rich inclusions are very much common in the charnockites and associated rocks in and around the MGB. Thus the presence of CO<sub>2</sub> bearing inclusions and its role in high-grade metamorphism and charnockite building processes is the unique feature in all the studies carried out so far. High-

density carbonic fluids, which corresponds to the peak metamorphic time is reported in most of the studies.

## **6.8 PRESENT STUDY**

Though the earlier fluid inclusion studies of the charnockites from the MGB of the SGT have given evidences for the involvement of CO<sub>2</sub> fluid in charnockite making process no much study has been carried out to know the relation of CO<sub>2</sub> influx and the graphite mineralization in the area. Some of this graphite is found to be giving the signatures of fluid origin (see Chapter V). So a detailed study on the influence of CO<sub>2</sub> influx in graphite mineralization is of much importance. From the studies on the mineralogical characteristics of the graphite, it has been noticed that these graphites are having a crystallization temperature of 700±100°C (see Chapter V). So the present study is aimed at finding out the temperature of entrapment of the CO<sub>2</sub> inclusions in the graphite bearing rocks and to discuss the role of CO<sub>2</sub> in graphite genesis.

### **6.8.1 Sample locations**

Fluid inclusions were studied from the charnockites of eleven localities in the southern part of the MGB (Fig 6.1). These localities are Valavoor (Sample Nos: G4, CK108), Punchavayal (Sample No: G5), Kannimala (Sample No: G6), Muvattupuzha (Sample No: CK6B), Mamala (Sample No: CK57G), Erumeli (Sample No: CK42), Kanjiramattom (Sample No: CK73), Manjamattom (Sample No: CK109), Supplapuram (Sample No: CT122) and Muthukudi (Sample No: CT125). Most of the samples selected for the study are graphite bearing. In some samples graphite is not visible

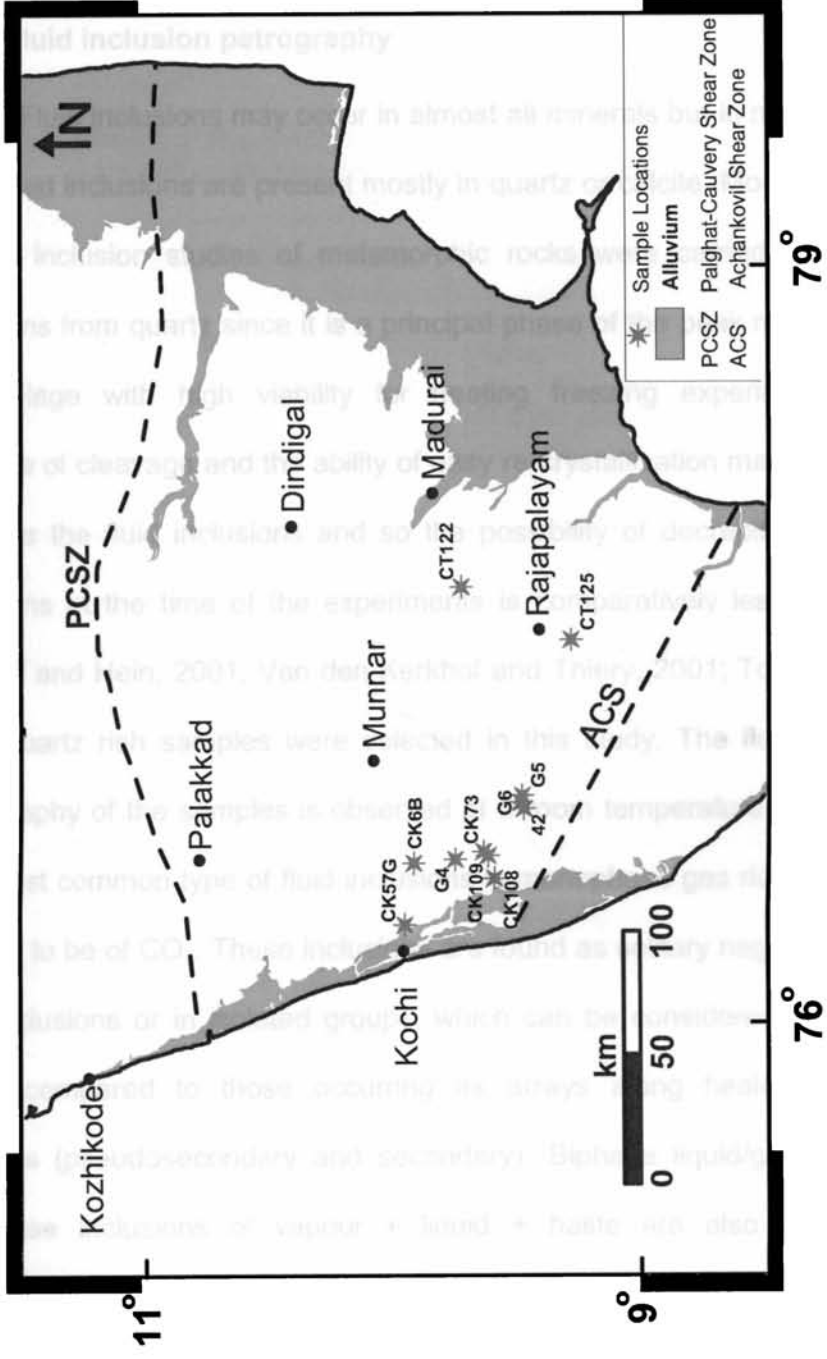


Fig. 6.1 Sample locations of fluid inclusion studies



megascopically but it is found in the weathered equivalent of the rock (laterite) in the area. Details about the sample location and the rock types are given in table 6.2.

### **6.8.2 Fluid inclusion petrography**

Fluid inclusions may occur in almost all minerals but in metamorphic rocks fluid inclusions are present mostly in quartz or calcite. More than 90% of fluid inclusion studies of metamorphic rocks were carried out in the inclusions from quartz since it is a principal phase of the peak metamorphic assemblage with high viability for heating freezing experiments. The absence of cleavage and the ability of easy re-crystallization make quartz to preserve the fluid inclusions and so the possibility of decrepitation of the inclusions at the time of the experiments is comparatively less (Van den Kerkhof and Hein, 2001; Van den Kerkhof and Thiery, 2001; Touret, 2001). Thus quartz rich samples were selected in this study. The fluid inclusion petrography of the samples is observed at a room temperature of 26-28°C. The most common type of fluid inclusions is monophasic gas rich which are inferred to be of CO<sub>2</sub>. These inclusions are found as solitary negative crystal type inclusions or in isolated groups, which can be considered of primary origin, compared to those occurring as arrays along healed or fresh fractures (pseudosecondary and secondary). Biphasic liquid/gas rich and polyphasic inclusions of vapour + liquid + halite are also noticed as pseudosecondary or secondary type. Some melt inclusions are also noticed in some of the samples. Brief description of the samples from the eleven localities studied and the nature of inclusions seen in them are given below.

**Table 6.2. Details of the location and the major rock types present there from which the samples for fluid inclusion studies are taken**

<b>Sample No.</b>	<b>Location / Place Name</b>	<b>Rock types in the location</b>
G4	Uzhavoor (Kerala)	Massive charnockite, Garnet biotite gneiss
G5	Punchavayal (Kerala)	Massive charnockite
G6	Mundakayam (Kerala)	Massive charnockite
6B	Muvattupuzha (Kerala)	Mafic medium grained charnockite
57G	Mamala (Kerala)	Massive charnockite
42	Erumeli (Kerala)	Massive charnockite
73	Kanjiramattam (Kerala)	Massive charnockite
108	Valavoor (Kerala)	Massive charnockite
109	Manjamattom (Kerala)	Mafic massive charnockite
122	Supplapuram (Tamil Nadu)	Charnockite, Garnet biotite gneiss, Pegmatites
125	Muthukudi (Tamil Nadu)	Charnockite, Garnet biotite gneiss

Two samples are studied from the Valavoor due to the heterogeneity observed in the rock types from adjacent quarries. In the location at Valavoor-1 (V1), the major rock type present is massive charnockite, which has been retrogressed to form garnet-biotite gneiss at several places. The presence of pegmatitic veins intruded in zigzag manner all over the charnockites gives some evidence for the cause of the retrogression. Graphite is found syngenetic to the pegmatites and gneisses. The sample for the fluid inclusion study is taken from the charnockite-gneiss contact zone.

Monophase, biphasic as well as polyphasic inclusions are present in the sample G4B. Monophase inclusions of variable dimensions and cavity shapes are found in isolated groups or as single inclusions, which can be considered as older generation fluids. These are but comparatively less in number and measure up to 20 micron size (Plate 6.1a). Most of the biphasic inclusions appear to be secondary or pseudosecondary. These are occurring as trails trapped in fractures that developed after the initial crystallization of the mineral grains in which they are found. Many of the trails occur entirely in the interior of the grains and do not extend to the grain boundaries. However fluid inclusion arrays crossing the grain boundaries are never noticed. The secondary/pseudosecondary biphasic inclusions are found very much distorted and leaked indicating post inclusion deformations in the rock (Plate 6.1b).

Valavoor-2 (V2) is a massive charnockite quarry, which is near to V1, but the retrogressive character noticed at V1 is not found in this exposure. Graphite is also absent here. The fluid inclusion petrography also

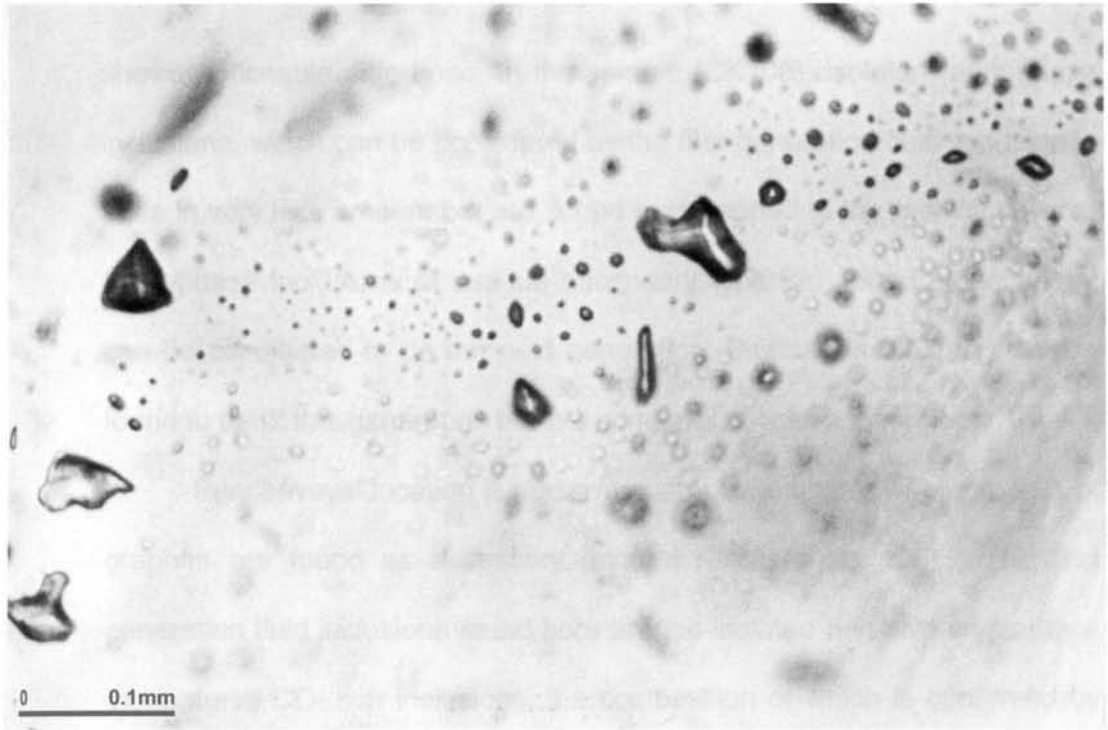


**PLATE 6.1a** Monophasic inclusions of variable dimensions and cavity shapes from sample G4B

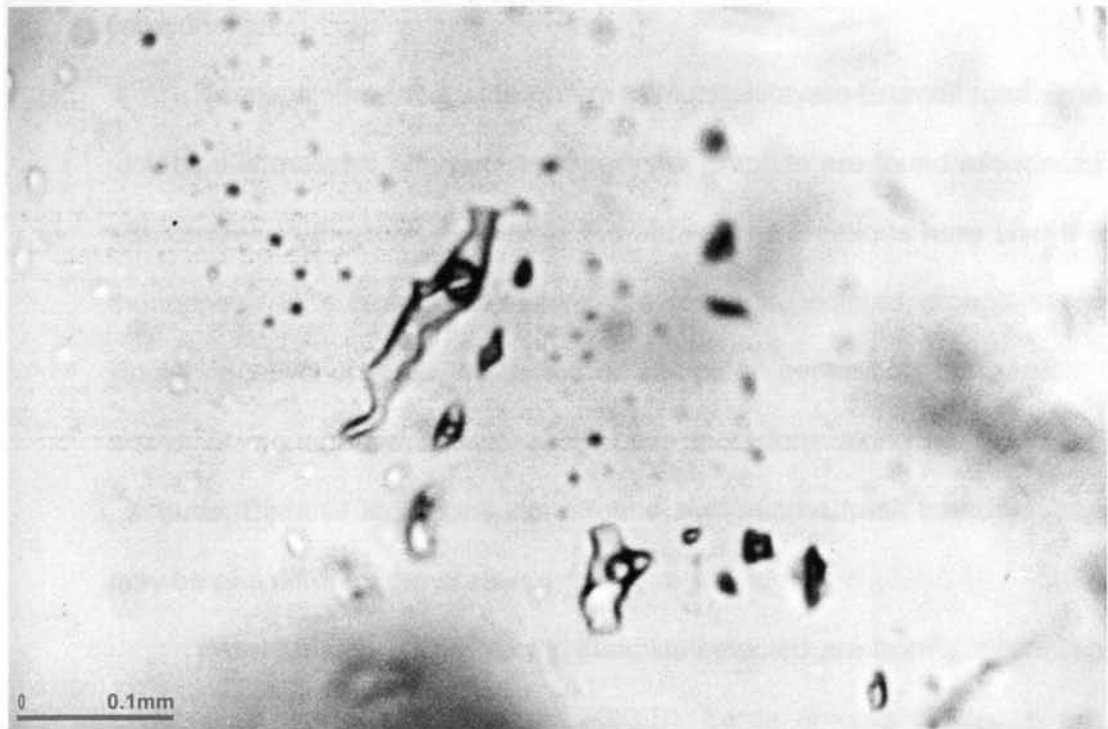


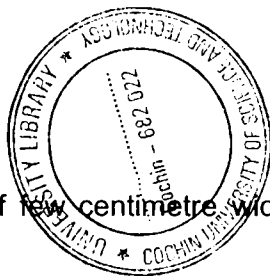
**PLATE 6.1b** Pseudosecondary biphasic inclusions from sample G4B showing leakage/distortion

shows noticeable difference. In the sample (CK108), isolated monophase inclusions, which can be considered as the first generation fluid inclusion is seen in very less amount but are, found post trapped to the melt inclusions. Monophase inclusions of pseudo secondary type i.e., found along arrays can be considered to be the next generation. Biphase inclusions are also found to be of this generation but are comparatively less in number.

Punchavayal location is massive charnockite quarry where specks of graphite are found as accessory mineral (Sample No. G5). The first generation fluid inclusions found here are the isolated negative crystal type monophase CO<sub>2</sub> rich inclusions, the composition of which is confirmed by microthermometry. The second-generation inclusions include both monophase as well as biphase. The biphase inclusions are of CO<sub>2</sub> + H<sub>2</sub>O components.

Kannimala is a roadside quarry in Mundakkayam-Erumeli road. The rock type is massive charnockite. Specks of graphite are found associated with biotites in the rock. Similar to the above said locations here also the monophase CO<sub>2</sub> bearing inclusions are found in isolated groups or as single negative crystals which forms the older generation, followed by arrays of monophase as well as biphase inclusions along healed micro fractures. Biphase inclusions alone found along some fresh fractures, and may be of a different generation.

From Muvattupuzha quarry, samples selected are from a migmatitic body associated with charnockite (CK6B). Large amount of biotites are found in the charnockite giving it a dark appearance. Migmatitic texture is within the charnockite characterised by alternating quartzo-feldspathic



09147

bands. Quartz veins of few centimetre widths are traversing all over the rock body.

The monophasic fluid inclusions found are inferred to be of comparatively older whereas the biphasic inclusions ( $\text{CO}_2 + \text{H}_2\text{O}$ ) and ( $\text{CO}_2$  gas +  $\text{CO}_2$  liquid +  $\text{H}_2\text{O}$ ) bearing polyphasic inclusions are also noticed as younger generation.

Medium grained charnockite (CK42) collected from Erumeli for the fluid inclusion studies only bear rare amount of isolated monophasic inclusions but rich in pseudosecondary/secondary biphasic inclusions. Presence of polyphasic inclusions or triple phase inclusions (liquid + gas + solid) is a peculiarity observed in the sample. The solid phase is identified as halite.

Mamala is an extensive charnockite hillock covering  $>1\text{km}^2$  showing much heterogeneity in the mineral assemblage at its different parts. Generally speaking the charnockite is massive in nature affected by a series of E-W trending vertical faults. The fault plains are characterised with considerable amount of mylonites and pseudotachylites. The presence of garnet, cordierite and thin flakes of graphite are noticed in some parts of the rock. Fluid inclusion wafers prepared for analysis are from less deformed part (CK57G). Isolated monophasic inclusions are rarely found in the samples, but those which noticed are of secondary/pseudosecondary origin which appeared like "rain droplets" (Plate 6.2).

Mafic charnockite (CK73) from Kanjiramattom is characterised with both monophasic and biphasic fluid inclusions. The first generation monophasic inclusions (the isolated ones seen in other locations) are not

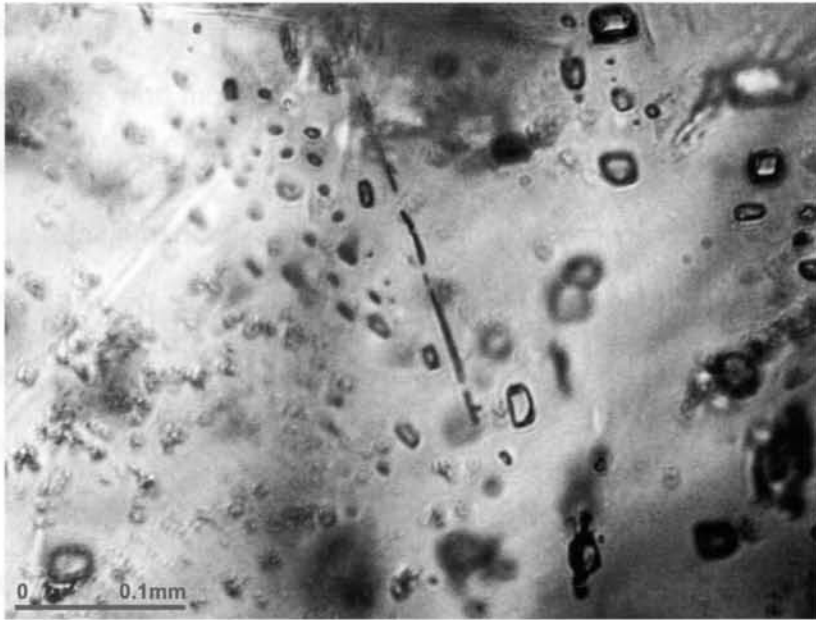


**Plate 6.2** Array of monophasic fluid inclusions from CK57G



**Plate 6.3** Biphasic leaked inclusions from sample CK.73

visible in the sample. Pseudosecondary type monophase inclusions along linear arrays are seen. Biphasic inclusions are also found to be of this generation, and most of them are CO<sub>2</sub> rich showing leakage of the second phase (Plate 6.3). This leaked phase is believed to be of H<sub>2</sub>O composition.

Manjamattom, which is also a massive charnockite exposure (CK109) near to Kanjiramattom is characterised mostly by biphasic pseudosecondary/secondary type fluid inclusions. Monophase inclusions are hardly seen.

Supplapuram and Muthukudi are two locations from Tamil Nadu. Major rock type found at Supplapuram is charnockite in contact with garnet-biotite gneiss. The gneiss is formed as a retrogressive counterpart of the charnockite. Flakes of graphite are very much visible along the foliation planes of the gneiss whereas in charnockite the graphites are found isolated or disseminated. Pegmatite veins of 5-10cm width have intruded the charnockite in a zigzag pattern. Fluid inclusions of the charnockite were studied (CT122). Primary monophase inclusions are rarely seen. Many arrays of secondary/pseudosecondary monophase inclusions are available. In this category biphasic inclusions are less in number.

Muthukudi is a large hillock composed of garnet-biotite gneiss within which small patches of charnockite are seen. The charnockites developed, gives arrested nature (Incipient charnockite). The inclusions found in the sample CT125 are mostly CO<sub>2</sub> rich monophase and are found in quartz as well as garnets. CO<sub>2</sub> + H<sub>2</sub>O biphasic inclusions are also found common (Plate 6.8) and both appears to be pseudosecondary in nature of almost the same generation. This sample is also devoid of primary type inclusions.



### 6.8.3 Chronology of the fluid inclusions

From all the samples selected for the fluid inclusion analysis, a general chronology of fluid trapping can be traced out based on fluid inclusion petrography. Even though some generations of fluid inclusions are not visible in some of the samples, may be due to some localized petrological changes, the overall picture can be described as below which can be further substantiated with the help of microthermometric studies (See section 6.9).

Chronologically the fluid inclusions can be grouped into three major generations. They are:

- i) Monophase carbonic inclusions with well-developed negative crystal shape seen isolated or in isolated groups in the samples. Based on fluid inclusion petrography this can be considered to be of primary origin (Plate 6.4) but since most of the host rocks are massive in nature and primarily grown minerals generally are not preserved (Van den Kerkhof and Hein, 2001) these inclusions can be termed 'early' or 'first generation'.
- ii) Monophase carbonic inclusions of pseudosecondary type (occurring in arrays mostly along healed fractures) (Plate 6.5). This can be considered to be the modified first generation fluid inclusions. Sometimes biphasic ( $\text{CO}_2 + \text{H}_2\text{O}$ ) inclusions are also found as pseudosecondary type, which may be of the same generation due to some heterogeneous trapping, or of

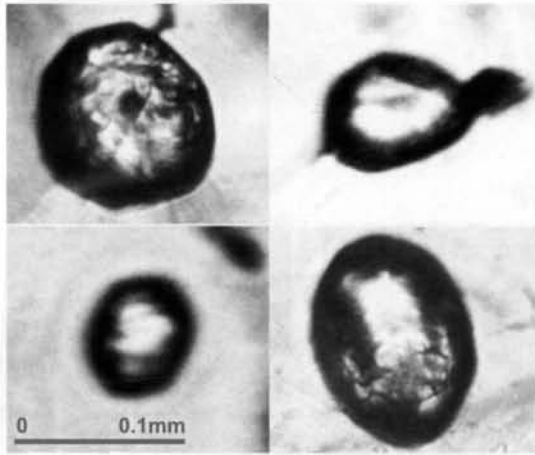
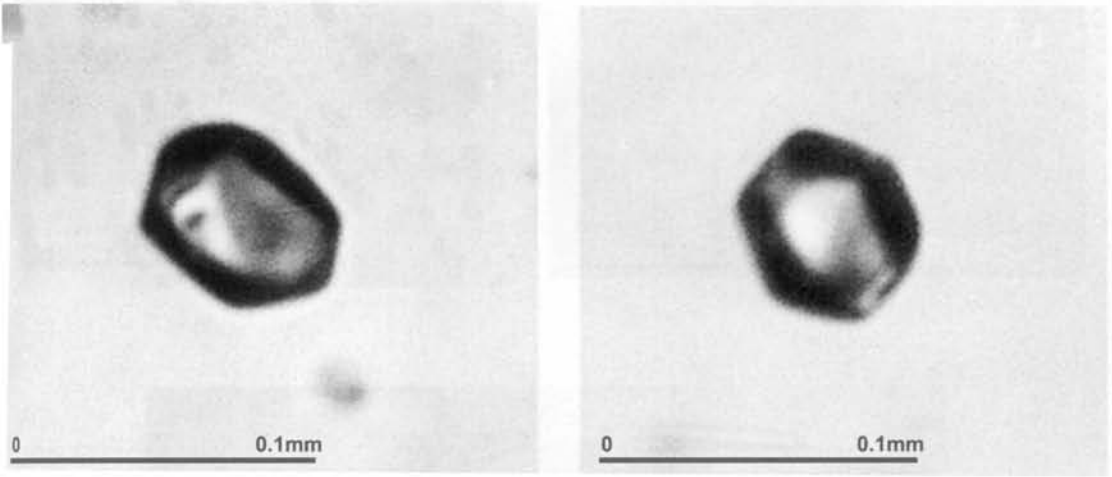
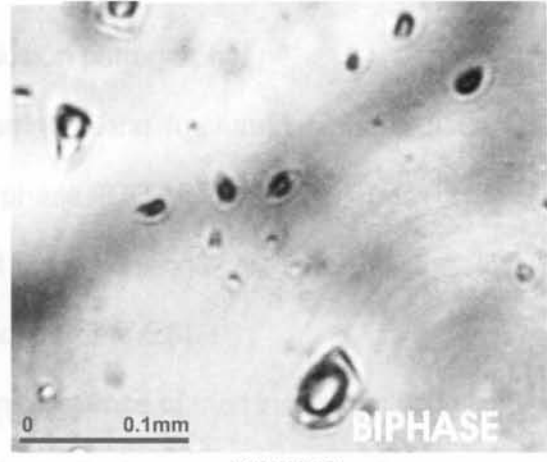
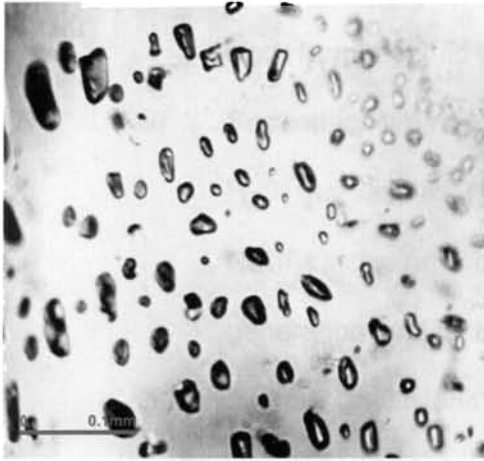


**Plate 6.4** First generation monophasic inclusions



BIPHASE

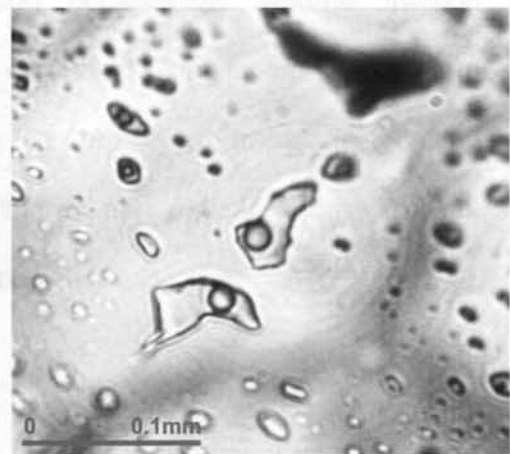
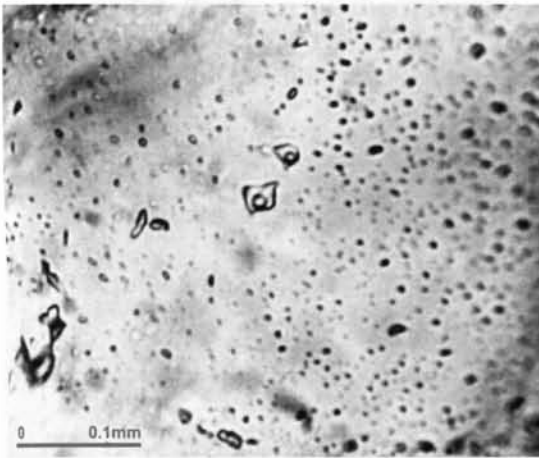
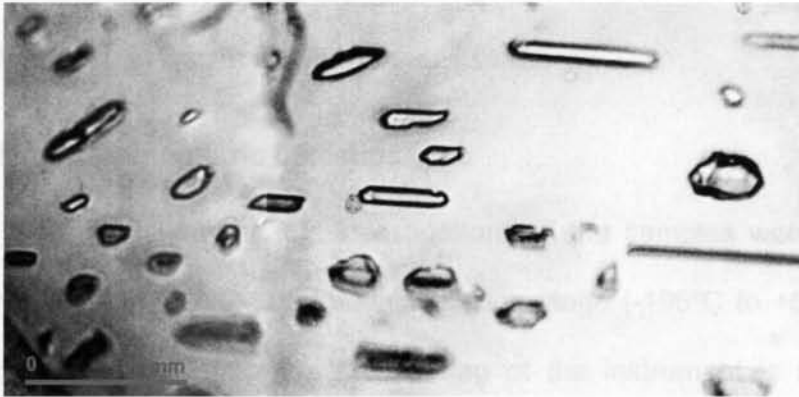


**Plate 6.5** Second-generation pseudosecondary monophasic/biphase inclusions

two different generations. Their relative chronology is not clear from the fluid inclusion petrography.

- iii) Secondary type (occurring along fractures) biphasic ( $\text{CO}_2 + \text{H}_2\text{O}$ ) as well as polyphasic ( $\text{CO}_2$  liquid +  $\text{CO}_2$  gas +  $\text{H}_2\text{O}$  +  $\text{NaCl}$ ) inclusions that can be considered to be the last generation fluid inclusions (Plate 6.6).

Other than fluid inclusions rare presence of melt inclusions is noticed in some of the samples and chronologically it appears to be earlier than all the types of fluid inclusions, i.e., the first generation of fluid inclusion, were post entrapped to the melt inclusions.

#### **6.8.4 Microthermometric Investigations**

The microthermometric investigations of the samples were carried out on a Linkam TMSG-600 heating-freezing stage ( $-196^\circ\text{C}$  to  $+600^\circ\text{C}$ ) at IIT Bombay (Plate 6.7). The thermal lag of the instrument is noted as  $\pm 1.1^\circ\text{C}$ . Fluid inclusions in quartz alone were investigated. The data obtained from microthermometry, and occasionally volume fraction estimates of the fluid inclusions were evaluated using computer program package FLUIDS-1 (Bakker, 2003) in order to transform melting temperatures, homogenization temperatures and optical volume fraction estimates into bulk compositions and densities.

##### **6.8.4a Freezing stage experiments**

The freezing stage experiments conducted in almost all samples in which both monophasic and biphasic inclusions were studied. From the analysis the presence of  $\text{CO}_2$  is confirmed by measuring the melting

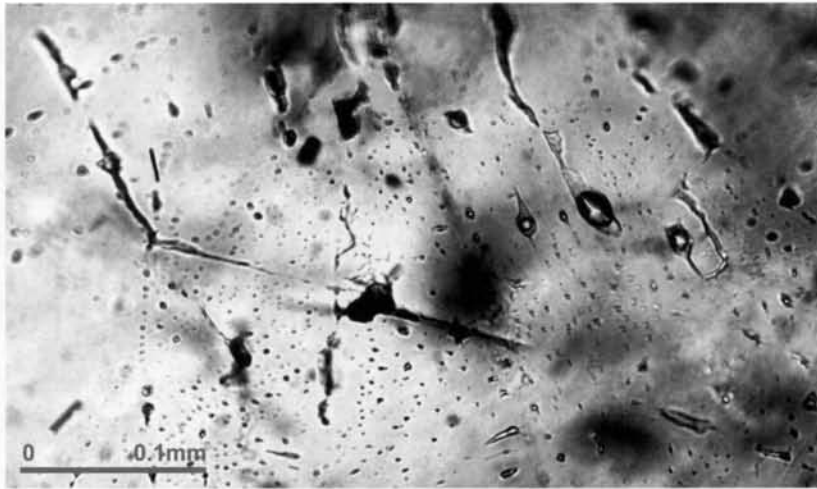
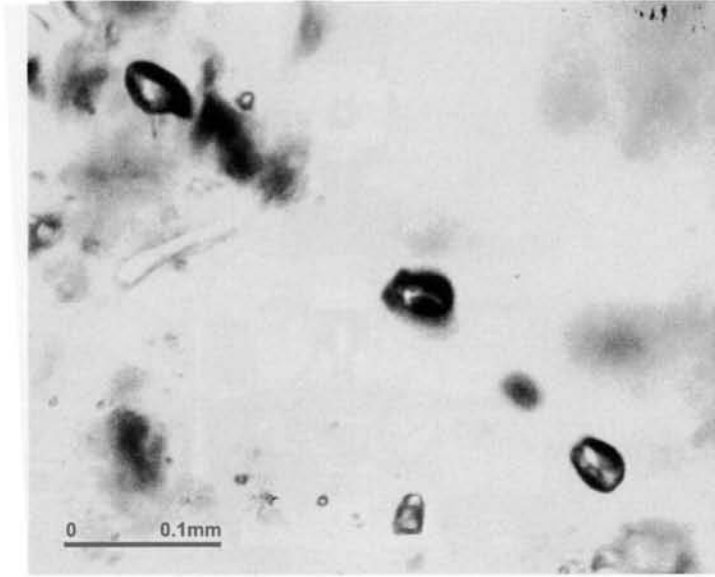
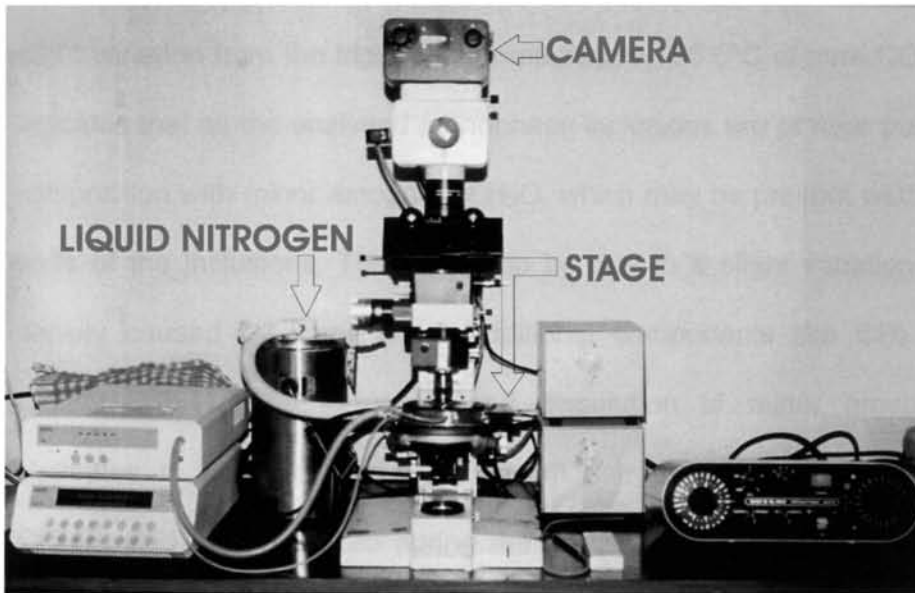


**Plate 6.6** Third generation secondary biphase inclusions



Linkam TMSG-600, Heating-Freezing stage attached to a Petrological Microscope

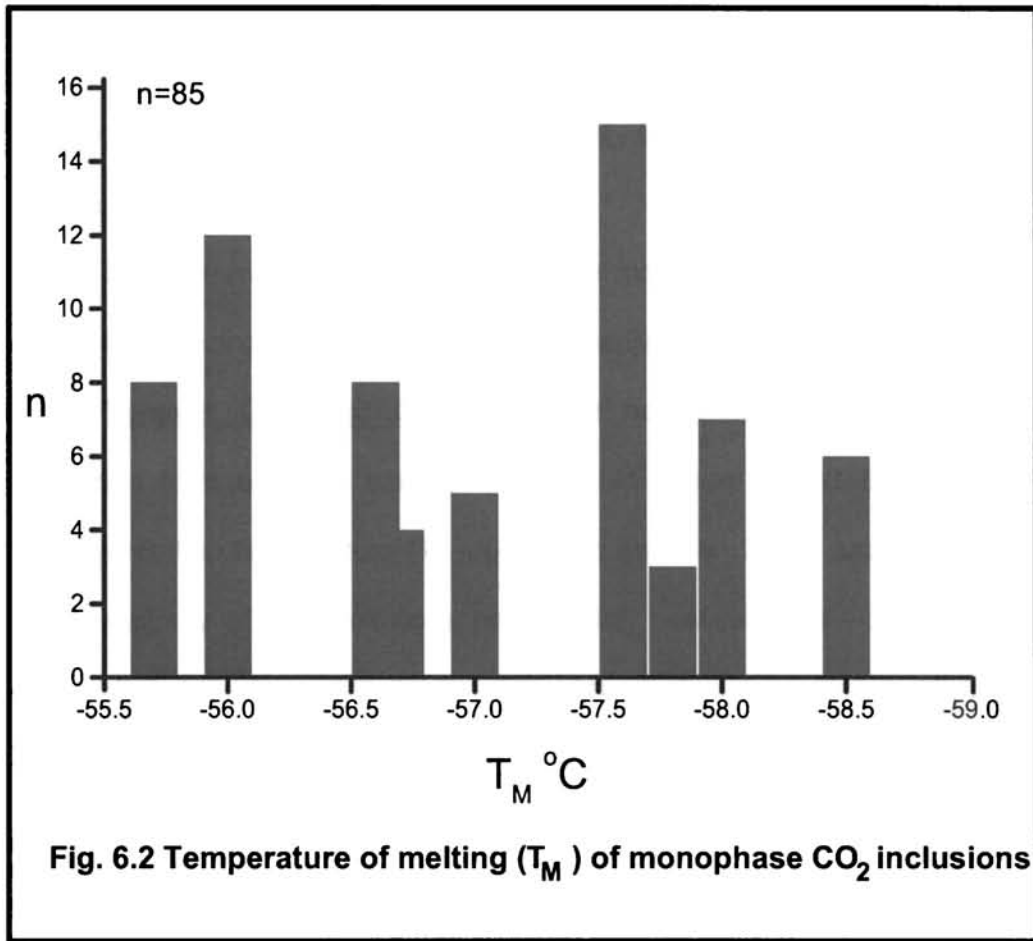


Fluid inclusion lab at IIT Bombay

temperature ( $T_M$ ) of the inclusions. In the given samples the  $T_M$  of  $CO_2$  inclusions ranges between ( $-55.7^\circ C$ ) to ( $-58.5^\circ C$ ) (Fig 6.2), which is having slight variation from the triple point temperature,  $-56.6^\circ C$  of pure  $CO_2$ . This indicates that all the analysed monophasic inclusions are of near pure  $CO_2$  composition with minor amounts of  $H_2O$ , which may be present wetting the walls of the inclusions. This may also be due to a slight variation in the density caused by some other additional components like  $CH_4$  or  $N_2$  (Touret, 1981). The formation and dissolution of minor amounts of clathrates in some of the inclusions in samples CK6, CK42, CK57G, CK108, CT122 and CT125 during the freezing-heating analysis supports this fact. It is also noted that  $T_M (CO_2)$  of these clathrate bearing inclusions falls exactly between  $-57.6^\circ C$  and  $-58.5^\circ C$ . However this contamination is less significant because  $CO_2$  inclusions of  $T_M$  up to  $-58^\circ C$  contain less than 8 mole percent methane (Burruss, 1981). But there are earlier findings which points that, a very few inclusions are capable of preserving their original density since majority of inclusions re-equilibrate to the changes in P-T conditions during the time of uplift (Sternner and Bodnar, 1989; Hollister, 1988; Bakker and Jensen, 1991) and the lower density inclusions are trapped during the late stage of evolution (Vitik and Bodnar, 1995a).

#### **6.8.4b Heating stage experiments**

As a liquid  $CO_2$  fluid inclusion cools, a vapour bubble eventually appears and on reheating it will disappear called the temperature of homogenization ( $T_H$ ). It is generally taken to be the isochore for that inclusion intersects the liquid-vapour boundary curve. In the present





samples the monophasic CO<sub>2</sub> inclusions are homogenising within a range of +9.4°C to +20.1°C and the CO<sub>2</sub> in the mixed carbonic aqueous inclusions are homogenising into a liquid phase at comparatively higher temperature (+21.7°C to +31°C) obviously due to low density (Fig 6.3). An example for a mixed CO<sub>2</sub> Liquid+ CO<sub>2</sub> Vapour + H<sub>2</sub>O inclusion (from sample CK 73) while freezing from room temperature (26.8°C) to -184°C and then heating up to the complete homogenisation temperature of 349°C is illustrated in Plate 6.8. From the picture the T<sub>M</sub> (CO<sub>2</sub>) is found at -56.7°C and T<sub>H</sub> (CO<sub>2</sub>) vapour bubble at 31°C.

The behaviour of biphasic/polyphasic inclusions from the samples during the freezing-heating analysis is summarised as below.

Samples G4B and G5: The total homogenisation of biphasic inclusions from both the samples is to liquid phase. For G4B the total homogenisation temperature (T<sub>H (TOT)</sub>) range between 200°C and 348°C in which majority of the inclusions homogenise between 343 –348°C (Fig 6.4a). Halite crystals are found in some of the inclusions, which are found dissolving at 210.6°C. In sample G5, the T<sub>H (TOT)</sub> is noticed at 380 °C.

Sample G6: The biphasic/polyphasic inclusions from sample G6 show a striking peculiarity that they are found homogenising into gaseous state at very high temperature at 800 to 1000°C. Only one or two inclusions are showing the T<sub>H (TOT)</sub> at a nominal range between 340 -380°C (Fig 6.4b). Clathrates are found to be forming at (-15) to (-20)°C and its dissolution at 10 to 12°C.

Sample CK6B: The T<sub>H (TOT)</sub> of the biphasic inclusions from this sample lies between 227 and 289°C. In the case of some polyphasic

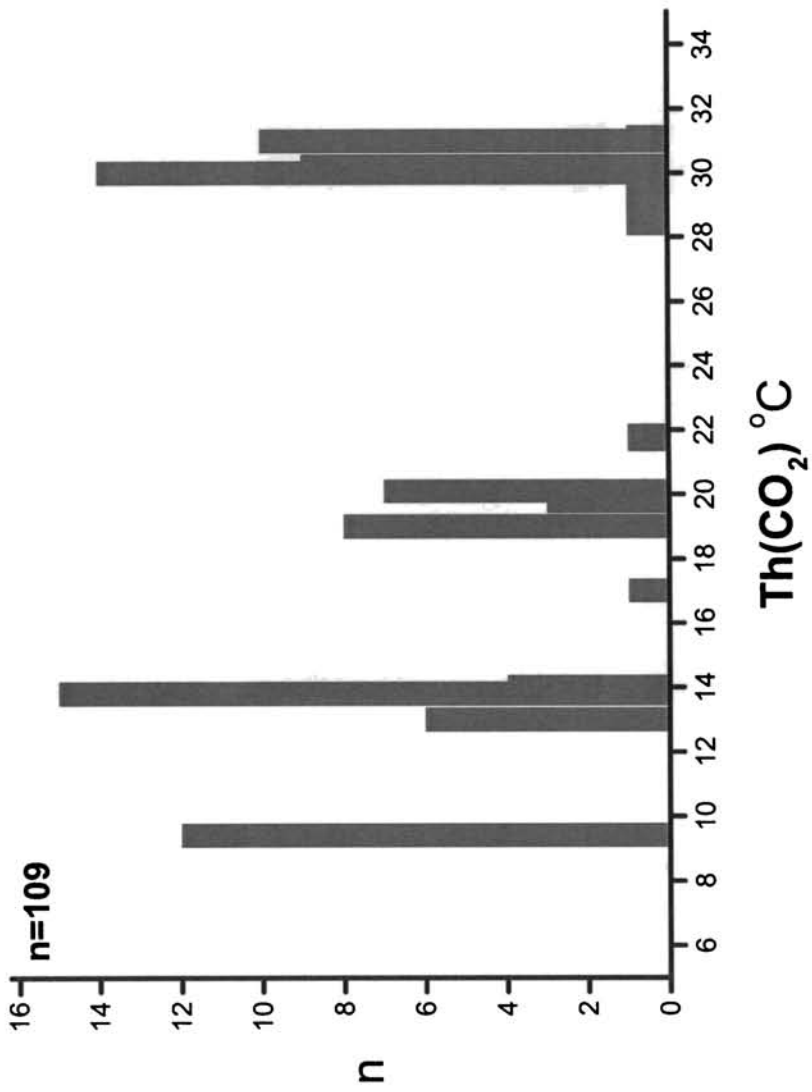
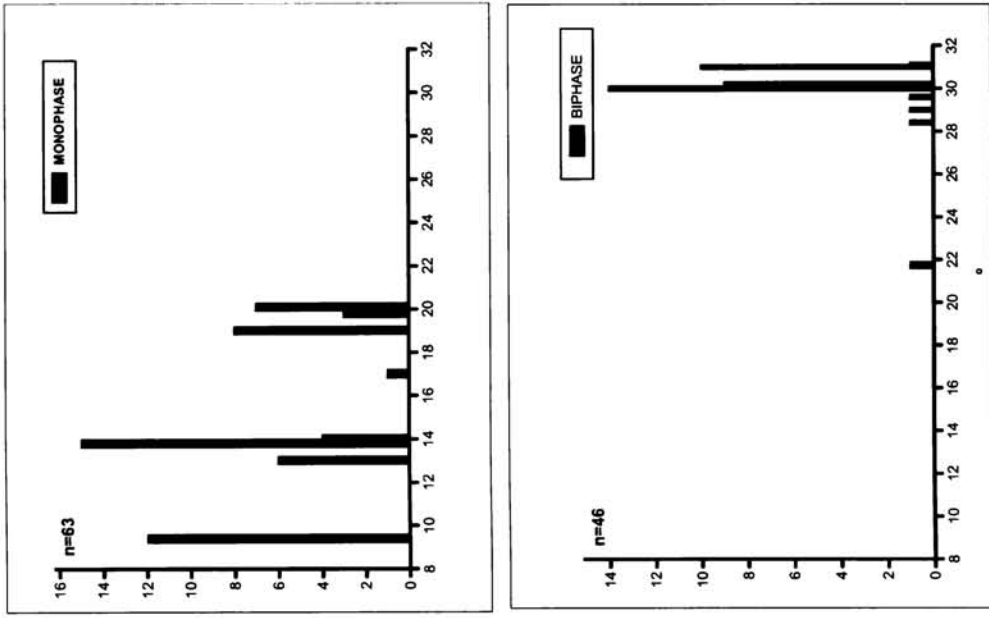


**Fig. 6.3** Temperature of homogenisation( $T_H$ ) of  $CO_2$  in monophase and biphasic inclusions

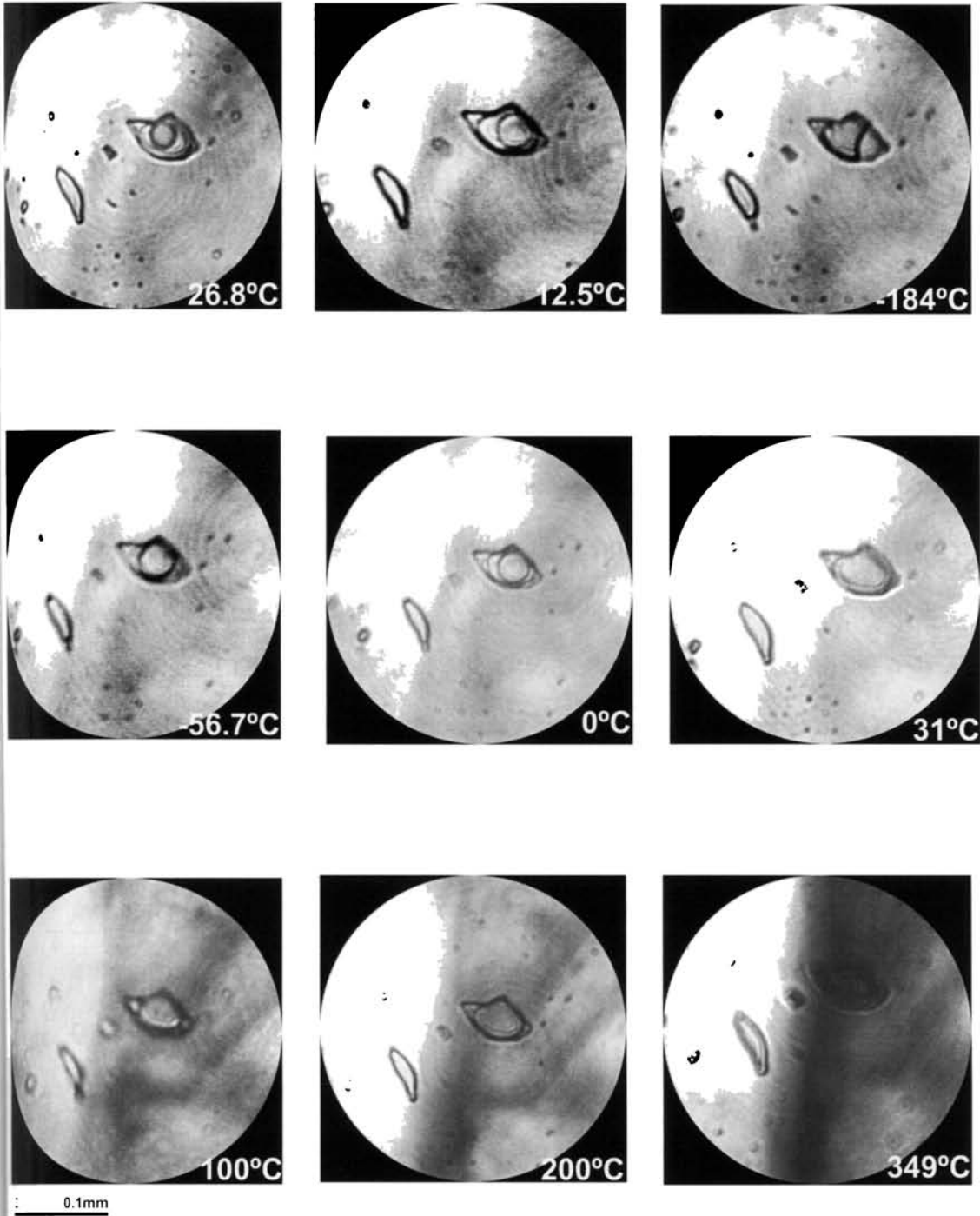


**Plate 6.8** Changes of a biphase inclusion from CK.73 while freezing and heating (see text for details)

inclusions, with halite crystals, the H<sub>2</sub>O bubbles are getting homogenized between 289°C and 300°C but the complete homogenization is occurring after the halite dissolution at 400-412°C (Fig 6.4c).

Sample CK42: Polyphase inclusions with a solid (halite) phase show T<sub>H</sub> (H<sub>2</sub>O) at 355°C-405°C (Fig 6.4d) homogenizing to both liquid as well as gas phase. The total homogenization is noted at 512 °C after the halite dissolution at 443°C. In some polyphase inclusions the Clathrates are found at (-16)°C and get dissolved at 10°C.

Sample CK57G: The biphasic gas rich inclusions from this sample are getting totally homogenised after H<sub>2</sub>O homogenization at 373 and 395 °C. But a majority of inclusions that are liquid rich in nature are getting homogenised between 147 and 165°C to both gas and liquid phases (Fig 6.4e). The presence of vapour-dominant and liquid-dominant inclusion pairs with similar homogenisation temperature is usually identified in geothermal waters at fluid boiling conditions (Norman *et al.*, 1996, 2001, 2002). So in this sample also it is an evidence for the boiling condition at the time of trapping of the inclusions and the inclusions are suspected to be of geothermal origin. Presence of Clathrate is noticed in some inclusions at (-15)°C and its dissolution at 10.3°C.

Sample CK108 and CK109: These samples show almost same type of biphasic inclusions. The T<sub>H</sub> (TOT) from both the locations is noted at a range of between 260 and 380°C (Fig 6.4f). In CK108 clathrate are formed at a temperature of (-18) to (-20)°C and its melting is noted at 8 - 16°C.

Sample CTN122: Polyphase inclusions from this sample is characterised by the presence of halite as well as clathrate. While heating,

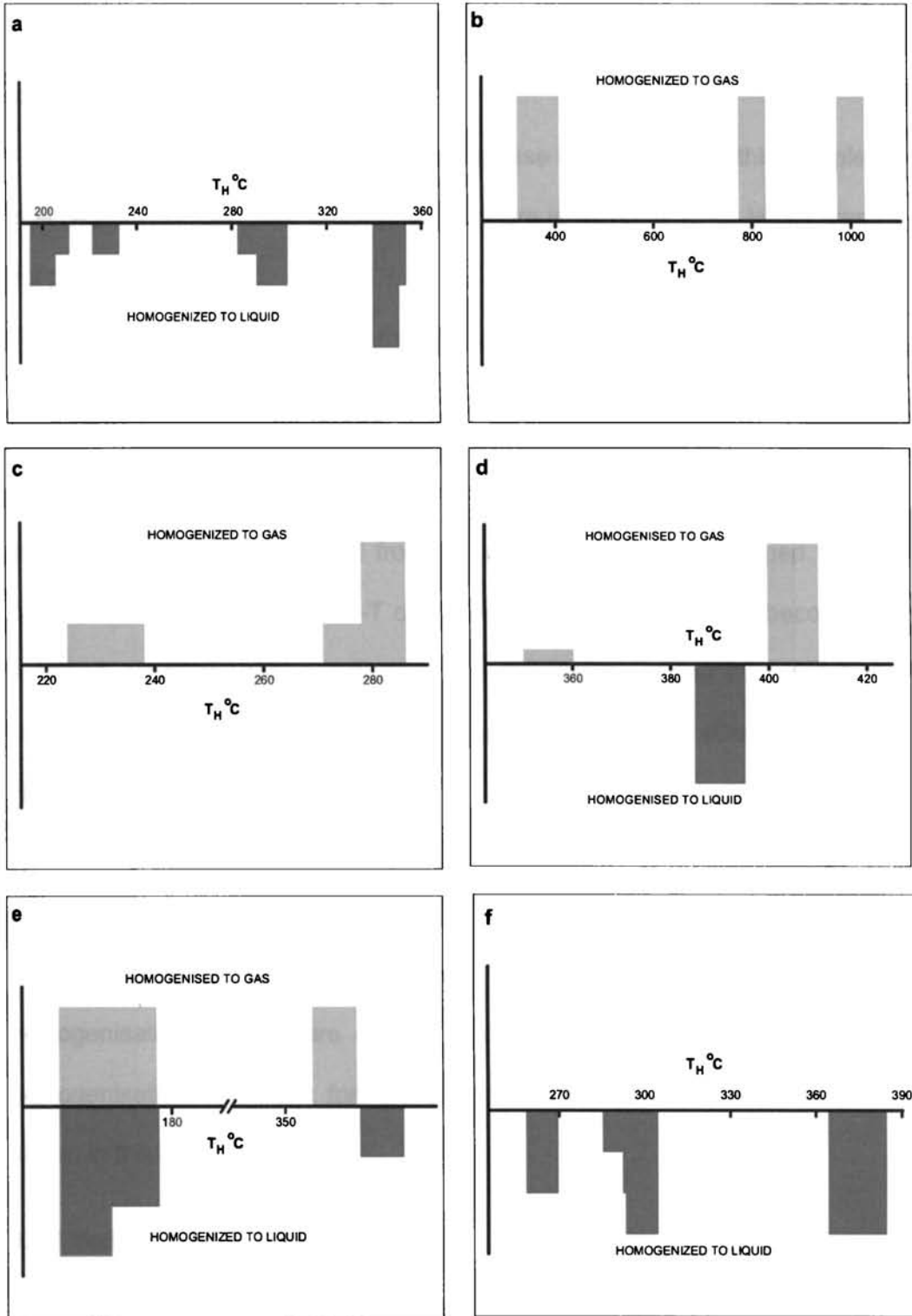


**Fig. 6.4** State of total homogenisation of the inclusions from different samples

clathrate dissolution is noticed at 10°C and halite dissolution at 564°C. The total homogenization is above 600°C.

Sample CTN125: The  $T_{H(TOT)}$  of biphasic inclusions from this sample is at 348-368°C. Clathrate melting temperature is found at 12°C. Halite was not present.

*(The data obtained from heating freezing studies are given in Appendix III)*

### **6.8.5 Density of CO<sub>2</sub> inclusions**

Information on the pressure temperature conditions of formation of any inclusions can be inferred from the density of the fluid trapped. The density is determined by the P-T condition at which the inclusion becomes a closed constant volume system. Thus the density of the fluid can be calculated from the homogenising temperature of the fluid (Crawford and Hollister, 1986).

The density of the monophasic CO<sub>2</sub> inclusions lies between 0.77g/cc and 0.87g/cc whereas the CO<sub>2</sub> in biphasic/polyphasic inclusions gives a density range of 0.58g/cc-0.75g/cc. The relationship between the homogenisation temperature of CO<sub>2</sub> and the density depending on the homogenisation state, put forward by Valakovich and Altunin (1968) as shown in the Fig. 6.5.

### **6.8.6 Salinity of H<sub>2</sub>O inclusions**

In H<sub>2</sub>O-NaCl system the compositional difference in inclusions is based on the salinity. For salinities <23.2 wt% NaCl the composition is determined from the ice melting temperature. The H<sub>2</sub>O containing NaCl up to the eutectic composition of 23.2wt% will show depression in the freezing

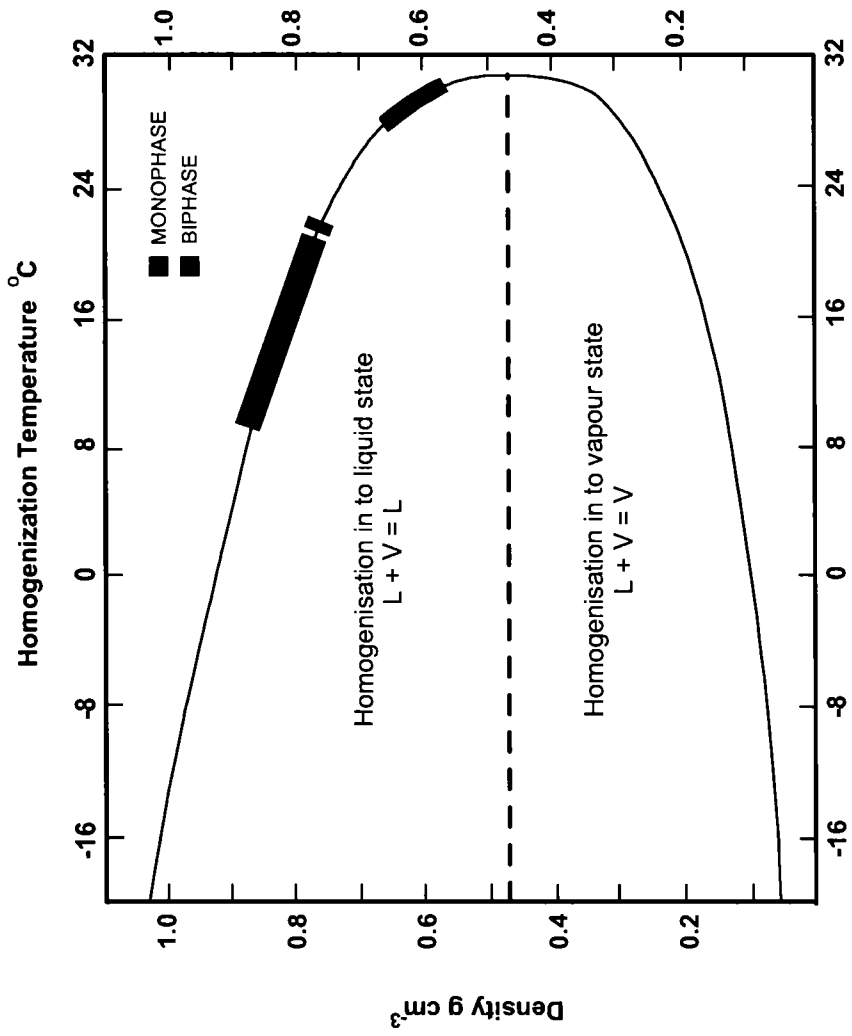


Fig.6.5 Relationship between temperature of homogenisation and density of CO<sub>2</sub> bearing inclusions (after Valakovich and Altunin, 1968)

point. Based on this Bodnar (1993) postulated an equation for salinity calculation,

$$\text{ie., Salinity (wt\%)} = 0.00 + 1.78\theta - 0.0442 \theta^2 + 0.000557\theta^3$$

(eq: 6.1)

where  $\theta$  is the freezing point depression in degree Celsius. But in the inclusions containing >26.3 wt% NaCl it is very difficult to determine the ice melting temperature and is always confused with the hydrohalite dissolution and the method is rather erroneous. Presence of clathrates also plays a negative effect in deriving the salinity from the melting temperature of ice (Bodnar, 1983). In this case the halite crystal dissolution temperature is more accurate for the salinity calculations (Bodnar and Vityk, 1994). Sterner *et al.* (1988) determined the solubility of halite under vapour-saturated conditions, which in turn is used to describe the salinity.

$$\text{i.e., Salinity (wt\%)} = 26.242 + 0.4928 \Psi + 1.42 \Psi^2 + 0.223 \Psi^3 + 0.04129 \Psi^4 + 6.295 \times 10^{-3} \Psi^5 - 1.967 \times 10^{-3} \Psi^6 + 1.1112 \times 10^{-4} \Psi^7 \quad (\text{eq:6.2})$$

where  $\Psi = T(^{\circ}\text{C})/100$ .

The equation is actually the solubility of NaCl in water from the peritectic temperature (0.1°C) to NaCl triple point (801°C). Based on this equation, a standard table of  $T_M$  (halite) vs Salinity (wt%) has been prepared from which the salinity can be easily extrapolated (Table 6.3).

Theoretically the equation is valid where the homogenisation of the three phases occurs simultaneously (Bodnar and Vityk, 1994) but can also be in a case where the liquid-vapour homogenisation is slightly higher than halite dissolution temperature (Chou, 1987).



**Table 6.3 Halite solubility in weight percent as a function of temperature calculated by Sterner et al. (1988)**

<b>T<sub>m</sub> (HALITE)</b>	<b>0</b>	<b>10</b>	<b>20</b>	<b>30</b>	<b>40</b>	<b>50</b>	<b>60</b>	<b>70</b>	<b>80</b>	<b>90</b>
0	26.2	26.3	26.4	26.5	26.7	26.8	27.0	27.2	27.4	27.7
100	28.0	28.3	28.6	28.9	29.3	29.7	30.1	30.5	30.9	31.4
200	31.9	32.4	32.9	33.5	34.1	34.7	35.3	36.0	36.7	37.4
300	38.2	38.9	39.8	40.6	41.5	42.4	43.3	44.3	45.3	46.4
400	47.4	48.5	49.7	50.8	52.0	53.3	54.5	55.8	57.1	58.4
500	59.8	61.1	62.5	63.9	65.3	66.8	68.2	69.6	71.1	72.5
600	74.0	75.4	76.9	78.3	79.7	81.1	82.5	83.9	85.3	86.6
700	87.9	89.2	90.5	91.8	93.0	94.2	95.4	96.6	97.7	98.9
800	100									

The samples G4B, CK6B, CK42 constitute of halite bearing inclusions. The respective salinity calculated for the inclusions are 32.4 wt%, 48.5 wt% and 52.0 wt%. The steps of halite dissolution in an inclusion from CK42 are illustrated in Plate 6.9.

## **6.9 INTERPRETATIONS FROM THE FLUID INCLUSION DATA**

An interpretation of fluid inclusion data can only be done by comparison with independent P-T estimates derived from co-existing minerals and a precise knowledge on the chronology of inclusions (Touret, 2001). The composition of fluids trapped together with the density data obtained from homogenisation temperatures can be used to construct representative isochores in pressure-temperature space. An inclusion can be trapped anywhere along the isochore, and even high density fluid inclusions are some times trapped at the lower P-T region of the isochore (Fonerav *et al.*, 2003; Santosh *et al.*, 2004).

In the present fluid inclusion study all the samples selected are graphite bearing and the inclusions are compositionally CO<sub>2</sub>, CO<sub>2</sub>+H<sub>2</sub>O,

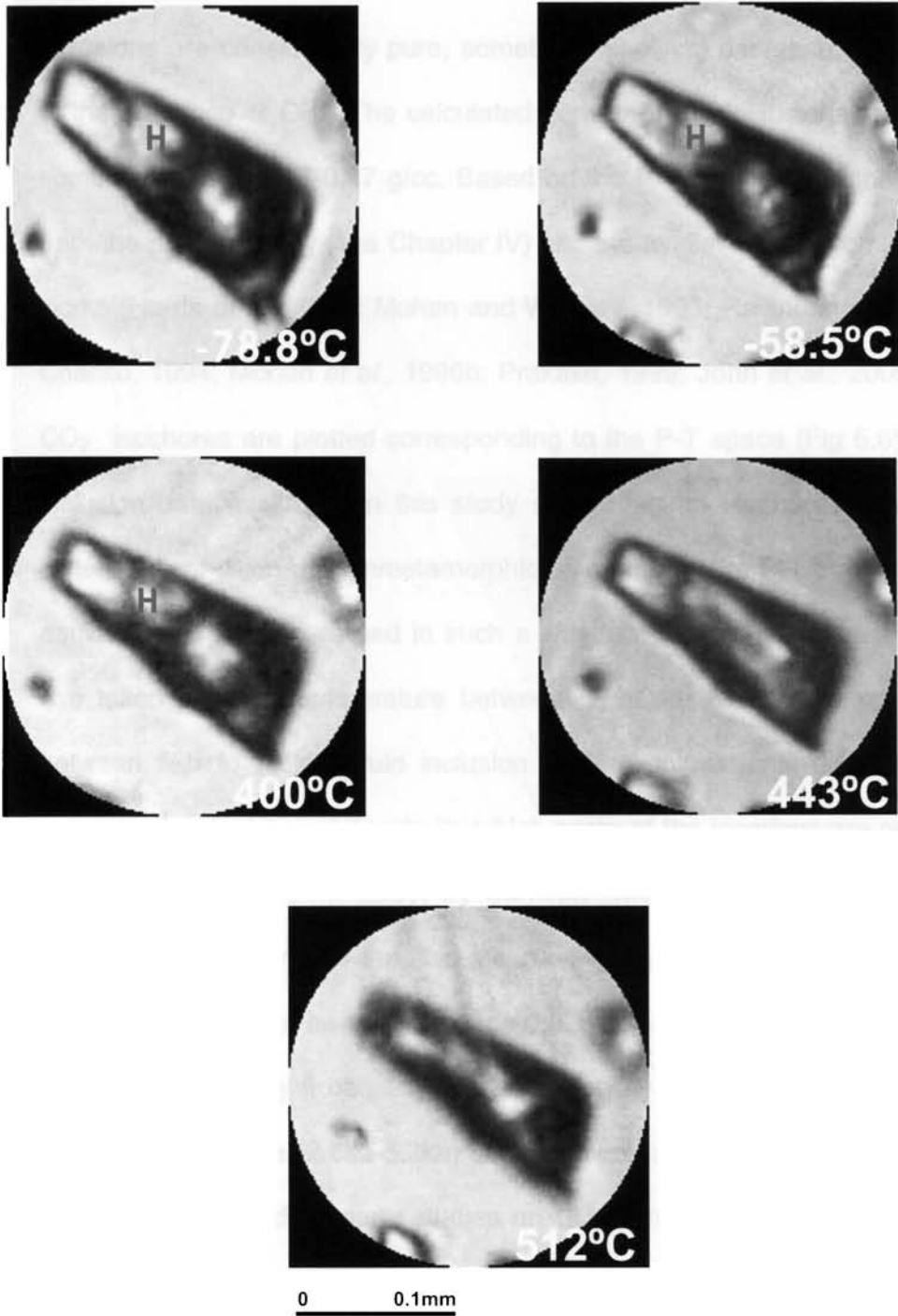


**PLATE 6.9** Dissolution of halite in an inclusion from CK42

CO<sub>2</sub>+H<sub>2</sub>O+ NaCl, with minor amounts of CH<sub>4</sub>. The monophasic CO<sub>2</sub> inclusions are considerably pure, sometimes showing decrease in T<sub>M</sub> due to the presence of CH<sub>4</sub>. The calculated density of the inclusions falls in a nominal range of 0.77-0.87 g/cc. Based on the P-T estimates of the MGB from the present study (see Chapter IV) and the available data from earlier works (Harris *et al.*, 1982; Mohan and Windley, 1993; Ravindrakumar and Chacko, 1994; Mohan *et al.*, 1996b; Prakash, 1999; John *et al.*, 2005) the CO<sub>2</sub> isochores are plotted corresponding to the P-T space (Fig 6.6). The inclusion data evaluated in this study show that the isochores does not satisfy the conditions of synmetamorphic entrapment. The P-T from mineral equilibria can be generalised in such a way that the MGB metamorphism has taken place at temperature between 600°C to 900°C and pressure between 5kb to 9.5kb. Fluid inclusion studies on carbonic fluids in the massive charnockites of Kerala (in which some of the locations are near to the locations of present study) by Santosh (1998) has estimated almost similar P-T conditions for the fluid inclusion entrapment and density of the inclusions is found to be lying between 0.92g/cc –1.10g/cc. In comparison, in the present study it can be noted that density (0.77g/cc - 0.87g/cc) as well as the pressure (2.6kb-5.2kb) derived is considerably low. This type of situation is reported in many studies on CO<sub>2</sub> rich fluid inclusions in high-grade terrains with considerable explanations. For instance, Frezzotti *et al.* (2004) stated that the degree of preservation of inclusions formed at high P-T conditions (granulites, eclogites) could not always give the same P-T of the formation of host rock. The feeble presence of H<sub>2</sub>O, ranging from 10mole% to 36mole% within these inclusions (usually difficult to detect

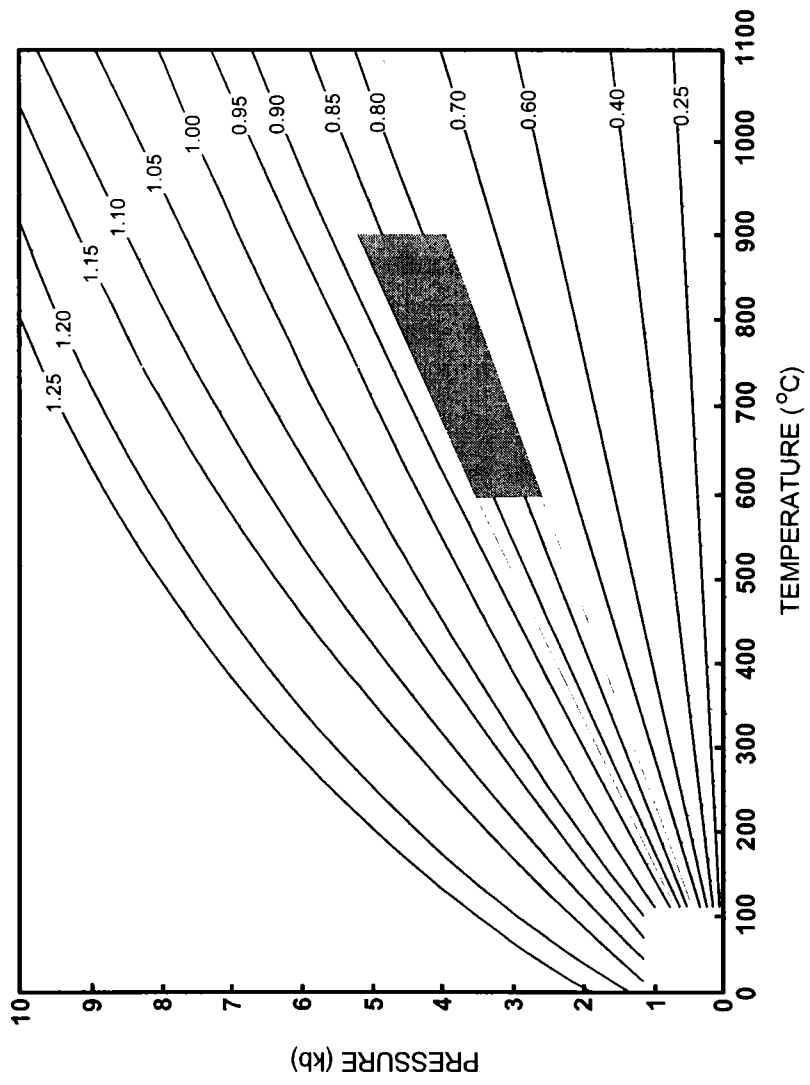


**Fig. 6.6 P-T diagram showing CO<sub>2</sub> isochores and proposed fields of inclusions in the present study**

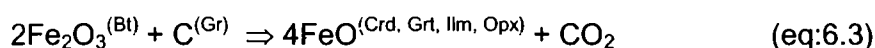
optically) can mislead the isochors to higher pressures (Brown and Lamb, 1986; Touret and Hansteen, 1988; Lamb *et al.*, 1991). To compensate this error an addition of 1 to 2 kb pressure can be applied to the calculated CO<sub>2</sub> pressure (Touret, 1987). The removal of water from inclusions by reactions involving hydrous daughter mineral like phlogopite (Touret and Hansteen, 1988) or preferential leaking of water through bulk diffusion or selective diffusion along twin boundaries and dislocations can also account for the above problem (Hall and Sterner, 1993). The effect of retrogressive metamorphism has also its own effect on the inclusions and there is no meaning in expecting the same density of trapping after some retrogressive changes (Vityk and Bodnar, 1995a).

Many such explanations can be attributed for the decrease in density and the calculated pressure of the inclusions in high-grade metamorphic rocks. But a special factor that is to be taken into consideration here is that the present samples are graphite bearing. The presence of graphite adds an important constraint on the thermodynamic behaviour of petrologic systems and indicates that in many cases metamorphic fluids are graphite saturated during both their generation and evolution, and at the times of their trapping as fluid inclusions (Cesare, 1995). The precipitation of graphite cause decrease in the fluid inclusion density and as a consequence the isochores extrapolated from the densities do not pass through the pressure temperature conditions at which the inclusion was trapped with pressure under estimates up to 2 kb (Cesare, 1995). For confirming this graphite forming mechanism further studies are needed using Raman spectroscopy to identify the graphite

precipitates within the fluid inclusion and characterizing them isotopically, because it is not visible under an optical microscope (Van den Kerkhof *et al.*, 1991; Wilmart *et al.*, 1991). However the limited range in the density of monophase inclusions and the very high temperature of homogenisation of some of the inclusions favour a model involving graphite precipitation accompanying peak metamorphism from carbonic fluids. This is in agreement with available graphite-crystallinity and stable isotope data on the MGB graphites, which is suggestive of the presence of fluid-derived as well as biogenic graphites in the terrain (see chapter 5). Further the MGB graphites are of high crystallinity indicative of their formation at high temperature (650-800 °C) (see chapter 5). The origin of graphite by any hydrothermal activity can be ruled out because these processes can only give low-crystalline graphite (Pasteris *et al.*, 1986; Pasteris, 1998; Pasteris, 1999). So the graphites formed will be very much along the progressive metamorphism of the terrain along or before the first generation fluid entrapment from multiple sources.

The interpretation of the evolution of the pseudosecondary inclusions described in this study is a difficult issue. The occurrence of CO<sub>2</sub> rich inclusions in granulite was a subject of considerable debate for several decades. The theory of carbonic metamorphism put forward by Newton *et al.*, (1980) is an almost accepted description on the source of CO<sub>2</sub> (Santosh, 1986a & b; Hansen *et al.*, 1984). Several other elucidations were put forward by many workers suggesting a post-metamorphic entrapment, peak metamorphic fluid trapping etc. However the exact picture on the source of CO<sub>2</sub> rich fluids in high-grade metamorphic rocks still remains

controversial that its source is from an external mantle or lower crustal source, or derived internally by the oxidation of graphite or pore fluid release during uplift (Jackson *et al.*, 1988 and the references there in). Cesare *et al.* (2005) has put forward the reaction producing CO<sub>2</sub> melt/fluid by the oxidation of graphite, from biotite bearing rocks during high temperature metamorphism. In the case of biotite bearing rocks where graphite is present the biotites are the only carriers of Fe<sup>3+</sup> will be get melted as temperature increases leading to iron reduction accompanied by the oxidation of carbon (graphite) producing CO<sub>2</sub>. The reaction is



There is a general rule in the case of high grade metamorphic rocks that a partial retrogression of peak metamorphic minerals will correspond to the greatest number of inclusions (Touret, 2001) i.e., in the present study even if the mineral equilibria gives a peak metamorphic temperature around 800°C the most visible inclusions shows much lower temperature. As Touret (2001) states these inclusions do not indicate an external independent source of fluids but only corresponds to the local re-equilibration of fluids (Vry and Brown, 1991) already present even since the pre-metamorphic stage. Re-equilibration of fluid inclusions may occur when the internal pressure of the inclusion is different from the external pressure. This makes the density changes of the fluid within the inclusions due to leaking or the change in volume of the inclusions. The morphology of the inclusions re-equilibrated under conditions of decompression (internal overpressure) or compression (internal underpressure) always differ. Three dimensional array of numerous tiny inclusions and fractures

surrounding a central inclusion, referred to as 'imposition halos' are characteristic of re-equilibration by internal under pressure (Sterner and Bodnar, 1989), whereas the presence of oriented planar arrays of numerous tiny secondary inclusions, termed 'decrepitation clusters', surrounding a central inclusion refers to an internal overpressure re-equilibration (Vityk and Bodnar, 1995b). In the present studied samples the morphology of re-equilibrated inclusions points to internal overpressure experience. Star like appearance of aqueous inclusions are indicative of this (Plate 6.10). A fluid inclusion study on enderbitic granulites from Bamble, Norway by Van den Kerkhof *et al.* (1994) describes a similar situation in which different densities of carbonic inclusions were noted at different parts of apparently homogeneous rock, which is interpreted as a result of local re-equilibration. It is concluded that only one inclusion out of 800 randomly selected inclusions is possibly of granulite facies, whereas the others were modified during subsequent stages of uplift and retrogression (Vitik and Bodnar, 1995a; Van den Kerkhof and Hein, 2001).

The presence of melt-inclusions points to the role of certain magmatic activity in the evolution of the host rock. Since the melt inclusions are pre-genetic to the fluid inclusions, it can be concluded that the carbonic metamorphism has taken place later to the melt activity. The youngest generation biphasic/polyphasic inclusion identified in the samples illustrate a late stage hydrothermal activity and the CO<sub>2</sub> densities from these CO<sub>2</sub>+H<sub>2</sub>O inclusions are comparatively low (0.58 -0.75 g/cc) which reveal that it is originated at a lower temperature. In the field it is noted that the charnockites of the present study are seen retrogressed to



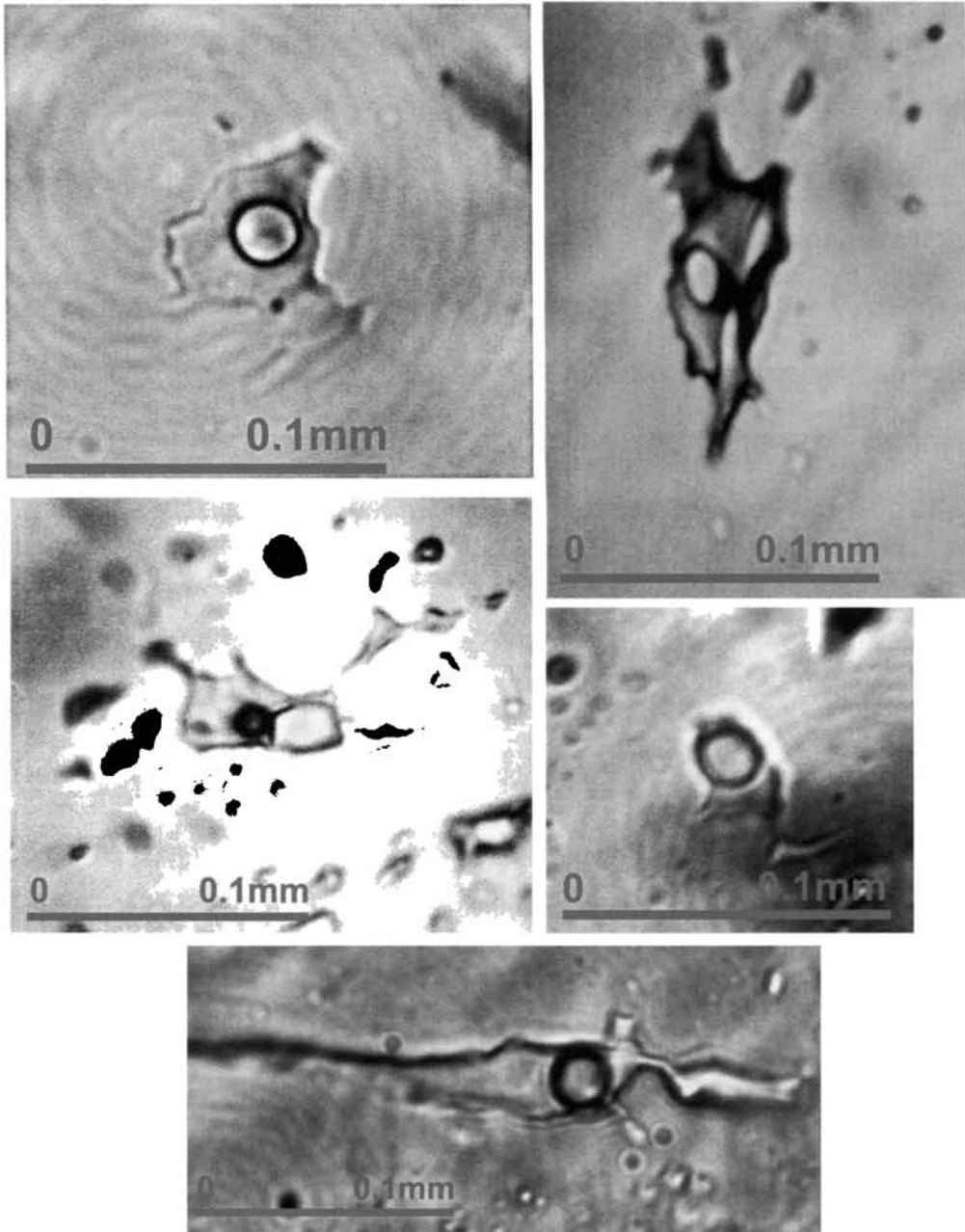


**Plate 6.10** 'Star' like appearance of aqueous inclusions indicating re-equilibration due to internal over pressure in the inclusions

biotite/hornblende-bearing gneisses at places controlled by fractures associated with pegmatitic veins and/or quartz veins. The presence of halites in this generation of inclusions points to an influx of some saline brine at the time of the retrogressive mechanism. Similarly the simultaneous occurrence of vapour-dominant and liquid-dominant inclusion pairs with similar homogenisation temperature denotes the fluid boiling conditions (Norman *et al.*, 1996, 2001, 2002). So in this sample it is also evident that the inclusions are of geothermal origin. Presence clathrates and its dissolution have been identified in many samples like G6, CK42, 57G, CK108, CK109 and CTN125. The high salinity of these inclusions is confirmed and it is calculated as 32.4 wt% - 52.0 wt% NaCl equivalent. A wide range of salinity can be expected as the increase in metamorphic grade with the highest levels tracking halite saturation (Yardley and Graham, 2002). The high fluid salinities can some times result from retrograde dehydration reactions in fluid-starved crystalline rocks (Bennett and Barker 1992; Yardley and Valley 1997). Thus the very high values of salinity can be attributed to such process.

The interaction of brine fluids and graphite can produce CO<sub>2</sub>-CH<sub>4</sub> rich fluids (Vapnik, *et al.* 2002). The immiscible nature of brine and carbonic fluids, which can persist together, even at very high magmatic temperatures (Shmulovich *et al.* 1994), gives the explanation for the coexistence of CO<sub>2</sub> inclusions and NaCl-CaCl<sub>2</sub>-H<sub>2</sub>O high salinity inclusions in same trails. However, as the source and chronology of the brine in relation to the host rock is not well established, it is difficult to discuss these aspects further.

## 6.10 CONCLUDING REMARKS

- The analysis of the fluid inclusions reveals the presence of three sets of fluid inclusions representing three important stages in the evolution of the terrain.
- The first generation is the monophasic CO<sub>2</sub> inclusions the composition of which is confirmed by freezing studies.
- Since the mineral equilibria based P-T estimates are much higher and the isochores of inclusions from the present study do not represent such a high P-T it can be inferred that none of the inclusions represent the peak metamorphic regime.
- Though petrographically they may be considered as primary fluid inclusions they do not represent a peak metamorphic entrapment owing to their lower density compared to the synmetamorphic high-density inclusions recorded elsewhere from the granulite-facies rocks from the SGT.
- The decrease in the density observed and the lower pressure estimates are interpreted to be due to the graphite precipitation from the fluids.
- An intermediate generation of pseudosecondary type biphasic/monophasic inclusions are the result of re-equilibration or modification of the first generation fluids.
- The total homogenisation temperature of more than 1000°C and the presence of melt inclusions points to a magmatic affinity for at least *some of the inclusions*.

- The youngest generation of fluids that caused the retrogression is low temperature (homogenising around 350 °C) high saline brine that has interacted with graphite to release CO<sub>2</sub> and this appears to be geothermal fluid.

# CHAPTER 7

## MONAZITE DATING

---

## 7.1 INTRODUCTION

Geochronological studies play an important role in the development of continental reconstruction theories for granulite terrains. Various techniques are employed now days in geochronology. K-Ar, Rb-Sr, Sm-Nd, U-Pb SHRIMP, single zircon evaporation and CHIME data have proved to be quite useful in Precambrian terrains. High spatial resolution dating of monazite by the electron-probe microanalyser (EPMA) enables systematic and detailed studies of small minerals like zircon and monazite. This technique called micro-geochronology or micro dating provides sometimes better information than any other method (Montel *et al.*, 1996). These minerals in granulite facies rocks often preserve cores that contain information on the age of the protoliths. It also gives the depositional age of the protoliths in case of metasedimentary rocks (Collins *et al.*, 2003). Dating of monazite with the electron microprobe has been successfully applied to magmatic and metamorphic rocks throughout the last two decades (Suzuki and Adachi, 1994; Montel *et al.*, 1996; Rhede *et al.*, 1996; Cocherie *et al.*, 1997) and provides a fast and cheap alternative to other insitu techniques like the ion-probe or laser ablation-ICP-MS. A comparative study on monazite dating by EPMA and SHRIMP isotopic ages from metamorphic rocks of Wymong craton USA by Dahl *et al.* (2005) found that the ages are internally consistent at various levels of observations and have proved that the EPMA dating is an accurate and precise method of age calculation for polymetamorphic terrains.

Monazite is a common and widespread LREE-bearing phosphate mineral, and is being used as an important accessory phase in reconstructing metamorphic pressure-temperature-time paths in multiply deformed orogenic terrains (Dahl *et al.*, 2005). Monazite can preserve multiple age and/or composition domains even within a single grain and provides detailed evidence of a complex history of growth, recrystallisation, dissolution, and re-growth during polyphase metamorphism (e.g., Lanzirotti and Hanson 1996; Williams *et al.*, 1999; Ayers *et al.*, 1999; Pyle and Spear 1999; Wing *et al.*, 2003).

A preliminary attempt on dating the MGB rocks with the EPMA based chemical technique is done here. Since monazites are rarely seen in charnockites of the MGB, in the present study the monazites from the associated gneisses and migmatites were analysed. An attempt is also made to compare the available geochronological data about the MGB from earlier works. The geochronological picture available from earlier studies on the metamorphic age of the rocks from the MGB has already been reviewed in chapter 1.

## **7.2 ELECTRON MICROPROBE DATING OF MONAZITE**

Electron microprobe has become a part of the geological analysis very early from the late 60's. This wide acceptance is due to many factors like its nondestructive methodology, high spatial resolution, capability to produce precise and accurate results, less time consumption etc. The basic use of electron microprobe is to analyse the major elements in minerals and very rarely some of the traces. The idea that the extrapolation of the

uranium, thorium and lead amounts from a mineral with the help of electron microprobes can bring out the age of that mineral resulted in the recently developed technique of monazite dating. The major limitation that can be noticed in this method is the scarcity of monazite in the rocks. It is not available as zircon or biotite. Especially it is very difficult to get monazite in Ca rich, mafic or intermediate rocks (Cuney and Friedrich, 1987).

This technique is as same as any other geochronological dating except that the U-Th-Pb concentrations are determined using the electron micro probe. The rest is simply calculating the age ( $\tau$ ) by solving the equation

$$\text{Pb} = \text{Th}/232[\exp (\Lambda^{232} \tau) -1] \times 208 + \text{U}/238.04 \times 0.9928 \times [\exp (\Lambda^{238} \tau) -1] \times 206 + \text{U}/238.04 \times 0.0072 \times [\exp (\Lambda^{235} \tau) -1] \times 207$$

(eq. 1)

Where Pb, U, Th are in ppm and  $\Lambda^{232}$ ,  $\Lambda^{235}$ ,  $\Lambda^{238}$  are the radioactive decay constants of  $^{232}\text{Th}$ ,  $^{235}\text{U}$  and  $^{238}\text{U}$  respectively.

In monazites Th and U are found in considerable amount and the radiogenic lead (\*Pb) accumulates very quickly (within 100My). A precise measurement is possible using an electron microprobe (Montel *et al.*, 1996). The analysis will give good result if and only if the non-radiogenic lead is negligible in the rock and the U/Th/Pb ratio is the product of the radioactive decay only.



## 7.3 ANALYTICAL TECHNIQUES

### 7.3.1 Monazite identification

As in conventional EPMA, in this technique also we make use of polished thin-sections. The main advantage is that the petrographical position of each dated monazite can be traced out and which will be of much help in the age interpretation. However, one of the drawbacks is that some times it will be a difficult task to locate monazite crystals using simple petrographic microscope. Therefore, sometimes scanning-electron microscopes (SEM) are made use for the identification of monazites. Monazite and zircon are usually confused under a petrological microscope and both are found coexisting in most of the samples. The distinction between them in polished thin sections with optical microscopy is rather easy when grain sizes are large. If the grains are rather smaller than this particular size it can be distinguished by the following methods explained by Montel *et al.* (1996) and Broun *et al.* (1998).

- i) If the grain is euhedral, zircons show two pyramids while the monazites display only one.
- ii) The more or less distinct, prismatic and euhedral shape of zircon, which contrasts with the predominantly rounded monazite grains.
- iii) Monazite shows a thin cleavage (100), while if any cleavage is seen in zircon will be coarser.
- iv) Extinction of monazite is 5-10° but the zircons show parallel extinction.

- v) The marked zoning of interference colors, which is characteristic of zircon but is absent or weakly expressed in monazite.
- vi) The occurrence and size of pleochroic halos those surrounding zircon were small and found only in biotite. In contrast, monazite, due to its high Th abundances; 10–20 wt.%, produced considerably larger halos in biotite and also cordierite. For the same reason, monazites are often surrounded by a halo in feldspar and garnet, which was never recognized in the case of zircon.
- vii) Monazites ( $n = 1.77-1.85$ ) have a lesser refractive index than zircon ( $n = 1.92-2.01$ )

SEM equipped with an analytical Energy Dispersive System (EDS) is a most efficient instrument to identify monazites. Back-scattered electron imaging is another tool, which gives a very bright image for monazites (Parrish, 1990; Montel, 1996; Braun *et al.*, 1998; Braun and Brocker, 2004).

### 7.3.2 Microprobe analysis

Microanalyses were performed with a Camebax electron microprobe at the Mineralogisch-Petrologisches Institut, Universität Bonn by Prof. Ingo Braun. The settings of the instrument was arranged as 20 kV and 50 nA, counting times were 30 (peak)/15 (background) s and 100/50 s, respectively. The U, Th, and Pb from the monazites were analysed simultaneously. The individual concentrations were calculated using ZAF

correction procedure with an average monazite composition for elements other than U, Th and Pb.

In electron microprobe dating the processing time for one data point is usually less than 5min. So large number (20-80) of imprecise ages (with errors between 50 and 100Ma), will be available from a single thin section within no time. Therefore a statistical procedure is necessary to improve the precision by averaging the data and to check the existence of unique or multiple age populations with a mathematical base. For the comparison of the geological model with the data available, the least-square concept is usually made use. Based on that we consider that in a single sample all of the analysed domains were formed at the same time or event. The least-square method then provides a best estimate of  $\tau$  (age) at a confidence level of  $\pm 2\sigma$ . This can be then given up to what extend the model is fulfilled by the data by calculating a numerical parameter; here it is MSWD (Mean Square of Weighted Deviates). For further confirmation a statistical test (here the  $\chi^2$  test at 5% confidence level) can be run. If the  $\chi^2$  tests yield a negative result then only it gives a non-ambiguous answer but then the MSWD will be high and we should have to reject the model. However, at low MSWD the  $\chi^2$ -test result will be positive and statistically the model cannot be rejected (but not necessary the proposed model is correct) (Braun *et al.*, 1998).

If the single age model is not acceptable we should extend it to two or more event models (Montel *et al.*, 1996). The quality of each population should also be taken in to account in addition to the statistical test. For

better geological interpretation the model obtained should be combined with other available data like the geological relationship between the domains (core-rim relationship), the petrographic relationship of individual grains, the composition-age relationship etc.

#### **7.4 FIELD RELATIONSHIP OF THE SAMPLES SELECTED FOR MONAZITE DATING**

Special attention has been taken in selecting the samples giving more emphasis that the sample locations should be representative for the entire MGB (Fig 7.1). In the area the monazites are hardly found in charnockites and so the rocks under study are gneisses, which often found in association with the charnockites. The field investigations reveal that the block consists of gneisses that are of retrogressed nature from the coexisting charnockites whereas some are migmatitic gneisses. The details about the samples are given in Table 7.1.

Thenmala: The location falls in the ACS. It is a quarry of garnet-biotite gneiss with highly folded foliations and traversed by many number of pegmatitic veins, which are also affected by the shear. The major minerals observed in thin section are garnet, biotite, quartz and feldspar. Accessory minerals include cordierite, opaques, zircon and monazite. Some opaques are associated with green spinel at their rims. The garnets are seen as porphyroblasts surrounded by magnetite and spinel (hercynite). Cordierites form some symplectitic intergrowth with quartz, biotite and spinel and are mostly concentrated at the rim of the garnet. This texture gives a picture of

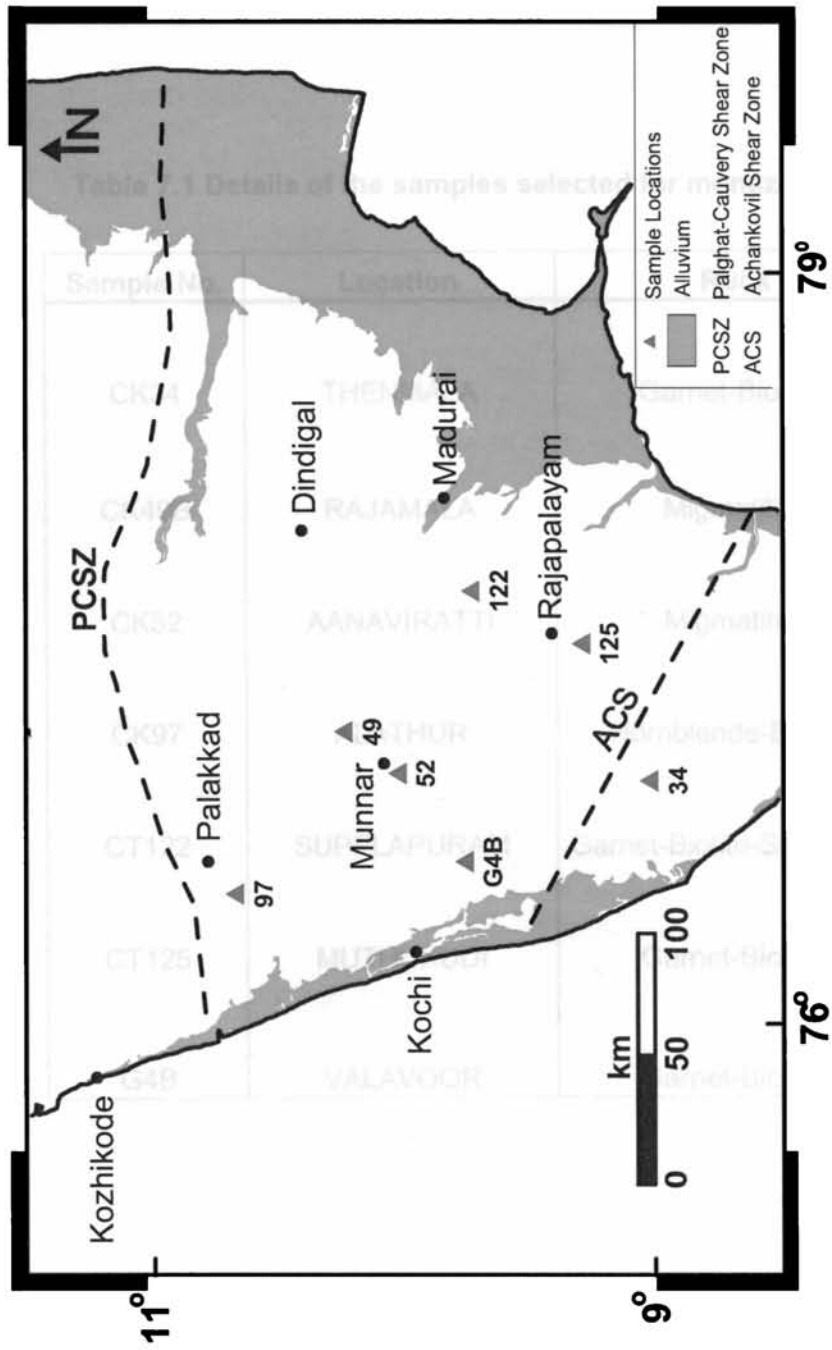


Fig. 7.1 Location of samples selected for monazite dating

**Table 7.1 Details of the samples selected for monazite dating**

<b>Sample No.</b>	<b>Location</b>	<b>Rock Type</b>
CK34	THENMALA	Garnet-Biotite gneiss
CK49B	RAJAMALA	Migmatitic gneiss
CK52	AANAVIRATTI	Migmatitic gneiss
CK97	ALATHUR	Hornblende-Biotite gneiss
CT122	SUPPLAPURAM	Garnet-Biotite-Sillimanite gneiss
CT125	MUTHUKUDI	Garnet-Biotite gneiss
G4B	VALAVOOR	Garnet-Biotite gneiss

garnet breakdown during some retrograde processes to form corona of cordierite–quartz symplectite along grain boundary.

Rajamala: The location is very near to the Munnar granitic intrusive and the rock type present is migmatitic gneiss. Mafic boudins of charnockitic composition are seen within the gneisses, giving an inference that the precursor charnockites have retrogressed to form the gneiss by the action of the granitic intrusion. Foliations show pygmatic folds and the mafic bands are concentrated with biotites (Plate 7.1).

Aanaviratti: This is a migmatitic gneiss exposure intruded by pink granitic veins and quartz veins. Some of the veins are found intruding discordant to the foliations of the gneiss. The foliations are highly deformed and show pygmatic and isoclinal folds. Mafic boudins of about 30-50 cm are seen as isolated pockets (Plate 7.2). From the field relation of these rocks a vague history, which can be drawn out is that, these mafic patches may be the relicts of precursor granulitic rock (charnockite) which may have got retrogressed due to an earlier granitic and quartz vein intrusion. Further the whole rock has undergone some tectonic disturbances and later on intruded by a second phase of granitic material which migmatized the retrogressed gneiss.

Alathur: The rock type found is hornblende-biotite gneiss in which charnockite patches are found parallel to the foliation planes. The charnockites are also showing gneissosity (Plate 7.3). K-feldspar forms the major mineral of the leucocratic bands in the gneisses. Garnets are also present. The monazite grains are found in the gneiss and so it is selected for the dating purpose.

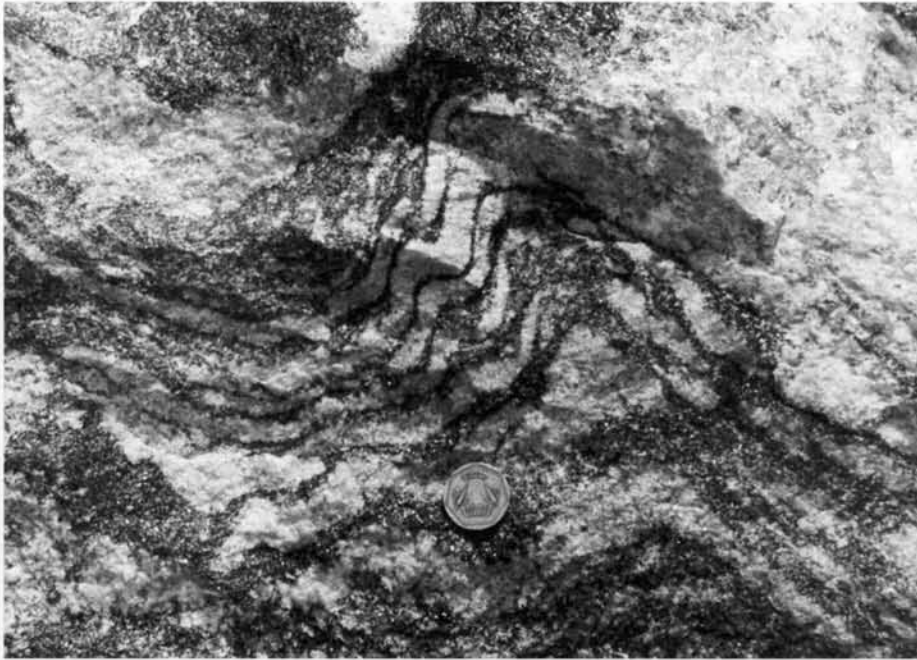


**Plate 7.1** Highly folded migmatitic gneiss from Rajamala

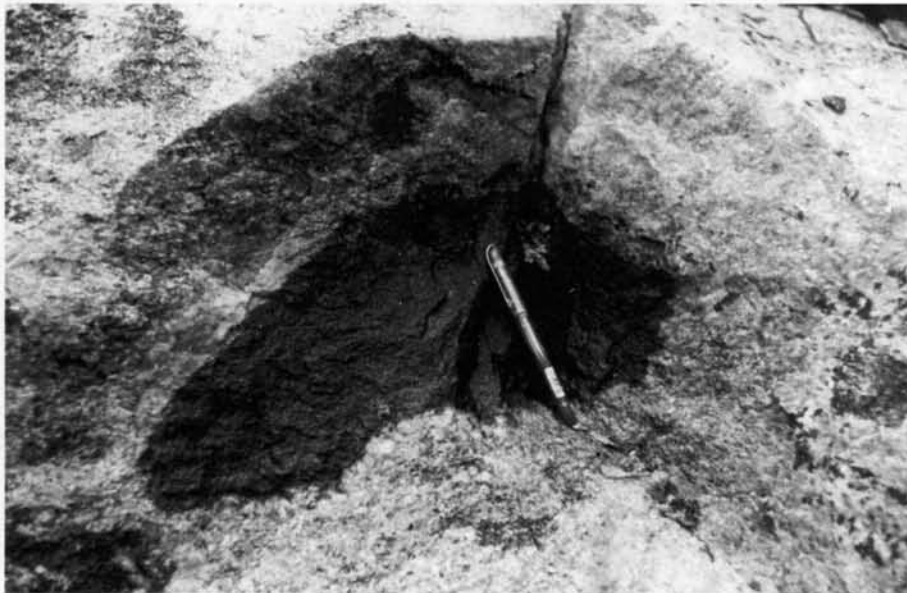


**Plate 7.2** Mafic bouding in the migmatitic gneiss from Aanaviratti





**Plate 7.3.** Charnockite patches found parallel to the gneissosity of hornblende-biotite gneiss from Alathur

The rock types and their field relations of the locations Supplapuram, Muthukudi, and Valavoor are discussed in detail in the previous chapters.

## 7.5 RESULTS AND DISCUSSION

The analysis carried out on samples from seven different locations from the MGB described above gives an apparent heterogeneity in Th-U-Pb composition and the age distribution forms in three different clusters. The Th concentration is having highest values approximately of 17wt% and a minimum of 2wt%. U shows highest concentration of ~ 0.84 wt% and minimum of ~0.04 wt% and that of Pb is at a maximum at about 0.45 wt% and minimum at ~0.07 wt%, but shows rather better homogeneity than Th concentration (Table 7.2).

Calculated ages of entire samples cluster around 469Ma (Ordovician), 546Ma (Cambrian) and 710Ma (Upper Proterozoic) (Fig 7.2). A plot on Th vs Pb (Fig 7.3) of the monazites from the samples also gives three isochrons, which concludes that there is only negligible amount of non-radiogenic lead and the system is closed. The U-TH-age diagram indicates that there is no relationship between individual ages and the U and Th abundance in monazites (Fig 7.4). That is why, in the figure the data points simply cluster along the mean values of the calculated ages without showing any relation to the U or Th concentration. So the Th equivalent age can be taken for more accuracy since monazites are always rich and more dependent on Th (Fig. 7.5).

**Table 7.2 Electron probe analytical results for monazites of different samples from MGB**

<b>N</b>		<b>Th(ppm)</b>	<b>±</b>	<b>U(ppm)</b>	<b>±</b>	<b>Pb(ppm)</b>	<b>±</b>	<b>t(Ma)</b>	<b>±</b>
1	r	55300	604	1400	344	1789	240	661	106
2	r	58400	617	1700	354	2188	243	754	102
3	c	51600	562	1600	347	1624	243	632	111
4	c	47700	696	2300	479	1389	185	557	95
5	r	56000	743	3100	470	1393	190	467	79
6	c	69800	816	3100	471	1791	188	497	66
7	r	79200	864	4200	484	2288	194	546	59
8	c	78600	861	4700	490	1689	187	401	54
9	r	69600	819	3100	481	1794	191	500	67
10	r	62300	778	4900	485	1992	194	563	70
11	r	34700	614	8400	526	1677	190	594	86
12	r	61000	773	1800	466	1800	191	596	82
13	c	47600	696	4500	479	1886	188	667	88
14	c	50400	710	2700	469	2228	188	825	98
15	c	36300	582	1900	413	730	193	382	117
16	c	84400	831	2400	427	1857	208	447	60
17	c	88100	841	1600	413	2357	208	560	61
18	c	30200	539	4400	442	1138	197	564	120
19	r	33500	562	3900	442	879	193	422	109
20	c	37400	588	3000	435	1065	195	500	111
21	c	23200	493	3600	431	903	191	570	148
22	r	24000	501	3300	445	916	191	581	150
23	c	28200	529	3500	433	913	192	510	129
24	c	45800	641	2300	427	1324	191	551	99
25	r	57400	709	2000	427	1138	197	396	81
26	c	55300	578	400	362	1285	242	505	109
27	c	82500	692	1400	363	2191	253	558	75
28	c	53800	570	1100	359	1288	243	498	108
29	r	60200	598	1100	363	1689	244	586	99
30	r	60400	599	800	344	1388	244	490	98
31	r	172800	999	3100	382	4473	281	543	40
32	c	173600	997	3000	375	4274	279	518	39
33	cfr	166600	976	3200	380	4270	280	535	41
34	r	91200	729	3400	371	2298	246	498	62
35	c	77300	674	2900	357	2096	246	536	73
36	c	78100	678	2900	360	2200	246	557	73
37	c	78700	681	2800	374	1996	246	504	72
38	c	70500	646	2000	363	2098	247	603	84
39	c	60800	604	2600	361	1596	242	512	89
40	c	54900	577	2100	366	1592	239	571	100
41	r	72600	655	2300	368	1897	243	526	78
42	c	101000	765	3600	372	2696	256	530	58
43	cfr	77200	674	2500	364	1994	246	519	74
44	c	76100	669	3000	373	1893	245	489	73
45	r	88300	858	3600	449	2484	207	550	57
46	c	34800	577	5600	458	1277	195	532	99
47	c	127000	1020	2800	466	2995	217	488	44
48	r	24500	488	1700	369	977	168	715	160
49	c	37700	576	2200	379	981	174	485	104

c= core, r = rim, cfr = presence of fracture

**Fig. 7.2** Weighted-histogram representation of the investigated samples. Shown are bell-shaped curves for each measurement, the sum curve for all individual ages and the statistically derived age populations (dashed lines)

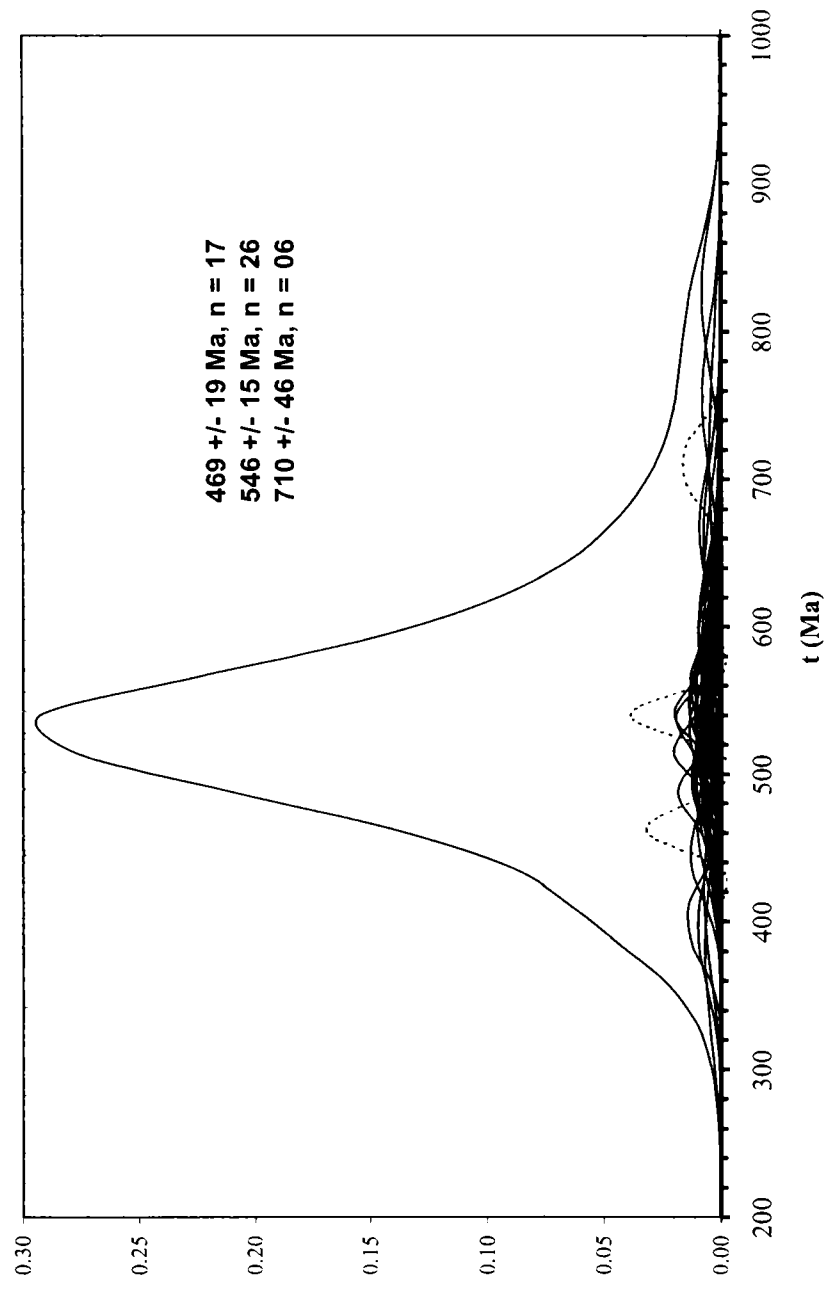


Fig. 7.3 Isochrons plotted from Th-Pb data

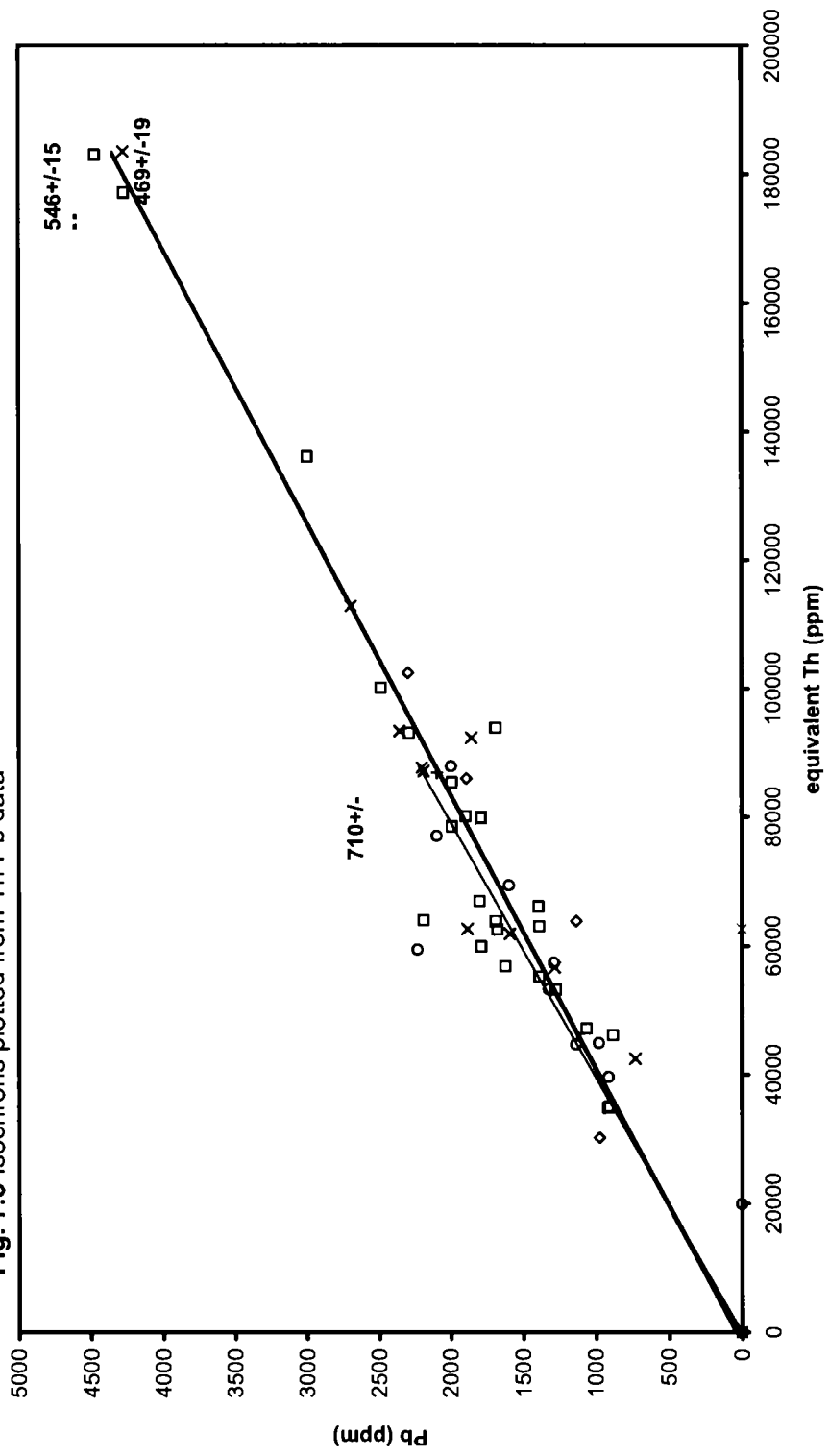


Fig. 7.4 U-Th-age diagram for the investigated samples displaying the relationship between individual ages and U-Th content. Solid line is the calculated mean age population and the dashed line represent standard deviation to each population.

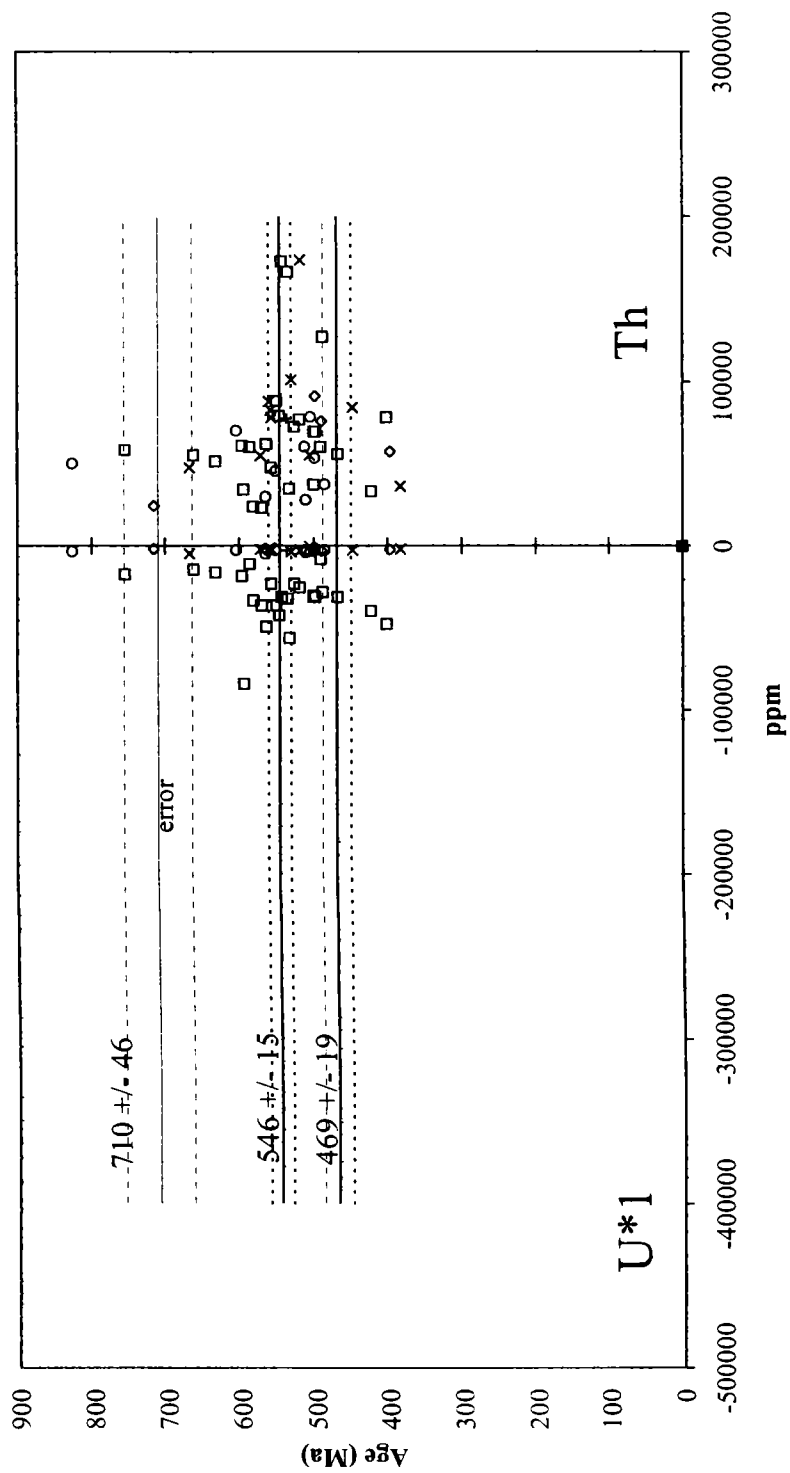
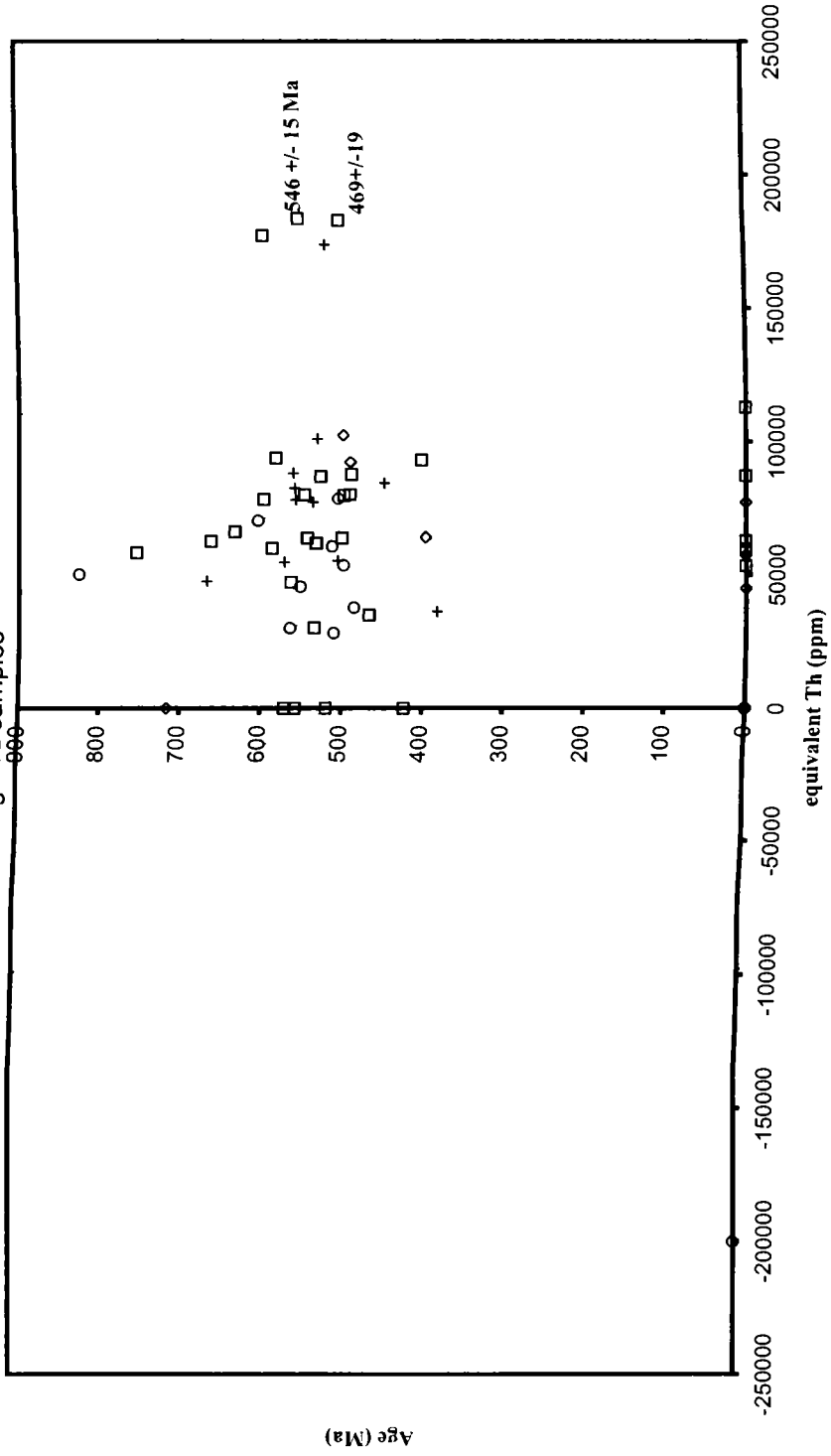


Fig. 7.5 Th equivalent age for the investigated samples



## 7.6 GEOLOGICAL IMPLICATIONS

The two major clusters of age falls in the range of  $500 \pm 50$  Ma from which the Pan-African imprint can be very well established. It was already known for the KKB and MGB that the Pan-African tectonothermal event was rather a reworking event than a crust forming one. The granitic intrusives of MGB have been found to be as part of the Pan-African orogeny (Rajesh and Santosh, 1996; Rajesh *et al.*, 1996). The present data highlights a high-grade metamorphic event too coinciding with this. Though earlier workers have recorded these events in other parts of the SGT (Hansen *et al.*, 1985; Choudhary *et al.*, 1992; Santosh *et al.*, 1992; Bartlett *et al.*, 1995; Jayananda *et al.*, 1995; Unnikrishnan-Warrier *et al.*, 1995) now it appears as a more significant event. The 710 Ma event, not hitherto recorded for this part of SGT obtained from the present analysis but could not be well established due to paucity of sufficient data.



# CHAPTER 8

## SUMMARY AND CONCLUSIONS

---

The study is a multifaceted investigation on charnockites and associated rocks (especially the gneisses) of the MGB to bring out the different aspects of their petrogenesis. The thermobarometric study is extended to the adjacent ACS, to make a regional appraisal of PT evolution of the terrains. The occurrence of graphite in the MGB and its inscrutable relation with the rocks of the terrain also form a matter of analysis in this study. The role of CO<sub>2</sub> in the genetic history of the charnockites as well as the graphite mineralization is also taken into account by analyzing the fluid inclusions in graphite bearing charnockites. EPMA-based monazite dating technique has been employed to date some of the gneisses from the MGB.

The MGB, a high-grade granulite facies terrain is characterized mostly by charnockites and different gneisses. The MGB is subdivided into a western block in Kerala - MBK and an eastern block in Tamil Nadu - MBTN, the two having some lithological differences that are noticed in this study also. The MBK is characterized by foliated charnockites and hornblende-biotite gneisses and MBTN characterized by massive charnockites and enderbites. The other rock types present in the MGB are mafic granulites, calc-silicate series of rocks, quartzites, many types of gneiss like biotite gneiss, garnet-biotite gneiss, garnet cordierite-sillimanite gneiss, migmatitic gneiss etc. Many granitoid intrusives and mafic dykes are also present. The block has experienced three major structural evolutionary events as evidenced from the mesoscopic field structures. Detailed field relationships of the different rock types are made out from the fieldwork and are confirmed by petrographic studies. This includes a variety

of prograde and retrograde reactions reflecting the polymetamorphosed nature of the area.

Detailed interpretation of reaction textures, mineral chemistry and estimation of pressure – temperature conditions of selected samples from the MGB and the ACS were done. The samples include mafic granulite, charnockite, garnet-biotite gneiss and garnet-cordierite gneiss. While most of the rocks show retrogressive textures, the mafic granulites exhibit some prograde reaction textures leading to the formation of pyroxenes preserved in them. The gneisses from the ACS give some typical mineral assemblages representing fluid as well as melt involved reactions.

Mineral chemistry of the major minerals in comparison with the minerals from similar rock types of adjacent blocks was also done. Pressure-temperature estimates of these rocks have been calculated using different models. Garnet–biotite thermometers are mostly used to estimate the temperature of the terrain since these minerals are common in almost all samples studied. Garnets show slight increase of FM towards the rim while they are in contact with biotites. This Fe-Mg exchange reaction can be elucidated as the cause of decrease in temperature from core to rim of garnets.

Compared to the ACS, the MGB shows a lower but a more or less constant pressure (4-5 kb). The cordierite bearing assemblages recorded highest pressures (8.2kb), owing to their proximity to major shear. Rim to core variation of pressure is also noted in both groups of samples, but only at a minor level.

The reaction textures and mineral chemistry of the samples from the MGB and the ACS reveal that both the domains exhibit contrasting P-T paths. The MGB samples express evidences for isobaric cooling whereas the ACS has experienced an isothermal decompression path. Peak-metamorphic temperatures are 1167 °C for the MGB and 910 °C for the ACS.

The occurrence, genesis and mineralogical characterization of graphite from the study area were another part of investigation. An attempt has also been made to bring out the temperature conditions of graphite formation in the terrain. Using different techniques like XRD and Raman spectroscopy the crystallite size and degree of crystallization of graphites were calculated. From X-ray diffractograms, concentrating in the (002) peak reflection of graphites the  $2\theta$ , d values and full width of the peak at half-maximum are estimated and from which the metamorphic temperature was calculated. The crystallite size ( $L_c$ ) along stacking direction is then calculated from Scherrer's equation. The Raman spectrum for a highly ordered, totally crystalline, pure carbon material that is properly called graphite gives a single first order Raman peak or ordered peak (O) at approximately  $1580\text{ cm}^{-1}$  and disordered peak or secondary peak (S) at about  $2725\text{ cm}^{-1}$ . In the present samples it shows an ordered peak at  $1584\text{ cm}^{-1}$  and disordered peak at  $2732\text{ cm}^{-1}$ .

The X-ray diffraction studies and the Raman spectroscopy suggest that the graphite occurring in the MGB is well ordered. The graphite crystallization is found to be an irreversible progressive reconstruction process even to the highest grades of metamorphism. The temperature of

formation of the graphite is found to be at  $700 \pm 100^{\circ}\text{C}$ . Preliminary carbon isotope results points to two different sources of carbon, i.e., the biogenic precursor and the carbonic fluid from the deeper crust for graphite mineralization in the MGB.

The fluid inclusion studies were pertained to a detailed investigation on the influence of  $\text{CO}_2$  influx in charnockitization as well as the graphite mineralization. It also aimed to find the temperature of entrapment of the  $\text{CO}_2$  inclusions in the graphite bearing rocks to reconfirm the temperature of graphite genesis.

Chronologically the fluid inclusions are found to be of three major generations. 1) Monophase carbonic inclusions with well-developed negative crystal shape seen isolated or in isolated groups in the samples. 2) Monophase carbonic inclusions of pseudosecondary type (occurring in arrays mostly along healed fractures). 3) Secondary type (occurring along fractures) biphasic ( $\text{CO}_2 + \text{H}_2\text{O}$ ) as well as polyphase ( $\text{CO}_2$  liquid +  $\text{CO}_2$  gas +  $\text{H}_2\text{O}$  +  $\text{NaCl}$ ) inclusions that can be considered to be the last generation fluid inclusions. From microthermometric investigations it is found that the monophase  $\text{CO}_2$  inclusions are considerably pure, sometimes with negligible amount of  $\text{CH}_4$ . The calculated density of the inclusions falls in a nominal range of 0.77-0.87 g/cc and show that the isochores does not satisfy the conditions of synmetamorphic entrapment. This type of situation is reported in many studies on  $\text{CO}_2$  rich fluid inclusions in high-grade terrains with considerable explanations. Here, the decrease in fluid inclusion density is due to the precipitation of graphite and consequently the isochores extrapolated from the densities do not pass through the pressure

temperature conditions at which the inclusion was trapped with pressure underestimates up to 2kb (Cesare, 1995). The interpretation of the evolution of the pseudosecondary inclusions described in this study pertains to the oxidation of graphite, from biotite bearing rocks during high temperature metamorphism. In the present study, even though the mineral equilibria gives a peak metamorphic temperature around 800°C the most visible inclusions shows much lower temperature pointing a condition of re-equilibration of the inclusions which in turn makes the density changes of the fluid within the inclusions due to leaking or the change in volume of the inclusions. The re-equilibration effect in the inclusions is confirmed from its peculiar morphology.

The presence of some melt-inclusions noticed in the samples points to the role of certain magmatic activity in the evolution of the host rock. From the fluid inclusion petrography it is evident that the melt inclusions are pre-genetic to the fluid inclusions. The very low densities (0.58 -0.75 g/cc) of the CO<sub>2</sub> present in the youngest generation of biphasic/polyphasic inclusion identified in the samples indicate a low temperature origin. The presence of saline brine within these inclusions and its high salinity indicates retrograde dehydration reactions. The coexistence of CO<sub>2</sub> inclusions and NaCl-CaCl<sub>2</sub>-H<sub>2</sub>O high salinity inclusions also indicates that the graphites present in the samples have reacted to the formation of those low-density carbonic inclusions.

Thus the fluid inclusion studies reveal the presence of three sets of fluid inclusions representing three important stages in the evolution of the terrain. The first generation is the monophasic CO<sub>2</sub> inclusions.

Petrographically they are considered as primary fluid inclusions but they owe comparatively lower density than the synmetamorphic inclusions recorded elsewhere from the granulite-facies rocks from the SGT. So they do not represent a peak metamorphic entrapment. The decrease in the density is interpreted to be due to the graphite precipitation from the fluids. Pseudosecondary biphasic/monophasic inclusions formed by the re-equilibration or modification of the first generation fluids are considered to be the second generation. The youngest generation fluids are the secondary inclusions within which high saline brine is incorporated. This fluid is considered as the causative for the retrogression and the release of secondary CO<sub>2</sub> when interacted with graphite.

Monazite dating carried out on samples from seven different locations from the MGB gives an apparent heterogeneity in Th-U-Pb composition and the age distribution forms three different clusters. The results give three ages for the entire samples from which two of them can only be considered as well defined. That is at 469Ma (Ordovician) and 546Ma (Cambrian). The third cluster at 710Ma (Upper Proterozoic) is neglected since the data is scarce. The two ages around  $500 \pm 50$  Ma corresponds with the Pan-African orogeny time. These ages confirms that a pronounced PanAfrican metamorphic event has occurred in the MGB as in many other parts of the SGT.

## REFERENCES

---



- Ayers, J. C., Miller C., Gorisch B., Milleman, J. (1999) Textural development of monazite during high-grade metamorphism: Hydrothermal growth kinetics, with implications for U,Th-Pb geochronology. *Am. Mineral.*, v. 84, pp. 1766-1780.
- Bakker R.J. (2003) Package FLUIDS 1. Computer programs for analysis of fluid inclusion data and for modelling bulk fluid properties. *Chem. Geol.*, v.194, pp. 3-23.
- Bakker, R.J. and Jensen, J.B.H. (1991) experimental post entrapment water loss from synthetic CO<sub>2</sub>-H<sub>2</sub>O inclusions in natural quartz. *Geochim. Cosmochim. Acta*, v. 55, pp. 2215-2230.
- Bartlett, J.M., Dougherty-Page, J.S., Harris, N.B.W. Hawkesworth, C.J. and Santosh, M. (1998) The application of single zircon evaporation and Nd model ages to the interpretation of polymetamorphic terrains: an example from the Proterozoic mobile belt of south India. *Contrib. Mineral. Petrol.* v. 131, pp. 181–195.
- Bartlett, J.M., Harris, N.B.W. Hawkesworth, C.J. and Santosh, M. (1995) New isotopic constraints on the crustal evolution of South India and Pan-African granulite metamorphism. In: M. Yoshida and M. Santosh (eds). *India and Antarctica during the Precambrian*. *Mem. Geol. Soc. India*, v. 34, pp. 391-397.
- Beckinsale, R., Drury, S.A. and Holt, R.W. (1980) 3.360 My old gneisses from the South Indian craton. *Nature*, v. 283, pp. 469-470.
- Belkin, H.E. (1994) Microthermometric investigation: Th and Tm. Practical and theoretical aspects. In: B. De Vivo and M.L. Frezzotti (eds) *Fluid inclusions in minerals: methods and applications*. Short course handbook of International Mineralogical Association, pp. 7-23.
- Benece, A.E. and Albee, A.L. (1968) Empirical correction factors for the electron microanalysis of silicates and oxides. *J. Geol.*, v.76, pp.382-403.
- Bennett, D.G. and Barker, A.J. (1992) High salinity fluids: the result of retrograde metamorphism in thrust zones. *Geochim. Cosmochim. Acta*, v. 56, pp.81–96.
- Beny-Bassez, C. and Rouzaud, J.N. (1985) Characterization of carbonaceous material by correlated electron and optical microscopy and Raman microspectroscopy. *Scanning Electron Microscopy*, pp. 119-132.
- Berman, R.G. (1991) Thermobarometry using multi-equilibrium calculations: a new technique with petrological applications. *Can. Mineral.*, v. 29, pp. 833-855.

- Bernatowicz, T.J., Amari, S., Zinner, E.K. and Lewis, R.S. (1991) Interstellar grains within interstellar grains. *Astrophys. J.*, v. 373, pp. L73-L76.
- Bhattacharya, A., Krishnakumar, K.R., Raith, M., Sen, S.K. (1991) An improved set of a-X parameters for Fe-Mg-Ca garnets and refinements of the orthopyroxene-garnet thermometer and the orthopyroxene-garnet-plagioclase quartz barometer, *J. Petrol.*, v. 32, pp. 629-656.
- Binu-Lal, S.S., Kehelpannala, K.V.W., Satish-Kumar, M. and Wada, H. (2003) Multistage graphite precipitation through protracted fluid flow in sheared metagranitoid, Digana, Sri Lanka: evidence from stable isotopes. *Chem. Geol.*, v. 197, pp. 253-270.
- Blundy, J.D. and Holland, T.J.B. (1990) Calcic amphibole equilibria and a new amphibole-plagioclase geothermometer. *Contrib. Mineral. Petrol.*, v.104, pp. 208-224.
- Bodnar, R.J. (1983) A method of calculating fluid inclusion volumes based on vapour bubble diameters and P-V-T-X properties of inclusion fluids. *Econ. Geol.*, v. 78, pp. 535-542.
- Bodnar, R.J. (1993) Revised equation and table for determining the freezing point depression of H<sub>2</sub>O-NaCl solutions. *Geochim Cosmochim Acta*, v. 49, pp. 1861-1873.
- Bodnar, R.J and Vityk, M.O. (1994) Interpretation of microthermometric data for H<sub>2</sub>O-NaCl fluid inclusions. In: B. De Vivo and M.L. Frezzotti (eds) *Fluid inclusions in minerals: methods and applications*. Short course handbook of International Mineralogical Association, pp. 117-130.
- Bohlen, S.R. (1991) On the formation of granulites. *J. Metamorph. Geol.*, v. 9, pp. 223-229.
- Bohlen, S.R. (1987) Pressure-temperature-time paths and a tectonic model for the evolution of granulites. *J. Geol.*, v.95, pp.617-632.
- Bohlen, S.R., Wall, V.J. and Boettcher, A.L. (1983) Geobarometry in granulites. In: S.K. Saxena (ed), *Advances in physical geochemistry*, Springer Verlag, Newyork, v. 3, pp. 141-171.
- Bonijoli, M, Oberlin, M. and Oberlin, A. (1982) A possible mechanism of natural graphite formation. *Inter. J. Coal Geol.*, v.1, pp. 283-312.
- Brandon, A.D. and Meen, K. (1995) Nd isotopic evidence for the position of southern most Indian terranes within East Gondwana. *Precamb. Res.*, v. 70, pp. 269-280.

- Braun, I. and Brocker, M. (2004) Monazite dating of granite gneisses and leucogranites from Kerala Khondalite Belt, southern India: implications for late Proterozoic crustal evolution in East Gondwana. *Int. J. Earth Sci. (Geol Rundsch)*, v. 93, pp. 13-22.
- Braun, I and Kriegsman, L.M. (2003) Proterozoic crustal evolution of southern most India and Sri Lanka. *Geophys.Res.Abs.*, v. 5, p. 87056.
- Braun, I., Montel, J-M. and Nicollet, C. (1998) Electron microprobe dating of monazites from high-grade gneisses and pegmatites of Kerala Khondalite Belt, southern India. *Chem. Geol.*, v. 146, pp. 65-85.
- Brett, R. and Higgins, G.T. (1967) Cliftonite in meteorites: a proposed origin. *Science*, v. 156, pp. 819-820.
- Brey, G.T. and Kohler, T. (1990) Geothermobarometry in four phase iherzolites, part II: new thermobarometers, and practical assessment of existing thermobarometers. *J. Petrol.*, v. 31, pp.1353-1378.
- Brown, P.E. and Lamb, W.M. (1986) Mixing of H<sub>2</sub>O-CO<sub>2</sub> in fluid inclusions: geobarometry and Archean gold deposits. *Geochim. Cosmochim. Acta*, v. 50, pp. 847-852.
- Brown, M. Mohan, A. and Prakash, D. (1992) Sapphirine assemblages, upper Palani Hills, Tamil Nadu, EOS, v. 73, p601.
- Brown, M and Raith, M. (1996) First evidence of ultrahigh-temperature decompression from the granulite province of southern India. *J. Geol. Soc. London*, v. 153, pp. 819-822.
- Burruss, R.C. (1981) Analysis of phase equilibria in C-O-H-S fluid inclusions. In: L.S. Hollister and M.L. Crawford (eds), *Fluid inclusions: application to petrology*. Mineral. Assoc. Canada., short course handbook No. 6, pp. 29-74.
- Buseck, P.R. and Bo-Jun, H. (1985) Conversion of carbonaceous material to graphite during metamorphism. *Geochim. Cosmochim. Acta*, v. 49, pp. 2003-2016.
- Cenki, B. and Kriegsman, L.M. (2005) Tectonics of the neoproterozoic southern granulite terrain, South India. *Precamb. Res.* (In Press)
- Cenki, B., Kriegsman, L.M. and Braun, I. (2002) Melt-producing and melt consuming reactions in the Achankovil cordierite gneiss, South India. *J. Metamorph. Geol.*, v. 20, pp. 543-561.
- Cesare, B. (1995) Graphite precipitation in C-O-H fluid inclusions: closed system compositional and density changes, and thermobarometric implications. *Contrib. Mineral. Petrol.*, v. 122, pp. 25-33.

- Cesare, B., Meli, S., Nodari, L. and Russo, U. (2005) Fe<sup>3+</sup> reduction during biotite melting in graphitic metapelites: another origin of CO<sub>2</sub> granulites. *Contrib. Mineral. Petrol.*, v. 149, pp. 129-140.
- Chacko, T., Mayeda, T.K., Clayton, R.N. and Goldsmith, J.R. (1991) Oxygen and carbon isotopic fractionation between CO<sub>2</sub> and calcite. *Geochim. Cosmochim. Acta*, v. 55, pp. 2867-2882.
- Chacko, T., Lamb, M., Farquhar, J. (1996) Ultra-high temperature metamorphism in the Kerala Khondalite Belt. In: M. Santosh, and M. Yoshida, (eds.), *The Archaean and Proterozoic terrains of southern India within East Gondwana*. *Gondwana Res. Mem. No.3*, pp. 157-165.
- Chacko, T., Ravindra Kumar, G.R. and Newton, R.C. (1987) Metamorphic P-T conditions of the Kerala (South India) khondalite belt: a granulite facies supracrustal terrain. *J. Geol.*, v. 95, pp. 343-350.
- Cherneva, Z and Gerdjikov, I. (2004) Retrograde overprint on high-grade metamorphic rocks from the deepest part of the Arda unit central Rhodope. *Bulgarian Geol. Soc. Ann. Scientif. Confer. "Geology"* 16-17 December 2004, pp. 6-8.
- Chou, I-M. (1987) Phase relation in the system NaCl-KCl-H<sub>2</sub>O. III. Solubilities of halite in vapour saturated liquids above 445°C and re-determination of phase equilibrium properties in the system NaCl-H<sub>2</sub>O to 1000°C and 1500 bars. *Geochim. Cosmochim. Acta*, v. 51, pp. 1965-1975.
- Choudhari, A.K., Harris, N.B.W., van Calsteren, P. and Hawksworth, C.J. (1992) Pan-African charnockite formation in Kerala, South India. *Geol. Mag.*, v. 129, pp.257-264.
- Clifford, T.N., Stumpf, E.F., Burger, A.J., McCarthy, T.S., and Rex, D.C. (1981) Geological-chemical and isotopic studies of Namaqualand granulites, South Africa: Grenville analogue. *Contrib. Mineral. Petrol.*, v. 77, pp. 225-250.
- Cocherie, A., Legendre, O., Peucat, J.J., and Koualmelan, A. (1997) In-situ Th-U-Pb dating using an electron microprobe: a powerful tool for complex polygenic monazites. *Terra. Abs.*, v.9, pp. 441.
- Collins A.S., Kroner, A., Fitzsimons, I.C.W. and Razakamanana. T. (2003) Detrital footprints of the Mosambique ocean: U/Pb SHRIMP and Pb evaporation zircon geochronology of metasedimentary gneisses in Eastern Madagascar. *Tectonophysics*, v. 375, pp. 77-99.
- Crawford, M.L. (1981) Fluid inclusions in metamorphic rocks-low and medium grade. In: L.S. Hollister and M.L Crawford (eds), *Fluid*

inclusions: application to petrology. Mineral. Assoc. Canada, short course handbook No. 6, pp. 157-181.

- Crawford, M.L. and Hollister, L.S. (1986) Metamorphic fluids: the evidence from fluid inclusions. In: J.V. Walther and B.J. Wood (eds), Fluid-rock interactions during metamorphism. *Adv. Phys. Geochem.*, v. 5, pp. 1-35.
- Cuney, M. and Friedrich, M. (1987) Physicochemical and crystal-chemistry controls on accessory mineral paragenesis in granitoids: implications for uranium metellogenesis. *Bull. Mineral.*, v. 110, pp. 235-247.
- Dahl, P.S., Hamilton, M.A., Jercinovic, M.J., Terry, M.P., Williams M.L. and Frei, R. (2005) Comparative isotopic and chemical geochronometry of monazite, with implications for U-Th-Pb dating by electron microprobe: an example from metamorphic rocks of the Wyoming craton (USA). *Am. Mineral.*, v. 90, pp. 619-638.
- Deer, W.A., Howie, R.A. and Zussman, J. (1966) An introduction to the rock-forming minerals. The English Language Book Society and Longman, England. 528p.
- de Waard, D. (1965) A proposed subdivision of the granulite facies. *Am. J. Sci.*, v. 263, pp. 455-461.
- de Waard, D.(1967) The occurrence of garnet in the granulite-facies terrane of the Adirondack Highlands and elsewhere, an amplification and a reply. *J. Petrol.*, v. 8, pp. 210-232.
- Dahl, P. S. (1980) The thermal-compositional dependence of Fe<sup>2+</sup> -Mg distributions between coexisting garnet and pyroxene: applications to geothermobarometry. *Am. Mineral.*, v. 65, pp. 854-866.
- Desai, S.D. (1968) Graphite. *Mineral Wealth*, v. 4, pp. 18-26.
- Desai, S.J., Patel, M.P. and Merh, S.S. (1978) Polymetamorphites of Balaram-Abu road area, north Gujarat southwest Rajasthan. *J. Geol. Soc. India*, v. 19, pp. 383-394.
- Diessel, C.F.K. and Offler, R. (1975) Change in physical properties of coalfield and graphitized phytoclasts with grade of metamorphism. *Neues Jahrb. Mineral., Montash. H.*, v. 1, pp. 11-26.
- Dissanayake, C.B. (1981) The origin of graphite of Sri Lanka. *Organ. Chem.*, v. 3, pp. 1-7.
- Drury, S.A., Harris, N.B.W., Holt, R.W. and Reeves-Smith, G.J. (1984) Precambrian tectonics and crustal evolution in South India. *J. Geol.*, v.92, pp. 3-20.

- Drury, S.A. and Holt, R.W. (1980) The tectonic framework of the South Indian craton: a reconnaissance involving LANDSAT imagery. *Tectonophysics*, v. 65, pp. T<sub>1</sub>-T<sub>15</sub>.
- Eckert, J.O., Newton, R. C. and Kleppa, O. J. (1991) The  $\Delta H$  of reaction and recalibration of garnet–pyroxene– plagioclase–quartz geobarometers in the CMAS system by solution calorimetry. *Am. Mineral.*, v. 76, pp. 148–160.
- Eichman, R. and Schidlowski, M. (1975) Isotopic fractionation between co-existing organic carbon-carbonate pairs in Precambrian sediments. *Geochim. Cosmochim. Acta.*, v. 39, pp. 589-595.
- Ellis, D.J. and Green, D.H. (1979) An experimental study of the effect of Ca up on the garnet-clinopyroxene exchange equilibria. *Contrib. Mineral. Petrol.*, v. 86, pp. 359-373.
- Eskola, P. (1915) On the relation between the chemical and mineralogical composition in the metamorphic rocks of the Orijarvi region. *Bull. Comm. Geol. Finlande*, No.44.
- Fareeduddin, Sharma, A.K. and Bose, U. (1991) Tectonic slices of high-grade rocks in the Delhi fold belt of north-central Rajasthan. *J. Geol. Soc. India*, v. 38, pp. 427-436.
- Farquhar, J. and Chacko, T. (1991) Isotopic evidence for involvement of CO<sub>2</sub>-bearing magmas in granulite formation. *Nature*, v.354, pp. 60-63
- Farquhar, J., Hauri, E. and Wang, J. (1999) New insights into carbon fluid chemistry and graphite precipitation: SIMS analysis of granulite facies graphite from Ponmudi, South India. *Earth Planet. Sci. Lett.*, v.171, pp. 607-621.
- Ferry, J.M. and Spear, F.S. (1978) Experimental calibration of the partition of Fe and Mg between biotite and garnet. *Contrib. Mineral. Petrol.*, v. 66, pp. 113-117.
- Fitzsimons, I.C.W. and Harley, S.L. (1994) The influence of retrograde cation exchange on granulite P-T estimates and a convergence techniques for the recovery of peak metamorphic conditions. *J. Petrol.*, v. 35, pp. 543-576.
- Fonarev, V.I., Santosh, M., Vasiukova, O.V. and Filimonov, M.B. (2003) Fluid evolution and exhumation path of the Trivandrum Granulite Block, southern India. *Contrib. Mineral. Petrol.*, v. 145, pp. 339-345.
- Fountain, D.M. and Salisbury, M.H. (1981) Exposed cross sections through the continental crust: implications for crustal structure, petrology and evolution. *Earth Planet. Sci. Lett.*, v. 56, pp. 236-277.

- Frezzotti, M.L., Cezare, B. and Scambelluri, M. (2004) Fluids at extreme P-T metamorphic conditions: the message from high-grade rocks. *Per. Mineral.*, v. 73, pp. 209-219.
- Ganguly, J. (1979) Garnet and clinopyroxene solid solutions and geothermometry based on Fe-Mg distribution coefficient. *Geochim. Cosmochim. Acta*, v. 43, pp. 1021-1029.
- Ganguly, J., and Kennedy, G.C. (1974) The energetics of natural garnet solid solutions. I. Mixing of the aluminosilicate end-members. *Contrib. Mineral. Petrol.*, v. 48, pp. 137-148.
- Ganguly, J. and Saxena, S.K. (1984) Mixing properties of aluminosilicate garnets: constraints from natural and experimental data, and applications to geothermobarometry. *Am. Mineral.*, v. 69, pp. 88-97.
- Ghosh, J.G., deWit, M.J. and Zartman, R.E. (2004) Age and tectonic evolution of Neoproterozoic ductile shear zones in the southern granulite terrain of India, with implications for Gondwana studies. *Tectonics*, v. 23, pp. 1-38.
- Ghosh, J.G., Zartman, R.E. and deWit, M.J. (1998) Re-evaluation of tectonic framework of southernmost India: new U-Pb geochronological and structural data, and their implication for Gondwana reconstruction. In: J. Almond, et al. (eds.), *Gondwana 10: Event Stratigraphy of Gondwana*. *J. Afr. Earth Sci.*, v.27/1A, p. 86.
- Goldman, D. S. and Albee, A. L. (1977) Correlation of Mg/Fe partitioning between garnet and biotite with 180/160 partitioning between quartz and magnetite. *Am. J. Sci.*, v. 277, pp. 750-767
- Goodwin, A.M. (1996) *Principles of Precambrian Geology*. Academic Press Ltd. London. 327p.
- Graham, e.M., and Powell, R. (1984) A garnet-hornblende geothermometer: calibration, testing, and application to the Pelona Schist, southern California. *J. Metamorph. Geol.*, v. 2, pp. 13-21.
- Green, D.H. and Ringwood, A.E. (1967) An experimental investigation of the gabbro to eclogite transition and petrological implications. *Geochim. Cosmochim. Acta*, v. 31, pp. 767-833.
- Grew, E.S. (1974) Carbonaceous material in some metamorphic rocks of New England and other areas. *J. Geol.*, v. 82, pp. 50-73.
- Grew, E.S. (1982) Sapphirine, Kohnertite and sillimanite + orthopyroxene in the charnockitic region of South India. *J. Geol. Soc. India*, v. 23, pp. 469-505.

- Griffin, G.M. (1967) X-ray diffraction techniques applicable to studies of diagenesis and low rank metamorphism in humid sediments. *J. Sed. Petrol.*, v. 37, pp. 1006-1011.
- GSI (Geological Survey of India) (1995). Geological and mineral map of Kerala and Tamil Nadu.
- Guidotti, C.V. (1984) Micas in metamorphic rocks. *Rev. Mineral.*, v. 13, pp. 357-467.
- Hall, D.L. and Sterner, M. (1993) Preferential water loss from synthetic fluid inclusions. *Contrib. Mineral. Petrol.*, v. 114, pp. 489-500.
- Hansen, E.C., Newton, R.C. and Janardhan, A.S. (1984) Fluid inclusions in rocks from the amphibolite facies gneiss to charnockite progression in southern Karnataka, India: direct evidence concerning the fluids of granulite metamorphism. *J. Metamorph. Geol.*, v. 2, pp. 249-264.
- Hansen E.C., Hickman N.H., Grant N.K. and Newton R.C. (1985) Pan-African age of "Peninsular Gneiss" near Madurai, South India (abstract). *EOS* v. 66, pp. 419-420.
- Harben, P.W. and Kuzvart, M. (1996) *Industrial minerals, a global geology*. Industrial Minerals Information Ltd. Surrey, England, 462p.
- Harley, S.L. (1998) On the occurrence and characterisation of ultrahigh-temperature (UHT) crustal metamorphism. In: P.J. Treloar and P.O'Brien (eds), *What controls metamorphism and metamorphic reactions?* *Geol. Soc. London Pub.*, pp. 75-101.
- Harley, S.L. (1989) The origin of granulites: a metamorphic perspective. *Geol. Mag.*, v. 126, pp 215-247.
- Harley, S.L. (1984) An experimental study of the partitioning of Fe and Mg between garnet and orthopyroxene. *Contrib. Mineral. Petrol.*, v. 86, pp. 359-373.
- Harris, N.B.W., Bartlett, J.M. and Santosh, M. (1996) Neodymium isotope constraints on the tectonic evolution of East Gondwana. *J. Southeast Asian. Earth Sci.*, v. 14, pp. 119-125.
- Harris, N.B.W., Holt, R.W. and Drury, S. A. (1982) Geobarometry, geothermometry, and Late Archaean geotherms from the granulite facies terrain of South India. *J. Geol.*, v.90, pp. 509-527.
- Harris, N.B.W., Santosh, M. and Taylor, P.N. (1994) Crustal evolution in South India: constraints from Nd isotopes. *J. Geol.*, v. 102, pp.139-150.



- Heier, K.S. (1973) Geochemistry of granulite facies rocks and problems of their origin. *Trans. Roy. Soc. London*, v. 273, pp. 429-442.
- Hodges, K.V. and Spear, F.S. (1982) Geothermometry, geobarometry and the  $Al_2SiO_5$  triple point at Mt. Moosilauke, New Hampshire. *Am. Mineral.*, v. 67, pp. 1118-1134.
- Hoinkes, G. (1986) Effect of grossular content in garnet on the partitioning of Fe and Mg between garnet and biotite: An empirical investigation on staurolite-zone samples from the Austroalpine Schneeberg complex. *Contrib. Mineral. Petrol.*, v. 92, pp. 393-399.
- Holland, T.H. (1900) The charnockite series, a group of Archaean hypersthentic rocks in Peninsular India. *Mem. Geol. Surv. India*, v. 28, Pt. 2.
- Holland, T. and Blundy, J. (1994) Non-ideal interactions in calcic amphibole and their bearing on amphibole plagioclase thermometry. *Contrib. Mineral. Petrol.*, v. 116, pp. 433-447.
- Hollister, L.S. (1988) On the origin of  $CO_2$  -rich fluid inclusions in migmatites. *J. Metamorph. Geol.*, v. 6, pp. 467-474.
- Howe, J.Y., Rawn, C.J., Jones, L.E. and Ow, H. (2003) Improved crystallographic data for graphite. *Powder Diffraction*, v. 18, No. 2, pp. 150-154.
- Howie, R.A. (1955) The geochemistry of charnockite series of Madras, India. *Trans. Roy.Soc. Edinburgh*, v.62, pp. 725-768.
- Indares, A.D. and Martignole, J. (2003) Towards the upper limits of the granulite facies. *J. Metamorph. Geol.*, v. 21, pp. 1-2.
- Jackson, D.H., Matthey, D.P. and Harris, N.B.W. (1988) Carbon isotope compositions of fluid inclusions in charnockites from southern India. *Nature*, v. 333, No.6169, pp. 167-170.
- Janardhan, A.S., Newton, R.C. and Smith, J.V. (1979) Ancient crustal metamorphism at low  $pH_2O$ : charnockite formation at Kabbaldurga, South India. *Nature*, v. 278, pp. 511-514.
- Jayananda, M., Janardhan, A.S. Sivasubramaniam, P. and Peucat, J-J. (1995a) Geochronologic and isotopic constraints on granulite formation in the Kodaikkanal area, southern India. In: M. Yoshida and M. Santosh (eds). *India and Antarctica during the Precambrian*. *Mem. Geol.Soc. India*, v. 34, pp. 373-390.
- Jayananda, M., Martin, H., Peucat, J-J and Mahabaleswar, B. (1995b) The late Archaean crust mantle interactions: Geochemistry of LREE

enriched mantle derived magmas. The Closepet batholith of southern India. *Contrib. Mineral. Petrol.*, v. 119, pp. 314-329.

- Jayananda, M and Peucat, J-J. 1996 Geochronological framework of southern India. In: M. Santosh and M. Yoshida (eds.), *The Archaean and Proterozoic terrains of southern India within East Gondwana*. *Gondwana Res. Mem. No.3*, pp. 53-75.
- John, M.M., Balakrishnan, S. and Bhadra, B.K. (2005) Contrasting metamorphism across Cauvery shear zone, south India. *J. Earth Syst. Sci.*, v. 114, No. 2, pp. 143-158.
- Kagi, H., Tsuchida, I., Wakatsuki, M., Takahashi, K., Kamimura, N., Iuchi, K. and Wada, H. (1994) Proper understanding of down-shifted Raman spectra of natural graphite: Direct estimation of laser-induced rise in sample temperature. *Geochim Cosmochim Acta*, v. 58, pp. 3527-3530.
- Katz, M.B. (1978) Tectonic evolution of the Archaean granulite facies belt of Sri Lanka-South India. *J. Geol. Soc. India*, v. 19, pp. 185-205.
- Katz, M.B. (1987) Graphite deposits of Sri Lanka: a consequence of granulite facies metamorphism. *Mineral. Deposit.*, v. 22, pp. 18-25.
- Kohn, MJ and Spear, FS. (1989) Empirical calibration of geobarometers for the assemblage garnet - hornblende - plagioclase - quartz. *Am. Mineral.*, v. 74, pp. 77-84.
- Kohn, MJ and Spear, FS. (1990) Two new geobarometers for garnet amphibolites with applications to southeastern Vermont. *Am. Mineral.*, v. 75, pp. 89-96.
- Krishnaswami, S. (1979) *India's mineral resources*, Oxford & IBH Pub. Co. New Delhi, 658p.
- Krogh, E.J. (1988) The garnet-clinopyroxene Fe-Mg geothermometer – a reinterpretation of existing experimental data. *Contrib. Mineral. Petrol.*, v. 99, pp. 44-48.
- Krogstad, E.J., Hanson, G.N. and Rajamani, V. (1991) U-Pb age of zircon and sphene for two gneiss terrains adjacent to the Kolar schist belt, South India: evidence for separate crustal histories. *J. Geol.*, v. 99, pp. 801-816.
- Kundu, A., D'Souza, M.J. and Mohan, A. (1998) Reaction textures in gneisses from Dallmannfjellet-Conrad area, Orwin range, central Dronning Maud land, East Antarctica: implication for metamorphic evolution. *J. Geol. Soc. India*, v. 52, pp. 709-719.

- Kwieceńska, B. and Petersen, H.I. (2004) Graphite, semigraphite, natural coke and natural char classification-ICCP system. *Inter. J. Coal Geol.*, v. 57, pp. 99-116.
- Lal, R.K. (1993) Internally consistent recalibrations of mineral equilibria for geothermobarometry involving garnet-orthopyroxene-plagioclase-quartz assemblages and their applications to South Indian granulites. *J. Metamorph. Geol.*, v. 11, pp. 855-866.
- Lamb, W.E., Brown, P.E. and Valley, J.W. (1991) Fluid inclusions in Adirondack granulites: *Contrib. Mineral. Petrol.*, v. 96, pp. 485-495.
- Landis, C.A. (1971) Graphitization of dispersed carbonaceous material in metamorphic rocks. *Contrib. Mineral. Petrol.*, v. 30, pp. 34-45.
- Lanzirotti, A. and Hanson, G. N. (1996) Geochronology and geochemistry of multiple generations of monazite from the Wepawaug Schist, Connecticut, USA: implications for monazite stability in metamorphic rocks. *Contrib. Mineral. Petrol.*, v. 125, pp. 332-340.
- Lee, H.Y. and Ganguly, J. (1988) Equilibrium compositions of coexisting garnet and orthopyroxene: experimental determinations in the system FeO-MgO-Al<sub>2</sub>O<sub>3</sub>-SiO<sub>2</sub> and applications. *J. Petrol.*, v. 29, pp. 93-113.
- Lloyd, G.E., Prasannakumar V. and McCaig, A.M. (2004) Kinematic and tectonomorphic evolution of the Palghat-Cauvery shear system and exhumation of the South India crustal blocks, IGC., Florence.
- Luque, F.J., Pasteris, J.D., Wopenka, B., Rodas, M. and Barrenechea, J.F. (1998) Natural fluid deposited graphite: mineralogical characteristics and mechanisms of formation. *Am. J. Sci.*, v. 298, pp. 471-498.
- Mahabaleswar, B. (1993) Geothermobarometry along the north south transect – a review. *Mem. Geol. Soc. India*, v. 25, pp. 303-312.
- Mahabaleswar, B., Jayananda, M., Peucat, J.J. and Shadakshara Swamy, S. (1995) Archaean high-grade gneiss complex from Satnur-Halagur-Sivasamudram areas, Karnataka, Southern India : petrogenesis and crustal evolution., *J. Geol. Soc. India*, v. 45, pp. 33-49.
- Mahadevan, T.M. (1992) Geological evolution of Chotanagpur gneissic complex in parts of Purulia district, West Bengal, India. *J. Geol.*, v. 64, pp. 1-22.
- Mahadevan, T.M. (1994) Deep continental structure of India – a review. *Mem. Geol. Soc. India*, v. 28, 569 p.

- Mahadevan, T.M. (1996) Deep continental structure and Precambrian evolution of the Indian peninsular shield. In: M. Santosh, and M. Yoshida, (eds.), *The Archaean and Proterozoic terrains of southern India within East Gondwana*. Gondwana Res. Mem. No.3, pp. 39-52.
- Majumdar, S.K. (1988) Crustal evolution of Choptanagpur gneissic complex and the mica belt of Bihar. In: D. Mukhopadhyaya (ed), *Precambrian of Eastern Indian Shield*. Mem. Geol. Soc India, v. 8, pp. 49-83.
- Markl, G, Bäuerle, J. and Grujic, D. (2000) Metamorphic evolution of Pan-African granulite facies metapelites from southern Madagascar. *Precamb. Res.*, v. 102, pp. 47-68.
- Meert, J.G. (2003) A synopsis of events related to the assembly of eastern Gondwana. *Tectonophysics*, v. 362, pp. 1-40.
- Meert, J.G., Van der Voo, R., Ayub, S., 1995. Paleomagnetic investigation of the Neoproterozoic Gagwe lavas and Mbozi Complex, Tanzania and the assembly of Gondwana. *Precamb. Res.*, v.74, pp. 225– 244.
- Miller, J.S., Santosh, M. Pressley, R.A, Clements, A.S. and Rogers, J.J.W. (1996) A Pan-African thermal event in southern India. *J Southeast Asian Earth Sci.*, v.14, pp. 127-136
- Miyashiro, A. (1961) Evolution of metamorphic belts. *J. Petrol.*, v. 2. No. 3, pp. 277-311.
- Mohan, A. (1996) The Madurai block. In: M. Santosh, and M. Yoshida, (eds.), *The Archaean and Proterozoic terrains of southern India within East Gondwana*. Gondwana Res. Mem. No.3, pp. 223-242.
- Mohan, A. and Jayananda, M. (1999) Metamorphism and isotopic evolution of granulites of southern India: Reference to Neoproterozoic crustal evolution. *Gondwana Res.*, v. 2, No. 2, pp. 151-162.
- Mohan, A., Lal, R.K. and Ackermann, D. (1985) Granulites of Ganguvarpatti, Madurai district, Tamil Nadu. *Indian J. Earth Sci.*, v.12, pp. 255-278.
- Mohan, A., Prakash, D. and Sachan, H.K. (1996a) Fluid inclusions from charnockites from Kodaikanal massif (South India): P-T record and implication for crustal uplift history. *Mineral. Petrol.*, v. 57, pp. 167-184.
- Mohan, A., Prakash, D and Motoyoshi, Y. (1996b) Decompressional P-T history in the sappherine –bearing granulites from Kodaikanal, southern India. Special issue on Precambrian India within East Gondwana. *J. Southeast Asian Earth Sci.*, v.14, pp. 231-243.

- Mohan, A and Windley, B.F. (1993) Crustal trajectory of sapphirine-bearing granulites from Ganguvarappatti, South India; evidence for an isothermal decompression path. *J. Metamorph. Geol.*, v. 11, pp. 867-878.
- Mostefaoui, S, Zinner, E, Hoppe, P., Stadermann, F.J. and El Goresy, A. (2005) In situ survey of graphite in unequilibrated chondrites: morphologies, C, N, O and H isotopic ratios. *Meteor. Planet. Sci.*, v. 40, No. 5, pp. 721-743.
- Montel, J-M., Foret, S., Veschambre. M., Nicollet, C. and Provost, A. (1996) Electron microprobe dating of monazite. *Chem. Geol.*, v. 131, pp. 37-53.
- Murthy, N.G.K. (1995) Proterozoic mafic dykes in southern peninsular India; A review. *Mem. Geol. Soc. India*, No. 33, pp. 81-98.
- Nambiar, C.G., Bhaskar Rao, B., Parthasarathy, R. and Fedkin, V.V. (1992) Geochemistry and genesis of charnockites and associated gneisses from northern Kerala, India. *High-grade metamorphics*. Theophrastus Pub. S.A., Athens, Greece, pp. 187-216.
- Nandakumar, V. and Harley, S.L. (2000) A reappraisal of the pressure-temperature path of granulites from the Kerala Khondalite Belt, southern India. *J. Geol.*, v. 108, pp. 687-703.
- Naqvi, S.M. and Rogers, J.J.W. (1987) *Precambrian geology of India*. Oxford Univ. Press, 223p.
- Nasir, S. (1991) New geothermometers for amphibolites, granulites and eclogites. *European. J. Mineral.*, v. 3, no. 1, pp. 110.
- Nasir, S. (1994) PTOXY: software package for the calculation of pressure-temperature oxygen fugacity using a selection of metamorphic geothermobarometers. *Comput. Geosci.*, v. 20, pp. 1297-1320.
- Nasir, S. and Abu-Aljarayesh, I., (1992) Empirical calibration of geothermometer for garnet amphibolite and granulite based on the assemblage garnet-clinopyroxene-hornblende. *Geochemistry*, v. 52, pp. 205-210.
- Nehru, C. E., and Wyllie, P. J. (1974) Electron microprobe measurement of pyroxenes coexisting with H<sub>2</sub>O-undersaturated liquid in the join CaMgSi<sub>2</sub>O<sub>6</sub>-Mg<sub>2</sub>Si<sub>2</sub>O<sub>6</sub>-H<sub>2</sub>O at 30 kilobars, with applications to geothermometry. *Contrib. Mineral. Petrol.*, v. 48, pp. 221-228.
- Newton, R.C. (1989) Metamorphic fluids in the deep crust. *Ann. Rev. Earth and Planet. Sci.*, v. 17, pp. 385-412.

- Newton, R.C. and Perkins, D., III (1982) Thermodynamic calibration of geobarometers for charnockites and basic granulites based on assemblages garnet-plagioclase-orthopyroxene (clinopyroxene)-quartz with application to high grade metamorphism. *Am. Mineral.*, v. 67, pp. 203-222.
- Newton, R.C., Smith, J.V. and Windley, B.F. (1980) Carbonic metamorphism, granulites and crustal growth. *Nature*, v. 288, pp. 45-50.
- Nickel, K.G. and Green, D.H. (1985) Empirical geothermobarometry for garnet peridotites and implications for the nature of the lithosphere, kimberlites and diamonds. *Earth Planet. Sci. Lett.*, v. 73, pp. 158-170.
- Norman, D.I., Blamey, N.J.F. and Moore, J.N. (2001) Overabundance of gaseous species and source of organic compounds in geothermal fluids. Proc.26<sup>th</sup> Workshop on Geothermal Reservoir Engg., Stanford University, Stanford California, January, 29-31, pp. 234-242.
- Norman, D.I., Blamey, N.J.F. and Moore, J.N. (2002) Interpreting geothermal processes and fluid sources from fluid inclusion organic compounds and CO<sub>2</sub>/N<sub>2</sub> ratios. Proc.27<sup>th</sup> Workshop on Geothermal Reservoir Engg., Stanford University, Stanford California, January, 28-30.
- Norman, D.I., Moore, J.N., Yonaka, B. and Musgrave, J. (1996) Gaseous species in fluid inclusions: a tracer of fluids and an indicator of fluid processes. Proc.21<sup>st</sup> Workshop on Geothermal Reservoir Engg., Stanford University, Stanford California, January, 22-24, pp. 233-240.
- Nutman, A.P., Chadwick, B., Ramakrishnan, K., Viswanatha, M.N. (1992) SHRIMP U-Pb ages of detrital zircon in Sargur supracrustal rocks in western Karnataka, southern India. *J. Geol. Soc. India*, v. 39, pp. 367-374.
- Parrish, R.R. (1990) U-Pb dating of monazites and its application to geological problems. *Can. J. Earth Sci.*, v.27, pp. 1431-1450.
- Parthasarathy, G. and Sharma, S.R. (2001) A comparative study on structural properties of graphite from Dharwar craton, India; a high temperature DTA study. *J. Geol. Soc. India*, v. 57, pp. 435-442.
- Parthasarathy, G., Sharma, S.R., Ravindran, T.R., Arora, A.K. and Hussain, S.M. (2003) Structural and thermal studies of graphite from East Antarctica. *J. Geol. Soc. India*, v. 61, pp. 335-343.

- Parthasarathy, G., Sreedhar, B. and Chetty, T.R.K. (2006) Spectroscopic and X-ray diffraction studies on fluid deposited rhombohedral graphite from the Eastern Ghats mobile belt, India. *Curr. Sci.*, v. 90, No. 7, pp. 995-1000.
- Pascoe, E.H. (1950) A manual of the geology of India and Burma. III edn., v. 1, 483p.
- Pasteris, J.D. (1998) The laser Raman microprobe as a tool for the economic geologist. In: M.A. McKibben, W.C. Shanks and W.I. Ridley (eds), *Application of microanalytical techniques to understanding mineralizing processes*. Soc. Econ Geologists, Denver, *Rev. Econ. Geol.*, v. 7, pp. 233-250
- Pasteris, J.D. (1999) Causes of the uniformly high crystallinity of graphite in large epigenetic deposits. *J. Metamorph. Geol.*, v. 17, pp. 779-787.
- Pasteris, J.D. and Chou, I.M. (1998) Fluid-deposited graphitic inclusions in quartz: comparison between KTB (German continental deep-drilling) core samples and artificially re-equilibrated natural inclusions. *Geochim. Cosmochim. Acta*, v. 62, pp. 109-122.
- Pasteris, J.D., Kuehn, C.A. and Bodnar, R.J. (1986) Applications of the laser Raman microprobe RAMANOR U-1000 to hydrothermal ore deposits: Carlin as an example. *Econ. Geol.*, v. 81, pp. 915-930.
- Pasteris, J.D. and Wopenka, B. (1991) Raman spectra of graphite as indicators of degree of metamorphism. *Can. Mineral.*, v. 29, pp. 1-9.
- Pattison, D.R.M. (2003) Petrogenetic significance of orthopyroxene-free garnet + clinopyroxene + plagioclase  $\pm$  quartz bearing metabasites with respect to amphibolite and granulite facies. *J. Metamorph. Geol.*, v. 21, pp. 21-34.
- Pearson, D.G., Davis, G. R. Nixon, P.H. and Milledge, H.J. (1989) Graphitized diamonds from a peridotite massif in Morocco and implications for anomalous diamond occurrences. *Nature*, v. 338, pp. 60-62.
- Perchuk, L. L. and Lavrentjeva, I. V. (1983) Experimental investigation of exchange equilibria in the system cordierite-garnet-biotite. In: S.K. SAXENA (ed.). *Kinetics and equilibrium mineral reactions*. *Adv. Phys. Geochem.*, v. 3, pp. 199-239
- Peucat, J-J., Mahabaleswar, B., and Jayananda, M. (1993) Age of younger tonalitic metamorphism and granulite metamorphism in the South Indian transition zone (Krishnagiri area): comparison with older Peninsular gneiss from Hassan-Gorur area. *J. Metamorph. Geol.*, v. 11, pp. 879-888.

- Peucat, J-J., Vidal, Bernad-Griffiths, J. and Condie, K.C. (1989) Sr. Nd and Pb. Isotopic systematics in the Archaean low-to high-grade transition zone in the southern India: syn accretion vs post accretion granulites. *J. Geol.*, v. 97, pp. 537-550.
- Prakash, D. (1999) Cordierite-bearing gneisses from Kodaikanal, South India: textural relationship and P-T conditions. *J. Geol. Soc. India*, v. 54, pp. 347-358.
- Pichamuthu, C.S. (1953) The charnockite problem. Mysore Geol. Assoc. Spec. Publ., Bangalore.
- Pichamuthu, C.S. (1961) Transformation of peninsular gneiss to charnockite, Mysore state, India. *J. Geol. Soc. India*, v. 21, pp. 221-229.
- Pichamuthu, C.S. (1979) Mineralogy of Indian charnockites. *J. Geol. Soc. India*, v. 20, pp. 257-276.
- Powell, R. (1978) The thermodynamics of pyroxene geotherms. *Phil. Trans.Roy. Soc. London, Series A*, 288, 457-469.
- Powell, R. (1985) Regression diagnostics and robust regression in geothermometer/ geobarometer calibration: the garnet-clinopyroxene geothermometer revisited. *J. Metamorph. Geol.*, v. 3, pp. 231-243.
- Pyle, J. M. and Spear, F. S. (1999) Yttrium zoning in garnet: coupling of major and accessory phases during metamorphic reactions. *Geol. Mat. Res.*, v. 1, pp. 1-49.
- Radhakrishna, T., Joseph, M., Thampi, P.K. and Mitchel, J.G. (1990) Phanerozoic mafic dyke intrusions from the high-grade terrain of southwestern India: K-Ar isotope and geochemical geochemical implications. In: A.J. Parker, P.C. Rickwood, and D.H. Tucker (eds), *Mafic dykes and emplacement mechanisms*, A.A, Balkema, Rotterdam, pp. 363-372.
- Radhakrishna, T., Poornachandra Rao, G.V.S., Mitchell, J.G. and Venkatesh, A. V. (1986) Proterozoic basic dyke activity in Kerala along the western coastal margin of India. *J. Geol, Soc. India*, v. 27, pp 245-253.
- Radhakrishna, B.P. and Naqvi, S.M. (1986) Precambrian continental crust of India and its evolution. *J. Geol.*, v. 94, pp. 145-166.
- Radhika, U.P. and Santosh, M. (1996) Shear zone hosted graphite in southern Kerala, India: implications for CO<sub>2</sub> infiltration. *J. Southeast. Asian. Earth Sci.*, v. 14, pp. 256-273.



- Radhika, U.P., Santosh, M. and Wada, H. (1995) Graphite occurrences in southern Kerala: characteristics and genesis. *J. Geol. Soc. India*, v. 45, pp. 653-666.
- Raheim, A. and Green, D. H. (1974) Experimental determination of the temperature and pressure dependence of the Fe-Mg partition coefficient for coexisting garnet and clinopyroxene. *Contrib. Mineral. Petrol.*, v. 48, pp. 179-203.
- Raith, M., Rasse, P., Ackermann, D. and Lal, R.K. (1983) Regional geothermobarometry in the granulite facies terrain of South India. *Trans. Roy. Soc. Edinburgh, Earth Sci.*, v. 73 (for 1982), pp. 221-244.
- Raith, M., Srikantappa, K.G., Ashamanjari and Spiering, B. (1990) The granulite terrane of the Nilgiri hills (Southern India): characterization of high-grade metamorphism. In: D. Vielzeuf and Ph. Vidal (eds), *Granulites and crustal evolution*. Kluwer Academic Publishers, pp. 339-365.
- Raith, M., Karmakar, S. and Brown, M. (1997) Ultra-high-temperature metamorphism and multistage decompressional evolution of sapphirine granulites from the Palani hills, southern India. *J. Metamorph. Geol.*, v. 15, pp. 379-399.
- Raja Rao, C.S., Poddar, B.C., Basu, K.K. and Dutta, A.K. (1971) Precambrian stratigraphy of Rajasthan – a review. *Rec. Geol. Surv. India*, v. 101(20), pp. 52-79.
- Rajesh-Chandran, R., Menon, R. D., Radhika, U.P., Santosh, M. and Yoshida, M. (1996) Proterozoic mineralizations in Kerala: summary characteristics and genesis. In: M. Santosh, and M. Yoshida, (eds.), *The Archaean and Proterozoic terrains of southern India within East Gondwana*. *Gondwana Res. Mem. No.3*, pp. 117-144.
- Rajesh H.M. (2004) The igneous charnockite-high-K alkali-calcic I-type granite-incipient charnockite association in Trivandrum Block, southern India. *Contrib. Mineral. Petrol.*, v. 147, pp. 346-362.
- Rajesh H.M and Santosh M. (1996) Alkaline magmatism in Peninsular India. In: M. Santosh and M. Yoshida (eds.), *The Archaean and Proterozoic terrains of southern India within East Gondwana*. *Gond. Res. Mem. No.3*, pp. 91-115.
- Rajesh H.M., Santosh M., Yoshida M. (1996) The felsic magmatic province in East Gondwana: implications for Pan-African tectonics. *J Southeast Asian Earth Sci.*, v.14, pp. 275–291.
- Rajesh H.M., Santosh M., Yoshida M. (1998) Dextral Pan-African shear along the southwestern edge of the Achankovil shear belt, South

- India: constraints on Gondwana reconstructions: a discussion: with reply by Sacks, P.E., Nambiar, C.G. and Walters, L.J. *J. Geol.*, v. 106, pp. 105-114.
- Ramakrishnan, M. (2003) Craton-mobile belt relations in southern granulite terrain. *Mem. Geol. Soc. India*, No.50, pp. 1-24.
- Rama Rao, B. (1945) The charnockite rocks of Mysore. *Mysore Geol. Dept. Bull.*, No. 18, 168p.
- Rao, J.S.R.K. and Rao, V.M. (1965) Occurrence and origin of graphite in parts of Eastern Ghats, South India. *Econ. Geol.*, v. 60, pp.1046-1054.
- Ravindra Kumar, G.R. (2004) Mechanism of arrested charnockite formation at Nemmara, Palghat region, southern India. *Lithos*, (In Press).
- Ravindra Kumar, G.R. (2005) Lithology and metamorphic evolution of granulite-facies segments of Kerala, southern India. *J. Geol. Soc. India*, v.66, No.2, pp. 253-254.
- Ravindra Kumar, G.R. and Chacko, T. (1994) Geothermobarometry of mafic granulites and metapelite from Palghat gap, petrological evidence for isothermal uplift and rapid cooling. *J. Metamorph. Geol.*, v. 12, pp. 479-492.
- Reymer, A. and Schubert, G. (1984) Phanerozoic and Precambrian crustal growth. In: A. Kroner (ed), *Proterozoic crustal evolution*. *Am. Geophys. Uni. Ser.*, v. 17, pp. 1-10.
- Reynolds, W.N. (1968) Physical properties of graphite. *Mater. Sci. Ser.* Elsevier, Amstardam.
- Rhede, D., Wendt, I., and Förster, H.J. (1996) A three-dimensional method for calculating independent chemical U/Pb- and Th/Pb-ages of accessory minerals. *Chem. Geol.*, v. 130, pp. 247-253.
- Roedder, E. (1979) Origin and significance of magmatic inclusions. *Bull. Mineral.*, v. 102, pp.487-510
- Roedder, E. (1984) Fluid inclusions. *Reviews in Mineralogy*, v. 12, Mineral. Soc. America. 646 p.
- Rumble, D. III, Duke, E.F. and Hoering, T. (1986) Hydrothermal graphite in New Hampshire: evidence of carbon mobility during regional metamorphism. *Geology*, v. 14, pp. 452-455.
- Sacks, P.E., Nambiar, C.G. and Walters, L.J. (1997) Dextral Pan-African shear along the southwestern edge of the Achankovil shear belt,

- South India: constraints on Gondwana reconstructions. *J. Geol.*, v. 105, pp. 275-284.
- Sandiford, M. and Powell, R. (1986) Deep crustal metamorphism during continental extension: modern and ancient examples: *Earth Planet. Sci. Lett.*, v. 79, pp. 151-158.
- Santosh, M. (1984) Nature of ore fluids in Odara rare metal pegmatite, Kerala, India. *N. Jb. Mineral. Mh.*, H.6, pp. 241-250.
- Santosh, M. (1986a) Carbonic metamorphism of charnockites in the southwestern Indian shield: a fluid inclusion study. *Lithos*, v. 19, pp. 1-10.
- Santosh, M. (1986b) Nature and evolution of metamorphic fluids in the Precambrian khondalites of Kerala, South India. *Precamb. Res.*, v. 33, pp. 283-302.
- Santosh, M. (1987) Cordierite gneiss of southern Kerala, India: petrology, fluid inclusions and implications for crustal uplift history. *Contrib. Mineral. Petrol.*, v. 96, pp. 343-356.
- Santosh M. (1989) Alkaline plutons, decompression granulites and late Proterozoic CO<sub>2</sub> influx in Kerala, South India. *Mem. Geol. Soc. India*, No.15, pp. 177-188.
- Santosh, M. (1991) Role of CO<sub>2</sub> in granulite petrogenesis: evidence from fluid inclusions. *J. Geosci.*, v. 34, pp. 1-53.
- Santosh, M. (1996) The Trivandrum and Nagercoil granulite blocks. In: M. Santosh and M. Yoshida (eds.), *The Archaean and Proterozoic terrains of southern India within East Gondwana*. *Gond. Res. Mem.* No. 3, pp.243-278.
- Santosh, M (1998) Fluid inclusion palaeopresures and source of carbonic fluids in the massive charnockites of Kerala, South India. *Mem. Geol. Soc. India*, No.11, pp. 91-99.
- Santosh, M., Jackson, D.H., Harris, N.B.W. and Matthey, D.P. (1991) Carbonic fluid inclusions in South India granulites: evidence for entrapment during charnockite formation. *Contrib. Mineral. Petrol.*, v. 108, pp. 318-330.
- Santosh, M., Kagami, H., Yoshida, M. and Nanda-Kumar, V. (1992) Pan-African charnockite formation in East Gondwana; geochronologic Sm-Nd and Rb-Sr petrogenetic constraints. *Bull. Ind. Geol. Assoc.*, v.25, pp.1-10.

- Santosh, M. and Nair, N.G.K. (1983a) Petrochemistry of the Chenganoor granite, Alleppey district, Kerala. *J. Geol. Soc. India*, v. 24, pp. 291-298.
- Santosh, M. and Nair, N.G.K. (1983b) Granite –molybdenite association in Kerala in relation to taphrogenic metallogeny. *Proc. Ind. Acad. Sci (Earth Planet. Sci)*, v. 92, pp. 297-310.
- Santosh M, Radhika, U.P. (1994) Carbonic metasomatism and charnockitic alteration. *J. Geol. Soc. India*, v. 43, pp. 191-199.
- Santosh M., Rajan P. K. and Nair, N.G.K. (1983) The Pariyaram granite, Trichur district, Kerala-its petrochemistry. *Bull. Ind. Geol. Assoc.*, v. 16, pp. 33-43.
- Santosh M. and Thara, K.G. (1985) The Mannapra syenite, central Kerala, India: geochemistry, petrogenesis and bearing on an orogenic magmatism. *Proc. Ind. Acad. Sci.*, v. 94, pp. 43-56.
- Santosh, M. and Tsunogae, T. (2003) Extremely high density pure CO<sub>2</sub> fluid inclusions in a garnet granulite from southern India. *J. Geol.*, v. 111, pp 1-16.
- Santosh, M., Tsunogae, T. and Yashikura, S. (2004) "Ultrahigh density" carbonic inclusions in ultrahigh-temperature crustal metamorphism. *J. Mineral. Petrol. Sci.*, v. 99 (Spl. Issue), pp. 164-179.
- Santosh, M. and Wada, H. (1993a) A carbon isotope study of graphite from the Kerala Khondalite Belt, southern India: evidence for CO<sub>2</sub> infiltration in granulites. *J. Geol.*, v. 101, pp. 643-651.
- Santosh, M. and Wada, H. (1993b) Microscale isotopic zonation in graphite crystals: Evidence for channeled CO<sub>2</sub> influx in granulites. *Earth Planet. Sci. Lett.*, v.119, pp. 19-26.
- Santosh, M., Wada, H., Satish-Kumar, M. and Binu-Lal, S.S. (2003) Carbon isotope "stratigraphy" in a single graphite crystal: implications for crystal growth mechanism of fluid deposited graphite. *Am. Mineral.*, v.88, pp. 1689-1696.
- Santosh, M., Yokoyama, K., Biju-Sekhar, S. and Rogers, J.J.W. (2003) Multiple tectonothermal events in the granulite blocks of southern India revealed from EPMA dating: implications on the history of super continents. *Gond. Res.* v. 6, pp. 29-63.
- Satish-Kumar, M. (2000) "Ultra high-temperature in Madurai granulites, southern India: evidence from carbon isotope thermometry. *J. Geol.*, v. 108, pp. 479-486.

- Satish-Kumar, M. and Wada, H. (2000) Carbon isotopic equilibrium between calcite and graphite in Skallen marbles, East Antarctica: evidence for the preservation of peak metamorphic temperatures. *Chem. Geol.*, v. 166. pp. 173-182.
- Satish-Kumar, M., Wada, H. and Santosh, M. (2002) Constraints on the application of carbon isotope thermometry in high- to ultrahigh-temperature metamorphic terranes. *J. Metamorph. Geol.*, v. 20, pp. 335-350.
- Satish-Kumar, M., Wada, H., Santosh, M. and Yoshida, M. (2001) Fluid-rock history of granulite facies humite marbles from Ambasamudram, southern India. *J. Metamorph. Geol.*, v. 19, pp. 395-410.
- Sengupta, P., Dasgupta, S., Bhattacharya, P.K. and Hariya, Y. (1989) Mixing behavior in quaternary garnet solid solution and an extended Ellis and Green garnet-clinopyroxene geothermometer. *Contrib. Mineral. Petrol.*, v. 103, pp. 223-227.
- Sen, S.K. (1970) Magnesium-iron compositional variance in hornblende pyroxene granulites: *Contrib. Mineral. Petrol.*, v. 29, pp. 76-88.
- Sen, S.K. and Ray, S. (1971) Breakdown reactions for natural hornblendes in granulite facies, *N. Jb. Mineral. Abh.*, v. 114, No., 3, pp. 301-319.
- Shabeer, K.P. (2004) Petrology and geochronology of granulite facies metamorphic rocks from the Kerala Khondalite Belt (KKB), southern India: implications to the partial melting processes and heat source. Unpublished Ph. D thesis. Department of Geosciences, Osaka City University, Japan. 205p.
- Sharma, S.R., Parthasarathy, G. and Kumar, B. (1998) X-ray diffraction studies on graphite from Dharwar craton. *J. Geol. Soc. India*, v. 51, pp. 517-522.
- Sharma, S.R., Parthasarathy, G., Ravindran, T.R., Arora, A.K. and Kumar, B. (2000) Laser Raman spectroscopic studies on graphites from Dharwar craton: a possible metamorphic grade indicator for the host rocks. *J. Geol. Soc. India*, v. 55, pp. 413-420.
- Shepherd, T.J., Rankin, A.H. and Alderton, D.H.M. (1985) A practical guide to fluid inclusion studies. Blackie & Son Ltd, Glasgow, 238 p.
- Shmulovich, K.I., Tkachenko, S.I. and Plyasunova, N.V. (1994) Phase equilibria in fluid systems at high pressures and temperatures. In: K.I. Shmulovich, B.W.D. Yardley and G.G. Gonchar (eds), *Fluids in the Crust: Equilibrium and Transport Properties* pp. 193-214. Chapman & Hall, London.

- Sinha-Roy, S., Mathai, J. and Narayanaswami (1984) Structure and metamorphic characteristics of cordierite-bearing gneiss of South Kerala. *J. Geol. Soc. India*, v. 25, pp. 231-244.
- Sivasubramanian, P., Natarajan, R. and Janardhan, A.S. (1991) Sapphirine-bearing assemblages from Perumalmai, Palani hills, Tamil Nadu. *J. Geol. Soc. India*, v. 38, pp. 532-537.
- Smeeth, W.F. (1916) Outline of the geological history of Mysore. *Mysore Geol. Dept. Bull.*, No.6, 26p.
- Soman, K., Lobzova, R.V., Sivadas, K.M. (1966) Geology, genetic type and origin of graphite in southern Kerala, India. *Econ. Geol.*, v. 81, pp. 997-1002.
- Soman, K. (2002) *Geology of Kerala*. Geol. Soc. India, Bangalore. 331p.
- Soto, J.I. and Soto, V.M. (1995) PT Mafic (v.20) software package for thermometry, barometry and activity calculations in mafic rocks using an IBM or compatible computer. *Comput. Geosci.*, v. 21, pp. 619-652.
- Spear, F.S. (1993) Metamorphic phase equilibria and pressure-temperature-time paths. *Mineral. Soc. Am. Mono.*
- Spear, F.S. (1995) *Metamorphic phase equilibria and pressure-temperature-time paths*: New York, Mineral. Soc. Am. 799p.
- Srikantappa, C. (1993) High-pressure charnockites of the Nilgiri hills, southern India. *Mem. Geol. Soc. India*, v. 25, pp. 95-110.
- Srikantappa, C. (1996) The Nilgiri Granulites. In: M. Santosh, and M. Yoshida, (eds.), *The Archaean and Proterozoic terrains of southern India within East Gondwana*. *Gondwana Res. Mem.* No.3, pp. 185-222.
- Srikantappa, C., Raith, M. and Spiering, B. (1985) Progressive charnockitization of a leptynite-khondalite suite in southern Kerala, India-evidence for formation of charnockites through decrease in fluid pressure? *J. Geol. Soc. India*, v. 26, pp. 849-872.
- Srikantappa, C., Raith, M. and Touret, J.L.R. (1992) Synmetamorphic high density carbonic fluids in the lower crust: Evidence from the Nilgiri granulites, southern India. *J. Petrol.*, v.33, pp. 733-760.
- Sterner, S.M., Hall, D.L. and Bodnar, R.J. (1988) Synthetic fluid inclusions. V. Solubility relations in the system NaCl-KCl-H<sub>2</sub>O under vapour saturated conditions. *Geochim. Cosmochim. Acta*, v. 52, pp. 989-1006.

- Sterner, S.M. and Bodnar, R.J. (1989) Synthetic fluid inclusions. VII. Re-equilibrium of fluid inclusions in quartz during laboratory stimulated metamorphic burial and uplift. *J. Metamorph. Geol.*, v. 7, pp. 243-260.
- Storm, L.C. and Spear, F.S. (2005) Pressure, temperature and cooling rates of granulite facies migmatitic pelites from the southern Adirondack highlands, New York. *J. Metamorph. Petrol.*, v. 23, pp. 107-130.
- Subramaniam, A.P. (1967) Charnockites and granulites of southern India. *Mémoires. Dansk Geol. Foren.*, v. 17, pp. 473-493.
- Sukumaran, S., Ravindra Kumar, G.R. and Srikantappa, C. (2005) Charnockite forming metamorphism in Palghat, southern India: a fluid inclusion study of gneiss, charnockite, charnoenderbite and pegmatite. *J. Geol. Soc. India*, v.66, pp. 679-694.
- Suzuki, K. and Adachi, M. (1994) Middle Precambrian detrital monazite and zircon from the Hida gneiss on Oki-Dogo island, Japan: their origin and implications for the correlation of basement gneiss of southwest Japan and Korea. *Tectonophysics*, v. 235, pp. 277-292.
- Tagiri, M. (1981) A measurement of graphitizing-degree by the X-ray powder diffractometer. *J. Japan. Assoc. Mineral. Petrol. Econ. Geol.*, v. 76, pp. 345-352.
- Tagiri, M. and Oba, T. (1986) Hydrothermal synthesis of graphite from bituminous coal at 0.5-5.0 kbar water vapour pressure and 300-600°C. *J. Japan. Assoc. Mineral. Petrol. Econ. Geol.*, v. 81, pp. 260-271.
- Tagiri, M. and Tsuboi, S. (1979) Mixed carbonaceous material in Mesozoic shales and sandstones from the Yamizo mountain system, Japan. *J. Japan. Assoc. Mineral. Petrol. Econ. Geol.*, v. 74, pp. 47-56.
- Thampi, P.K. Nair, P.K.R and Balasubramonian, G. (1993) Petrochemistry and tectonic evolution of Munnar granite, Idukki district, Kerala. *Curr. Sci.*, v. 64, pp. 238-243.
- Thompson, A.B. (1983) Fluid absent metamorphism. *J. Geol. Soc. London*, v. 140, pp. 533-547.
- Toriumi, M and Nomizo, A. (2000) Diffusion-controlled garnet growth during Sambagawa metamorphism. *Structur. Geol.*, v. 44, pp. 47-57.
- Tracy, R.J., Robinson, P. and Thompson, A.B. (1976) Garnet composition and zoning in the determination and pressure of metamorphism, central Massachusetts. *Am. Mineral.*, v. 61, pp. 762-775.

- Thrower, P.A. and Mayor, R.M. (1978) Point defects and self diffusion in graphite. *Physica. Status. Solidi.*, v. 47, pp.11-37.
- Touret, J. (1981) Fluid inclusions in high grade metamorphic rocks. In: L.S. Hollister, and M.L. Crawford, (eds), *Fluid inclusions: application to petrology*. Min. Assoc. Can., short course handbook No. 6, pp. 182-208.
- Touret, J.L.R. (1987) Fluid inclusions and pressure-temperature estimates in deep-seated rocks. In: H.C. Helgeson (ed), *Chemical transport in Metasomatic Processes*, NATO ASI Series C: Math. Phys. Sci., v. 218, pp. 91-121.
- Touret, J.L.R. (1992) Fluid inclusions in subducted rocks. *Proc. Koninklijke Ned. Acad. Wetensch*, v. 95, pp. 385-403.
- Touret, J.L.R. (2001) Fluids in metamorphic rocks. *Lithos*, v. 55, pp. 1-25.
- Touret, J.L.R. and Hansteen, T.H. (1988) Geothermobarometry and fluid inclusions in a rock from the Doddabetta charnockite complex, Southwest India. *Ren Soci. Ital. Mineral. Petrol.*, v. 43, pp. 65-82.
- Tuinstra F. and Koenig, J.L. (1970) Raman spectrum of graphite. *J. Chem. Phys.*, v. 53, pp. 1126-1130.
- Turner, F. J. (1948) Mineral and structural evolution of the metamorphic rocks. *Mem. Geol. Soc. Am.*, v. 30, 342p.
- Tyrrell. G.W. (1926) *The principles of petrology*. B.I. Pub. Pvt. Ltd, Bombay, 349p.
- Unnikrishnan-Warrier, C., Yoshida, M., Kagami, H. and Santosh, M. (1995) Sm-Nd and Rb-Sr mineral isochron ages of Madras charnockites and an evolution of garnet geochronometry in granulites. In: M. Yoshida and M. Santosh (eds.), *India and Antarctica during the Precambrian*. *Mem. Geol. Soc. India*, No. 34, pp. 253-260.
- Valakovich, M.P and Altunin, U.V. (1968) *Thermophysical properties of Carbon dioxide*. Collets. London.
- Valley, J.W. and O'Neil, J.R. (1981)  $^{12}\text{C}$  and  $^{13}\text{C}$  exchange between calcite and graphite: a possible thermometer in Grenville marbles. *Geochim. Cosmochim. Acta.*, v. 45, pp. 411-419.
- Van den Kerkhof, A.M. and Hein, U.H. (2001) Fluid inclusion petrography. *Lithos*, v. 55, pp. 27-47.
- Van den Kerkhof, A.M. and Thiery, R. (2001) Carbonic inclusions. *Lithos*, v. 55, pp. 49-68.



- Van den Kerkhof, A.M., Touret, J.L.R., Majer, C. and Jansen, J.B.H. (1991) Retrograde methane-dominated fluid inclusions from high temperature granulites of Rogaland, southwestern Norway. *Geochim. Cosmochim. Acta*, v. 55, pp. 2533-2544.
- Van den Kerkhof, A.M., Touret, J.L.R., Kreulen, R. (1994) Juvenile CO<sub>2</sub> in enderbites of Tromoy near Arendal, southern Norway: a fluid inclusion and stable isotope study. *J. Metamorph. Geol.*, v. 12, pp. 301-310.
- Vapnik, Y., Bushmin, S. and Sheglova, T. (2002) Fluid characteristics of metamorphic and metasomatic rocks of kyanite deposits of the Bolshie Keivy thrust structure, eastern Baltic shield. *Metallogeny of Precambrian shields. Abs. Int. Symp. Kyiv, Ukrain, September, 2002.*
- Varghese, S. (1990) Fluid-rock interactions in the high-grade terrains of South India: a mineralogic and thermodynamic study. Unpublished Ph.D. thesis. IISC, Bangalore.
- Vityk, M.O. and Bodnar, R.J. (1995a) Do fluid inclusions in high-grade metamorphic terranes preserve metamorphic density during retrograde decompression? *Am. Mineral.*, v.80, pp. 641-644.
- Vityk, M.O. and Bodnar, R.J. (1995b) Natural and synthetic re-equilibration textures of fluid inclusions in quartz (Marmarosh Diamonds): Evidence for refilling under conditions of compressive loading. *Europ. J. Mineral.*, v. 7, pp. 1071-1087.
- Vry, J.K. and Brown, P.E. (1991) Texturally early fluid inclusions in garnet: evidence of the pro-grade metamorphic path? *Contrib. Mineral. Petrol.*, v. 108, pp. 271-282.
- Wada, H. and Ito, R. (1990) Stable isotope analysis of small amounts of carbon dioxide and its application to the microscale isotopic zoning of graphite crystals in metamorphic rocks. *Mass Spectro.*, v. 38, pp. 287-294.
- Wada, H., Tomita, T., Iuchi, K., Ito, M. and Morikiyo, T. (1994) Graphitization of carbonaceous matter during metamorphism with reference to carbonate and pelitic rocks of contact and regional metamorphism, Japan. *Contrib. Mineral. Petrol.*, v. 118, pp. 217-228.
- Wells, P.R.A. (1979) Chemical and thermal evolution of Archaean crust, southern West Greenland. *J. Petrol.*, v. 20, pp. 187-226.
- Williams, M.L., and Grambling, J.A. (1990) Manganese, ferric iron, and the equilibrium between garnet and biotite. *Am. Mineral.*, v. 75, pp. 886-908.

- Williams, M. L., Jercinovic, M.J., Terry, M.P. (1999) Age mapping and chemical dating of monazite using the electron microprobe: deconvoluting multistage tectonic histories. *Geology*, v. 27, pp. 1023-1026.
- Wilmart, E., Clochiatti, R., Duechesene, J.C. and Touret, J.L.R. (1991) Fluid inclusions in charnockites from the Bjerkreim-Soknedal massif (Rogaland, southwestern Norway): fluid origin and insitu evolution. *Contrib. Mineral. Petrol.*, v. 108, pp. 453-462.
- Wing, B. N., Ferry, J. M., and Harrison, T. M. (2003) Prograde destruction and formation of monazite and allanite during contact and regional metamorphism of pelites: Petrology and geochronology. *Contrib. Mineral. Petrol*, v. 145, pp. 228–250
- Wopenka, B. and Pasteris, J.D. (1993) Structural characterization of kerogens to granulite facies graphite: applicability of Raman microprobe spectroscopy. *Am. Mineral.*, v.78, pp. 533-557.
- Wood, B.J. (1974) Solubility of alumina in orthopyroxene coexisting with garnet. *Contrib. Mineral. Petrol.*, v. 46, pp. 1-15.
- Wood, B.J. and Banno, S.S. (1973) Garnet-orthopyroxene and orthopyroxene-clinopyroxene relationship in simple and complex systems. *Contrib. Mineral. Petrol.*, v. 42, pp. 253-265.
- Yardley, B.W.D. and Graham, J.T. (2002) The origin of salinity in metamorphic fluids. *Geofluids*, v. 2, pp. 249-256.
- Yardley, B.W.D. and Valley, J.W. (1997) The petrologic case for a dry lower crust. *J. Geophys. Res.*, v. 102, pp.12173–12185.
- Yedekar, D.B., Jain, S.C., Nair, K.K.K. and Dutta, K.K.K (1990) The Central Indian collision suture. *Geol. Surv. India, Spl. Pub.*, v. 28, pp. 1-43.
- Yoshida, M., Bindu, R.S., Kagami, H., Rajesham, T., Santosh, M. and Shirahata, H. (1996) Geochronologic constraints of granulite terranes of South India and their implications for the Precambrian assembly of Gondwana. *J. Southeast Asian Earth Sci.*, v. 14, No.3/4, pp. 137-147.
- Yui T.F., Huang, E. and Xu, I. (1996) Raman spectrum of carbonaceous material: a possible metamorphic grade indicator for low-grade metamorphic rocks. *J. Metamorph. Geol.*, v. 14, pp. 115-124.

